

**LEVEL** *12*



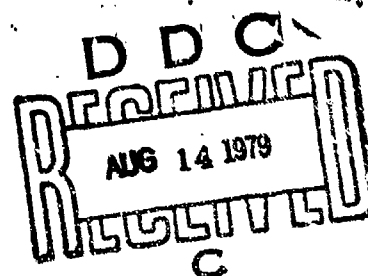
AD A072748

**RADC-TR-79-154**  
Final Technical Report  
June 1979

## **CROSS POLARIZATION INTERFERENCE REDUCTION TECHNIQUES**

**Harris Corporation**

Bruce E. Gillingham  
Charles A. Baird  
M. Guy Pelchat



APPROVED FOR PUBLIC RELEASE; DISTRIBUTION UNLIMITED

DDC FILE COPY


**ROME AIR DEVELOPMENT CENTER**  
**Air Force Systems Command**  
**Griffiss Air Force Base, New York 13441**

**79 08 14 020**

This report has been reviewed by the DC Information Office (OI) and is releasable to the National Technical Information Service (NTIS). At NTIS it will be releasable to the general public, including foreign nations.

RADC-TR-79-154 has been reviewed and is approved for publication.

APPROVED:



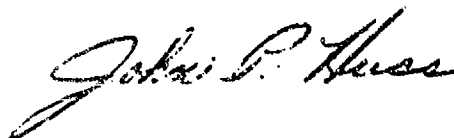
FREDERICK D. SCHMANDT  
Project Engineer

APPROVED:



FRED I. DIAMOND  
Technical Director  
Communications and Control Division

FOR THE COMMANDER:



JOHN F. HUSS  
Acting Chief, Plans Office

If your address has changed or if you wish to be removed from the RADC mailing list, or if the addressee is no longer employed by your organization, please notify RADC (DCCT) Griffiss AFB NY 13441. This will assist us in maintaining a current mailing list.

Do not return this copy. Repair or destroy.

UNCLASSIFIED

SECURITY CLASSIFICATION OF THIS PAGE (When Data Entered)

REPORT DOCUMENTATION PAGE		READ INSTRUCTIONS BEFORE COMPLETING FORM
1. REPORT NUMBER RADC-TR-79-154	2. GOVT ACCESSION NO.	3. RECIPIENT'S CATALOG NUMBER
4. TITLE (and Subtitle) CROSS POLARIZATION INTERFERENCE REDUCTION TECHNIQUES	5. TYPE OF REPORT & PERIOD COVERED Final Technical Report Sep 77 - Dec 78	6. PERFORMING ORG. REPORT NUMBER N/A
7. AUTHOR(s) Bruce E. Gillingham Charles A. Baird M. Guy Pelchat	8. CONTRACT OR GRANT NUMBER(s) F30602-77-C-0100	
9. PERFORMING ORGANIZATION NAME AND ADDRESS Harris Government Communication System Division P.O. Box 37 Melbourne, FL 32901	10. PROGRAM ELEMENT, PROJECT, TASK AREA & WORK UNIT NUMBERS 62702F 45192113	
11. CONTROLLING OFFICE NAME AND ADDRESS Rome Air Development Center (DCCT) Griffiss AFB NY 13441	12. REPORT DATE June 1979	13. NUMBER OF PAGES
14. MONITORING AGENCY NAME & ADDRESS (if different from Controlling Office) Same	15. SECURITY CLASS. (of this report) UNCLASSIFIED	15a. DECLASSIFICATION/DOWNGRADING SCHEDULE N/A
16. DISTRIBUTION STATEMENT (of this Report) Approved for public release; distribution unlimited.		
17. DISTRIBUTION STATEMENT (of the abstract entered in Block 20, if different from Report) Same		
18. SUPPLEMENTARY NOTES RADC Project Engineer: Frederick D. Schmandt (DCCT)		
19. KEY WORDS (Continue on reverse side if necessary and identify by block number) Digital Microwave Polarization Frequency Reuse		
20. ABSTRACT (Continue on reverse side if necessary and identify by block number) The objective of this program was to design, fabricate and test the optimum algorithm developed on the previous contract (Contract F30602-76-C-0041) to improve the performance of cross-polarization on line-of-sight (LOS) digital microwave channels. Specifically, an adaptive equalizer which would function with cross-polarization discrimination ratios from 5 dB to 40 dB and provide up to 20 nanoseconds of linear and parabolic group delay compensation was desired.		

DD FORM 1 JAN 73 1473

UNCLASSIFIED

SECURITY CLASSIFICATION OF THIS PAGE (When Data Entered)

417 224

UNCLASSIFIED

SECURITY CLASSIFICATION OF THIS PAGE(When Data Entered)

An experimental equalizer was constructed and successfully tested both in the laboratory and at RADC. All primary design objectives were met with the exception of automatic operation in the copolar mode. Theoretical limitations of the performance measurement technique used in the equalizer restrict copolar operation to a manual mode. In the automatic cross-polar mode, the equalizer can reduce an input cross-polarization discrimination ratio (CPDR) of 5 dB to a CPDR near 25 dB with the modem signal meeting FCC 19311 requirements over an LC8D radio. Non-dispersive cross-pole interference can be reduced by 25 dB. In back-to-back modem tests, the equalizer's residual interference level is near the design objective of -40 dB.

Accession For		<input checked="checked" type="checkbox"/>
NTIS GRA&I		<input type="checkbox"/>
DDC TAB		<input type="checkbox"/>
Unannounced Justification		
By _____		
Distribution/		
Availability Codes		
Dist.	Avail and/or special	
A		

UNCLASSIFIED

SECURITY CLASSIFICATION OF THIS PAGE(When Data Entered)

# CROSS POLARIZATION INTERFERENCE

## REDUCTION TECHNIQUES

### TECHNICAL REPORT

#### SUMMARY

The primary objective of this program was the construction and test of an adaptive equalizer providing improved performance of cross polarization on line-of-sight (LOS) digital microwave channels.

On a prior contract (F30602-76-C-0041), a general analysis of the use of dual polarized communication on LOS links was performed. The study resulted in a conceptual design of an equalizer that could automatically remove cross-polarization interference, providing greatly reduced bit error rates with the modems used on the LOS channels. The equalizer operates with constant envelope signalling techniques and was optimized for use with the Broadband Modem II implemented on a previous contract (F30602-76-C-0434). Two Broadband Modems operating on cross-polarized channels can provide 4 bits of data per second per hertz of RF bandwidth.

The experimental equalizer was constructed and successfully tested, both in the laboratory and the Rome Air Development Center (RADC). All design requirements were met with the exception of automatic operation in the copolar mode. Theoretical limitations of the performance measurement technique used in the equalizer restrict copolar operation to a manual mode. The equalizer provides the required 20 ns of linear and parabolic group delay compensation at the band edges

(70 MHz  $\pm$  7 MHz). In addition, it can provide 8 ns of straight delay compensation and more than 3 dB of linear, parabolic, and cubic amplitude correction at the band edges.

In the automatic cross-polar mode, the equalizer can reduce an input cross-polarization discrimination ratio (CPDR) of 5 dB to a CPDR close to 25 dB with the modem signal filtered by a LC8D radio with a FCC 19311 microwave filter. Starting with a CPDR of 10 dB, the interference can be reduced to a CPDR near 28 dB. The residual interference level is down more than 30 dB from the signal level. For nondispersive cross-polarization interference, the equalizer can be modified to reduce a 5 dB CPDR to the residual interference level of -30 dB.

Without the amplitude modulation induced by the FCC 19311 filter, the breadboard equalizer's residual interference level is close to the design objective of -40 dB. A CPDR of 10 dB can be reduced to a CPDR of better than 30 dB, and a CPDR of 5 dB can be reduced to a CPDR near 28 dB. Additional tests demonstrated that the equalizer can track time varying interference at a 1 Hz rate without degradation and up to a 10 Hz rate with less than 1.5 dB degradation in the vicinity of a  $1 \times 10^{-7}$  BER.

## TABLE OF CONTENTS

<u>Paragraph</u>	<u>Title</u>	<u>Page</u>
1.0	INTRODUCTION .....	1-2
1.1	Objective .....	1-2
1.2	Approach .....	1-2
1.3	Results .....	1-2
1.4	Report Organization .....	1-3
2.0	ANALYTICAL RESULTS .....	2-2
2.1	Summary of Results From Previous Contract.....	2-2
2.1.1	Comparative Link Availability .....	2-2
2.1.2	Description of the Conceptual Design .....	2-3
2.1.2.1	Performance Measurement Circuitry .....	2-6
2.1.2.2	Control Logic Description .....	2-7
2.2	Correction Network Implementation .....	2-11
2.2.1	Evolution of the Correction Network Implementation .....	2-15
2.2.2	Simultaneous Copolar and Cross-Polar Equalization .....	2-18
2.2.3	Selection of Tap Spacing .....	2-21
2.2.4	Control Loop Coupling With the Notch Filter Network ....	2-22
3.0	HARDWARE DESCRIPTION .....	3-2
3.1	Cross-Polarization Interference Reduction Equalizer Unit Level Description .....	3-2
3.2	Equalizer Description .....	3-6
3.3	Control Circuitry Description .....	3-11
4.0	TEST RESULTS .....	4-2
4.1	In-Plant Tests .....	4-2
4.1.1	Equalizer Results .....	4-2
4.1.2	Main Signal Path Results .....	4-18
4.1.3	Performance Testing Results .....	4-38
4.1.3.1	Two B/Hz Test Results .....	4-52
4.1.3.2	One B/Hz Test Results .....	4-62
4.1.4	RADC Witnessed In-Plant Testing Results .....	4-69
4.2	RADC Tests .....	4-69
4.2.1	FCC 19311 Waveguide Filter Results .....	4-69
4.2.2	Performance Verification Testing Results .....	4-78
4.2.3	Radio/Simulator Performance Testing Results .....	4-78
4.2.3.1	2 B/Hz Radio/Simulator Results .....	4-82
4.2.3.2	1 B/Hz Radio/Simulator Results .....	4-86
5.0	CONCLUSIONS AND RECOMMENDATIONS .....	5-2
5.1	Conclusions .....	5-2
5.2	Recommendations .....	5-2

# TABLE OF CONTENTS (Continued)

<u>Paragraph</u>	<u>Title</u>	<u>Page</u>
	APPENDICES	
A	Achievable Time Delay .....	A-1
B	Decorrelator .....	B-1
C	Test Plan .....	C-1
D	Achievable S/N Improvement .....	D-1
E	References . . . . .	E-1

# LIST OF ILLUSTRATIONS

<u>Figure</u>	<u>Title</u>	<u>Page</u>
1	8.0 GHz Link Availability Versus System Margin .....	2-4
2	Basic Block Diagram .....	2-5
3	Performance Measurement Circuitry .....	2-7
4	Block Diagram of Control Logic .....	2-9
5	Approximate Sketch of Interference Versus In-Phase Weight Setting .....	2-10
6	Mathematical Description of Transmission and Correction Network Characteristics .....	2-13
7	Conventional Tapped Delay Line Correction Network .....	2-14
8	Special Multitap Correction Network .....	2-16
9	Notch Filter Correction Network .....	2-17
10	Cross-Polar Equalization .....	2-19
11	Copolar Equalization .....	2-20
12	MMSE Versus Tap Spacing for TDL Filters Adjusted to Match a 4-Pole Butterworth .....	2-23
13	Equivalent Form of Notch Filter Network Using Standard Tapped Delay Line .....	2-24
14	CPIRE Front Panel .....	3-3
15	CPIRE Block Diagram .....	3-4
16	Equalizer Block Diagram .....	3-7
17	Notch Filter Block Diagram .....	3-9
18	Weight Block Diagram .....	3-10
19	Control Circuitry Block Diagram .....	3-12
20	Effect of Weight A1 on Amplitude Response - Horizontal Channel .....	4-4
21	Effect of Weight A1 on Group Delay - Horizontal Channel .....	4-5
22	Effect of Weight A1 on Amplitude Response - Vertical Channel .....	4-6
23	Effect of Weight A1 on Group Delay - Vertical Channel .....	4-7
24	Effect of Weight B1 on Amplitude Response - Horizontal Channel .....	4-8
25	Effect of Weight B1 on Group Delay - Horizontal Channel .....	4-9
26	Effect of Weight B1 on Amplitude Response - Vertical Channel .....	4-10
27	Effect of Weight B1 on Group Delay - Vertical Channel .....	4-11
28	Effect of Weight C1 on Amplitude Response - Horizontal Channel .....	4-12
29	Effect of Weight C1 on Group Delay - Horizontal Channel .....	4-13
30	Effect of Weight C1 on Amplitude Response - Vertical Channel .....	4-14
31	Effect of Weight C1 on Group Delay - Vertical Channel .....	4-15

# LIST OF ILLUSTRATIONS (Continued)

<u>Figure</u>	<u>Title</u>	<u>Page</u>
32	Effect of Weight A2 on Group Delay - Horizontal Channel .....	4-16
33	Effect of Weight A2 on Group Delay - Vertical Channel ..	4-17
34	Effect of Weight A2 on Amplitude Response - Horizontal Channel .....	4-19
35	Effect of Weight A2 on Amplitude Response - Vertical Channel .....	4-20
36	Effect of Weight B2 on Group Delay - Horizontal Channel .....	4-21
37	Effect of Weight B2 on Amplitude Response - Horizontal Channel .....	4-22
38	Effect of Weight B2 on Group Delay - Vertical Channel ..	4-23
39	Effect of Weight B2 on Amplitude Response - Vertical Channel .....	4-24
40	Effect of Weight C2 on Group Delay - Horizontal Channel .....	4-25
41	Effect of Weight C2 on Amplitude Response - Horizontal Channel .....	4-25
42	Effect of Weight C2 on Group Delay - Vertical Channel ..	4-27
43	Effect of Weight C2 on Amplitude Response - Vertical Channel .....	4-28
44	Attenuation of Weight D1 with Positive Control Voltages - Horizontal Channel .....	4-29
45	Attenuation of Weight D1 with Negative Control Voltages - Horizontal Channel .....	4-30
46	Attenuation of Weight D2 with Positive Control Voltages - Horizontal Channel .....	4-31
47	Attenuation of Weight D2 with Negative Control Voltages - Horizontal Channel .....	4-32
48	Attenuation of Weight D1 with Positive Control Voltages - Vertical Channel .....	4-33
49	Attenuation of Weight D1 with Negative Control Voltages - Vertical Channel .....	4-34
50	Attenuation of Weight D2 with Positive Control Voltages - Vertical Channel .....	4-35
51	Attenuation of Weight D2 with Negative Control Voltages - Vertical Channel .....	4-36
52	Horizontal Channel Amplitude Response With Input Filter (35 MHz-105 MHz) .....	4-37
53	Horizontal Channel Amplitude Response With Input Filter (63 MHz-77 MHz) .....	4-39
54	Horizontal Channel Delay With Input Filter .....	4-40
55	Horizontal Channel Group Delay With Input Filter .....	4-41
56	Horizontal Channel Amplitude Response Without Input Filter .....	4-42
57	Horizontal Channel Delay Without Input Filter .....	4-43
58	Horizontal Channel Group Delay Without Input Filter ....	4-44

# LIST OF ILLUSTRATIONS (Continued)

<u>Figure</u>	<u>Title</u>	<u>Page</u>
59	Vertical Channel Amplitude Response With Input Filter (35 MHz-105 MHz) .....	4-45
60	Vertical Channel Amplitude Response With Input Filter (63 MHz-77 MHz) .....	4-46
61	Vertical Channel Delay With Input Filter .....	4-47
62	Vertical Channel Group Delay With Input Filter .....	4-48
63	Vertical Channel Amplitude Response Without Input Filter .....	4-49
64	Vertical Channel Delay Without Input Filter .....	4-50
65	Vertical Channel Group Delay Without Input Filter .....	4-51
66	BBM II 2 B/Hz Performance With Cross-Polarization Interference .....	4-53
67	CPIRE Horizontal Channel 2 B/Hz Performance Without Input Filter .....	4-55
68	CPIRE Vertical Channel 2 B/Hz Performance Without Input Filter .....	4-56
69	Dispersive Cross-Polarization Test Filter Amplitude Response (35 MHz-105 MHz) .....	4-57
70	Dispersive Cross-Polarization Test Filter Amplitude Response (63 MHz-77 MHz) .....	4-58
71	Dispersive Cross-Polarization Test Filter Group Delay Characteristics .....	4-59
72	CPIRE Horizontal Channel 2 B/Hz Dispersive Cross-Pole Performance Without Input Filter .....	4-60
73	CPIRE Vertical Channel 2 B/Hz Dispersive Cross-Pole Performance Without Input Filter .....	4-61
74	CPIRE Horizontal Channel 2 B/Hz Dynamic Cross-Pole Performance Without Input Filter .....	4-63
75	CPIRE Vertical Channel 2 B/Hz Dynamic Cross-Pole Performance Without Input Filter .....	4-64
76	CPIRE Horizontal Channel 2 B/Hz Performance With Input Filter .....	4-65
77	CPIRE Vertical Channel 2 B/Hz Performance With Input Filter .....	4-66
78	BBM II 1 B/Hz Performance With Cross-Polarization Interference .....	4-67
79	CPIRE Horizontal Channel 1 B/Hz Performance Without Input Filter .....	4-68
80	CPIRE Vertical Channel 1 B/Hz Performance Without Input Filter .....	4-70
81	CPIRE Horizontal Channel 1 B/Hz Dispersive Cross-Pole Performance Without Input Filter .....	4-71
82	CPIRE Vertical Channel 1 B/Hz Dispersive Cross-Pole Performance Without Input Filter .....	4-72
83	CPIRE Horizontal Channel 1 B/Hz Dynamic Cross-Pole Performance Without Input Filter .....	4-73

# LIST OF ILLUSTRATIONS (Continued)

<u>Figure</u>	<u>Title</u>	<u>Page</u>
84	CPIRE Vertical Channel 1 B/Hz Dynamic Cross-Pole Performance Without Input Filter .....	4-74
85	CPIRE Horizontal Channel 1 B/Hz Performance With Input Filter .....	4-75
86	CPIRE Vertical Channel 1 B/Hz Performance With Input Filter .....	4-76
87	CPIRE Horizontal Channel 2 B/Hz Performance Without Input Filter ....	4-77
88	BBM II Performance With FCC 19311 Filters .....	4-79
89	CPIRE Horizontal Channel 2 B/Hz Performance Without Input Filter .....	4-80
90	CPIRE Vertical Channel 2 B/Hz Performance Without Input Filter .....	4-81
91	BBM II 2 B/Hz Performance Over LC8D Radio With Cross-Polarization Interference .....	4-83
92	CPIRE Horizontal Channel 2 B/Hz Performance With LC8D Radio/Simulator Without Equalization .....	4-84
93	CPIRE Vertical Channel 2 B/Hz Performance With LC8D Radio/Simulator Without Equalization .....	4-85
94	CPIRE Vertical Channel 2 B/Hz Performance With LC8D Radio/Simulator With Equalization .....	4-87
95	CPIRE Vertical Channel 2 B/Hz Performance With LC8D/ Radio/Simulator - Equalizer Bypassed .....	4-88
96	CPIRE Vertical Channel 1 B/Hz Performance With LC8D Radio/Simulator .....	4-89
97	CPIRE Vertical Channel 1 B/Hz Performance With LC8D Radio/Simulator - Equalizer Bypassed .....	4-91
B-1	Decorrelator Block Diagram .....	B-3
B-2	Decorrelator Front Panel .....	B-4
B-3	Decorrelator Horizontal Output Amplitude Response .....	B-5
B-4	Decorrelator Vertical Output-Amplitude Response .....	B-6
B-5	Decorrelator Horizontal Output Delay .....	B-7
B-6	Decorrelator Vertical Output Delay .....	B-8
C-1	CPIRE Basic Block Diagram .....	C-3
C-2	In-Plant Test Configuration .....	C-5
C-3	$E_b/N_0$ Test Setup .....	C-6
C-4	Decorrelator Block Diagram .....	C-7
C-5	Cross Polarization Test Setup .....	C-8
C-6	RADC Test Configuration .....	C-11
D-1	Cross-Polarization Interference Cancellation Scheme .....	D-3
D-2	Achievable $(S/N)_0$ Bounds .....	D-4

## Evaluation

Increased use of digital communications is resulting in a significant increase in congestion, particularly in the microwave frequency bands. Bandwidth efficient modulation techniques are required to alleviate this congestion. Several approaches have been taken to improve bandwidth efficiency (see RADC Research & Technology Plan, TPO R3B). One approach involves the use of one carrier frequency on orthogonal polarization which doubles the amount of data that can be communicated in a given bandwidth.

Rain, turbulence, and multipath can severely affect the separation between polarizations, particularly over long microwave links. These effects limit the use of cross polarization because of the high availability requirements for LOS microwave. By the use of adaptive algorithms effects caused by the media can be counteracted permitting cross polarized transmission with high reliability. The hardware developed was demonstrated under this effort to effectively remove cross-polarization interference under the quite restrictive test conditions investigated. In addition to eliminating interference the hardware can track both amplitude and delay functions induced by cross polarization interference. This later capability allows detailed studies into the cross polarization interference mechanism.

A follow-on test program is suggested to more fully define the capabilities of the hardware, to evaluate its capabilities when utilized in conjunction with additional modulation types, and to characterize the cross polarization phenomena in order to determine ways to more effectively combat its effects.

  
FREDERICK D. SCHMANDT  
Project Engineer

**SECTION 1.0**  
**INTRODUCTION**

## 1.0 INTRODUCTION

### 1.1 Objective

The objective of this program was to design, fabricate and test the optimum algorithm developed on a previous contract (F30602-76-C-0041)<sup>1</sup> to improve the performance of cross polarization on line-of-sight (LOS) digital microwave channels. Specifically, an adaptive equalizer which would function with cross-polarization discrimination ratios from 5 dB to 40 dB and provide up to 20 nanoseconds (ns) of linear and parabolic group delay compensation was desired.

### 1.2 Approach

The program consisted of two main phases. During the first phase, general analytical work on the cross-pole problem was continued, as well as detailed computer simulation of a specific equalizer design. In the second phase, a breadboard cross-polarization interference reduction equalizer was constructed and tested both in the laboratory, and on a microwave radio.

### 1.3 Results

The experimental equalizer was tested successfully both in the laboratory and the Rome Air Development Center (RADC). All design requirements were met with the exception of automatic operation in the copolar mode. Theoretical limitations of the performance measurement technique used in the equalizer (refer to Paragraph 2.2.2) limit copolar operation to a manual mode. In the automatic cross-polar mode, the equalizer can reduce an input cross-polarization discrimination ratio (CPDR) of 5 dB to a CPDR close to 25 dB with the modem signal filtered by an LC8D radio with an FCC 19311 microwave filter. Starting with a CPDR of 10 dB, the interference can be reduced to a CPDR near 28 dB. The residual interference level is down more than 30 dB from the signal level. For nondispersive cross-polarization interference, the equalizer can be modified to reduce a 5 dB CPDR to the residual interference level of -30 dB.

Without the amplitude modulation induced by the FCC 19311 filter, the breadboard equalizer's residual interference level is close to the design objective of -40 dB. A CPDR of 10 dB can be reduced to a CPDR of better than 30 dB, and a CPDR of 5 dB can be reduced to a CPDR near 28 dB.

1.4      Report Organization

The results of the analytical effort are presented in Section 2.0. The design and construction of the experimental equalizer are discussed in Section 3.0. In Section 4.0 the test program and results are presented. Conclusions and recommendations are presented in Section 5.0.

SECTION 2.0  
ANALYTICAL RESULTS

## 2.0 ANALYTICAL RESULTS

The majority of the conceptual design for the cross-pole correction device was completed on a previous RADC contract (Contract F30602-76-C-0041). This effort included general analytical work on the cross-pole problem, as well as detailed computer simulation of a specific design. This section will present a brief summary of that work, together with a discussion of the major changes required during the hardware implementation.

### 2.1 Summary of Results From Previous Contract

During the conceptual design phase conducted under the previous contract a general analysis of the use of dual polarized communication on LOS links was performed. A review of the physical and statistical properties of cross-polar interference led to the development of a procedure to quantitatively define the interference problem and compare alternative interference reduction and bandwidth capacity expanding techniques. This work indicated the utility of adaptive cross-pole interference reduction methods. Consequently, a thorough investigation of the design trade-offs associated with the application of adaptive interference reduction to LOS microwave links was performed and resulted in the design of a specific system. The mathematical analysis of this design led to the development of both general performance estimates for dual polarized links and a system model through which specific component parameters were chosen.

#### 2.1.1 Comparative Link Availability

Utilizing data gathered from the literature, in conjunction with approximations which were developed relating cross-polar interference to degradation in signal-to-noise ratio, a procedure for computing the probability that a link of a given quality would be available was developed. These statistics were computed for links employing both circular and linear orthogonal polarizations, as well as for those which utilized modulation techniques to increase bandwidth efficiency. In this manner, the relative costs (in terms of link power requirements) of these alternatives were assessed. This investigation indicated that in all cases, dual linear polarization is less susceptible to rain-induced cross-polar interference than is circular polarization. Other generalizations from these results are

limited by the relevance of the rain statistics used to the specific link being considered. That is, the procedure developed is a generally applicable method, but it requires that accurate rain statistics be compiled for the specific application being considered. Similarly, the effects of non-rain-induced interference (e.g., multipath) are also very dependent upon applications and do not lead to easily generalized results.

One example of these results is shown in Figure 1. These computations were performed for a 16 km link at 8 GHz. The four curves in the figure are: a) the basic link where frequency reuse is not employed and the system margin must compensate for direct attenuation only; b) cross-polar links employing dual linearly polarized waves; c) cross-polar links employing dual circularly polarized waves; and d) links where capacity is doubled using 16 rather than 4-phase modulation. These curves indicate the reduction in availability for a fixed link margin (and similarly, the increased system margin required for a fixed availability) resulting from frequency reuse links and non-frequency reuse links. It is apparent as longer links are considered, the family of curves on each figure must rise indicating an increased probability of a given amount of rain on the link. Due to the limited amount of path rain data available in the literature, quantitative estimates of such increases are difficult. Note that the use of a polarization correction technique will reduce the cross-polarization coupling, effectively moving the dual polarization curves on each figure toward the lower one. Consequently, to realize this improvement, the design of a specific correction method was pursued.

#### 2.1.2 Description of the Conceptual Design

As shown in the last paragraph, if dual polarized links are to be employed, additional link margin is required for each cross-pole channel to perform on a par (maintain same availability) with a single polarization (basic) link. This is necessitated by the additional interference introduced by the cross-pole coupling. This interference, and the need for additional power margin, can be avoided by the use of adaptive interference reduction circuits. The block diagram of such a device is shown in Figure 2 and consists of three major components; the adjustable correction network, the performance measurement device, and the controller. Associated with each of

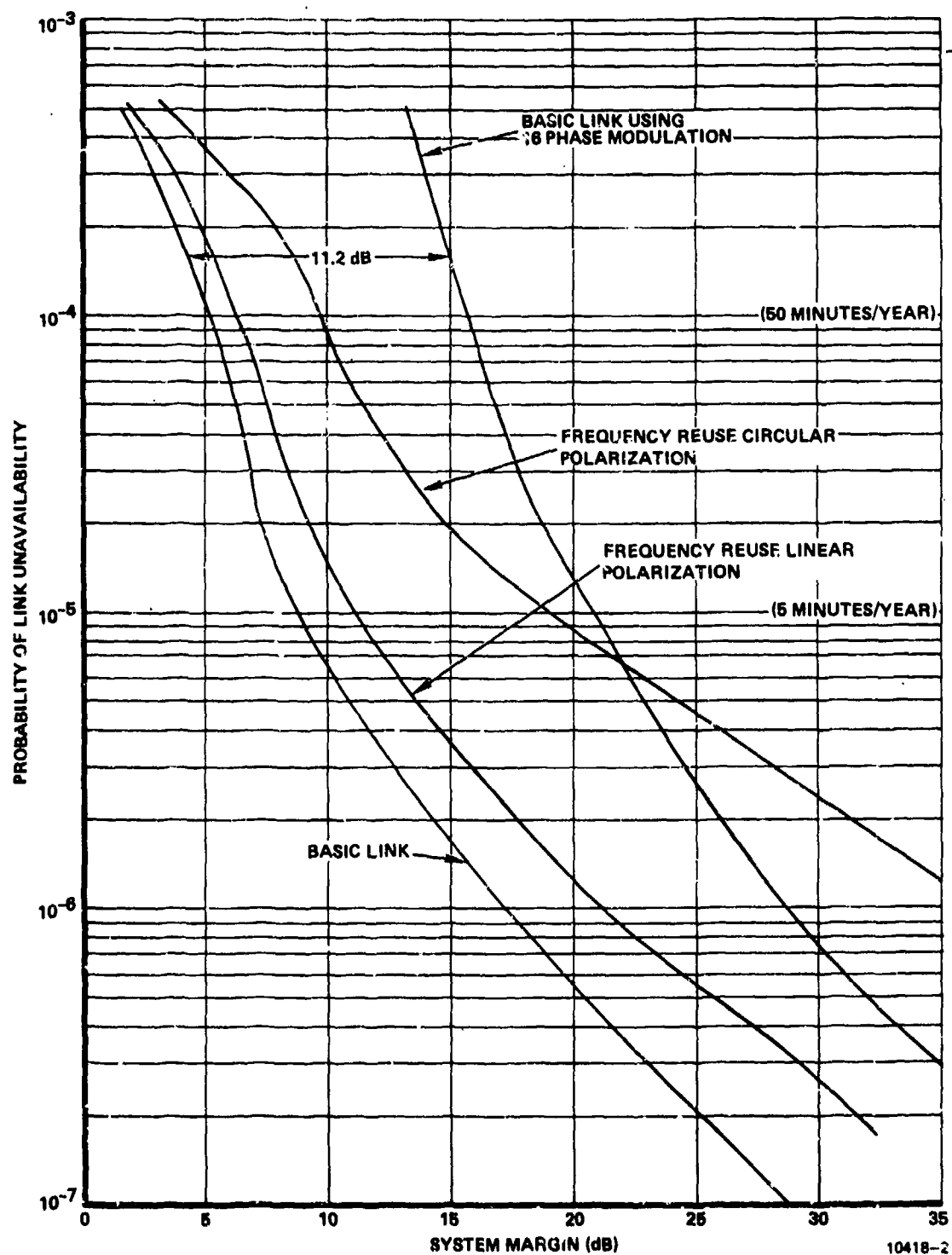


Figure 1. 8.0 GHz Link Availability Versus System Margin

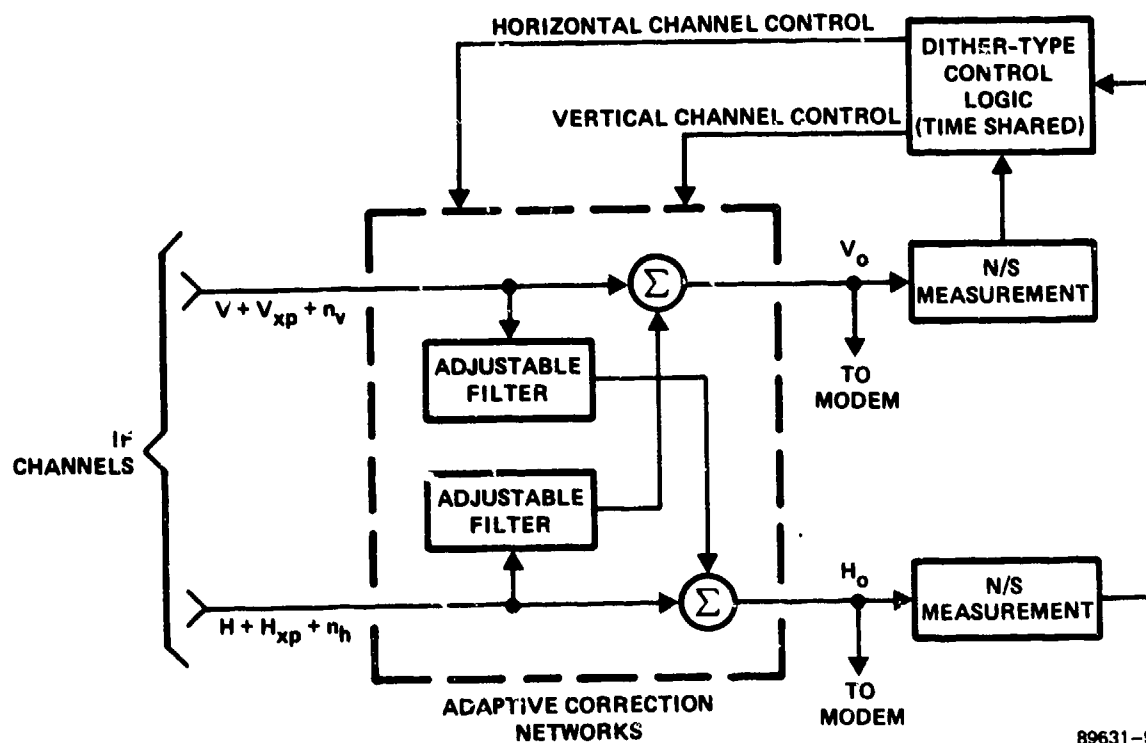


Figure 2. Basic Block Diagram

these components are a number of design considerations and trade-offs which are discussed in detail in the previous report.

The basic design philosophy used was to postulate what appeared to be the simplest approach suitable to the problem and verify that its performance would be adequate. For example, the dither-type gradient control method is quite simple to implement, but the injected dither can potentially limit the system performance. It was demonstrated that this was not a limitation. Also, the efficient use of this type of control requires the availability of an easily measured performance index. To accomplish this the technique to measure the interference-induced envelope fluctuation was developed. The use of this was indicated by the fact that the DCS signal formats were nominally constant envelope; however, the technique is applicable only when some fluctuations are present since it requires that the interference produce additional measurable envelope fluctuations. For the correction network implementation, the simplest procedure would be to use the single adjustable complex weight  $w = w_i + jw_q$ , which would be adequate for relatively narrowband systems. However, since the measured radio characteristics examined indicate nonnegligible dispersion between channels over the required bandwidth and insufficient data is available on the dispersive nature of the media, more sophisticated multitap networks were used. For each of these multitap network designs the frequency response is a function of several adjustable complex weights  $w_i$ .

The circuitry illustrated in Figure 2 is designed to interface the radios at IF with nominally vertical and horizontal channels being shown. These signals are contaminated with cross-polar interference  $V_{xp}$  and  $H_{xp}$  and thermal noise  $n_v$  and  $n_h$ . Both the dither-type controller and the N/S (inverse signal-to-noise ratio) performance measurement circuits have been implemented as designed on the previous contract, and will be briefly described in this section. The adjustable correction network, on the other hand, has undergone several modifications during the present implementation phase. These modifications will be discussed in Paragraph 2.2.

#### 2.1.2.1 Performance Measurement Circuitry

The performance measurement technique is a direct-type method based on measuring the inverse of the signal-to-noise ratio. The network is

designed to operate with nominally constant envelope desired signal formats and for a given weight setting on the adjustable correction network it measures the interference by measuring the power in the envelope fluctuations. (Note that non-interference-induced envelope fluctuations can be tolerated, as long as the interference produces measurable envelope variations.) A block diagram of this circuitry is shown in Figure 3. The

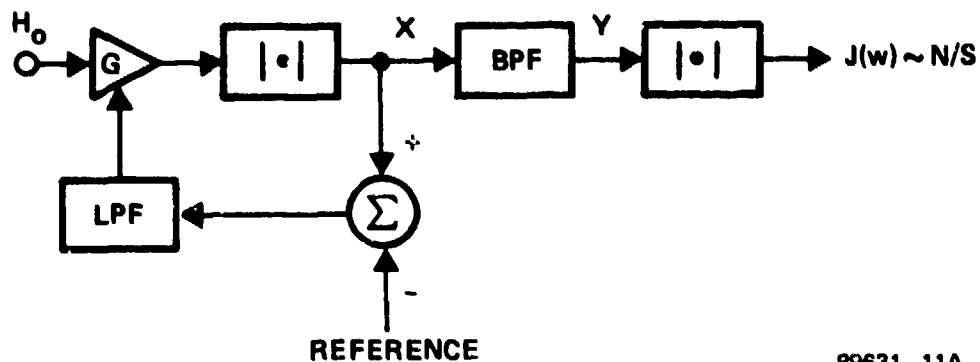


Figure 3. Performance Measurement Circuitry

89631-11A

variable gain amplifier, magnitude detector and gain control keep the signal level at X constant so that fluctuations in the desired signal level will not affect the interference measurement. The bandpass filter then removes the dc terms due to the desired signal components. Finally, the second magnitude detector measures the average power level of the remaining noise terms. Its output is written as  $J(w)$  to indicate its functional dependence on the correction network weight settings and is directly proportional to the inverse signal-to-noise ratio,  $N/S$ .

#### 2.1.2.2 Control Logic Description

The circuitry described in the last section allows the measurement of the interference as a function of the adjustable weight settings and thereby provides the capability of measuring the gradient of the interference with respect to these weight settings, i.e., the weights  $w_i$  and  $w_q$ . This gradient information

$$\frac{\partial J}{\partial w_i} = \nabla J_i \quad \text{and} \quad \frac{\partial J}{\partial w_q} = \nabla J_q$$

can then be used to drive the weights to where the gradients are zero, the

defining relations for the optimum weights. The interference measurement,  $J$ , is a quadratic function of the weights  $w_i$  and  $w_q$ , and therefore, the vanishing of the gradients will define unique weight settings which minimize the interference and thereby maximize the signal-to-interference ratio. Figure 4 illustrates the block diagram of a control technique which utilizes a dithering signal to develop the gradient of the interference with respect to the weights and the associated circuitry to drive the correction network weights to their optimum (zero gradient) values. For control of the multitap correction networks this control logic is time shared between four complex tap weights.

The circuitry illustrated in Figure 4 can be described in the following manner. The square wave source generates two orthogonal waveforms, each of which is used to dither one of the correction network weights by  $\pm\Delta$ , a square wave of magnitude  $\Delta$ . In this manner the interference measurement network gives, for example, (for the in-phase weight)  $J(w_i + \Delta_i)$  and  $J(w_i - \Delta_i)$  over the positive and negative values for the dither waveform. The quadrature weight is dithered simultaneously with an orthogonal ( $90^\circ$  phase shifted) square wave, with the separate effects on the interference measurement being extracted with the synchronous detectors (multiplier - LPF combination) shown in the figure. For example, the output  $X$  of the in-phase weight synchronous detector becomes

$$X = \text{sgn}(\Delta_i) J(w_i + \Delta_i) \quad (2-1)$$

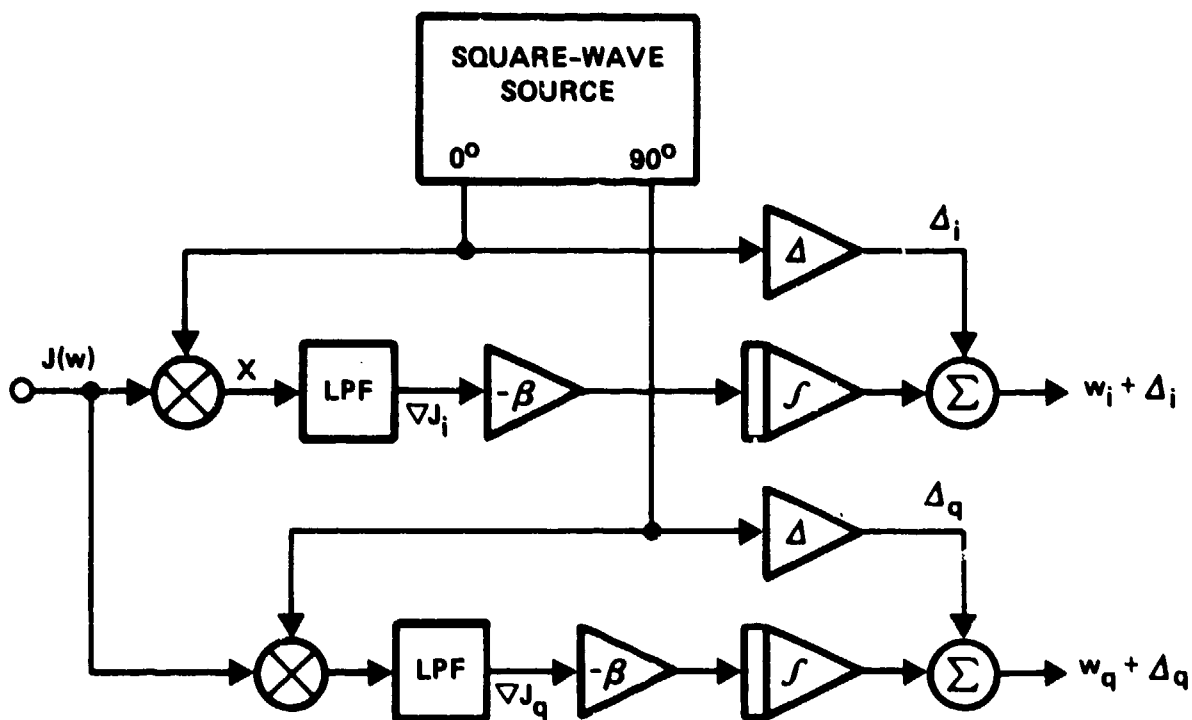
which is  $J(w_i + \Delta_i)$  when  $\Delta_i > 0$  and  $-J(w_i - \Delta_i)$  when  $\Delta_i < 0$ .

Consequently, the output of the LPF averages this waveform to generate the approximate gradient  $\nabla J$  of  $J(w)$  with respect to  $w_i$  as

$$\nabla J(w_i) = \lim_{\Delta \rightarrow 0} \frac{J(w_i + \Delta_i) - J(w_i - \Delta_i)}{2\Delta_i} \quad (2-2)$$

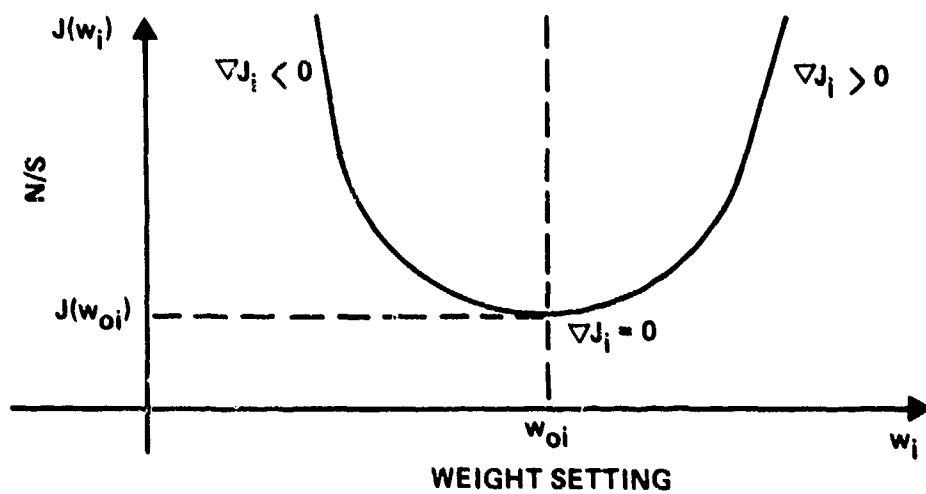
$$\sim X = \frac{J(w_i + \Delta_i) - J(w_i - \Delta_i)}{2\Delta_i} = \nabla J_i$$

As mentioned above, the interference  $J$  is quadratic in the weights, with an approximate sketch of this functional relationship being shown in Figure 5. This figure illustrates that the minimum interference  $J(w_{0i})$  corresponds to the point where  $\nabla J_i = 0$  and the quadratic nature of



89631-12

Figure 4. Block Diagram of Control Logic



89631-18A

Figure 5. Approximate Sketch of Interference Versus In-Phase Weight Setting

this curve gives  $\nabla J_i > 0$  if  $w_i > w_{0i}$  and  $\nabla J_i < 0$  if  $w_i < w_{0i}$ . These relationships allow the optimum weight to be found with a simple integration circuit as used in Figure 4. That is,

$$\frac{dw_i}{dt} = -\beta \nabla J_i \quad (2-3)$$

where  $\frac{dw_i}{dt}$  is zero when  $\nabla J_i = 0$  and the weight remains constant, while non-zero  $\nabla J_i$  tends to drive the weight toward the optimum (zero gradient) value. The quadrature weight control is described similarly. More detail concerning gain settings (e.g.,  $\beta$  value) and loop bandwidth is discussed in the final report for the previous contract.<sup>1</sup>

As described above, the synchronous detectors include a low-pass filter (LPF) to average the output and form the required gradient. This averaging will remove the dither generated square wave due to the average or dc value of the performance measure at the particular operating point. For instance, at the optimum weight setting this square wave will be of magnitude  $J(w_0)$ . Since the control loop already contains an integrator, some averaging will be present and the additional LPF could cause stability problems. In fact, for high signal-to-noise ratios, the value of  $J(w_0)$  will be quite small, and as long as it is small compared to the effect of the weight dither, its effect will be negligible. An alternative to the LPF after the synchronous detector is to remove the dc at the input to the detector with a high-pass filter. This alternative was used in both the simulations run on the previous contract and with the present hardware implementation.

## 2.2 Correction Network Implementation

The purpose of the correction network is to undo the coupling (deorthogonalization) of the two polarizations which has occurred in the media and other parts of the system. The primary considerations in its design are where it is placed in the system and the type of network to be used. These considerations reduce to trade-offs of bandwidth versus S/N loss and hardware simplicity. The decoupling is accomplished by coupling the signal from one channel, properly weighting it, and adding it back into the other channel to undo the media induced coupling. For very narrowband

systems where the relative dispersion between the two channels is small, a single adjustable complex weight would function as an adequate correction method. However, in general, a more sophisticated correction network is required which allows the adjustment of a frequency dependent transfer characteristic across the bandwidth of interest. This section will discuss the several alternative techniques which were considered for the present application.

To develop a general description of the correction networks, consider the mathematical description illustrated in Figure 6. In this figure,  $s_1$  and  $s_2$  represent the two orthogonally polarized transmitted signals while  $r_1$  and  $r_2$  are the received signals which have been coupled and distorted due to the transmission system. In general, this coupling and distortion can be modeled as frequency dependent transfer functions as shown where

$$r_1(\omega) = s_1(\omega) H_{11}(\omega) + s_2(\omega) H_{12}(\omega) \quad (2-4)$$

$$r_2(\omega) = s_1(\omega) H_{21}(\omega) + s_2(\omega) H_{22}(\omega) \quad (2-5)$$

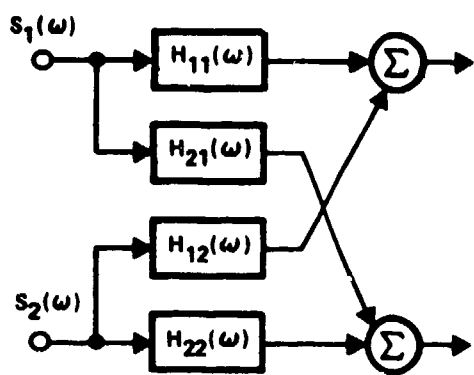
Modeling the correction networks as transfer functions  $w_{12}(\omega)$  and  $w_{21}(\omega)$  as shown in the figure, the cross coupling can be removed by forming

$$\begin{aligned} s_1'(\omega) &= r_1(\omega) - w_{21}(\omega) r_2(\omega) = r_1(\omega) - \frac{H_{12}(\omega)}{H_{22}(\omega)} r_2(\omega) \\ &= s_1(\omega) \left[ H_{11}(\omega) - \frac{H_{21}(\omega) H_{12}(\omega)}{H_{22}(\omega)} \right] \end{aligned} \quad (2-6)$$

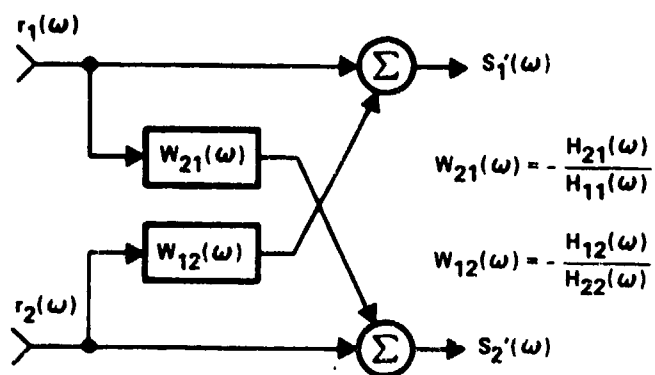
and

$$\begin{aligned} s_2'(\omega) &= r_2(\omega) - w_{12}(\omega) r_1(\omega) = r_2(\omega) - \frac{H_{21}(\omega)}{H_{11}(\omega)} r_1(\omega) \\ &= s_2(\omega) \left[ H_{22}(\omega) - \frac{H_{21}(\omega) H_{12}(\omega)}{H_{11}(\omega)} \right] \end{aligned} \quad (2-7)$$

As described above, the correction networks must provide the transfer functions  $w_{12}(\omega) = -H_{12}(\omega)/H_{22}(\omega)$  and  $w_{21}(\omega) = -H_{21}(\omega)/H_{11}(\omega)$ . These transfer characteristics can quite generally be approximated by the conventional tapped delay line equalizer shown in Figure 7. In this figure the weights  $w_i$  are complex quantities with the length (number of taps) and time delay per tap depending on the specific



TRANSMISSION SYSTEM  
TRANSFER CHARACTERISTICS



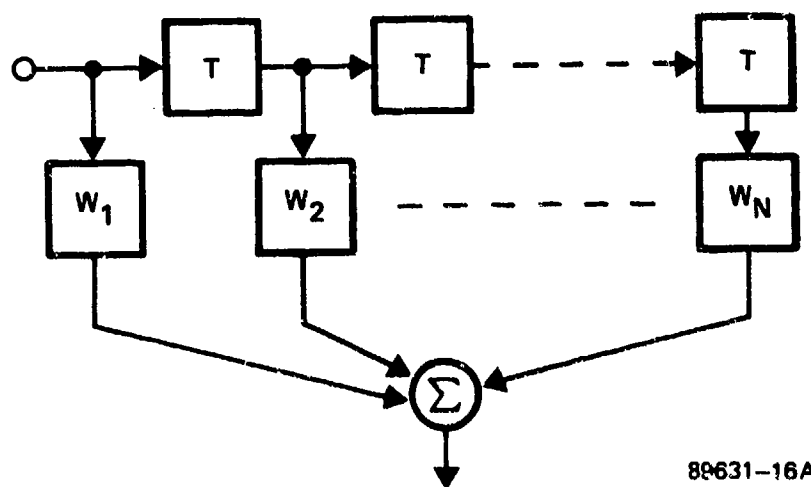
CORRECTION NETWORK  
MODEL

$$w_{21}(\omega) = -\frac{H_{21}(\omega)}{H_{11}(\omega)}$$

$$w_{12}(\omega) = -\frac{H_{12}(\omega)}{H_{22}(\omega)}$$

89631-16

Figure 6. Mathematical Description of Transmission and  
Correction Network Characteristics



89631-16A

Figure 7. Conventional Tapped Delay Line Correction Network

transfer characteristics to be equalized. Several modifications of this form for the correction network were considered for the hardware implementation.

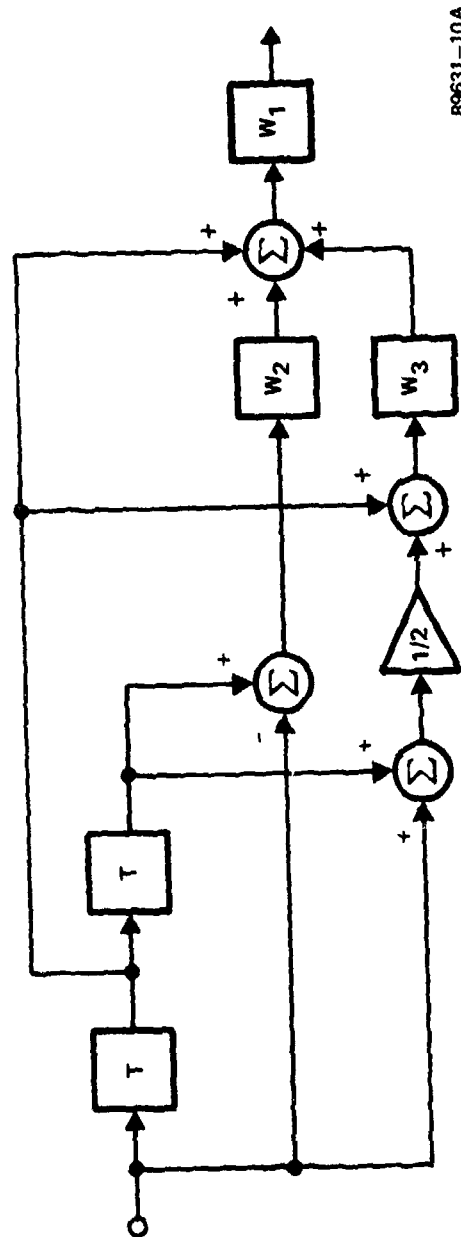
#### 2.2.1 Evolution of the Correction Network Implementation

As described in the last paragraph, the function of the correction network is to provide the required transfer characteristic to properly modify the received signal. This allows it to be used to cancel the interference it has induced in the cross-polar channel. Generally stated, it must be designed to synthesize a transfer function which can be represented in the Taylor series expansion

$$W(\omega) = A + B\omega + C\omega^2 + \dots \quad (2-8)$$

The conventional tapped delay line discussed above could be used. However, in the previous contract a special correction network was developed which allowed separate and uncoupled control of the constant (A), linear (B), and quadratic (C) terms in the frequency response. This device has the advantage of providing uncoupled control of each of these functions and allows the final setting of the network to be correlated with these specific characteristics of the transmission system. That is, when the adaptive control circuits have stabilized, the weight settings on this special correction network would indicate the form of the coupling that the system has caused. Figure 8 illustrates the form of this special network where  $w_1$  controls the constant term,  $w_2$  the linear and  $w_3$  the quadratic term. A detailed discussion of its development is presented in the final report for the previous contract.

During the initial design effort for the hardware implementation phase of this project an alternative correction method was configured. This resulted from a mathematically simpler realization of the desired transfer function as presented in Equation 2-8. This simplification leads to less complex hardware (fewer parts count), while retaining the desirable controllability characteristics as well as the unique relationship between the weight settings and the coefficients of the Taylor expansion. This network is illustrated in Figure 9 and consists of a series of notch filters  $B(\omega)$ , the outputs of which are properly delayed and weighted by  $w_0$ ,  $w_L$ ,  $w_Q$  and  $w_C$  and finally summed. The transfer function of this network can be derived by considering the transfer function of the notch filter  $B(\omega)$



89631-10A

Figure 8. Special Multitap Correction Network

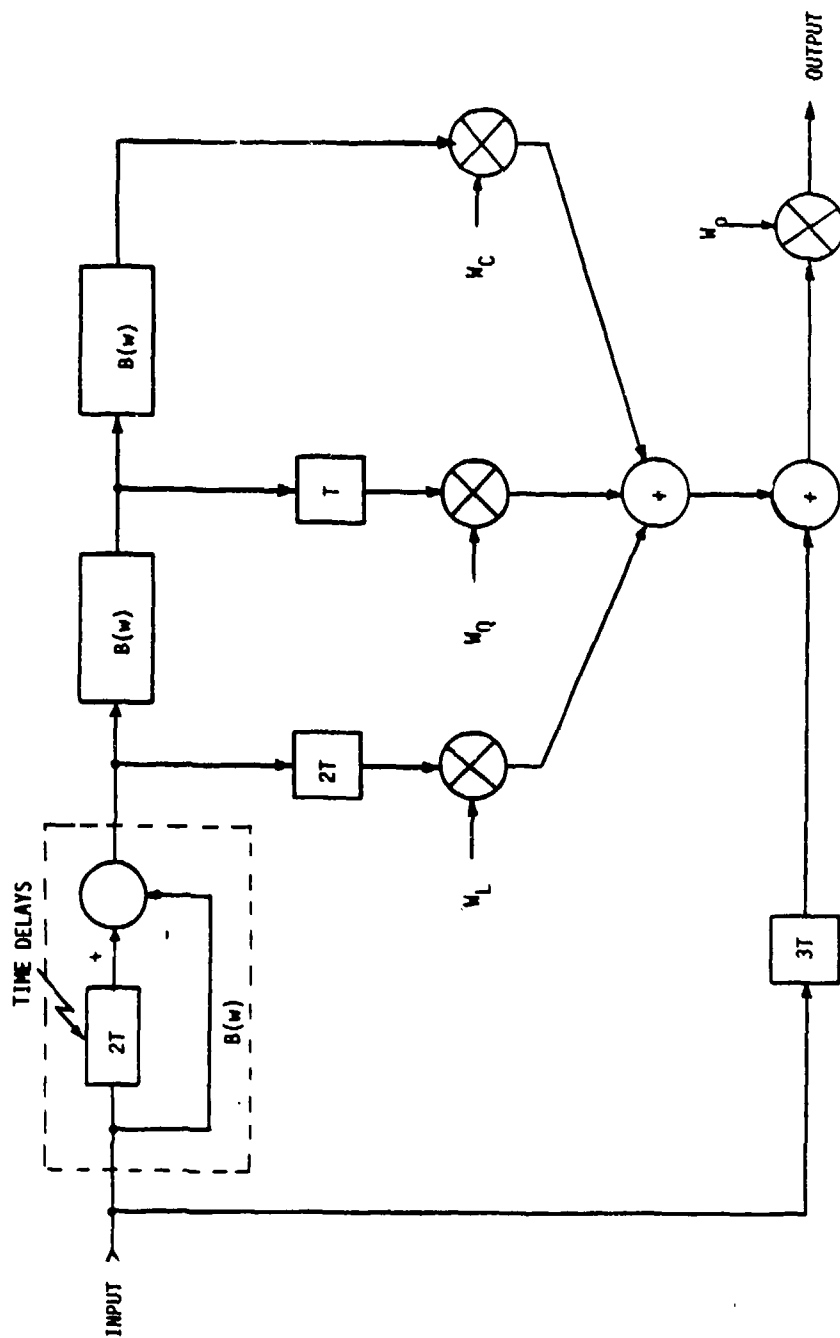


Figure 9. Notch Filter Correction Network

$$B(\omega) = e^{-j\omega 2T} - 1 = e^{-j\omega T} (e^{-j\omega T} - e^{+j\omega T}) \quad (2-9)$$

$$= -2je^{-j\omega T} \sin \omega T$$

Consequently, the overall transfer function  $H(\omega)$  is proportional to

$$H(\omega) \sim w_0 (1 + w_L \sin \omega T + w_Q \sin^2 \omega T + w_C \sin^3 \omega T) \quad (2-10)$$

If  $T$  is chosen such that  $\omega T$  is small this gives

$$H(\omega) \sim w_0 (1 + w_L \omega T + w_Q \omega^2 T^2 + w_C \omega^3 T^3) \quad (2-11)$$

the desired power series in  $\omega$ . Note that an additional term has been included here to give control of up to a cubic function of frequency.

### 2.2.2 Simultaneous Copolar and Cross-Polar Equalization

Figure 10 shows the original configuration of the cross-polarization canceller with equalization. Equalization is necessary for complete cancellation because the wave shape of the vertical signal on the vertical port is not the same as it is on the horizontal port; i.e.,  $\hat{s}_v$  does not match  $s_v$  in shape. Similarly,  $s_h$  does not match  $\hat{s}_h$  in shape. Thus, Equalizer 1 transforms  $s_v$  to  $\hat{s}_v$  and Equalizer 2 transforms  $s_h$  to  $\hat{s}_h$ . Complete cancellation is then possible by making  $W_1 = E_2$  and  $W_2 = E_1$ . Note that if no cross-polarization coupling exists, then  $E_1 = E_2 = 0$  and the equalizers are effectively removed from the dual channel receiving network.

Complete cross-polarization decoupling can also be achieved if the equalizers are configured as in Figure 11. Equalizer 1 is now adjusted to transform  $\hat{s}_h$  to  $s_h$  and Equalizer 2 transforms  $\hat{s}_v$  to  $s_v$ . Note that with this configuration the equalizers remain in the receiving network even in the absence of cross-polarization coupling. This configuration was suggested on March 16, 1978, during the critical design review. At the present time we believe that this new configuration does not work with the amplitude fluctuation sensing technique employed during this study although it should work with other performance criteria. In particular, it should work well if the rms opening of the eye pattern were used as a performance measure. We will now discuss the difficulty with this new configuration.

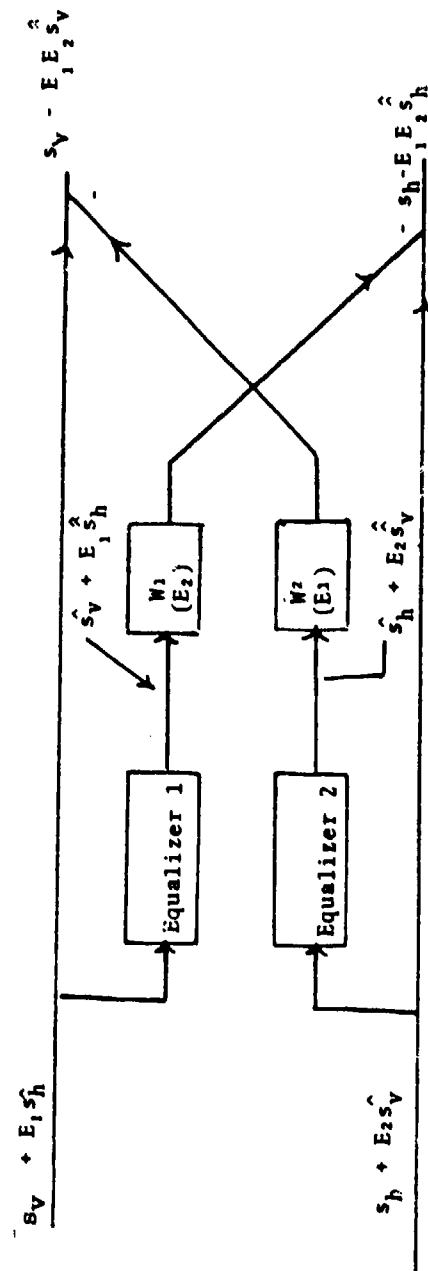


Figure 10. Cross-Polar Equalization

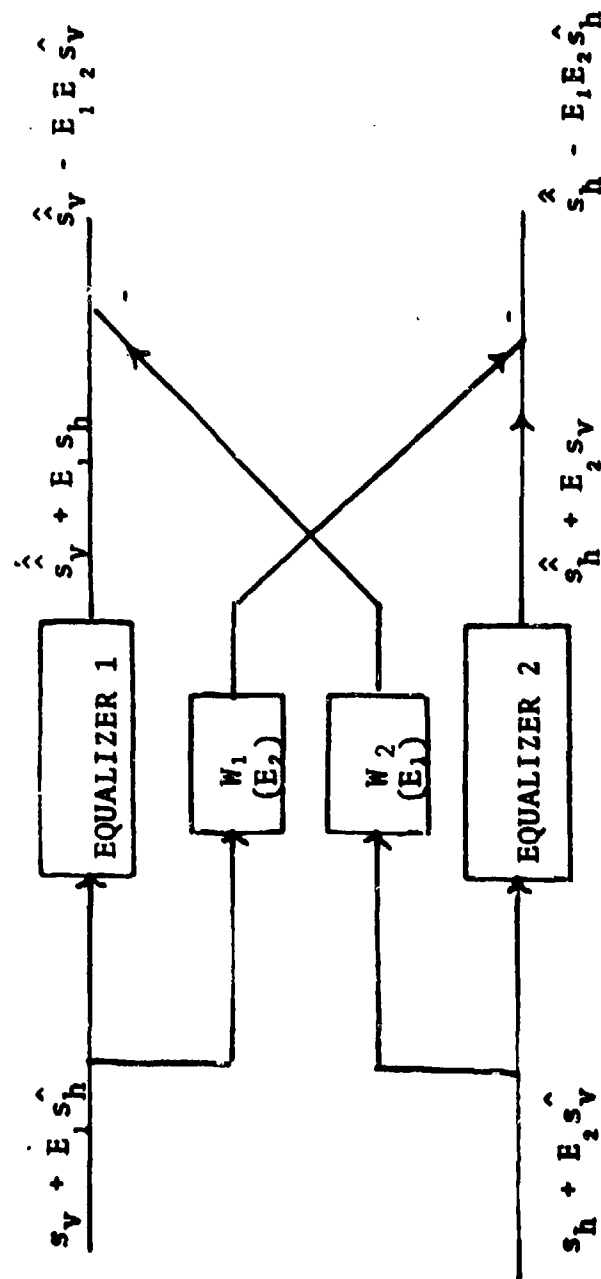


Figure 11. Copolar Equalization

In order for the AM fluctuation criterion to be workable, it must be that undesirable distortion causes amplitude fluctuations. This is always true when the distortion is due to cross-polarization coupling because the two desired signals are uncorrelated and hence have random relative phase. But copolar distortion terms are correlated with the desired signals. For example, it is possible for the distortion to be in phase quadrature with the desired signal and hence primarily cause phase modulation of the desired signal. Filters with even phase response and odd amplitude response cause quadrature distortion while filters with odd phase response and even amplitude response cause in-phase distortion. Since even phase response and odd amplitude response distortions cannot be detected by our AM measuring equipment, we cannot expect the configuration of Figure 11 to be workable as we verified experimentally. However, as mentioned earlier, it should work well with a suitable performance criteria such as the closure of the eye pattern at the output of the demodulator.

### 2.2.3 Selection of Tap Spacing

As mentioned in Paragraph 2.2.1, the tap spacing (time delay) in the notch filter must be chosen small so that the resultant transfer function of the overall correction network approximates the Taylor expansion as shown in Equation 2-11. Strictly speaking, the derivation required that  $\sin \omega T \approx \omega T$  ( $\omega \equiv \Delta \omega = \omega_c + \omega_o$ , where  $\omega_c$  is the center frequency and  $\omega_o$  is the operating frequency), however, for the desired qualitative behavior the sine function should merely remain monotonic. That is,  $-\pi/2 < \Delta \omega T < \pi/2$  will yield the desired behavior. In the present implementation T was chosen as  $2T = 1/70$  MHz, consequently over the 14 MHz bandwidth of interest  $-0.05 < \Delta \omega T < 0.05$ , and the desired behavior is guaranteed.

To allow further study of the tap spacing requirement, and also give confidence that the correction network will be able to adjust its transfer function over an adequate range, a computer simulation was developed. This simulation allowed an arbitrary tapped delay line filter to be specified (that is, a given number of taps, tap spacings, and tap configuration) and the required tap weights to match (in a minimum mean square error (MMSE) sense) a specified frequency characteristic was computed.

Also, besides the optimal tap weightings, the program computed the mean square error (MSE) in the resulting fit, indicating how well the particular filter can match the specified characteristic. Figure 12 shows the results of using this program to compute how well several types of tapped delay line (TDL) filters can match a 4-pole Butterworth filter characteristic which is 3 dB down at the edge of the 14 MHz bandwidth. The results for both a 4 and 6 tap standard tap delay line (see Figure 6), as well as the 4-tap notch filter correction network used in the cross-pole device are displayed, together with the error that would be associated with a single complex weight. These plots also indicate that the notch filter device will perform well if the tap spacing is small. Additional simulations for various Chebychev filters, and for a frequency response which matched the measured radio characteristics were also run, all of which indicated satisfactory performance.

#### 2.2.4 Control Loop Coupling With the Notch Filter Network

The last paragraph indicated that the notch filter network should exhibit satisfactory steady-state behavior, since it was demonstrated that if the proper weights are used, the resultant transfer characteristic could match a variety of desired frequency responses. Since this device is to be used in an adaptive manner, it is also important that it is easily controlled. This problem can be studied by examining the coupling, or correlation, between the various tap signals which must be weighted and combined. If the correlation between these signals is small, then their contribution to the output should be relatively independent of each other, and likewise the weight settings and control should be uncoupled. This is particularly important in the present application, since the control circuitry is to be time-shared between the four adjustable complex weights and it is desirable not to have to cycle through the weights a large number of times or go into a limit-cycle type behavior.

To compute the correlation between the tap signals consider the equivalent form of the notch filter network shown in Figure 13. This form was constructed by tracing the various paths through the notch filter network and represents the linear combination of taps on a standard tapped delay line that will produce the same response as the notch filter network. If the tap signals  $X_i$ ,  $i = 1, 7$  are collected as the column vector  $X$ , then

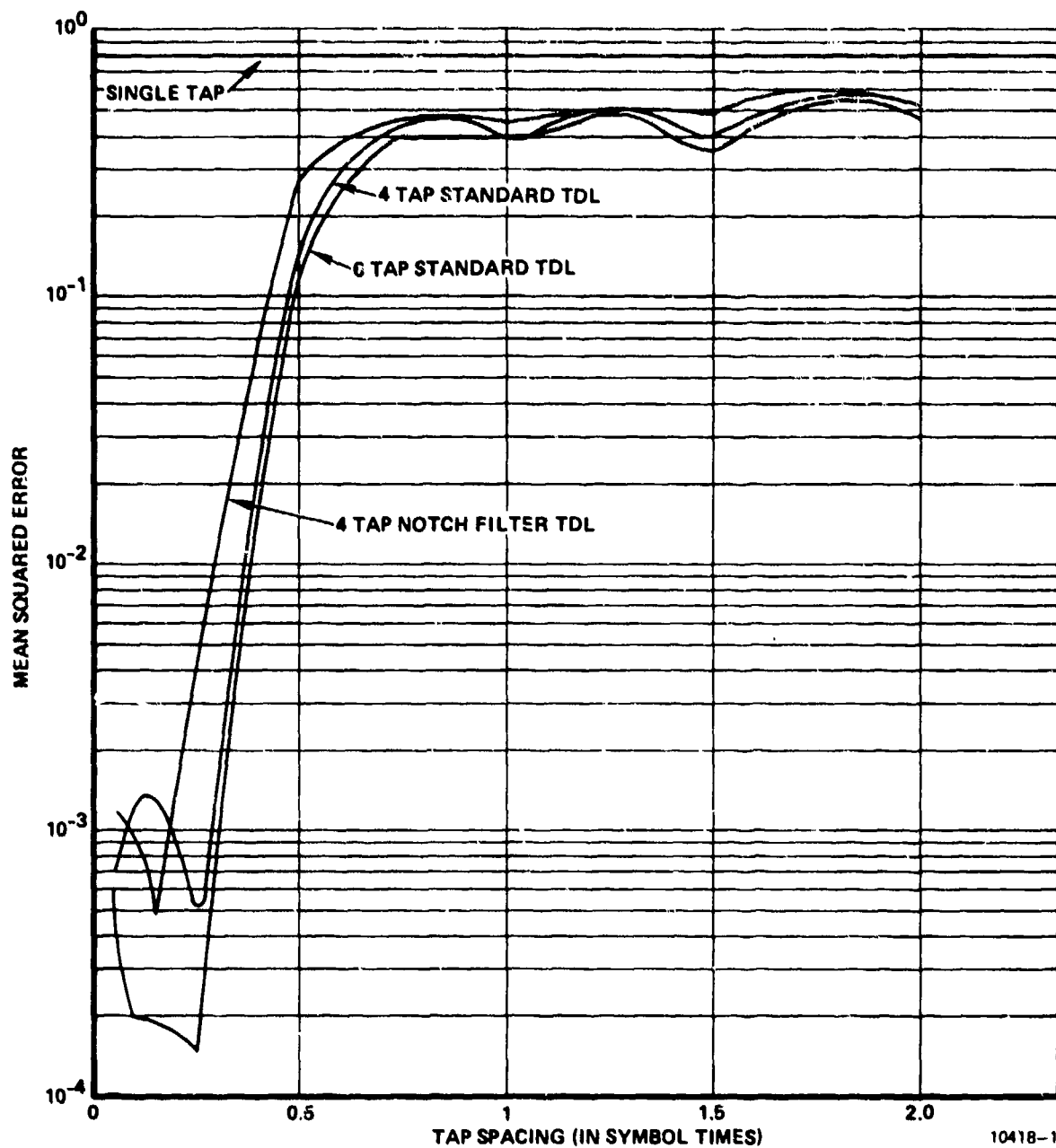


Figure 12. MMSE Versus Tap Spacing for TDL Filters  
Adjusted to Match a 4-Pole Butterworth

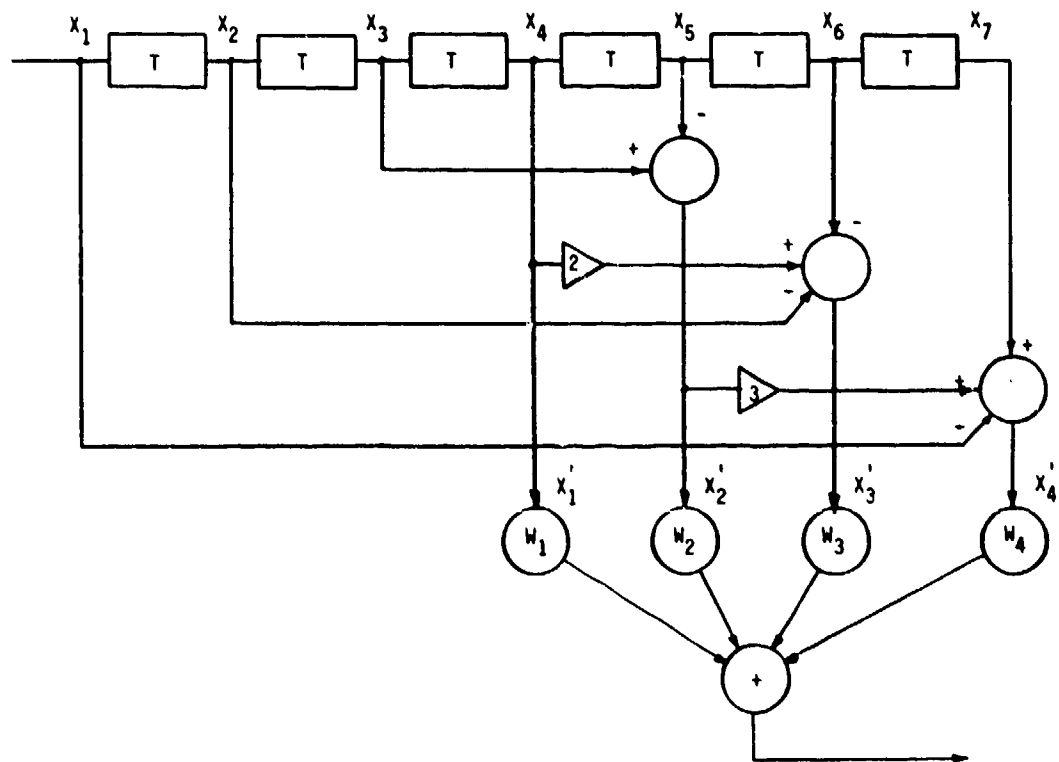


Figure 13. Equivalent Form of Notch Filter Network Using Standard Tapped Delay Line

the correlation matrix associated with these signals can be written as  $R = E(XX^T)$  where  $R_{ij} = E(X_i X_j)$ . Also, as shown in the figure, the signals  $X_i$  are those which must be weighted in the notch filter network. Since these signals are merely a linear combination of the  $X_i$  they can be represented as  $X' = PX$  where the transformation matrix  $P$  is given by

$$P = \begin{bmatrix} 0 & 0 & 0 & 1 & 0 & 0 & 0 \\ 0 & 0 & +1 & 0 & -1 & 0 & 0 \\ 0 & -1 & 0 & 2 & 0 & -1 & 0 \\ -1 & 0 & 3 & 0 & -3 & 0 & +1 \end{bmatrix}$$

For the small tap spacings used in the present implementation, the signals  $X_i$  would be highly correlated, and the correlation matrix would take the approximate form

$$R = \begin{bmatrix} 1 & 1-\Delta & 1-2\Delta & 1-3\Delta & 1-4\Delta & 1-5\Delta & 1-6\Delta \\ 1-\Delta & 1 & 1-\Delta & 1-2\Delta & 1-3\Delta & 1-4\Delta & 1-5\Delta \\ 1-2\Delta & 1-\Delta & 1 & 1-\Delta & 1-2\Delta & 1-3\Delta & 1-4\Delta \\ 1-3\Delta & 1-2\Delta & 1-\Delta & 1 & 1-\Delta & 1-2\Delta & 1-3\Delta \\ 1-4\Delta & 1-3\Delta & 1-2\Delta & 1-\Delta & 1 & 1-\Delta & 1-2\Delta \\ 1-5\Delta & 1-4\Delta & 1-3\Delta & 1-2\Delta & 1-\Delta & 1 & 1-\Delta \\ 1-6\Delta & 1-5\Delta & 1-4\Delta & 1-3\Delta & 1-2\Delta & 1-\Delta & 1 \end{bmatrix}$$

where  $\Delta$  is a small positive number. Consequently, all the off-diagonal terms of  $R$  are close to unity, indicating high correlation and potentially difficult controllability. On the other hand, since  $X' = PX$ , then  $R' = E(X'X'^T)$  is the correlation matrix for the notch filter network which can be represented as  $R' = E(PXX^T P) = PRP^T$ .

Computing  $R'$  then gives

$$R' = E(X'X'^T) = \begin{bmatrix} 1 & 0 & 4\Delta & 0 \\ 0 & 4\Delta & 0 & 8\Delta \\ 4\Delta & 0 & 8\Delta & 0 \\ 0 & 8\Delta & 0 & 24\Delta \end{bmatrix}$$

In this case, the off-diagonal terms are either zero or quite small, indicating much less coupling and therefore improved controllability characteristics for the notch filter network.

SECTION 3.0  
HARDWARE DESCRIPTION

### 3.0 HARDWARE DESCRIPTION

An experimental breadboard equalizer incorporating the baseline concepts described in Section 2.0 was constructed. The actual hardware is described in this section. The Cross Polarization Interference Reduction Equalizer is first described as a unit. The equalizer and control sections are then treated separately.

#### 3.1 Cross Polarization Interference Reduction Equalizer Unit Level Description

The Cross Polarization Interference Reduction Equalizer (CPIRE) is an adaptive equalizer designed to automatically compensate for cross-polarization interference between two orthogonally polarized microwave modem channels. The hardware is packaged in an 8.75 inch high chassis designed to be mounted in a standard 19-inch rack. The unit contains integral power supplies and cooling fan. It should be noted that as cooling air is drawn into the chassis from the top, a minimum space of 3.5 inches is required above the unit. All front panel jacks are BNC type. The 70 MHz IF input and output connectors are designed to interface with 75 ohm circuits. They may be easily modified for 50 ohm circuits, however, by removing the transformers located behind the front panel.

A photograph of the CPIRE front panel is shown in Figure 14.

The CPIRE operates by adjusting the phase and amplitude of an equalized version of one channel and summing it with the other to cancel the interference. The equalizer is capable of linear, parabolic, and cubic amplitude correction as well as straight delay and linear and parabolic group delay correction. Equalization compensates for dispersive cross-polarization mechanisms by adjusting a component of a received channel to match the interference on the other channel, allowing cancellation. Dual equalizers and cross-pole weight circuits allow simultaneous operation on both received channels.

A basic block diagram is shown in Figure 15. An input filter is provided for each channel for use where large amounts of out-of-band noise are present. The filters are 28 MHz wide, 4 pole, 0.05 dB Chebyshev bandpass filters centered at 70 MHz. For use where IF bandwidths are limited to less than 28 MHz, the filters are unnecessary and may be easily bypassed by changing four SMA connector cables within the chassis.

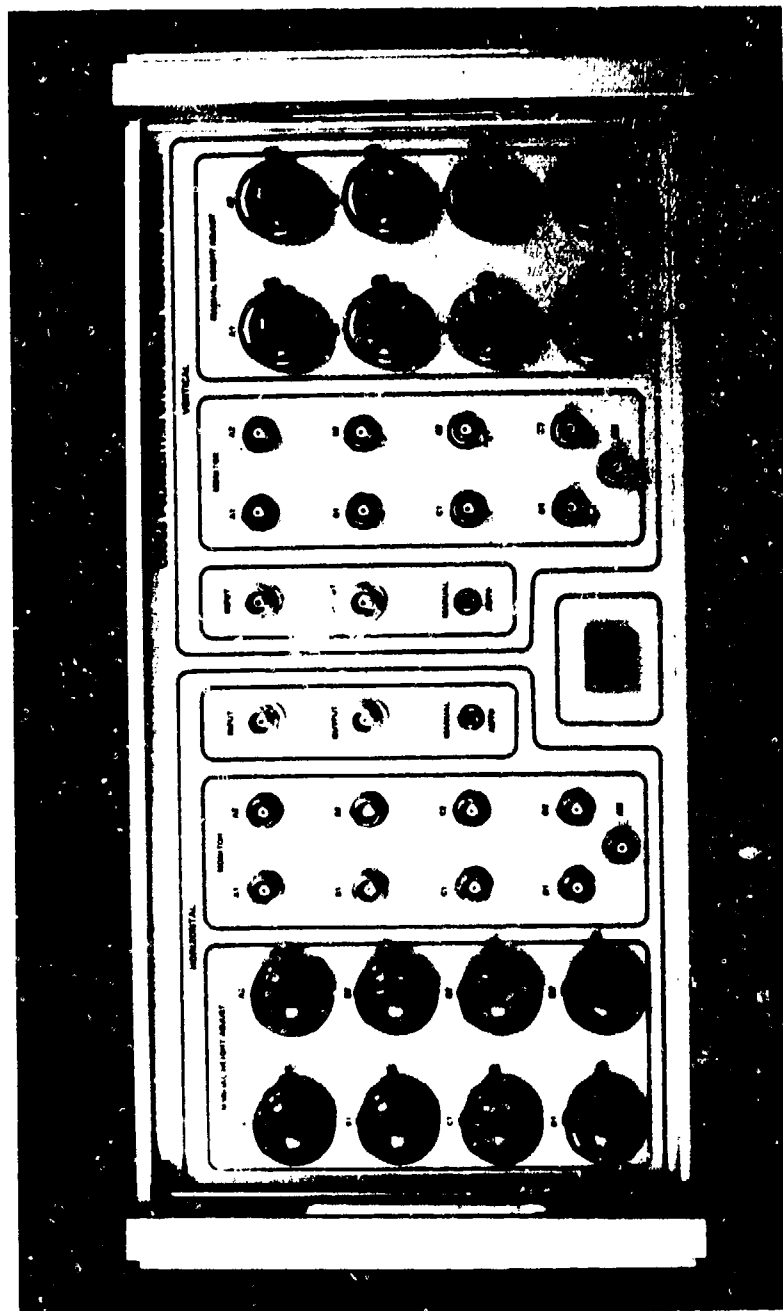


Figure 14. CPIRE Front Panel

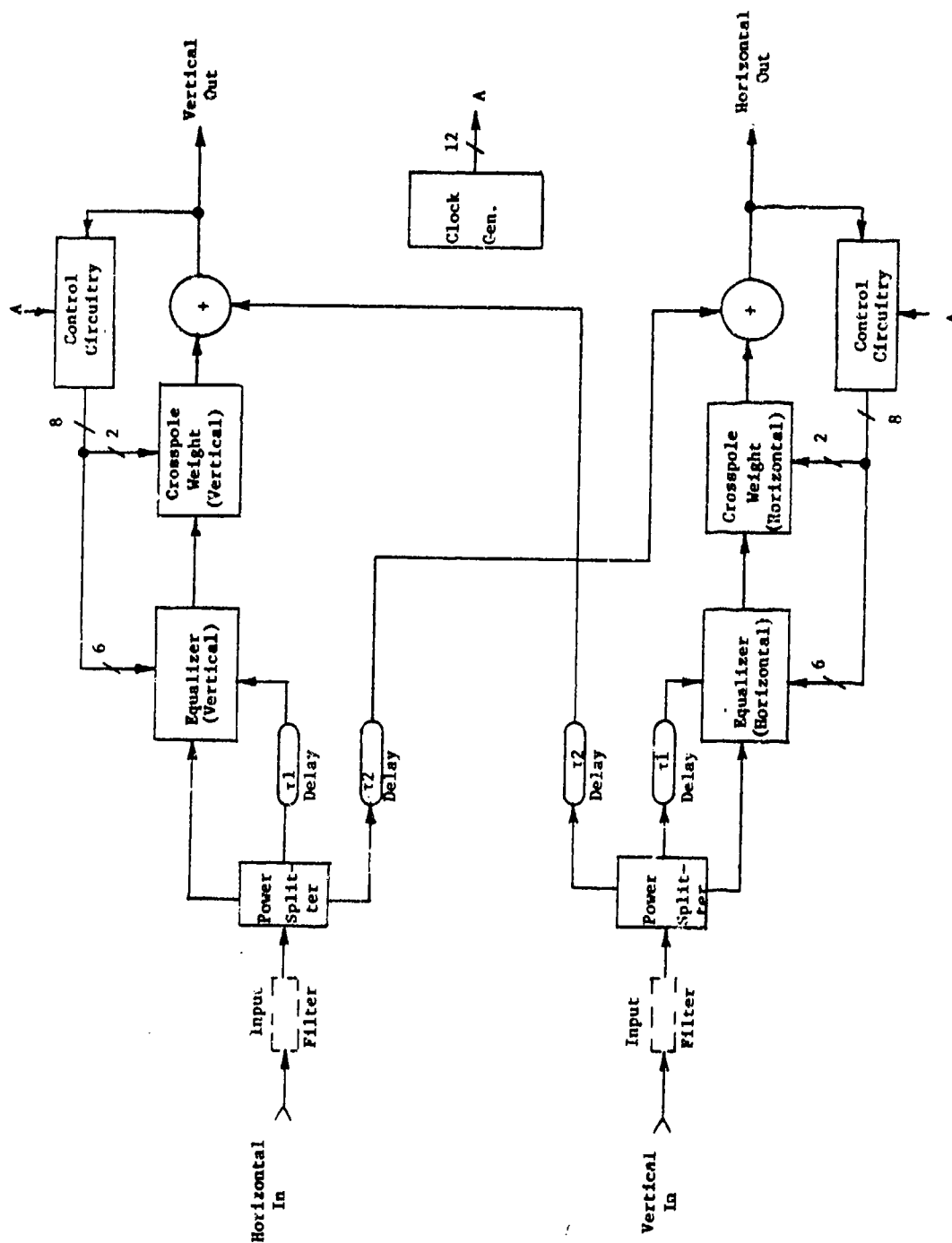


Figure 15. CPIR Block Diagram

After filtering, each channel is split three ways. The main signal path is delayed by  $\tau_2$  and fed to a summer where the cross-polarization interference cancelling signal is added. The output of the summer is the main channel output. The delay,  $\tau_2$ , compensates for delays in the equalizer and cross-pole weight. The other two components of the input signal are fed to the equalizer. One path is direct, the other delayed by  $\tau_1$ . The equalizer output is adjusted in phase and amplitude by the cross-pole weight and then summed with the main signal path of the other channel.

A secondary output of the summer drives the control circuitry for that channel. A performance monitor produces an error voltage and subsequently the weight control voltages for the equalizer and cross-pole weights. There are three complex weight pairs in each equalizer and one pair in each cross-pole weight. A clock generating circuit is common to both channels. Four separate dither clocks are produced, each with adjustable phase as well as the four pairs of enable lines used in the control circuitry. The length and separation between enable pulses are adjustable via on-card DIP switches.

While the CPIRE is primarily intended for use as an automatic cross-pole equalizer, it may also be operated in other modes. The two front panel toggle switches disable the automatic control circuitry and enable the front panel manual weight controls. These are 10-turn precision potentiometers with locking turn-dials. When set to midposition (a turn-dial indication of 5) the weight control voltages are set to 0, corresponding to maximum attenuation. As the controls are rotated counterclockwise toward an indication of 0, the control voltage increases to +10 volts and the weight attenuation decreases. Rotation of the controls clockwise toward an indication of 10 produces an increasing negative control voltage. This also reduces weight attenuation but with a 180 degree phase shift.

The manual weight controls grouped with a channel's input and output connectors affect the output of that channel. The first three pairs of controls, A1 through C2, are the equalizer controls. A1 and A2 affect linear amplitude and straight delay, respectively. B1 adjusts parabolic

amplitude and B2 adjusts linear group delay. C1 provides cubic amplitude adjustment and C2 provides parabolic group delay adjustment. D1 and D2 form the complex cross-pole weight. The weight monitor outputs correspond to the similarly labeled manual controls. They function in manual as well as automatic modes. The weight monitor outputs are isolated and are capable of supplying 10 mA with a source impedance of 100 ohms. The BNC jack labeled AM MONITOR provides a relative indication of the amount of residual cross-polarization interference. Its output ranges from near zero with no interference to approximately +10 volts with a cross-polarization discrimination ratio of 5 dB. It has the same drive characteristics as the weight monitors. It should be noted that the AUTO/MANUAL switch for the Vertical Channel must be in the AUTO position for automatic operation of the Horizontal Channel.

Without internal modification, the CPIRE may be used as a single channel, manual copolar equalizer. Either set of controls may be used. To use the HORIZONTAL controls, the input is applied to the VERTICAL INPUT and the output is taken from the HORIZONTAL OUTPUT. The AUTO/MANUAL switch should be in the MANUAL position and one of the cross-pole weights (D1 or D2) should be set to an extreme for minimum loss. The chosen control, D1 or D2, may be used as a gain adjustment. Minimum insertion loss in the manual copolar mode is approximately 3 dB. To use the Vertical Controls, the input is applied to the HORIZONTAL INPUT and the output taken from the VERTICAL OUTPUT. No signal should be applied to the other input as it will be summed with the equalizer output.

In order to operate the CPIRE as a dual channel manual copolar equalizer, it is necessary to remove the semiridged delay lines from connectors B2 and M2 which are accessible by removing the top cover of the chassis. Operation is then the same as single channel operation.

### 3.2 Equalizer Description

A block diagram of the equalizer portion of the CPIRE is shown in Figure 16. The direct signal path from the input power splitter drives a series of three cascaded notch filters. The output of each notch filter goes to a weight. The weights are complex and thus are capable of shifting phase through 360 degrees and can adjust amplitude over a 40 dB range. The

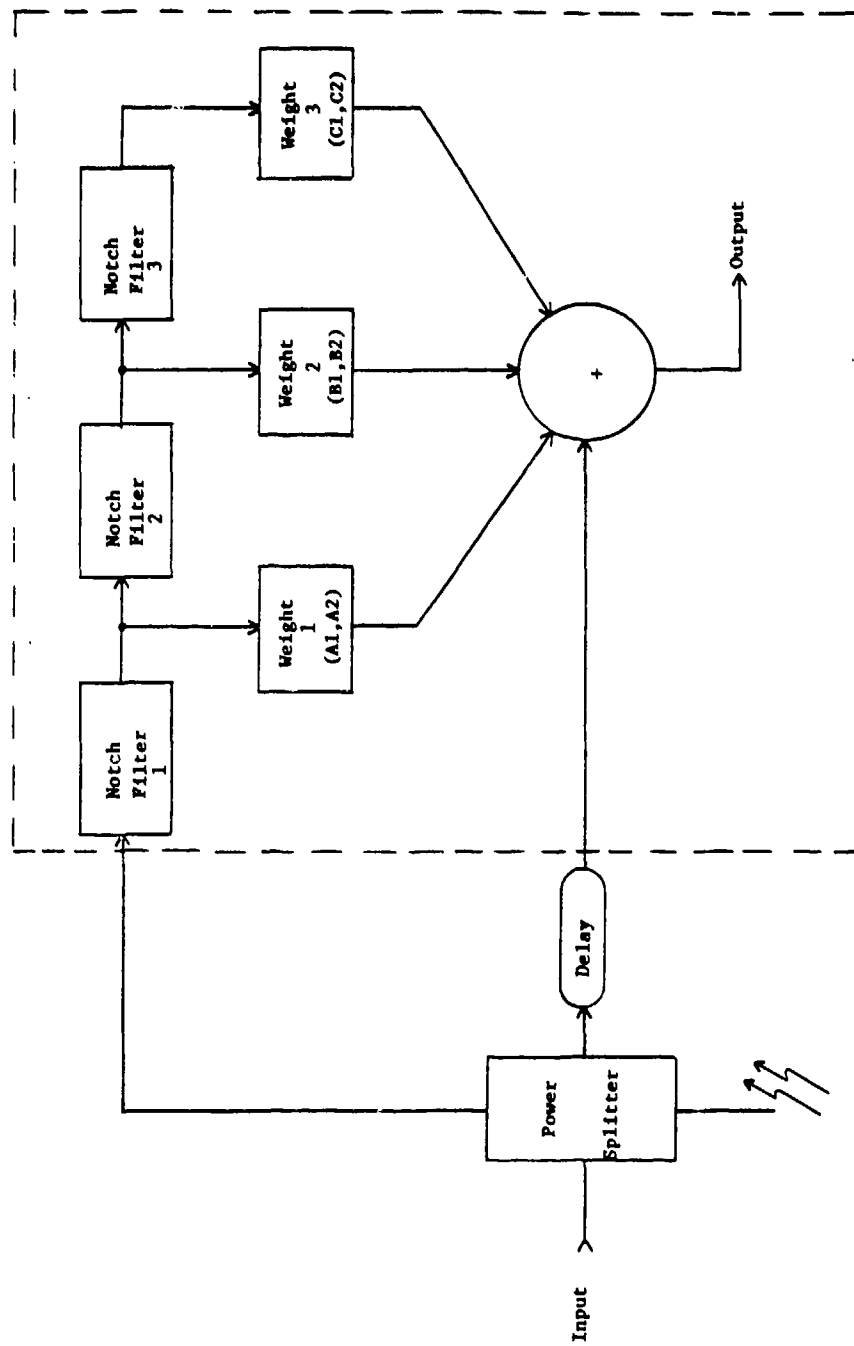


Figure 16. Equalizer Block Diagram

weight outputs are all summed with the delayed portion of the input signal. The delay is equal to that incurred through all three notch filters and final weight. The outputs of the first two weights are also aligned in time with the other summer inputs with delay lines. When the weights are all set to maximum attenuation (control voltage = 0), only the main path remains and the input passes unequalized. The first weight adjusts linear amplitude and straight delay. The second weight adjusts parabolic amplitude and linear delay. Finally, the third weight adjusts cubic amplitude and parabolic group delay.

The notch filters are detailed in Figure 17. The notch function is achieved by splitting the input in phase, delaying one side and summing the resulting signals together 180 degrees out of phase. The delay,  $\tau$ , is made equal to one period at 70 MHz or 14.29 ns. Thus, with a 70 MHz input, the delayed portion is shifted 360 degrees and arrives in phase with the other signal at the summer. Summed 180 degrees out of phase, the inputs cancel, producing no output. This produces the null or notch at 70 MHz. At either side of 70 MHz, the degree of cancellation is a function of frequency shift from the center. A phase shift of 180 degrees is incurred as the frequency is swept through 70 MHz.

A block diagram of a weight is shown in Figure 18. The input signal is split and fed to two electronically controlled attenuators. Attenuation is a function of input current. Reversing the current direction introduces a 180 degree phase shift in the output. The attenuator outputs are summed with a quadrature hybrid. Since the signals they adjust are 90 degrees out of phase, the attenuators are independent. The in-phase attenuators adjust amplitude response while the quadrature attenuators adjust group delay characteristics. The fourth or cross-pole weight is similar in construction but as the phase relationships between channels and interference are not fixed, no distinction can be made between the two weight control elements. The quadrature summation of the attenuator outputs along with the phase inversion capability of the attenuators permits any phase shift from 0 to 360 degrees and any amplitude over the approximate 40 dB range of the attenuators.

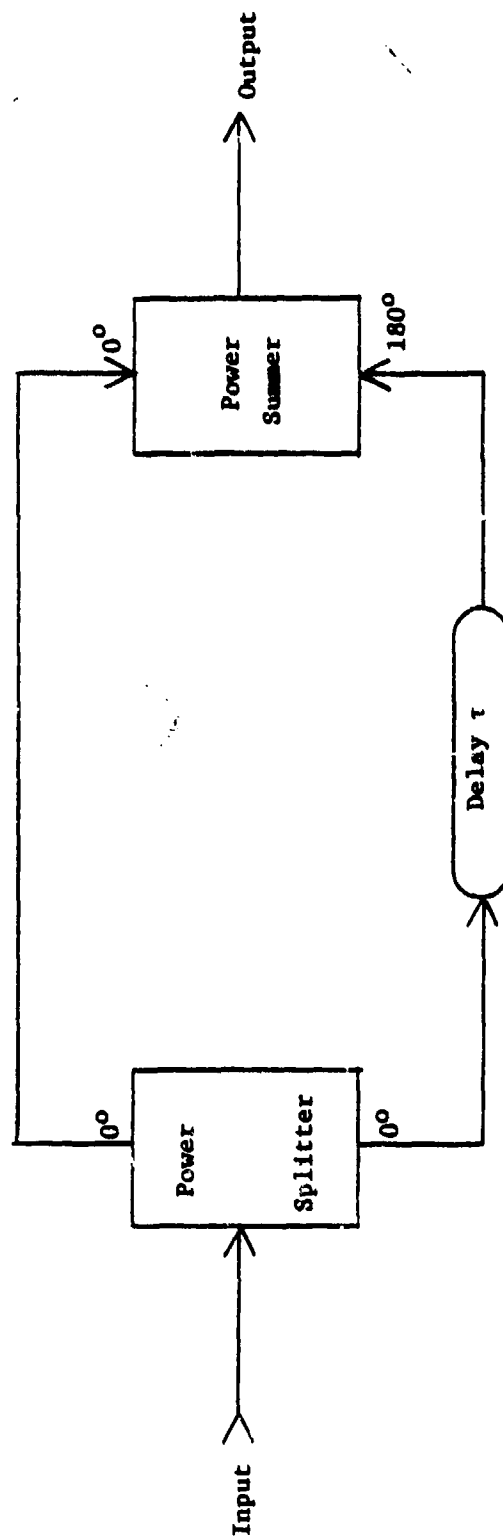


Figure 17. Notch Filter Block Diagram

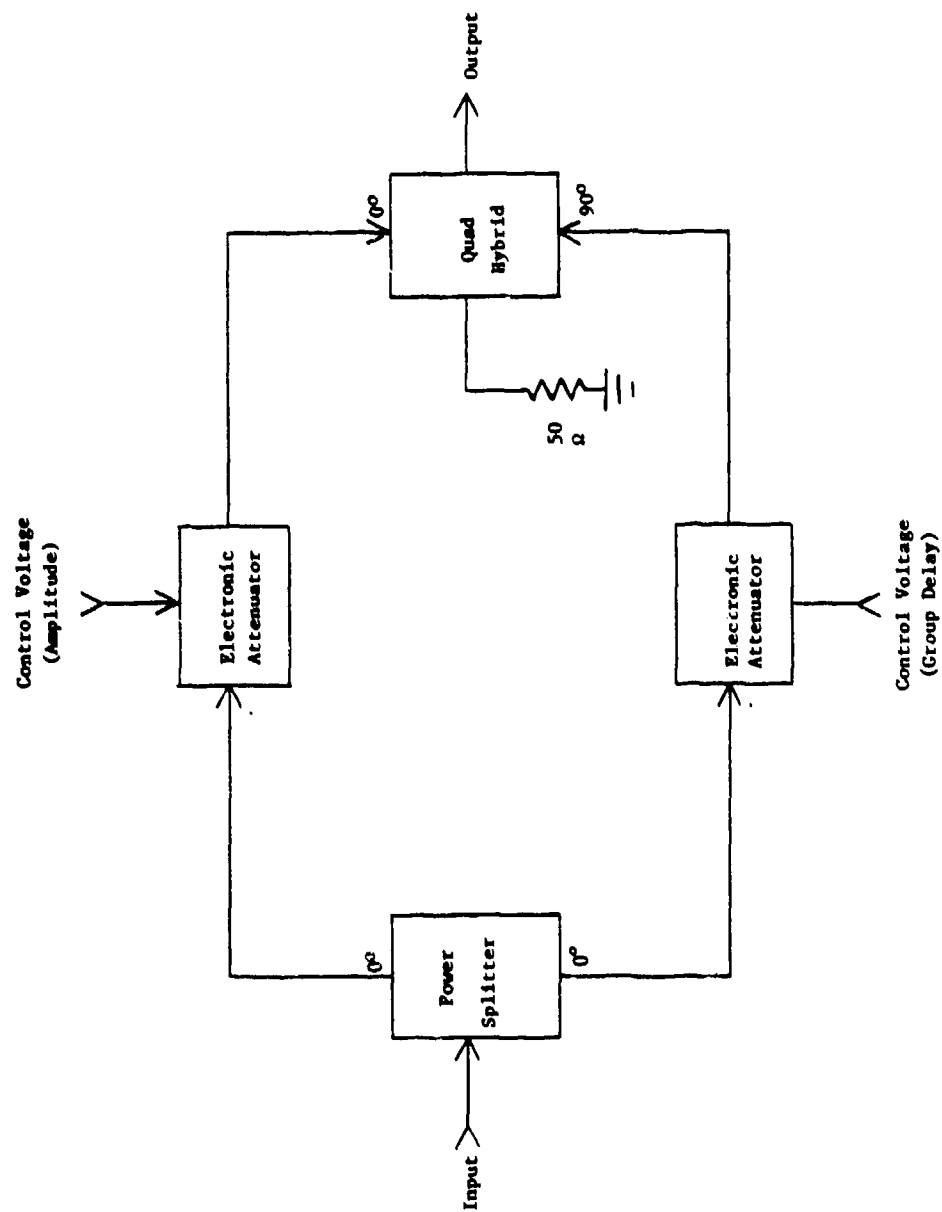


Figure 18. Weight Block Diagram

### 3.3 Control Circuitry Description

Automatic control of weight settings is accomplished by measuring the amount of cross-polarization-interference-induced amplitude modulation (AM) on the envelope of the output signal. Weights are set to minimize AM using a "dither" technique.

A simplified block diagram of the weight control circuitry is shown in Figure 19. In the actual implementation, there are four pairs of integrators that may be switched sequentially to the detector outputs. For simplicity, only one pair of integrators is shown in the figure. An AGC loop consisting of a gain controlled amplifier, absolute value circuit, error comparator, and low pass filter makes the input signal level independent of weight setting. The parameters of the AGC are chosen such that the circuit can remove dither-induced amplitude modulation at an approximate rate of 10 kHz but not effect cross-pole-induced AM at half-symbol-rate frequencies (6.705 MHz). The output of the absolute value circuit is bandpass filtered, extracting the envelope from the input signal. The power in the envelope is measured with a second absolute value circuit and a bandpass filter. The filter is chosen so that dither-rate fluctuations in amplitude modulation power can be observed. The filter output goes to two quadrature synchronous detectors. The detectors are driven by the square wave dither signals that are also summed with the weight control voltages. Synchronous detection allows the integrator to receive an error signal that is always of the proper polarity to drive the weight control voltage to the point where the envelope AM is minimized. The quadrature detectors allow both halves of each complex weight to be adjusted simultaneously. The integrators help set the loop bandwidth and act as storage elements for the weight setting.

Loop gain is proportional to  $\beta \Delta$  where  $\beta$  is the integrator gain constant and  $\Delta$  is the dither size. Increasing loop gain decreases acquisition time and allows the loops to track faster changes in cross polarization interference. However, increasing the integrator gain decreases loop stability and increases integrator drift. Increasing dither size increases the residual interference left after the cross-pole interference is canceled. Thus, loop parameters must be chosen to obtain

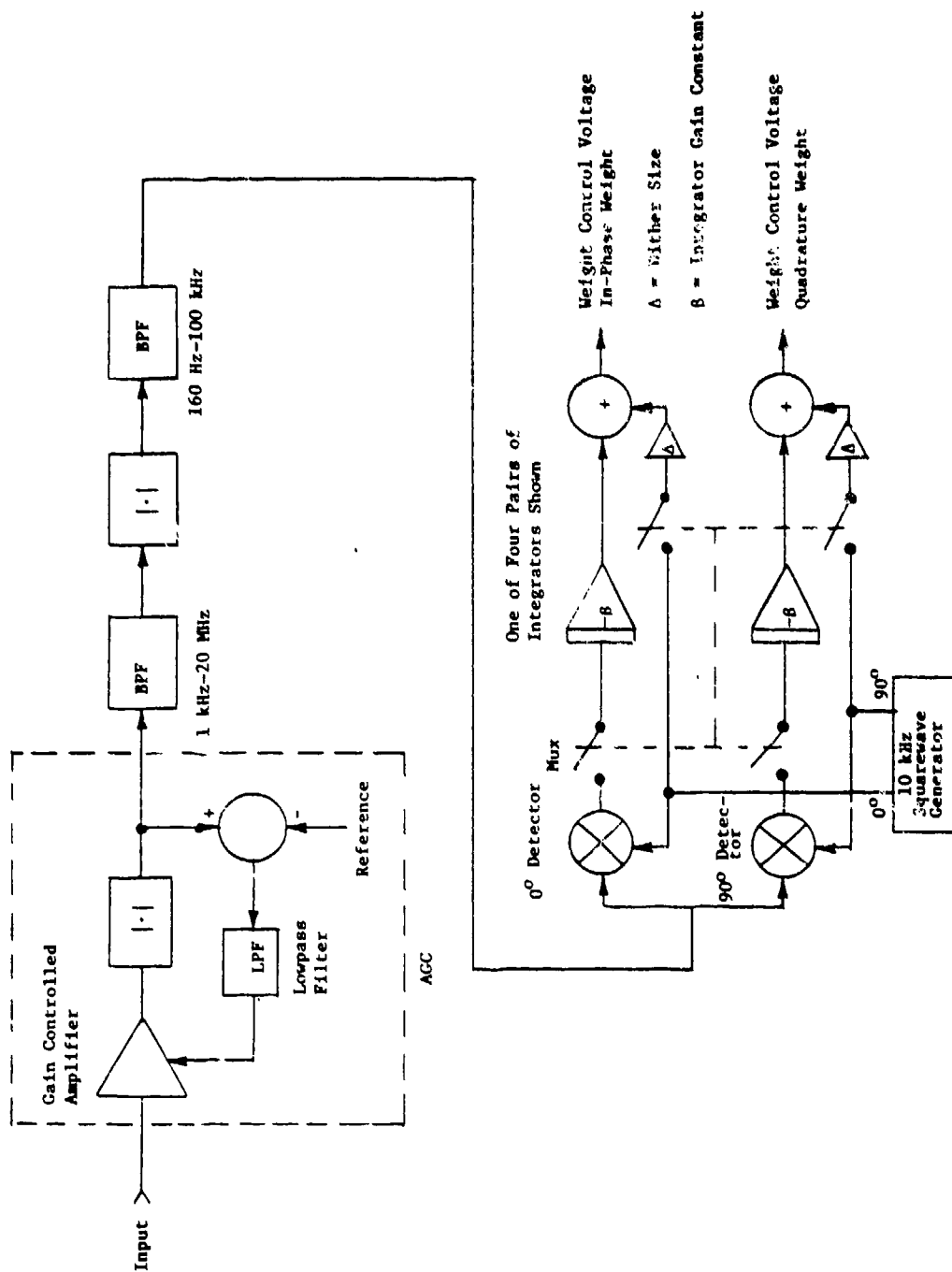


Figure 19. Control Circuitry Block Diagram

desired trade-off between speed and residual interference. Further considerations include an increase in loop jitter as loop gain is decreased. This jitter also contributes to residual interference.

Weight control voltages are adjusted in pairs with a MUX control circuit. The quadrature dither clocks are applied to one pair of weights at a time. While one pair of weights is being dithered, the other pairs are held constant by the integrators. Each weight is updated at a 25 percent duty cycle. The sequence is weights A-B-C-D. The MUX parameters are controlled by the clock generator circuit which is common to both channels. The nominal 90 degree phase shift between quadrature clocks is adjustable. Also, the phases of the two dither signals relative to the detector clocks are adjustable, allowing compensation for phase shifts in the control circuitry. The number of dither cycles applied to a weight during the dither time ("dwell") may be chosen as any integer value between 0 and 15. It is also possible to select a "wait" time between weight selections. This may also be any integer value of dither cycles between 0 and 15. All of these MUX parameters affect loop performance as well as the basic loop parameters of dither size, integrator gain, and filter bandwidths. The MUX control signals are derived from a 20 MHz crystal oscillator. Dither frequency is 9.77 kHz.

A linearization network is included in the path between the integrator output summer and the actual weight control element. This is necessary to stabilize loop gain over the weights' operating range. The weight monitors measure the voltage at the output of the linearization network rather than at the integrator output. For this reason, the weight monitor voltage versus weight attenuation characteristic is very nonlinear. This configuration allows the monitors to function in MANUAL as well as AUTOMATIC, since the manual control voltages are added after the linearization network. Insertion of the manual control voltage ahead of the linearization network would decrease stability and ease of adjustment.

SECTION 4.0  
TEST RESULTS

#### 4.0 TEST RESULTS

The test program was performed at Harris GCSD in Melbourne, Florida, and at RADC in Rome, N.Y. The in-plant tests consisted of three main groups. The first group of tests were performed on the notch filter equalizer section of the CPIRE with an HP8505A Network Analyzer to characterize its performance. The second group of tests again employed the Network Analyzer to characterize the main signal path of the CPIRE with the equalizer controls set to the neutral or mid-point positions. The third group of tests were run in conjunction with a GFE Broadband Modem II (BBM II) built by Harris on a previous contract (F30602-76-C-0434).<sup>2</sup> Two BBM II Modems on cross-polarized microwave channels are capable of 4 Bits per second per hertz of RF bandwidth operation. Bit-error rate measurements were performed with additive thermal noise in the presence of cross-polarization interference with and without the CPIRE. The RADC tests consisted of tests similar to those run at Harris to verify performance, and tests with the BBM II signal passing through an LC80 radio connected back-to-back with the simulator.

In this Section, the test results are presented. CPIRE performance was good and all primary design goals were met except for automatic copolar operation (see Paragraph 2.2.2). In addition, performance with a constant envelope signal came very close to meeting all design objectives.

##### 4.1 In-Plant Tests

This paragraph presents data acquired at Harris GCSD during performance testing and RADC witnessed in-house testing.

##### 4.1.1 Equalizer Results

The equalizer portion of the CPIRE was tested separately in the manual mode using an HP8505A Network Analyzer. Equalizer characteristics were plotted automatically. Design goals for the equalizer were 20 nanoseconds of compensation at the band edges ( $\pm 7$  MHz) for linear and parabolic group delay. No design goals were set for absolute delay adjustment or amplitude compensation. Amplitude compensation range is a consequence of the group delay adjustment range. An analysis of achievable

time delays for this implementation is given in Appendix A. Maximum theoretical adjustment range is 11 ns for the straight delay term, 22 ns for the linear term and 33 ns for the parabolic term. Overload constraints prevent the attainment of these maximums.

Equalizer weights were tested one at a time with all other weights set to 0 volts as measured at the weight monitor outputs. Measurements were made over a 14 MHz band centered at 70 MHz with weight monitor output voltage as a parameter. The first set of curves shows the effect of the three amplitude weights A1, B1, and C1. Ideally, the amplitude weights should have no effect on delay. To test the degree of independence, group delay as well as amplitude measurements were made for each weight. Figure 20 shows the amplitude response effect of weight A1 of the Horizontal Channel. The set of curves are quite linear and demonstrate a control range exceeding  $\pm 3$  dB at the band edges. The effect of this control on group delay is shown in Figure 21 for the extreme control settings of  $\pm 10$  volts. The effect is minor and is much less for smaller control voltages. The jagged curve is a characteristic of the HP8505A measurement technique. All group delay curves should be mentally averaged, and the fine detail ignored. Likewise, the frequency scale plotted by the machine is only approximate. Curves for the vertical channel A1 weight are given in Figures 22 and 23. Here, the adjustment range is slightly greater as is the effect on delay at the band edges.

Weight B1 of the Horizontal Channel is characterized in Figures 24 and 25. The amplitude adjustment is parabolic and fairly symmetrical. Range exceeds 3 dB at the band edges. Weight B1 also contributes little delay distortion. Figures 26 and 27 display the same information for the Vertical Channel. Performance is very similar to that of the Horizontal channel.

The third amplitude weight, C1, of the Horizontal Channel provides the cubic amplitude adjustment shown in Figure 28. Again, somewhat more than 3 dB of adjustment is obtained at the band edges. The effect on group delay is shown in Figure 29. C1 of the Vertical Channel is depicted in Figures 30 and 31.

The first of the group delay weights is A2 and it provides flat delay adjustment. This is shown for the Horizontal Channel in Figure 32, and for the Vertical Channel in Figure 33. The range is approximately  $\pm 8$  ns on

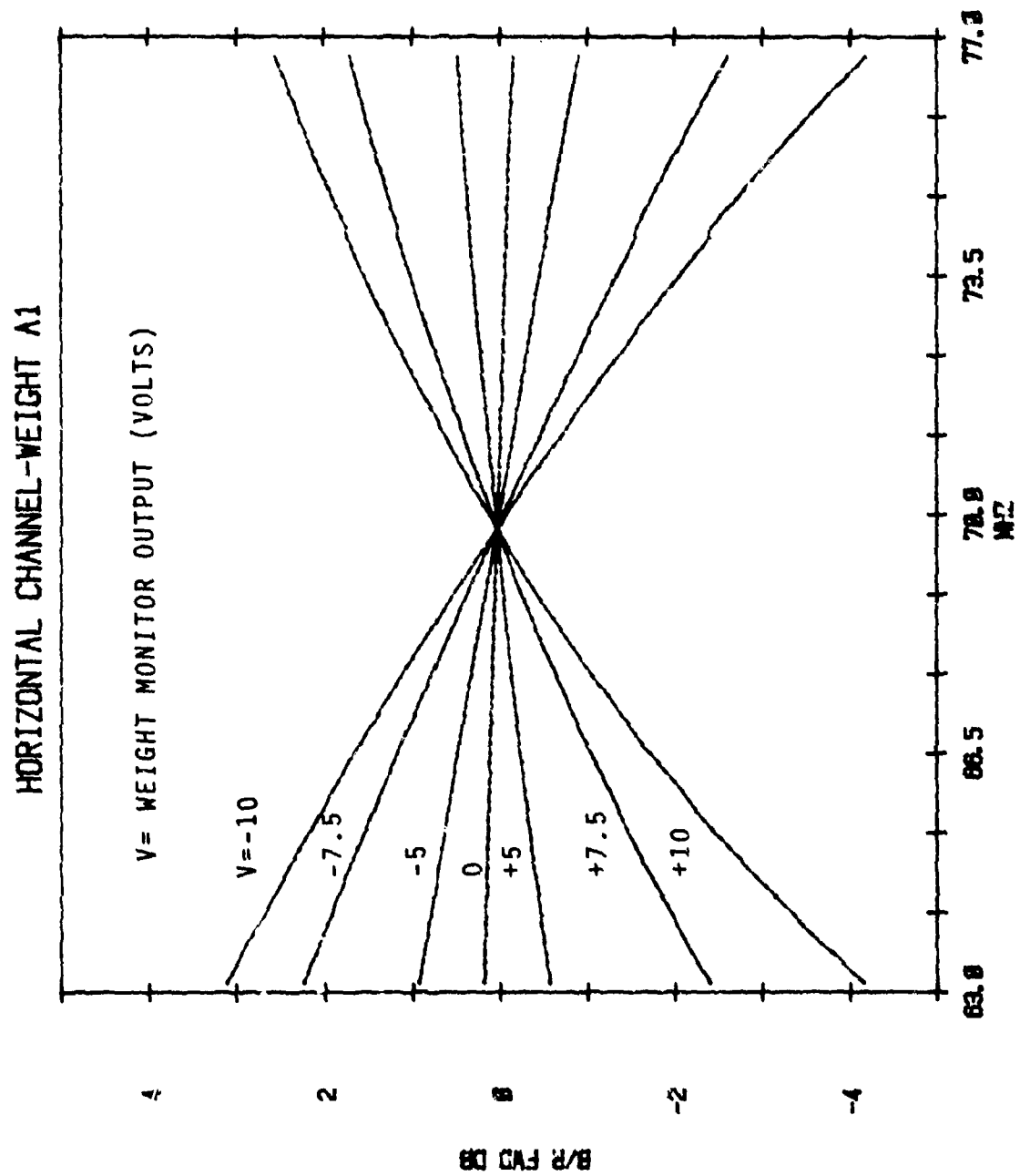


Figure 20. Effect of Weight A1 on Amplitude Response - Horizontal Channel

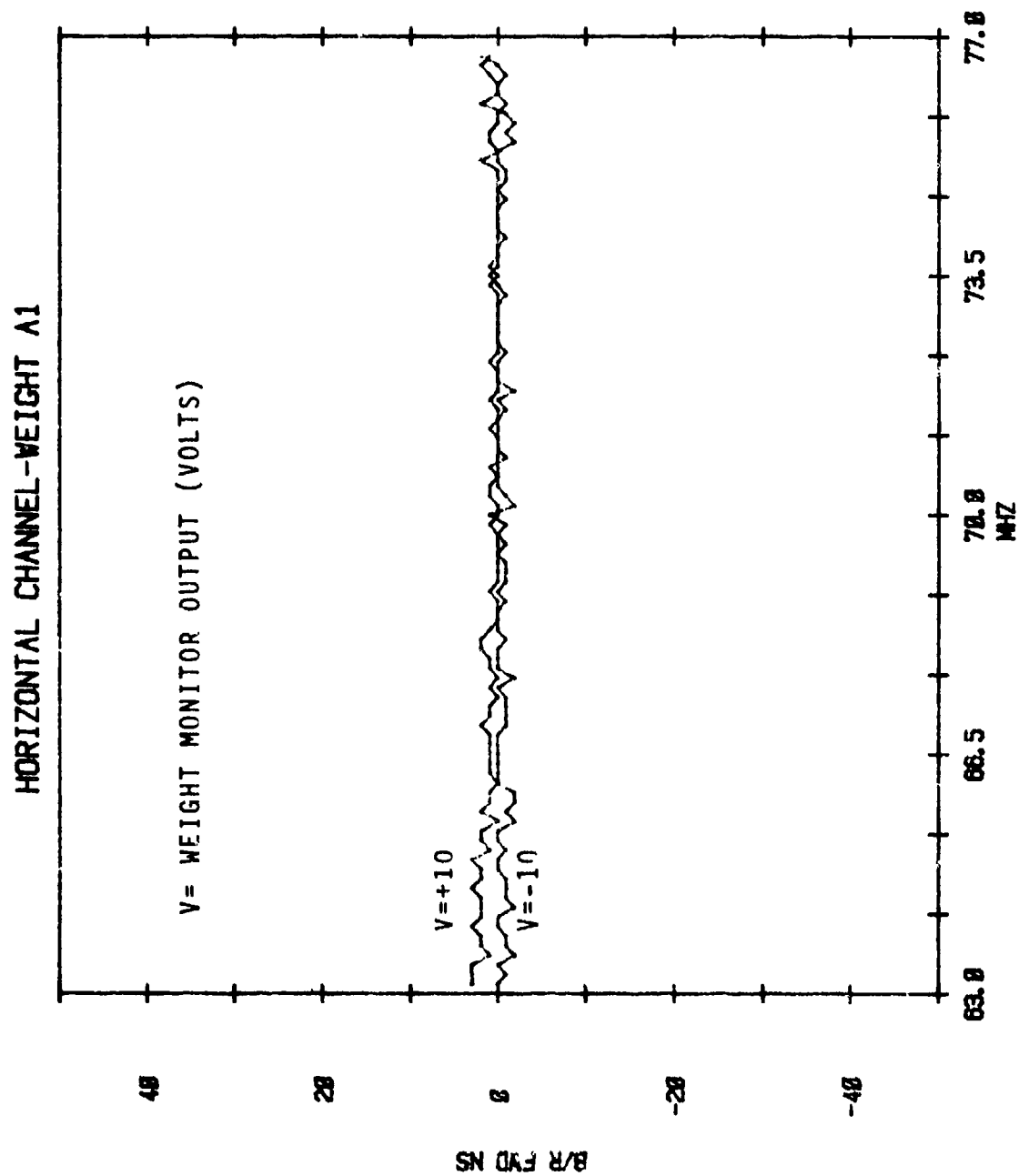


Figure 21. Effect of Weight A1 on Group Delay - Horizontal Channel

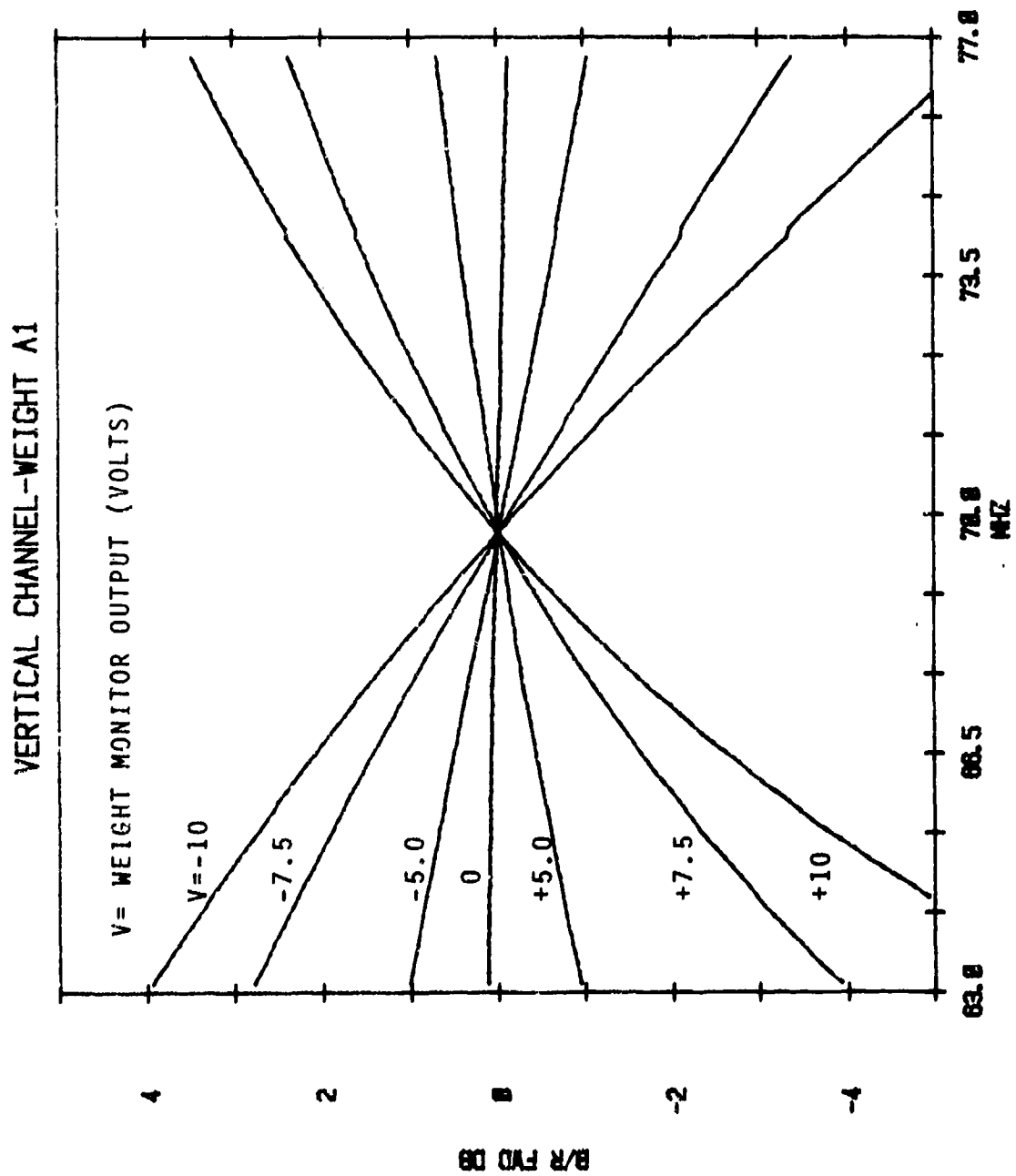


Figure 22. Effect of Weight A1 on Amplitude Response - Vertical Channel

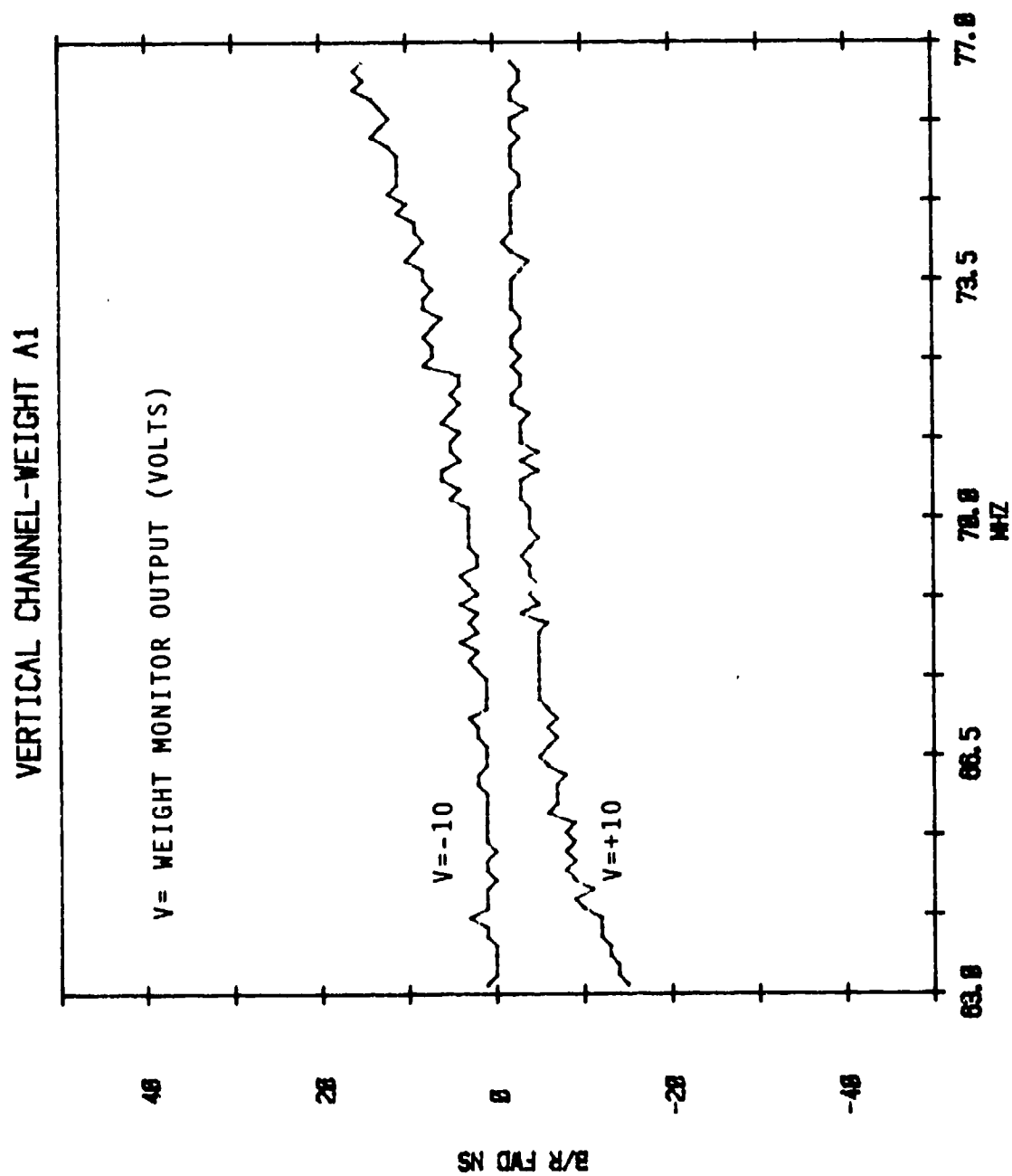


Figure 23. Effect of Weight A1 on Group Delay - Vertical Channel

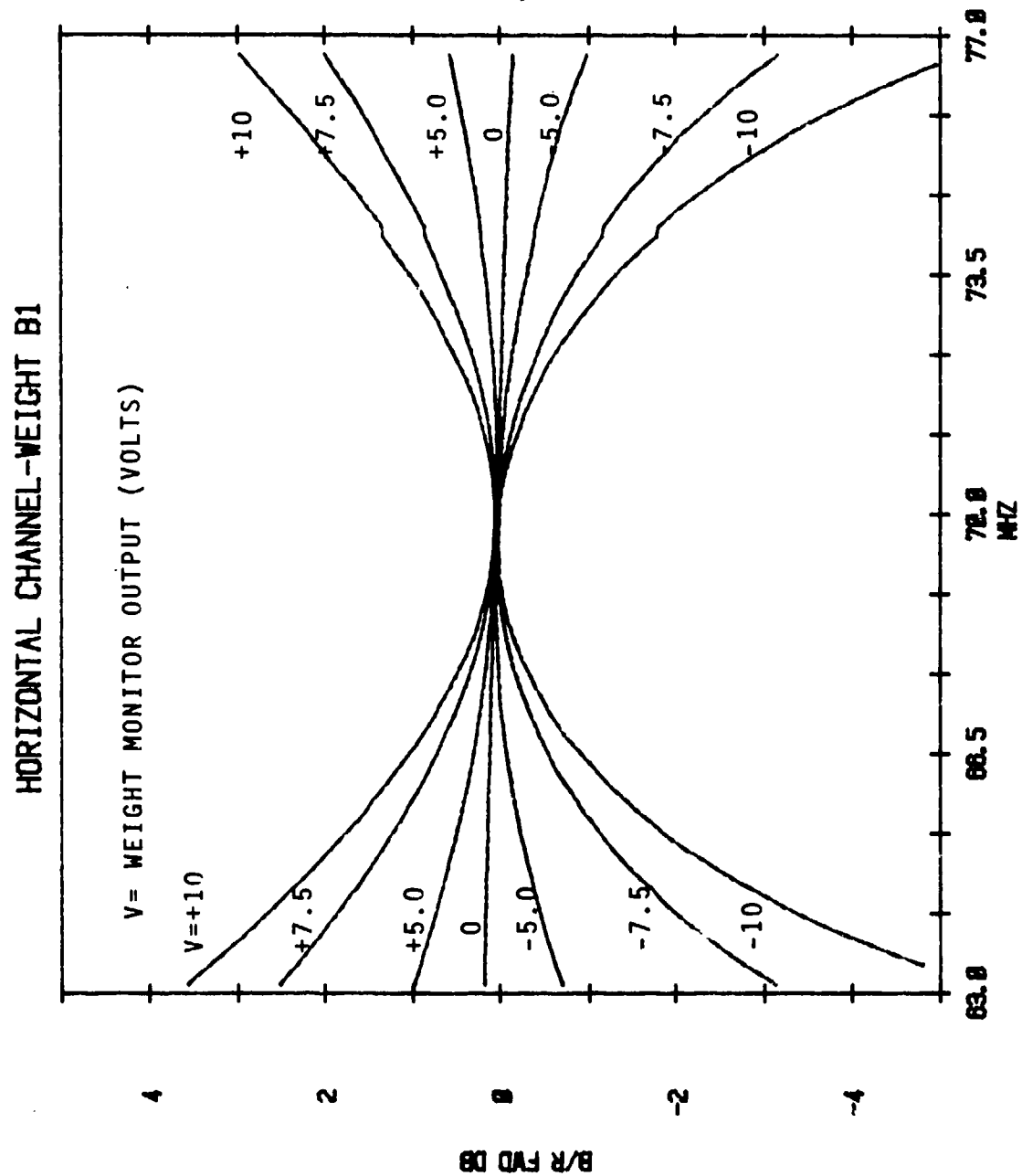


Figure 24. Effect of Weight B1 on Amplitude Response - Horizontal Channel

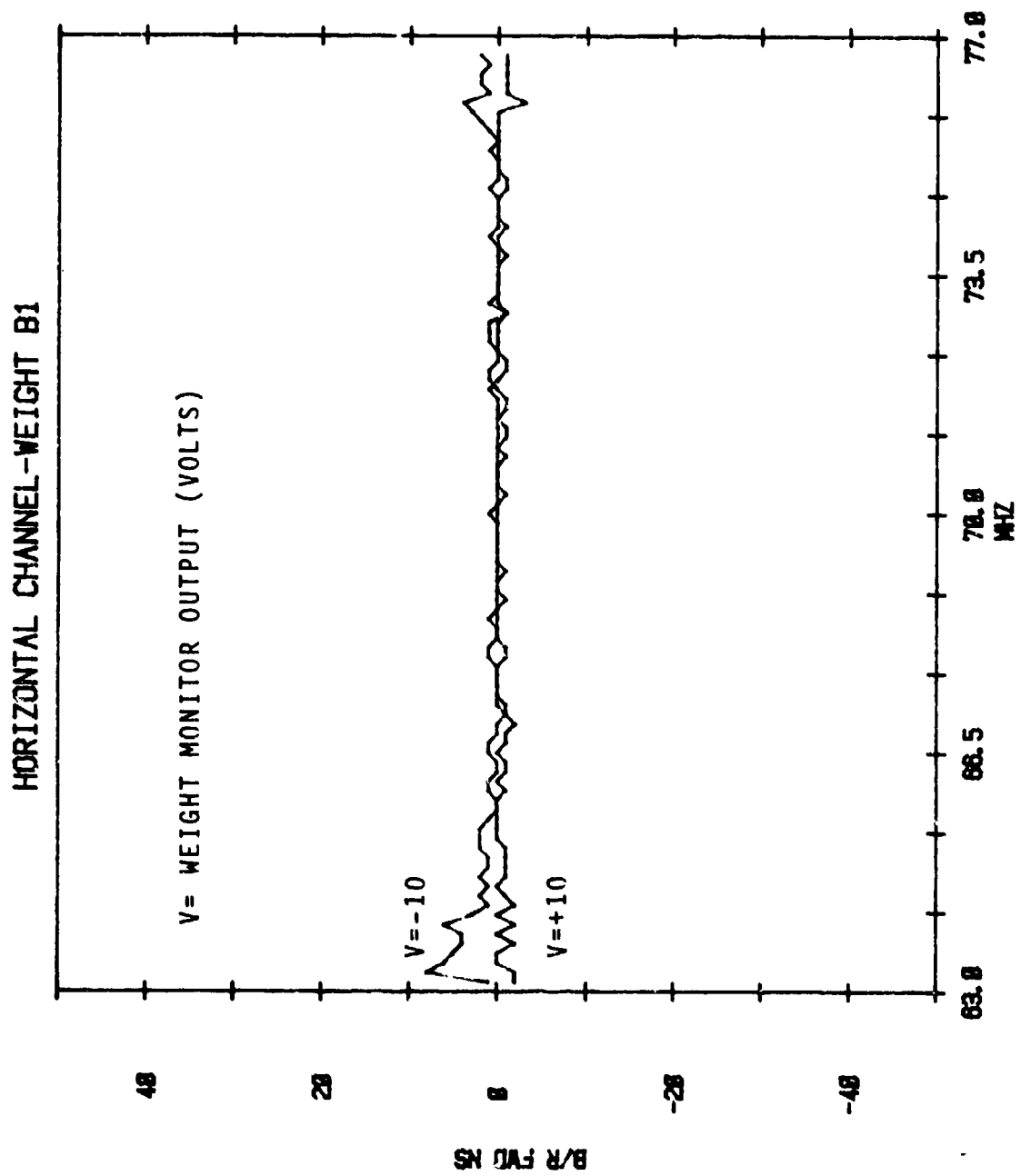


Figure 25. Effect of Weight B1 on Group Delay - Horizontal Channel

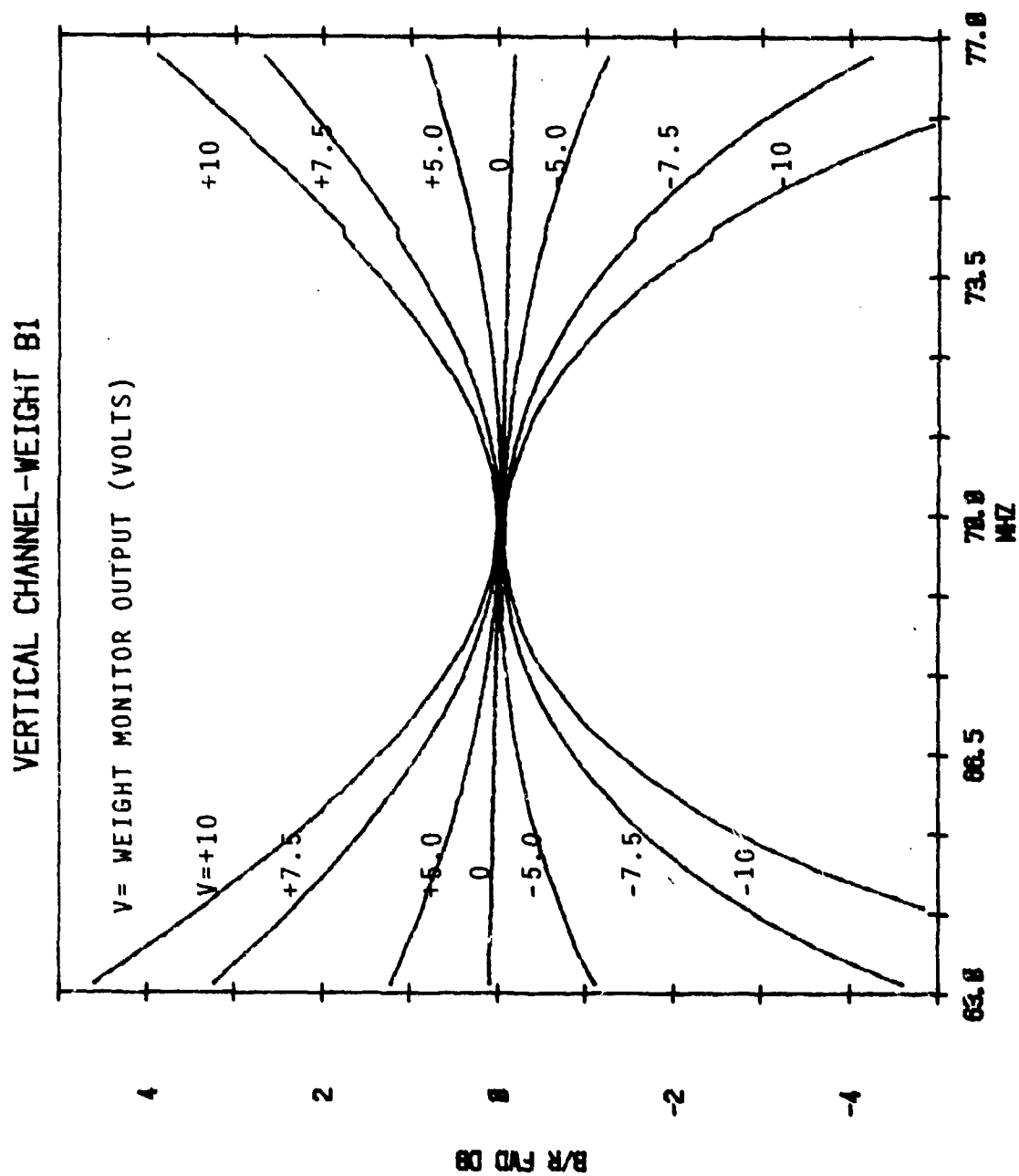


Figure 26. Effect of Weight B1 on Amplitude Response - Vertical Channel

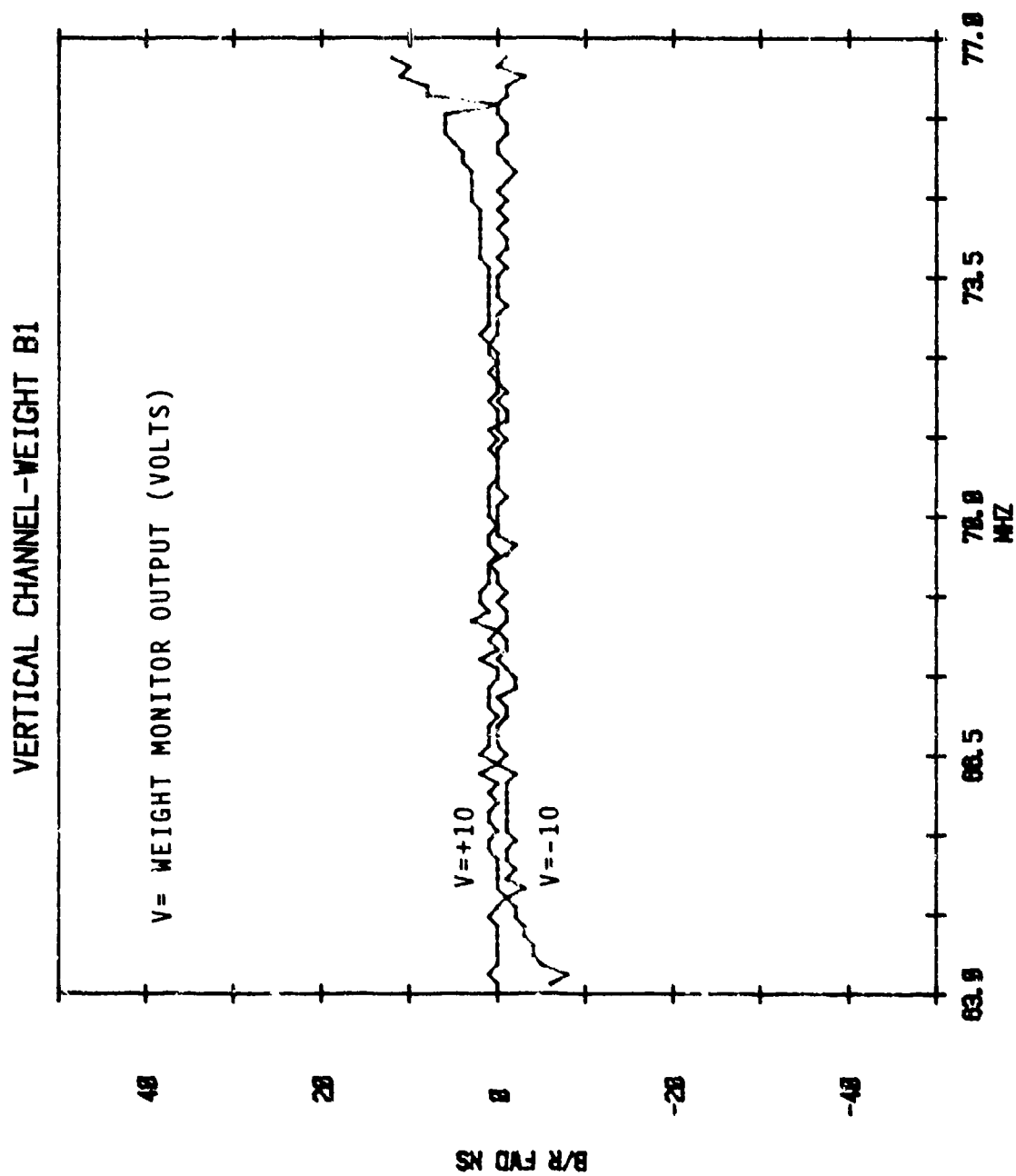


Figure 27. Effect of Weight B1 on Group Delay - Vertical Channel

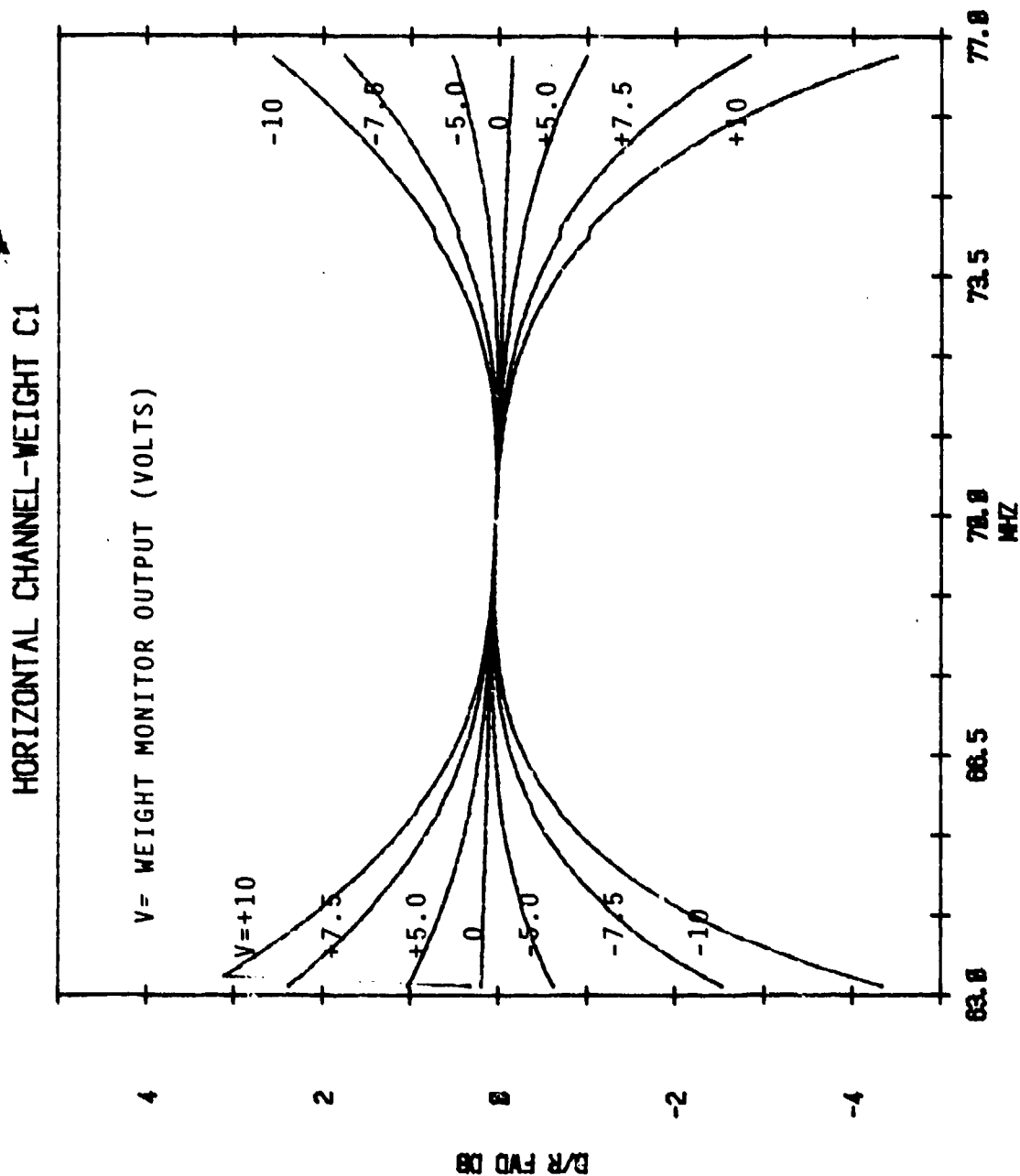


Figure 28. Effect of Weight C1 on Amplitude Response - Horizontal Channel

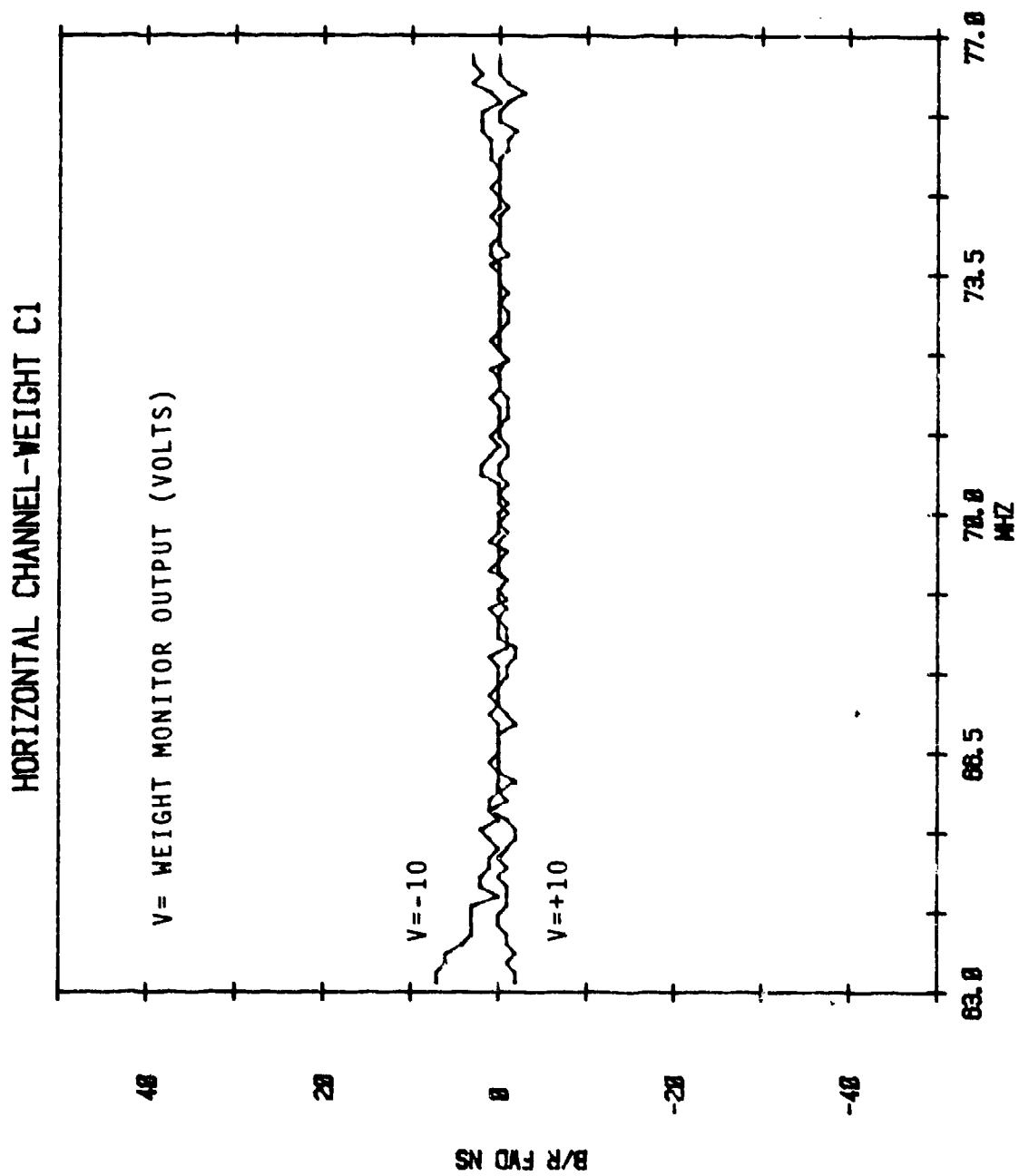


Figure 29. Effect of Weight C1 on Group Delay - Horizontal Channel

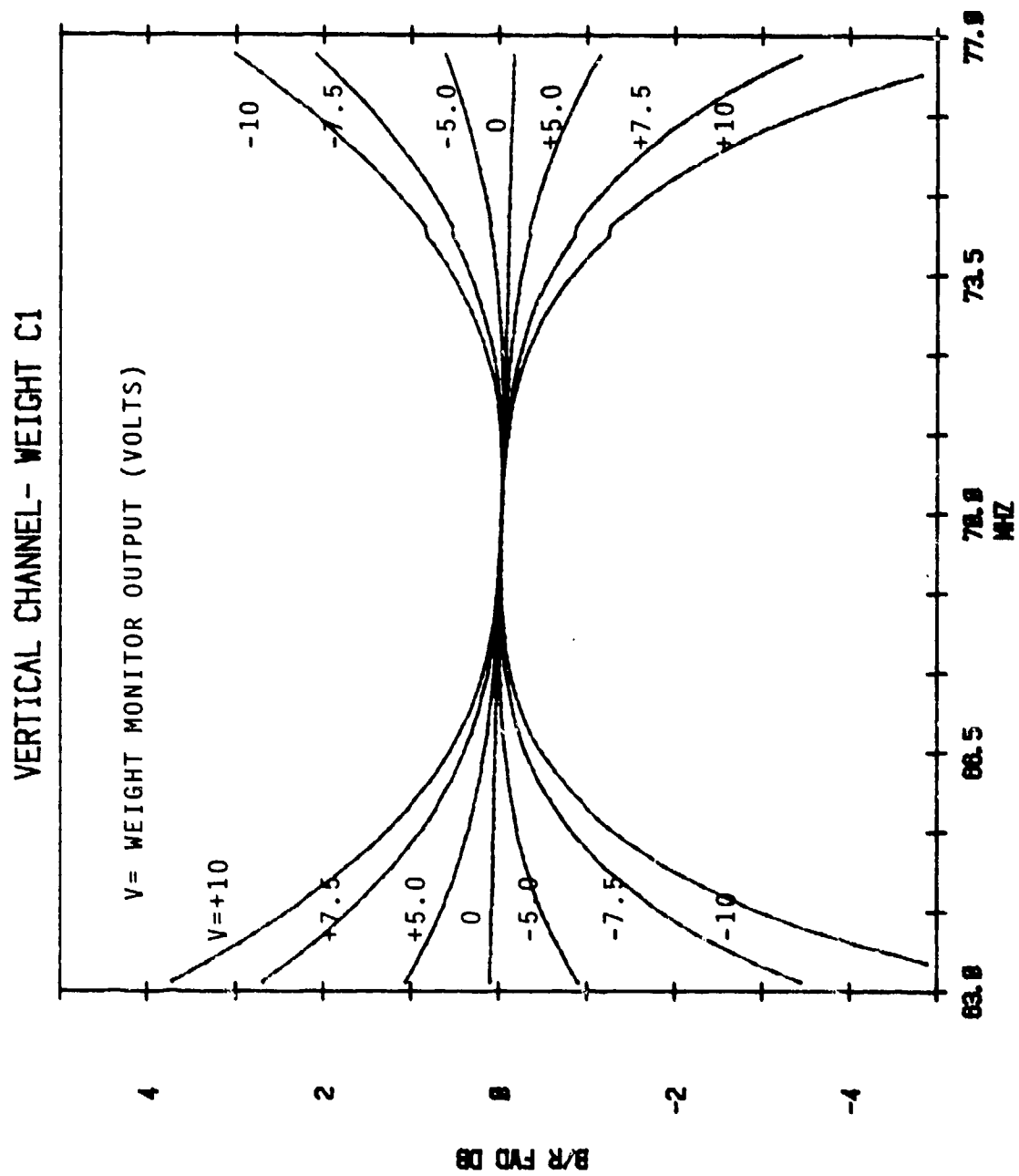


Figure 30. Effect of Weight C1 on Amplitude Response - Vertical Channel

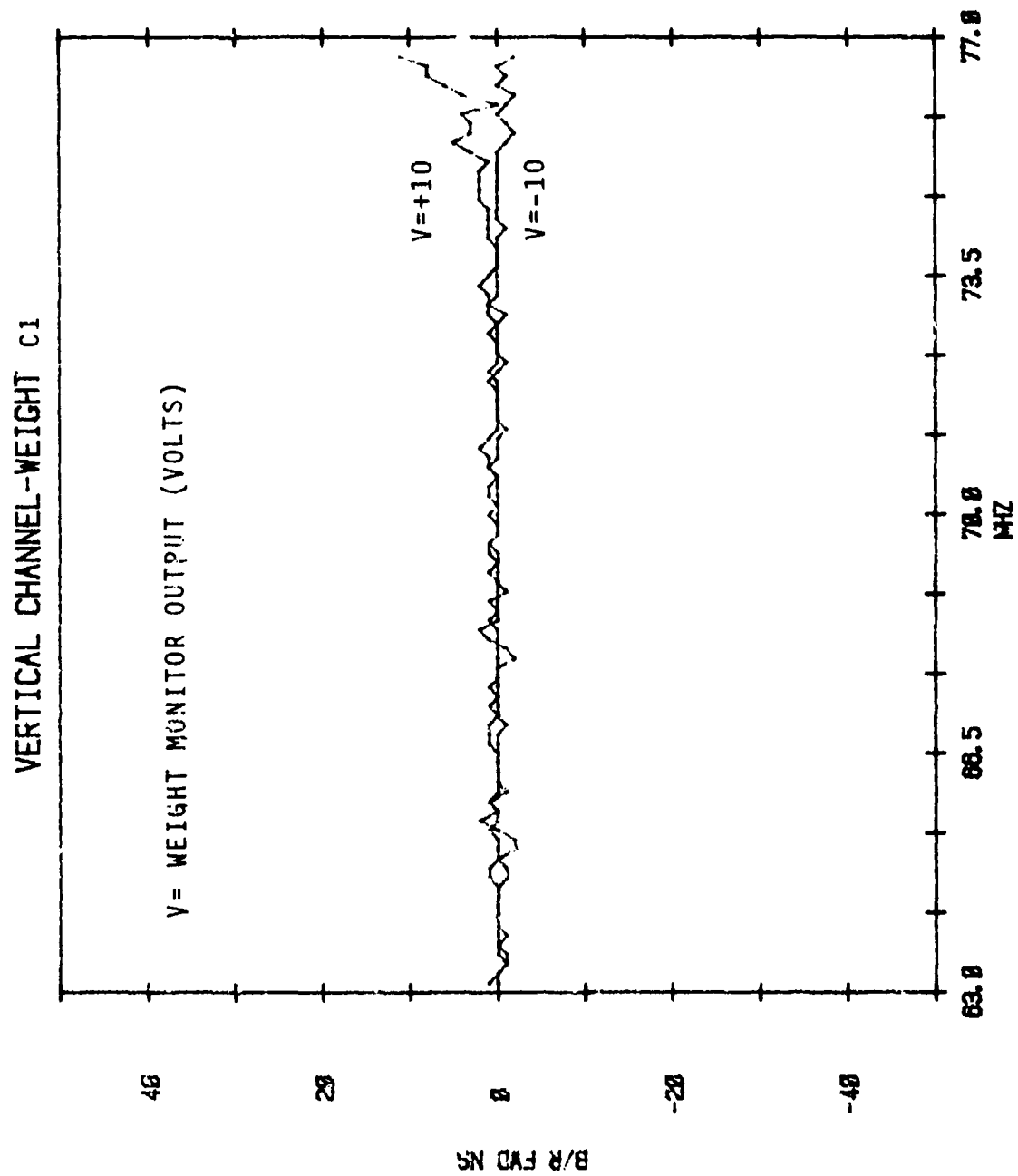


Figure 31. Effect of Weight C1 on Group Delay - Vertical Channel

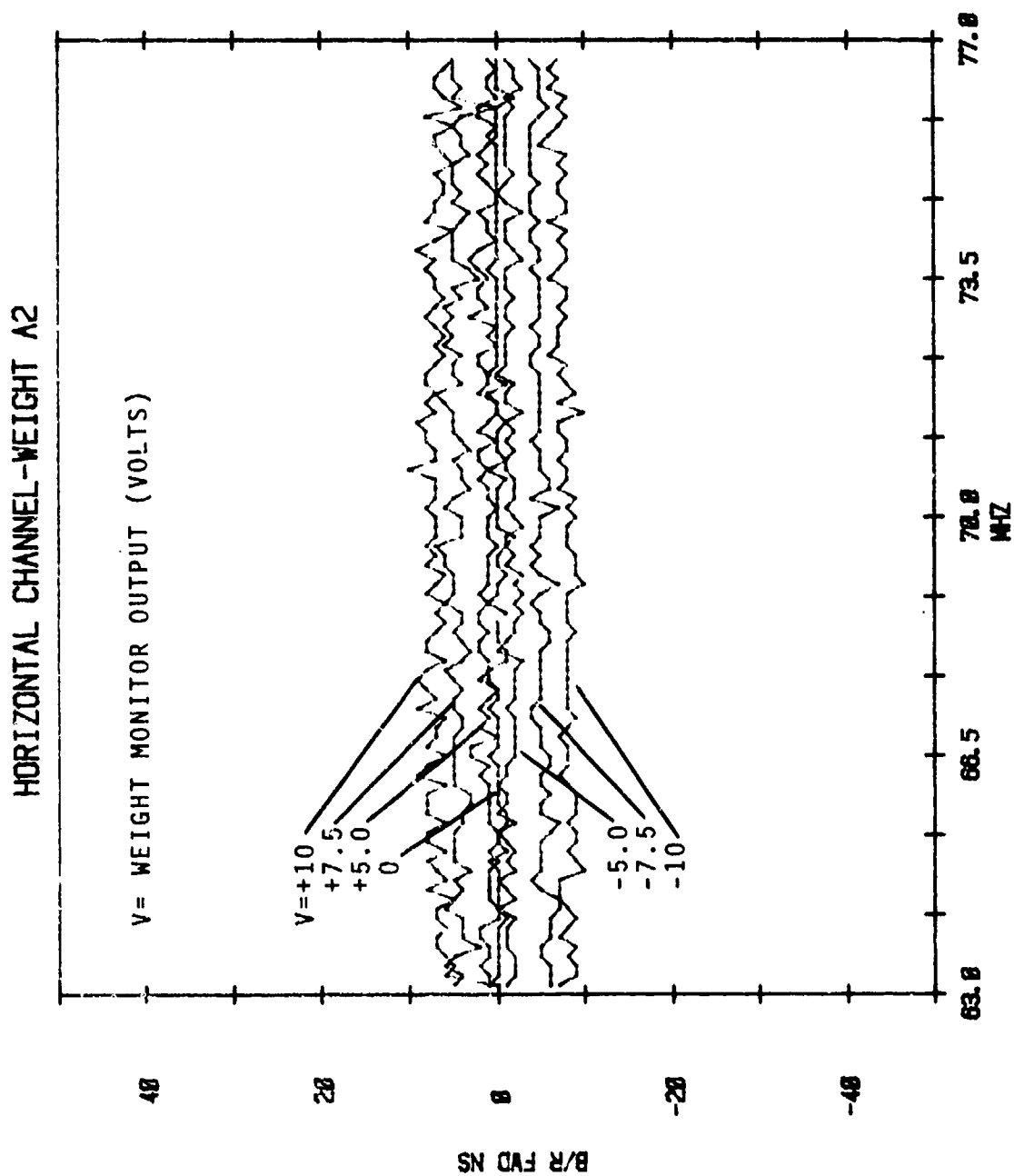


Figure 32. Effect of Weight A2 on Group Delay - Horizontal Channel

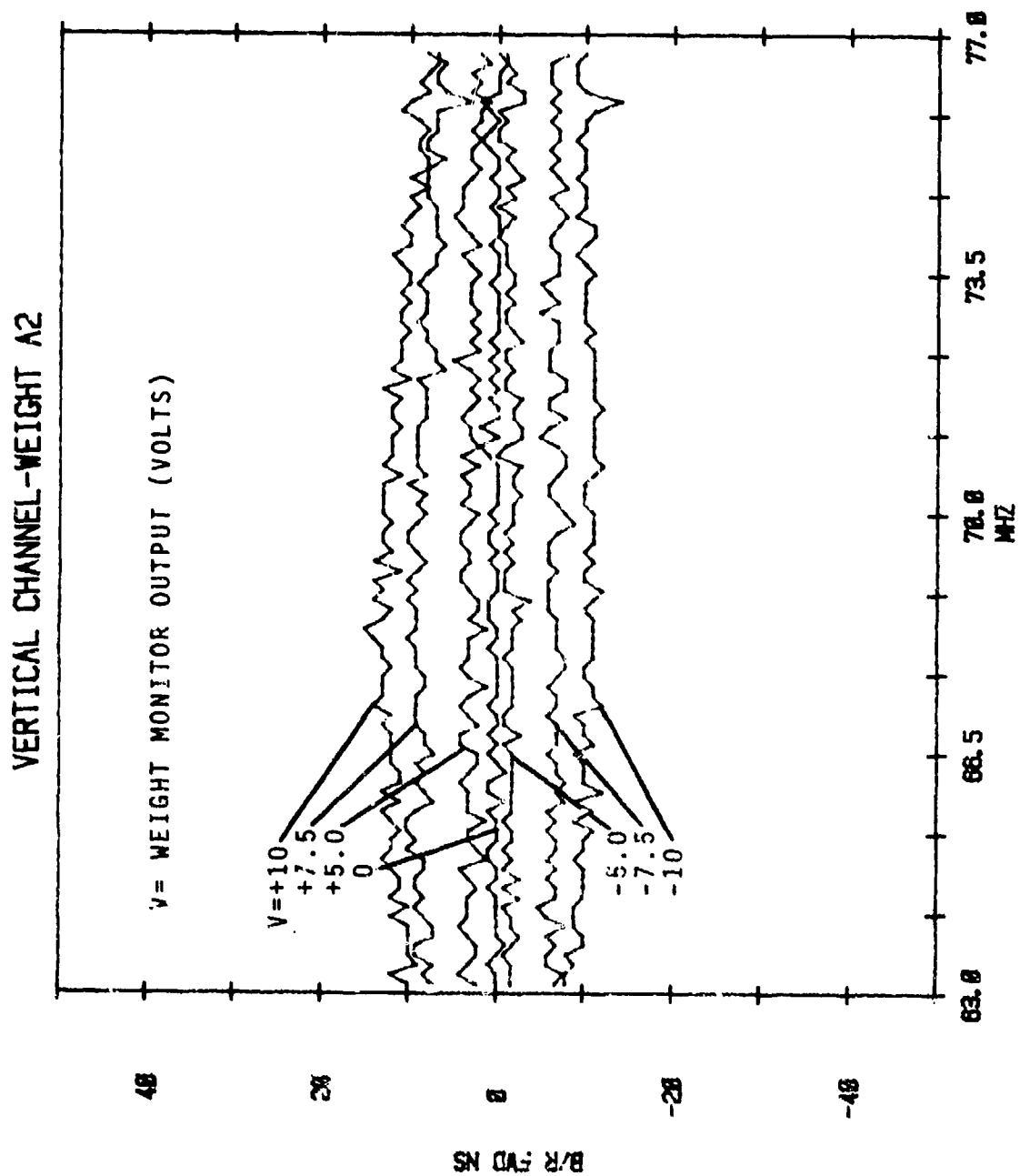


Figure 33. Effect of Weight A2 on Group Delay - Vertical Channel

the Horizontal Channel and  $\pm 10$  ns on the Vertical Channel. Theoretically, all delay weights should have a small parabolic effect on amplitude response. This is apparent in Figure 34 which depicts the amplitude effects of A2 on the Horizontal Channel. A 1 dB rise is evident at the lower band edge. Referring to Figure 35 for the Vertical Channel, it may be seen that the effect is approximately 1.75 dB. This is a result of the slightly greater control range. While this may seem like a fairly large amplitude distortion, it should be remembered that this is for an extreme control setting. The effect diminishes rapidly for lower control settings. Extremes only are shown for clarity.

The linear delay weight, B2, of the horizontal channel is characterized in Figures 36 and 37. Range is close to 20 ns at the band edges and is fairly linear for deviations below 10 ns. Similar curves are shown for the Vertical Channel in Figures 38 and 39.

Group delay characteristics of weight C2 of the Horizontal Channel are given in Figure 40. The parabolic adjustment exceeds 20 ns at the band edges. Amplitude distortion caused by this weight is less than 1 dB as seen in Figure 41. Refer to Figures 42 and 43 for delay and amplitude adjustment characteristics of weight C2 of the Vertical Channel.

The cross-pole weights, D1 and D2, measured independently affect only amplitude. Figure 44 shows attenuation of weight D1 of the Horizontal Channel with positive control voltages as a parameter. Figure 45 has negative control voltages as a parameter. The Horizontal Channel's D2 weight is characterized in Figures 46 and 47. Minimum attenuation is approximately 3 dB and maximum attenuation exceeds 35 dB. If weights D1 and D2 are simultaneously adjusted for minimum power output, an attenuation exceeding 40 dB is possible. Adjustment of both weights allows cancellation of various leakage components. Attenuation curves for weights D1 and D2 for the Vertical Channel are given in Figures 48, 49, 50, and 51.

#### 4.1.2. Main Signal Path Results

The input to output transfer characteristics of the CPIRE were measured and results are presented in this paragraph. Figure 52 shows the amplitude response of the Horizontal Channel with input filter from 35 MHz to 105 MHz. These end points represent the points of maximum out-of-band gain

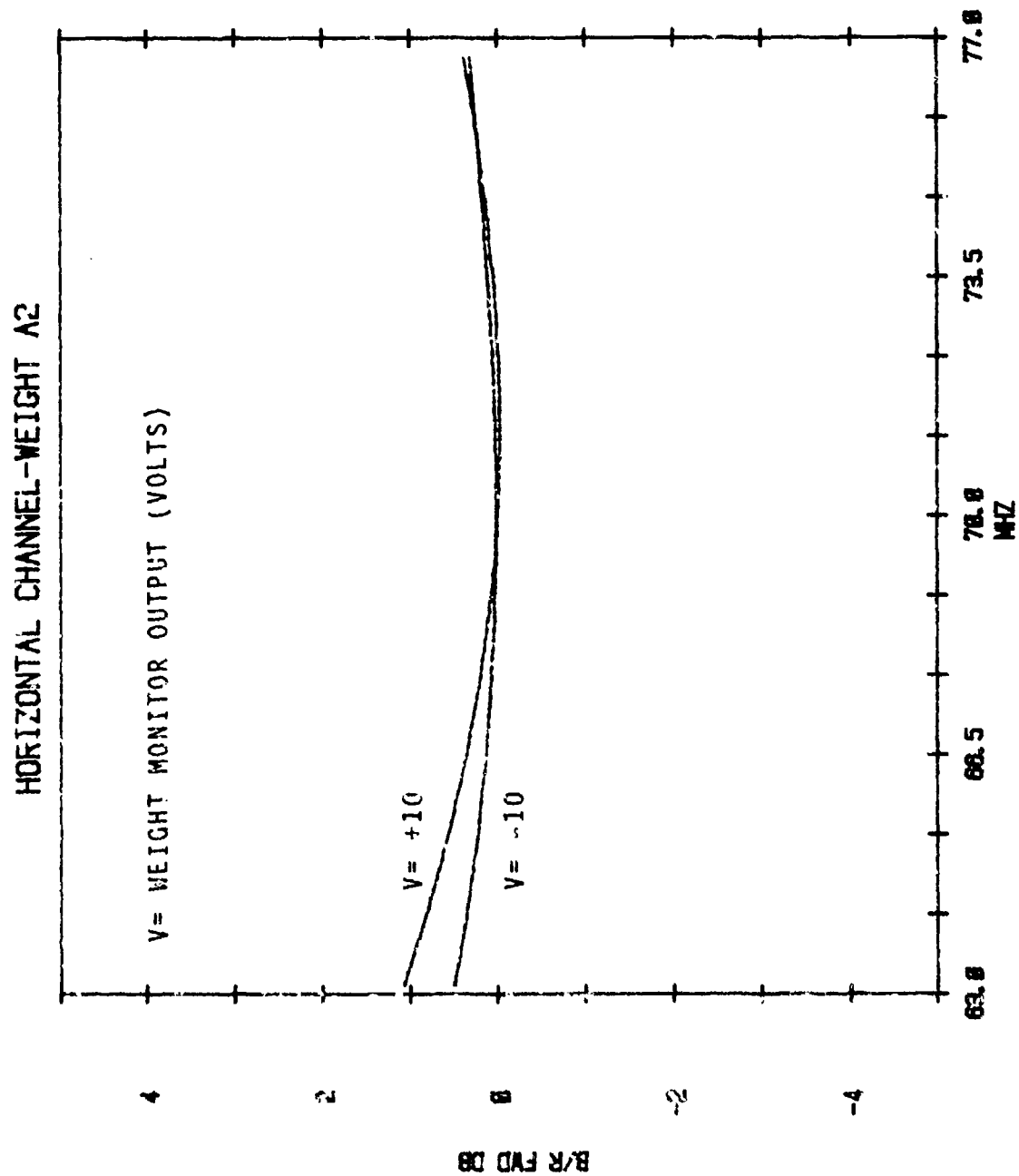


Figure 34. Effect of Weight A2 on Amplitude Response - Horizontal Channel

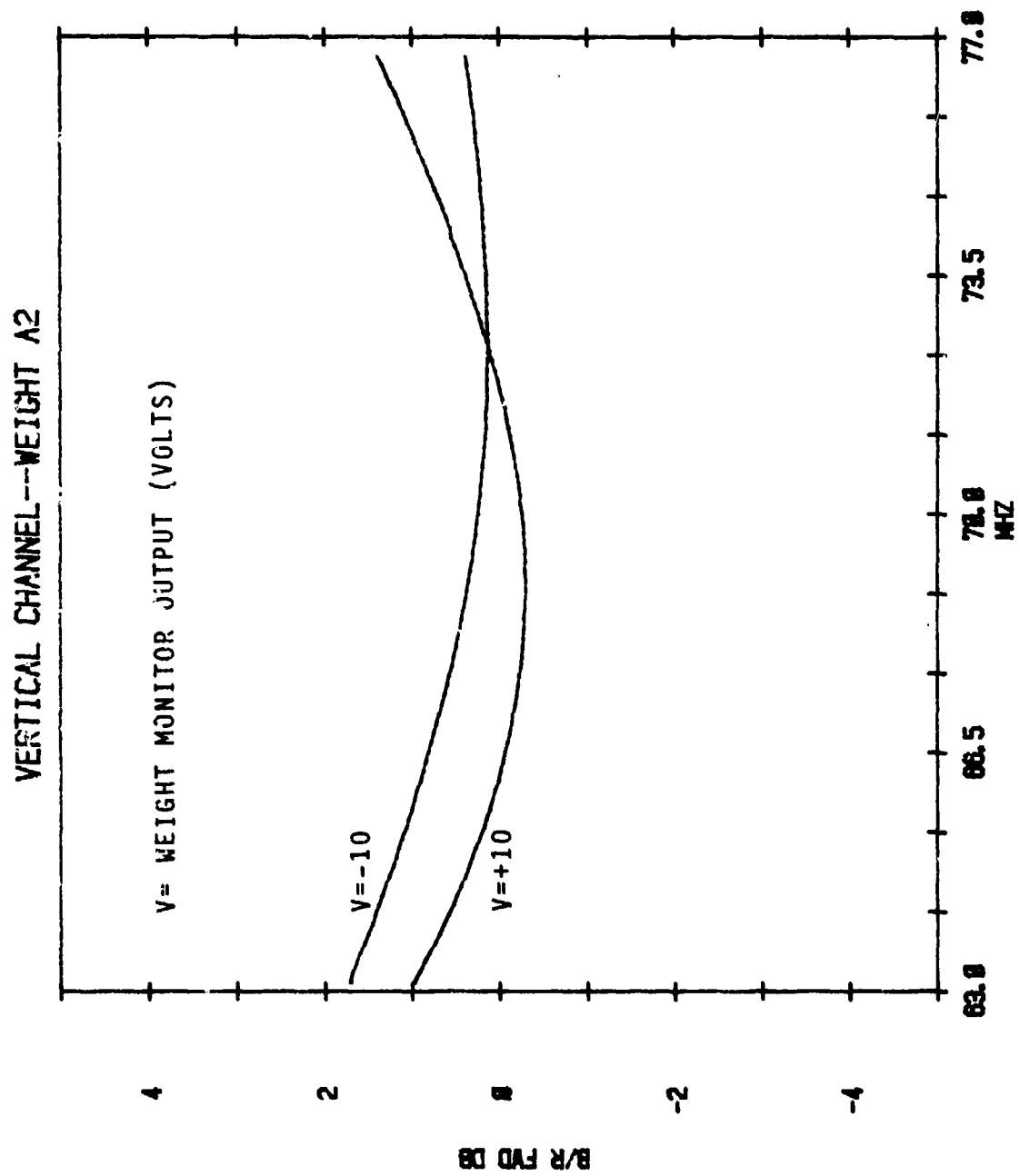


Figure 35. Effect of Weight A2 on Amplitude Response - Vertical Channel

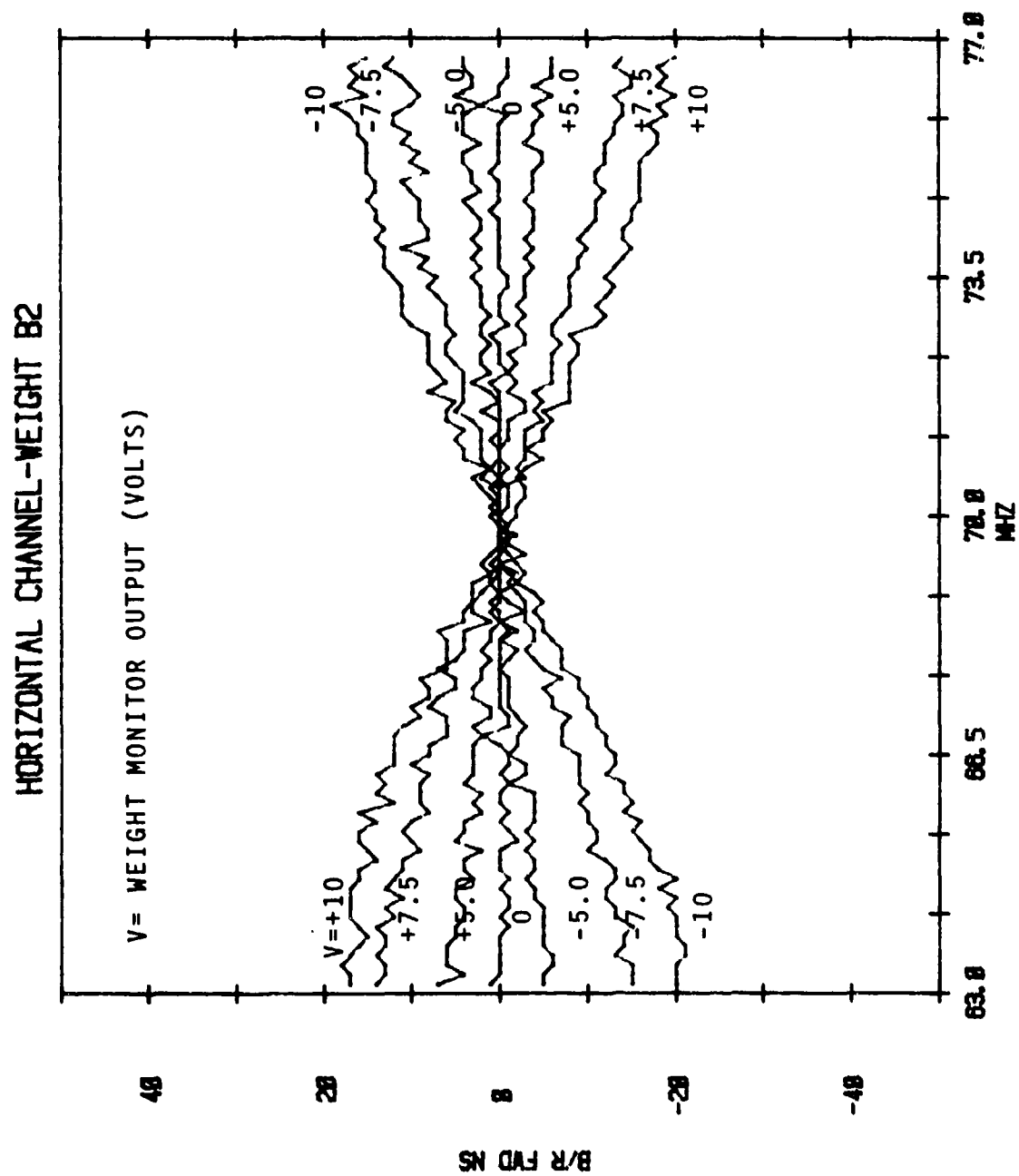


Figure 36. Effect of Weight B2 on Group Delay - Horizontal Channel

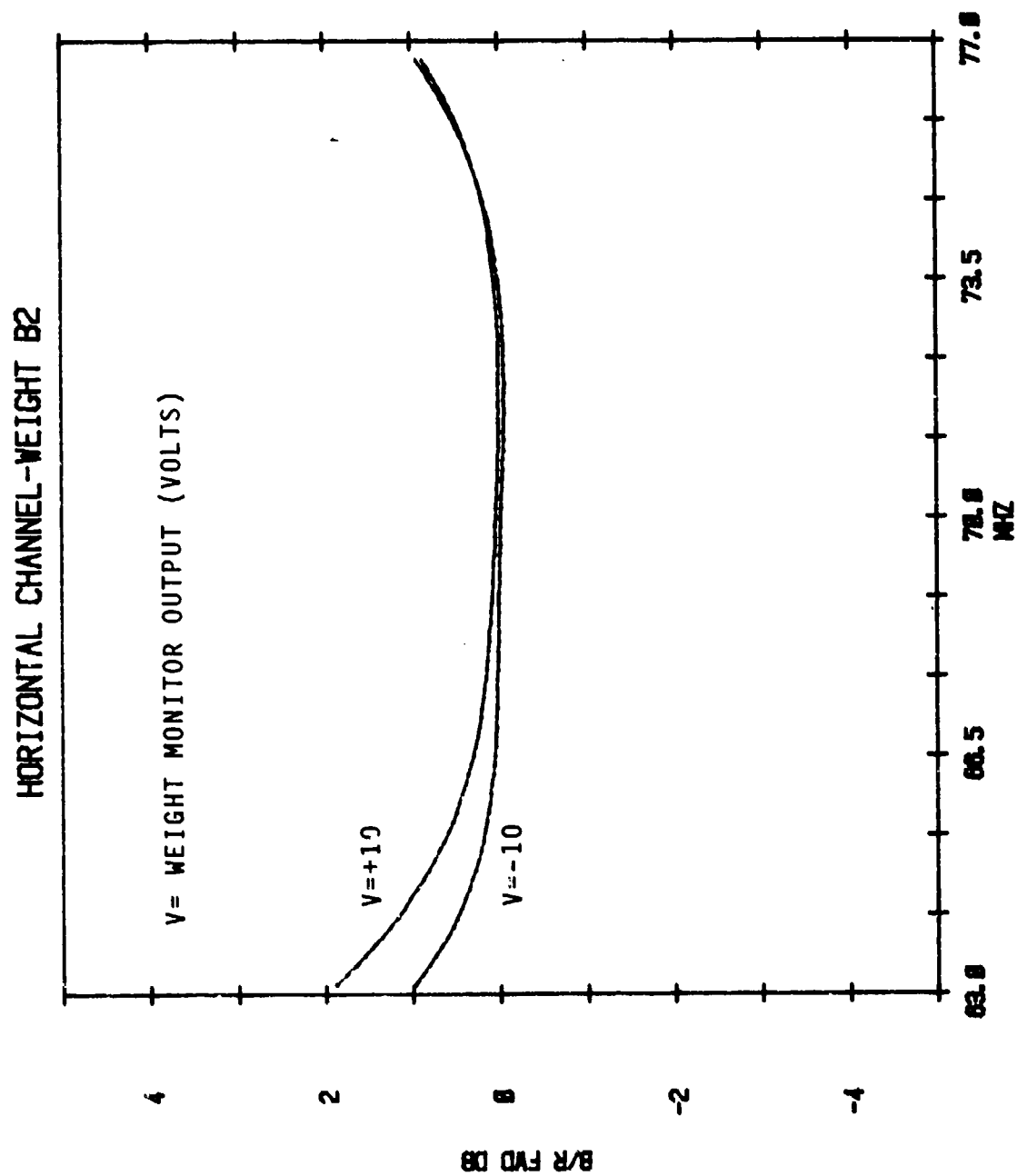


Figure 37. Effect of Weight B2 on Amplitude Response - Horizontal Channel

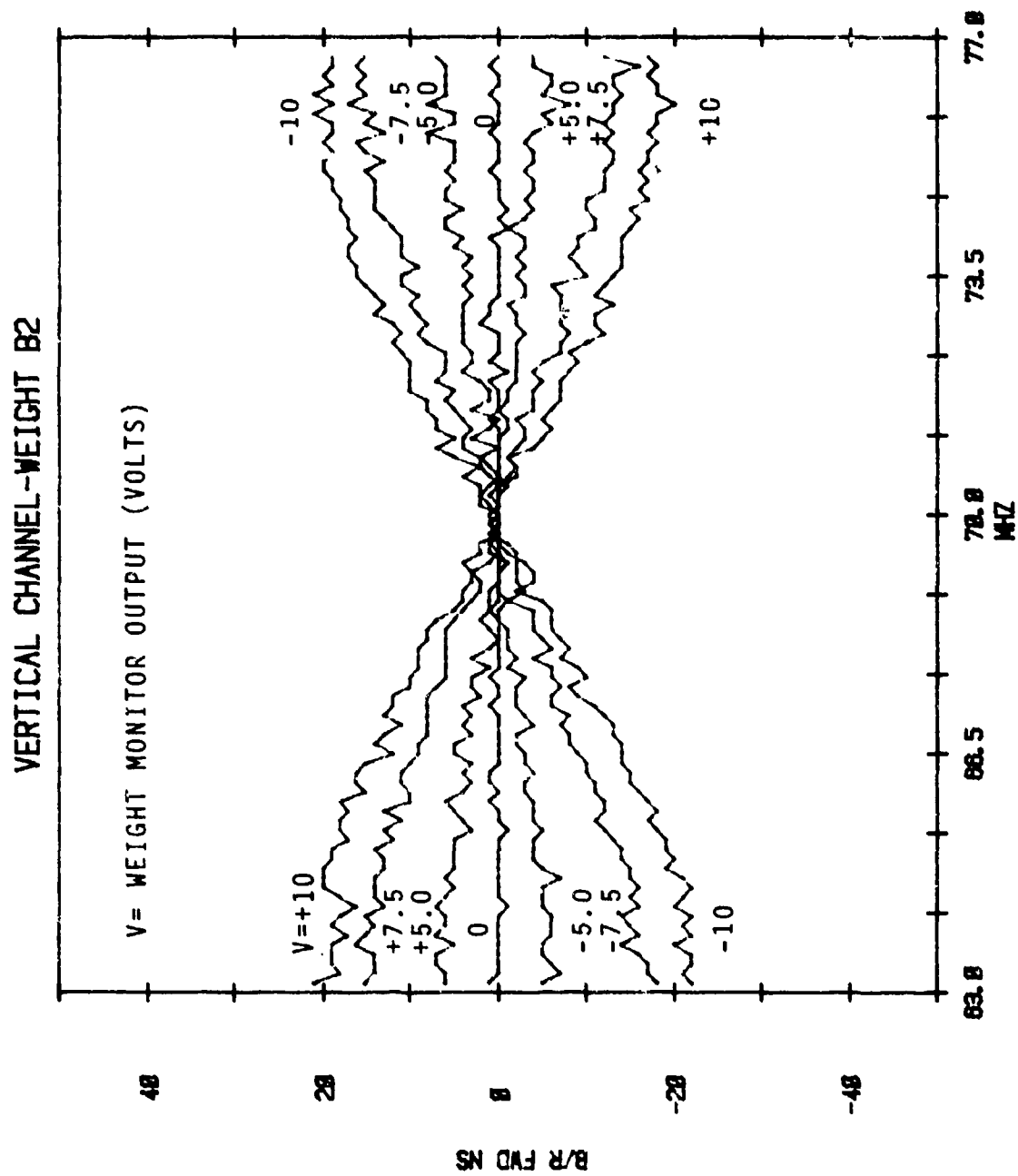


Figure 38. Effect of Weight B2 on Group Delay - Vertical Channel

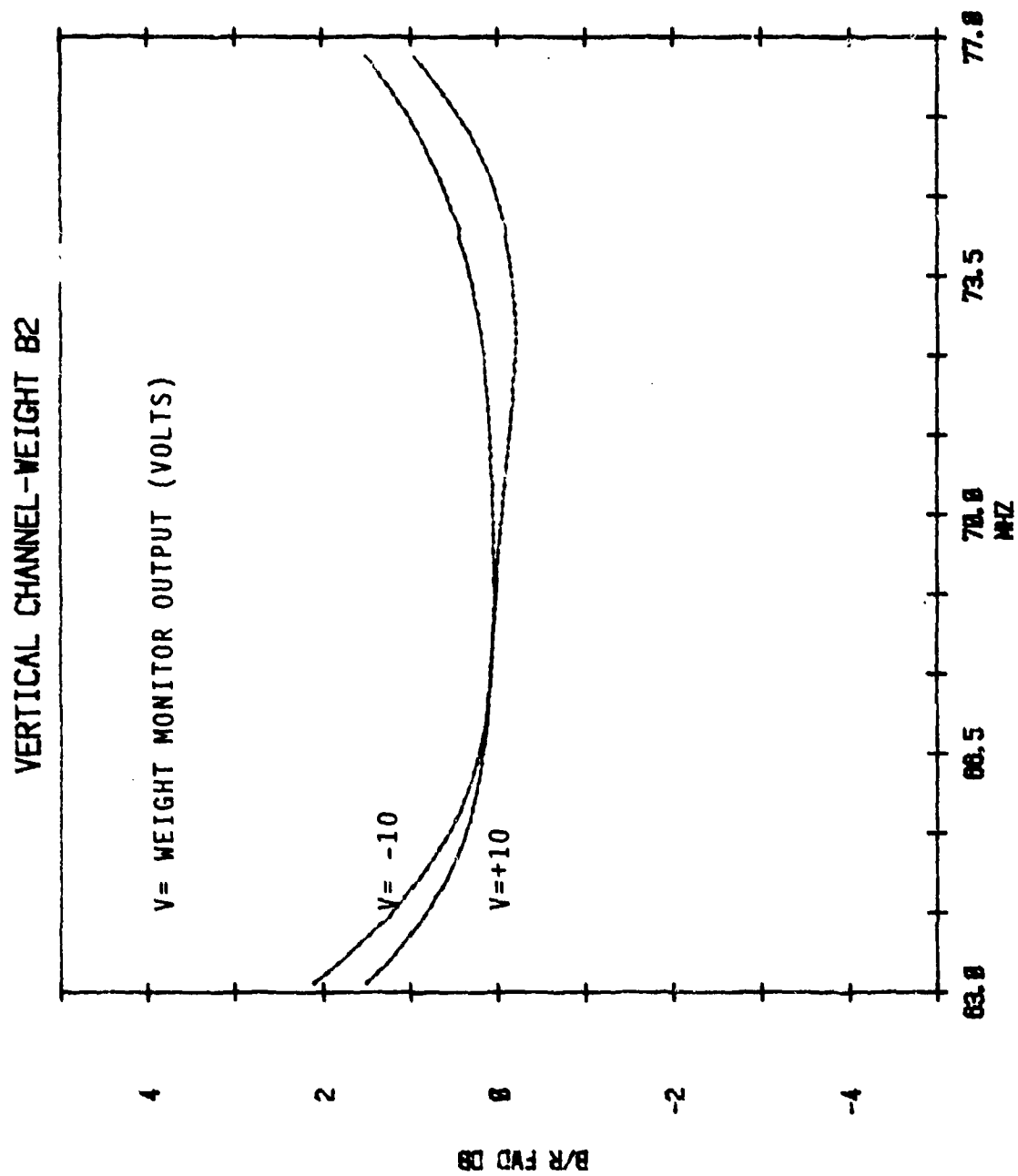


Figure 39. Effect of Weight B2 on Amplitude Response - Vertical Channel

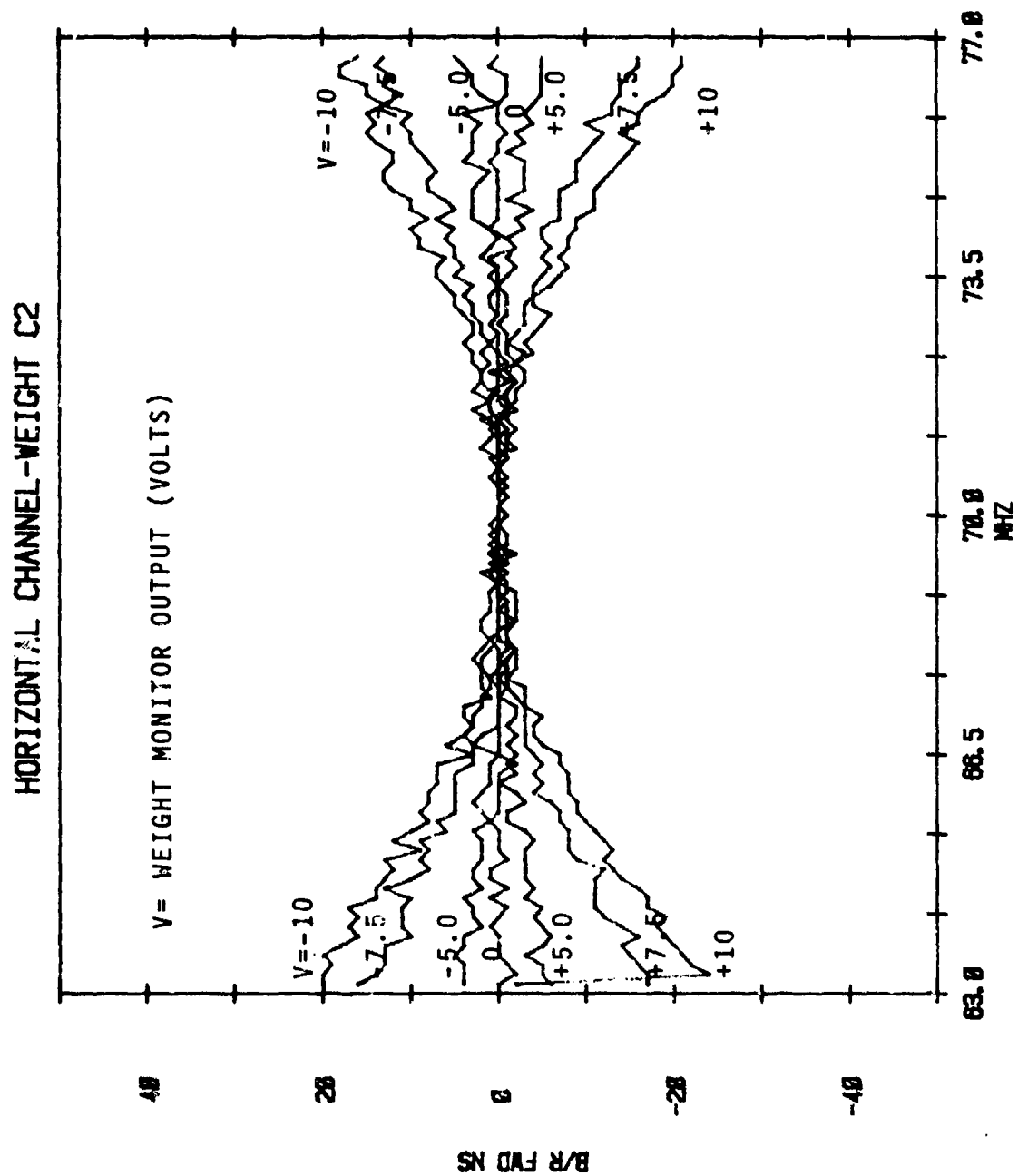


Figure 40. Effect of Weight C2 on Group Delay - Horizontal Channel

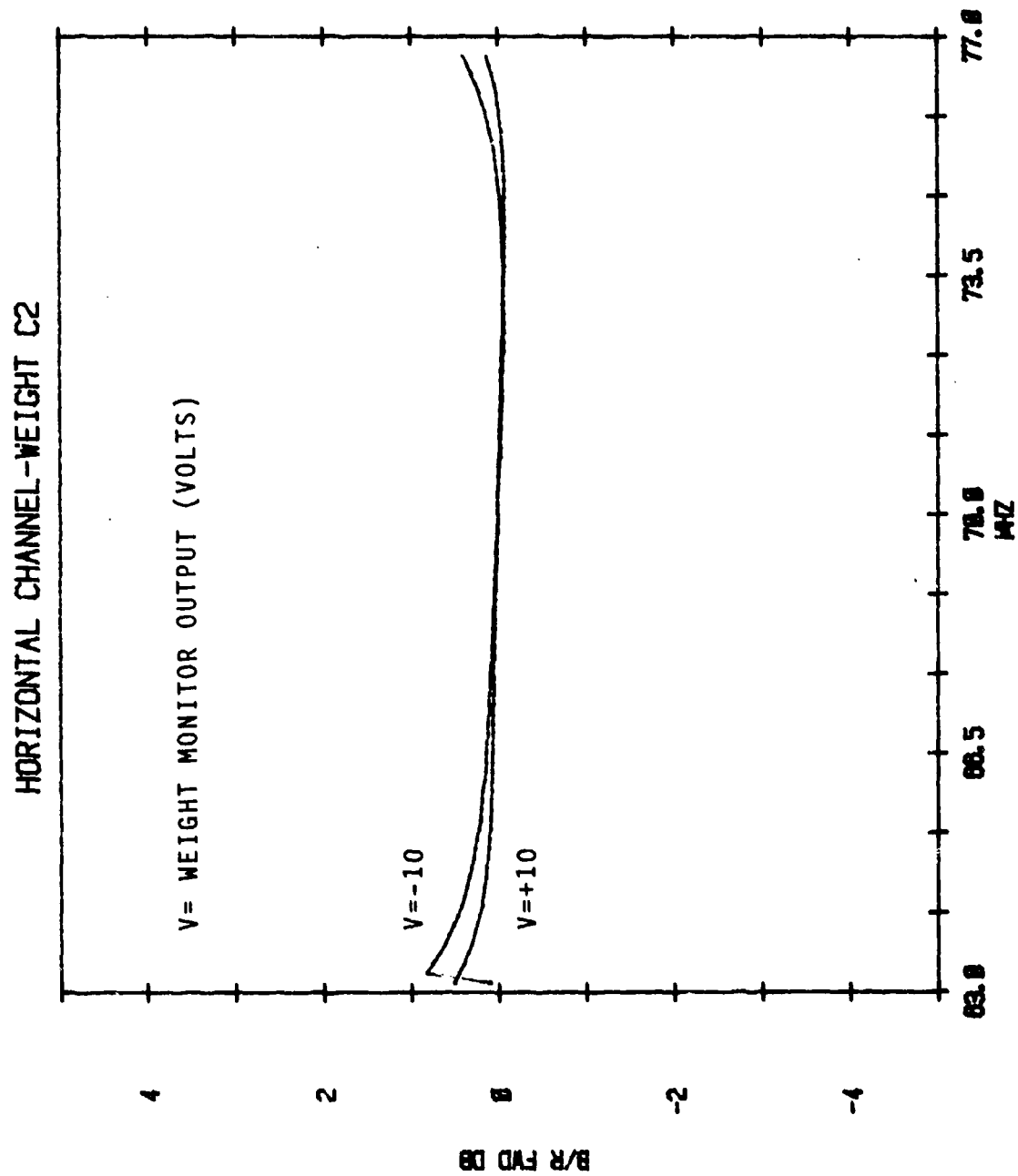


Figure 41. Effect of Weight C2 on Amplitude Response - Horizontal Channel

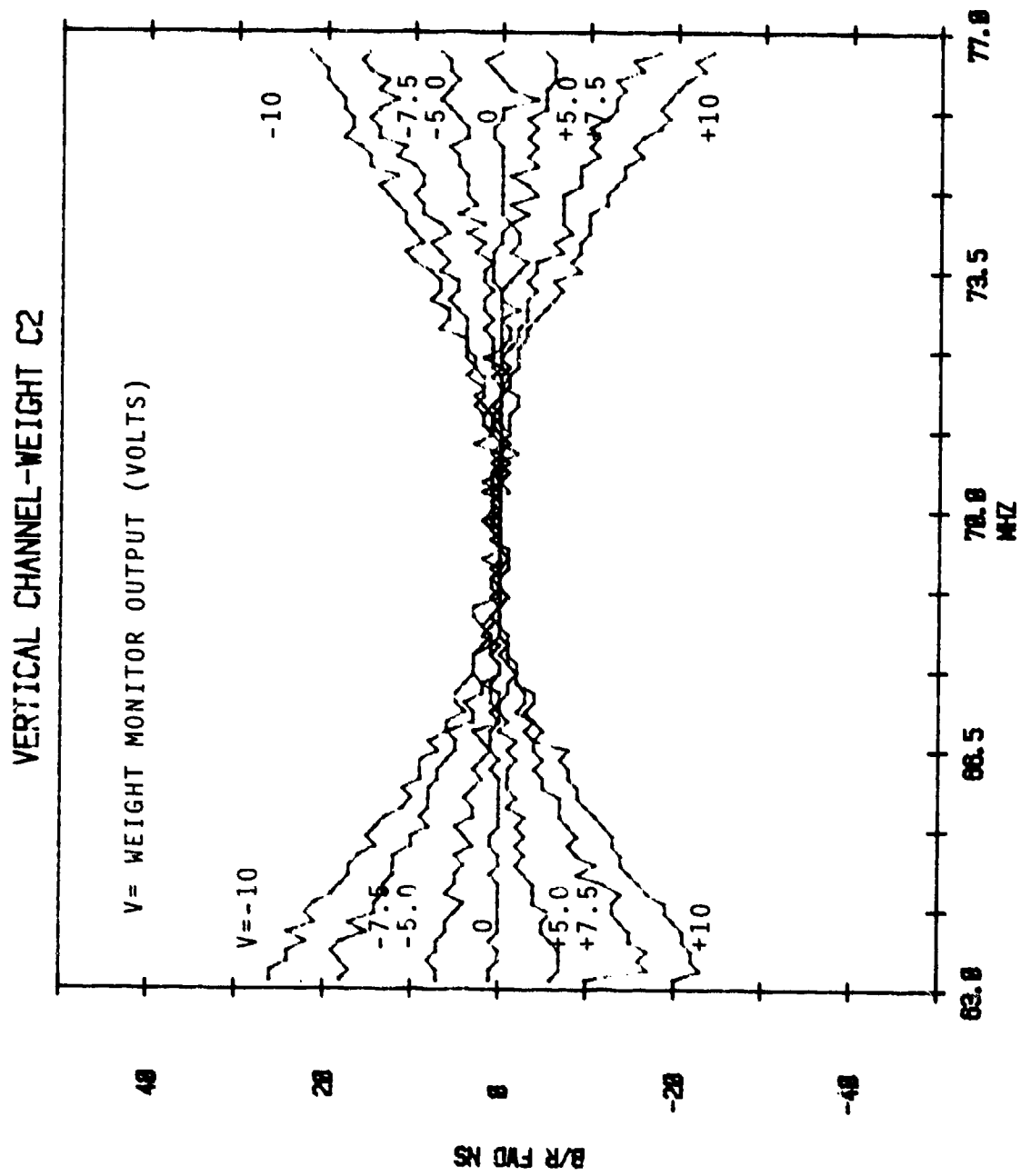


Figure 42. Effect of Weight C2 on Group Delay - Vertical Channel

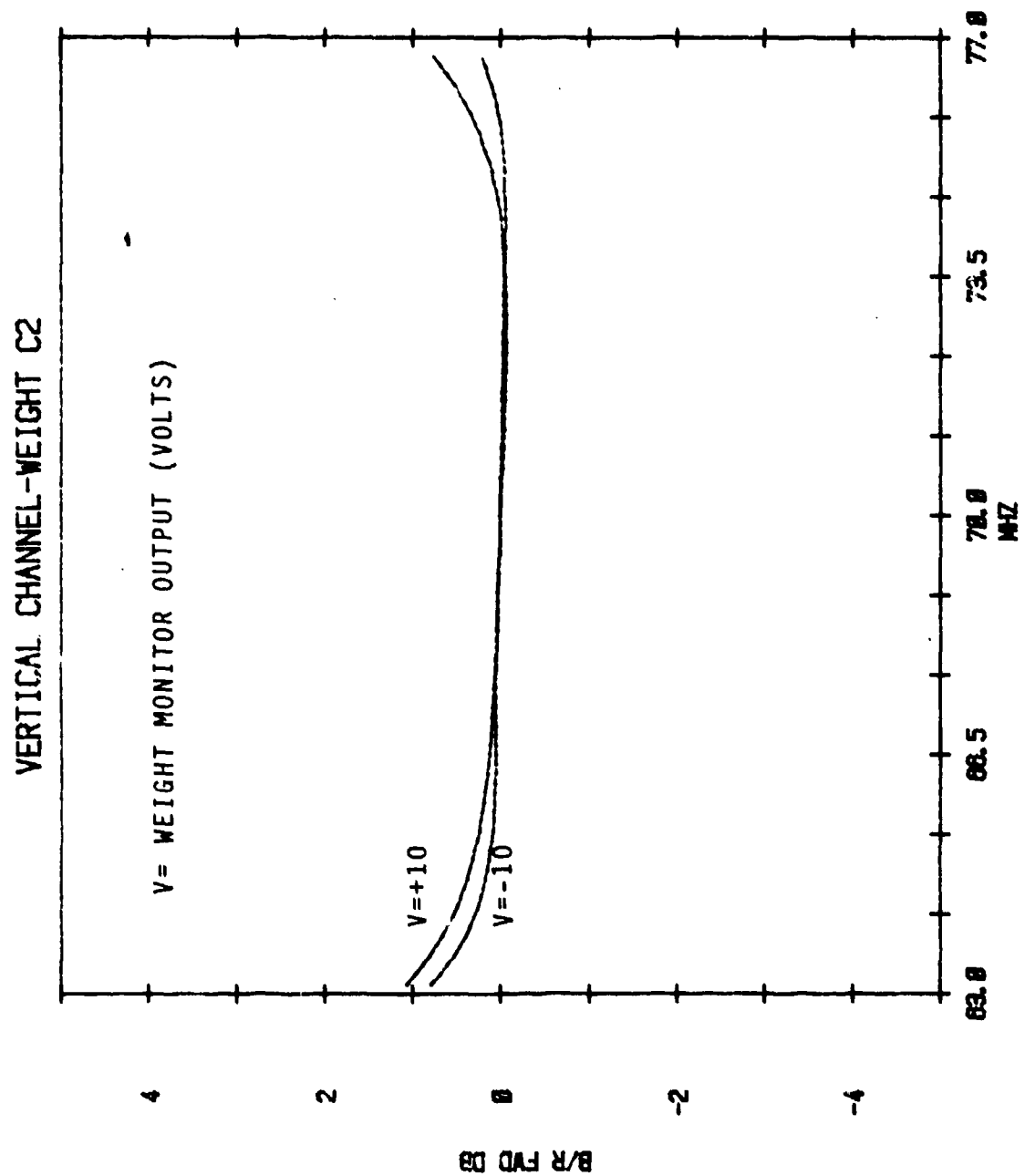


Figure 43. Effect of Weight C2 on Amplitude Response - Vertical Channel

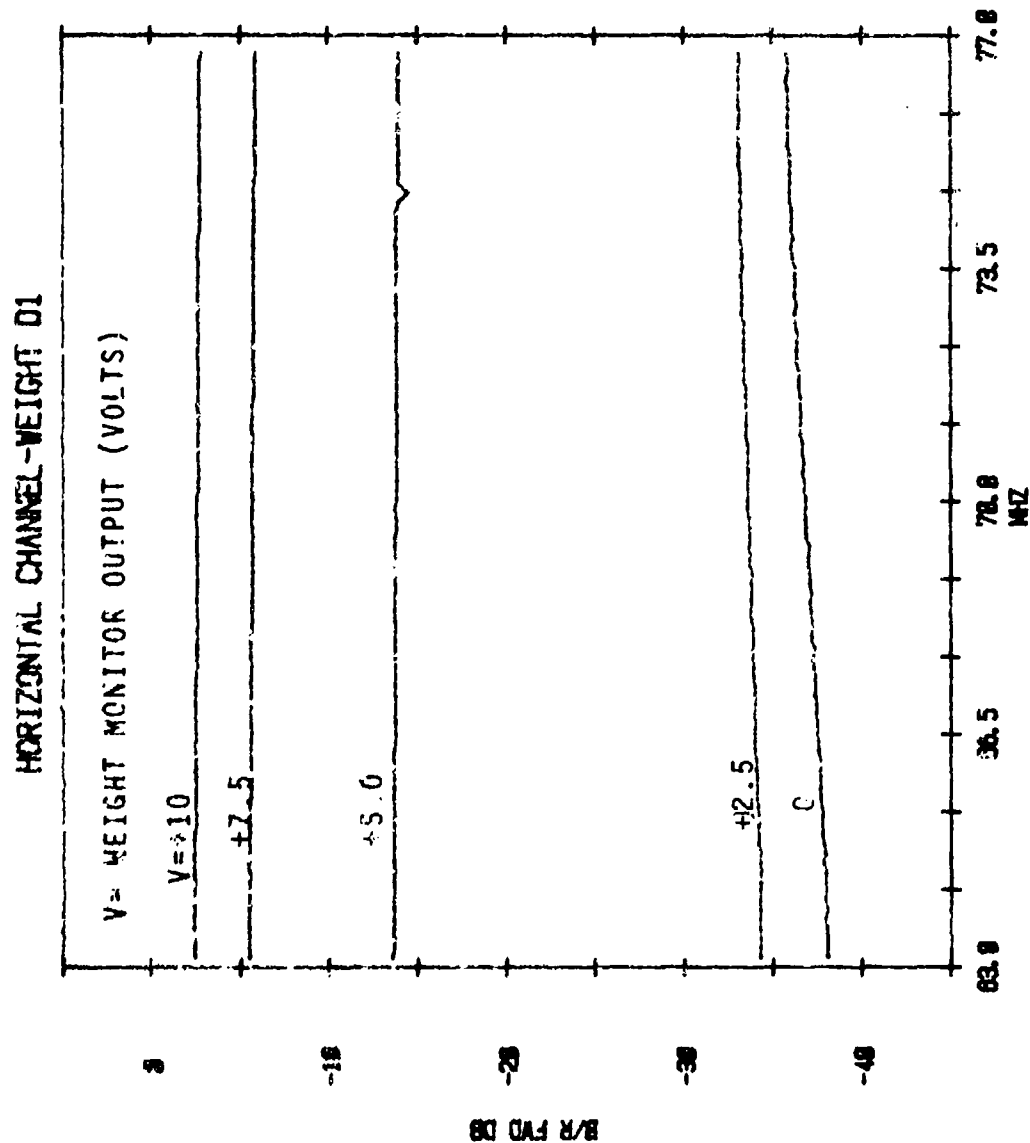


Figure 44. Attenuation of Weight D1 with Positive Control Voltages - Horizontal Channel

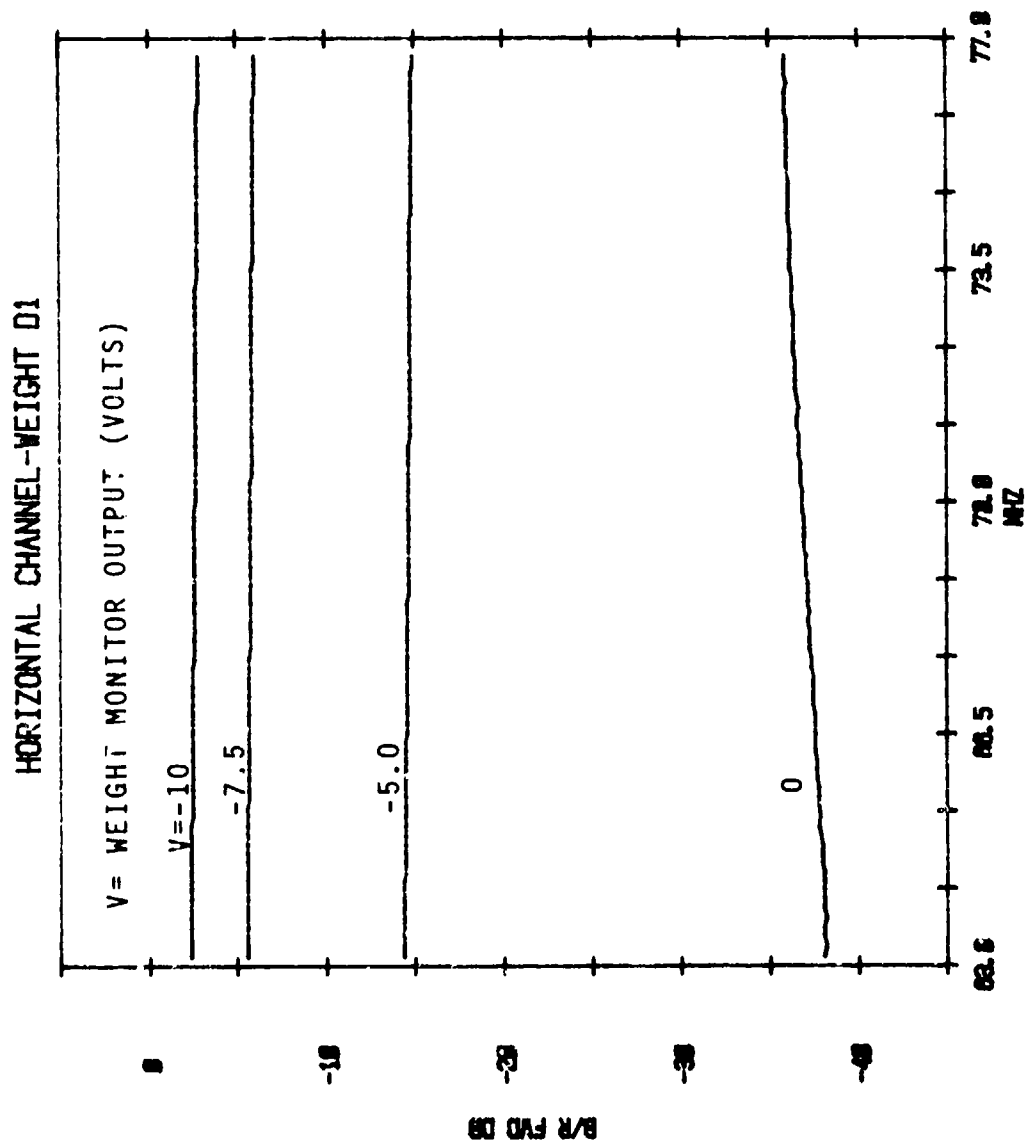


Figure 45. Attenuation of Weight D1 With Negative Control Voltages - Horizontal Channel

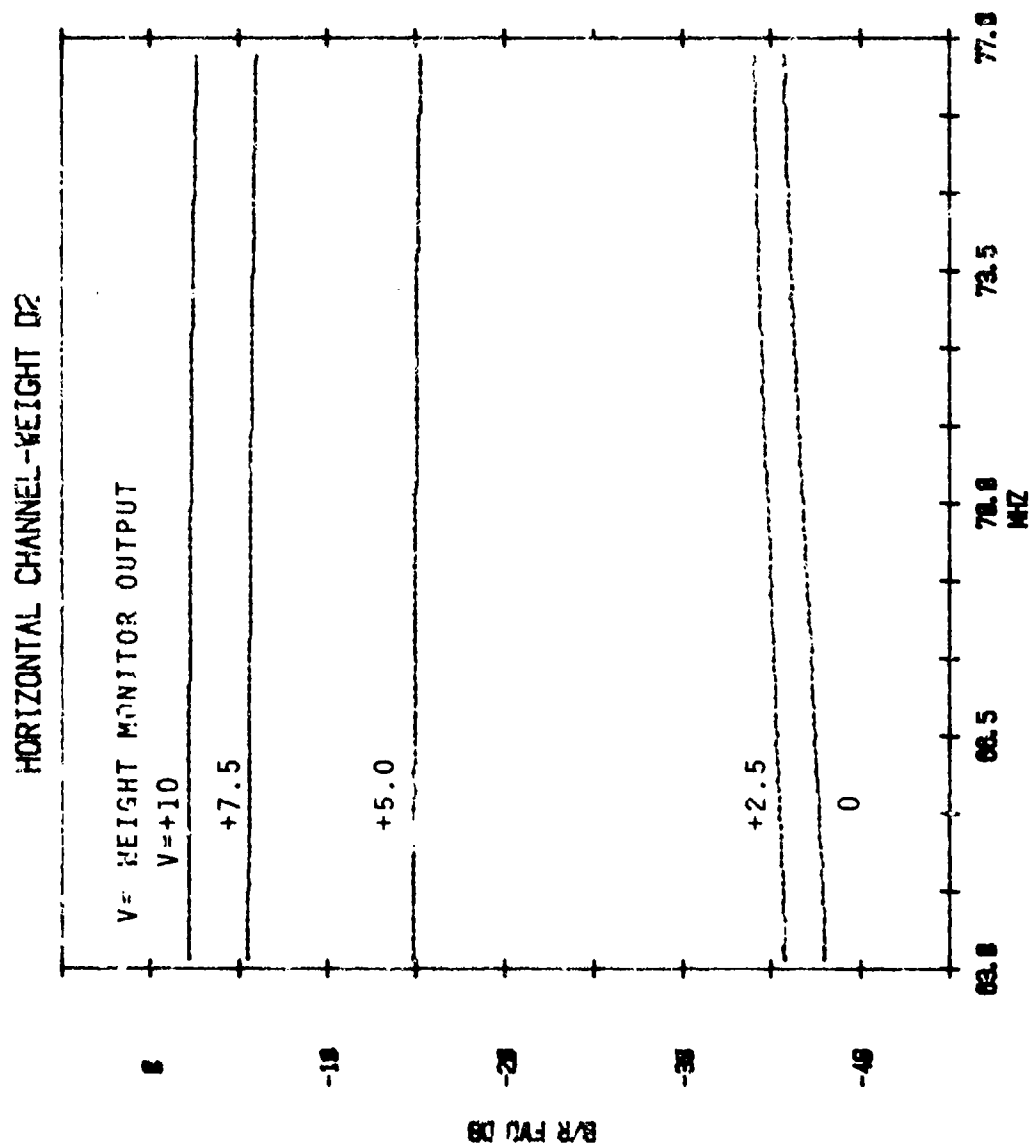


Figure 46. Attenuation of Weight D2 with Positive Control Voltages - Horizontal Channel

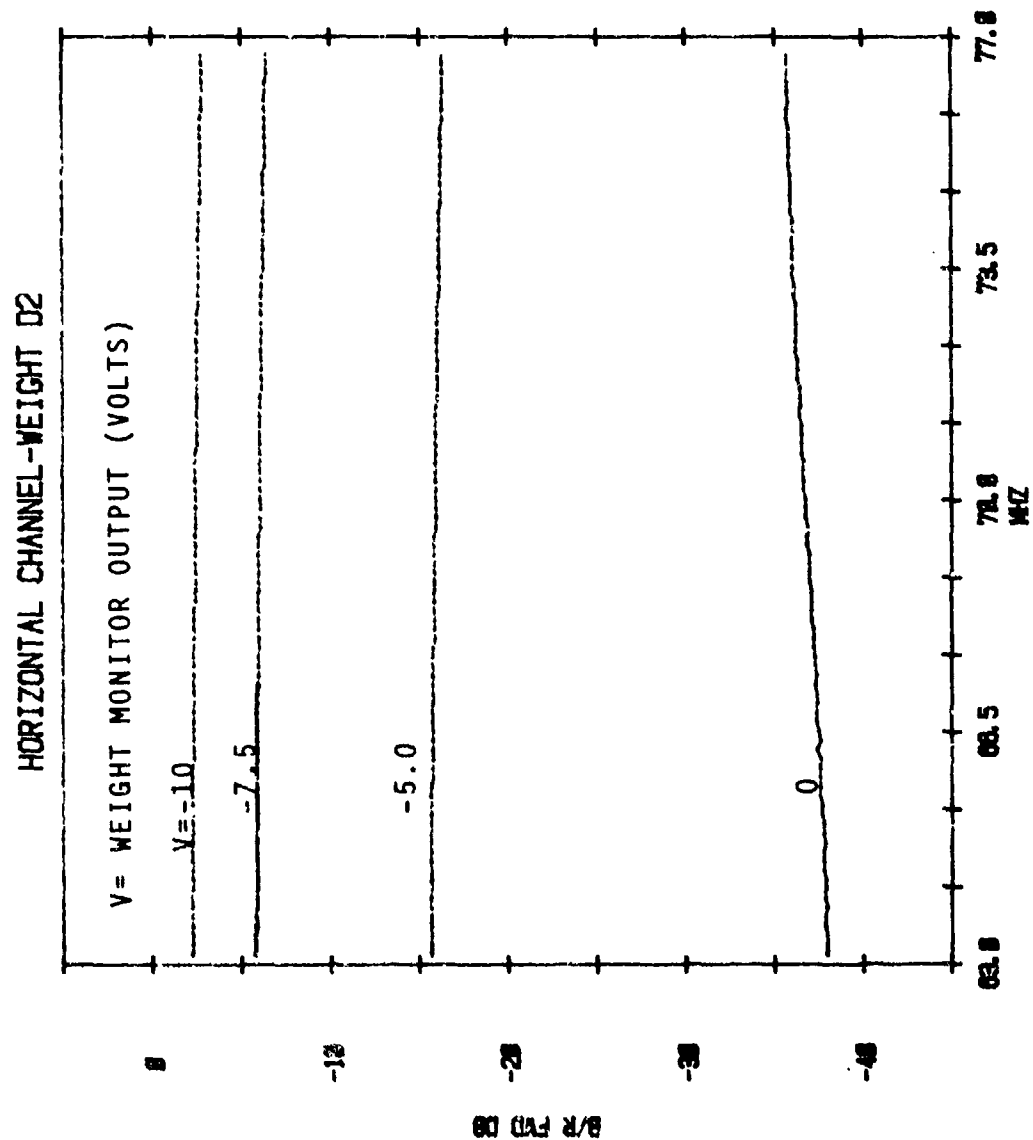


Figure 47. Attenuation of Weight D2 with Negative Control Voltages - Horizontal Channel

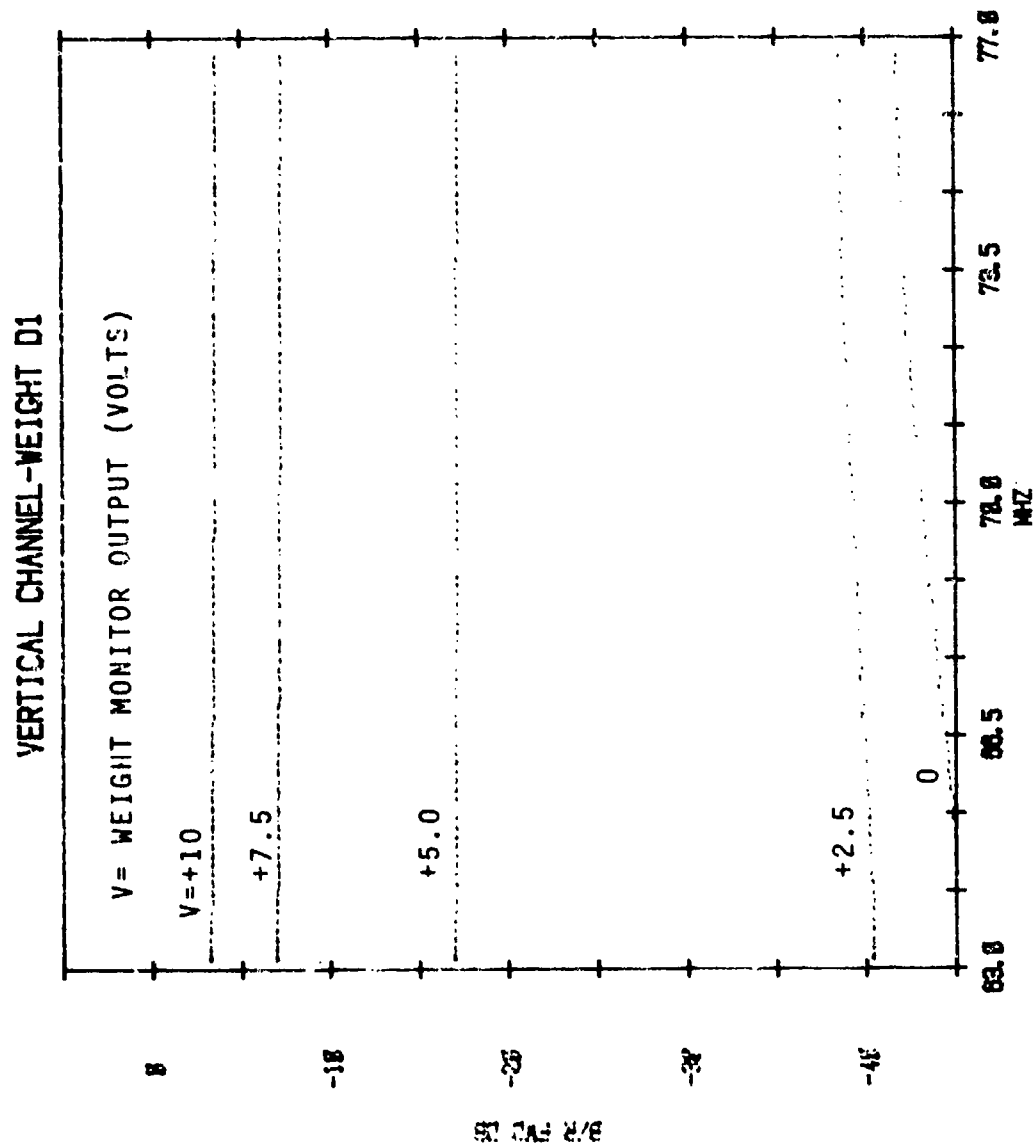


Figure 48. Attenuation of Weight D1 with Positive Control Voltages - Vertical Channel

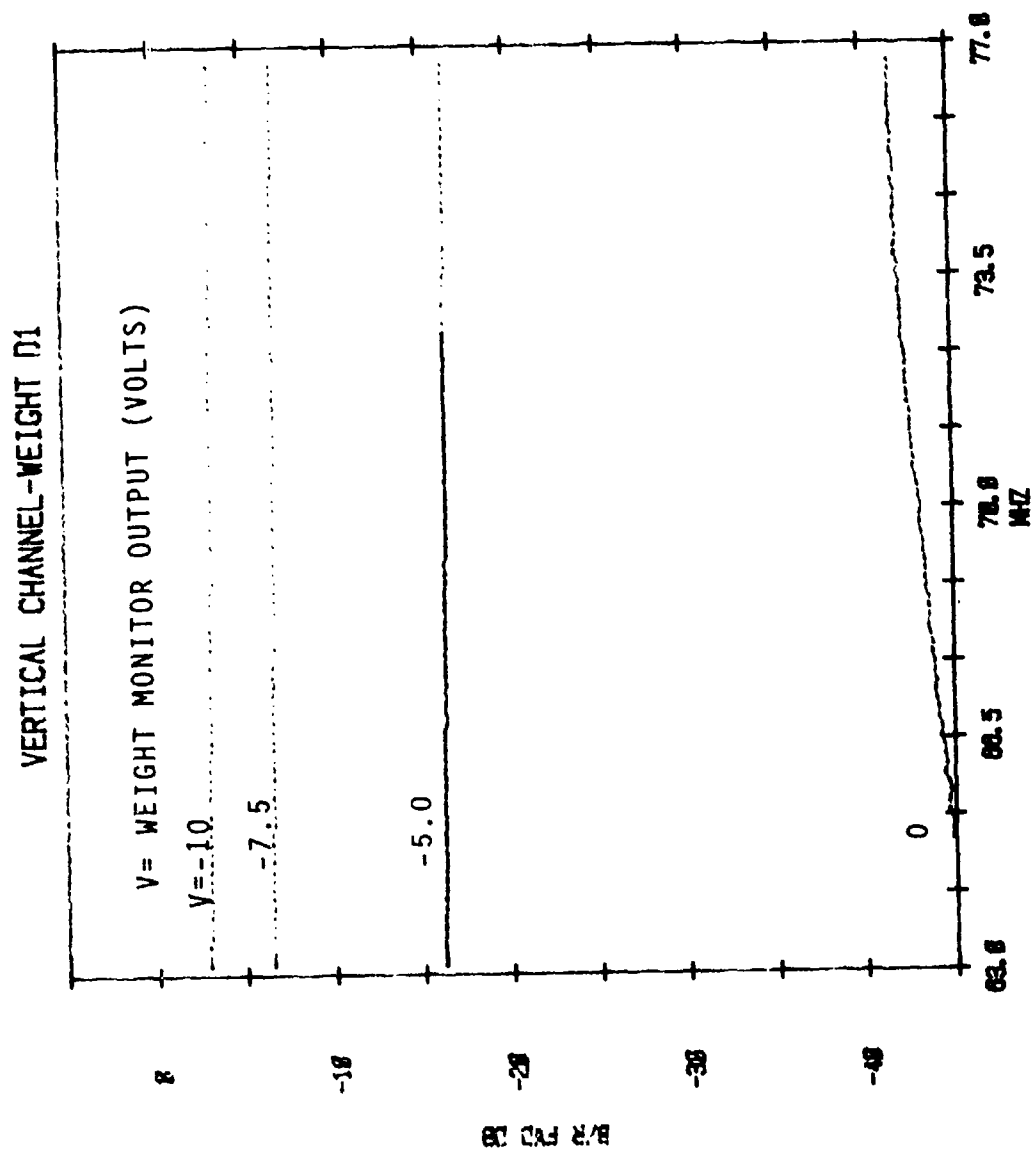


Figure 49. Attenuation of Weight D1 with Negative Control Voltages - Vertical Channel



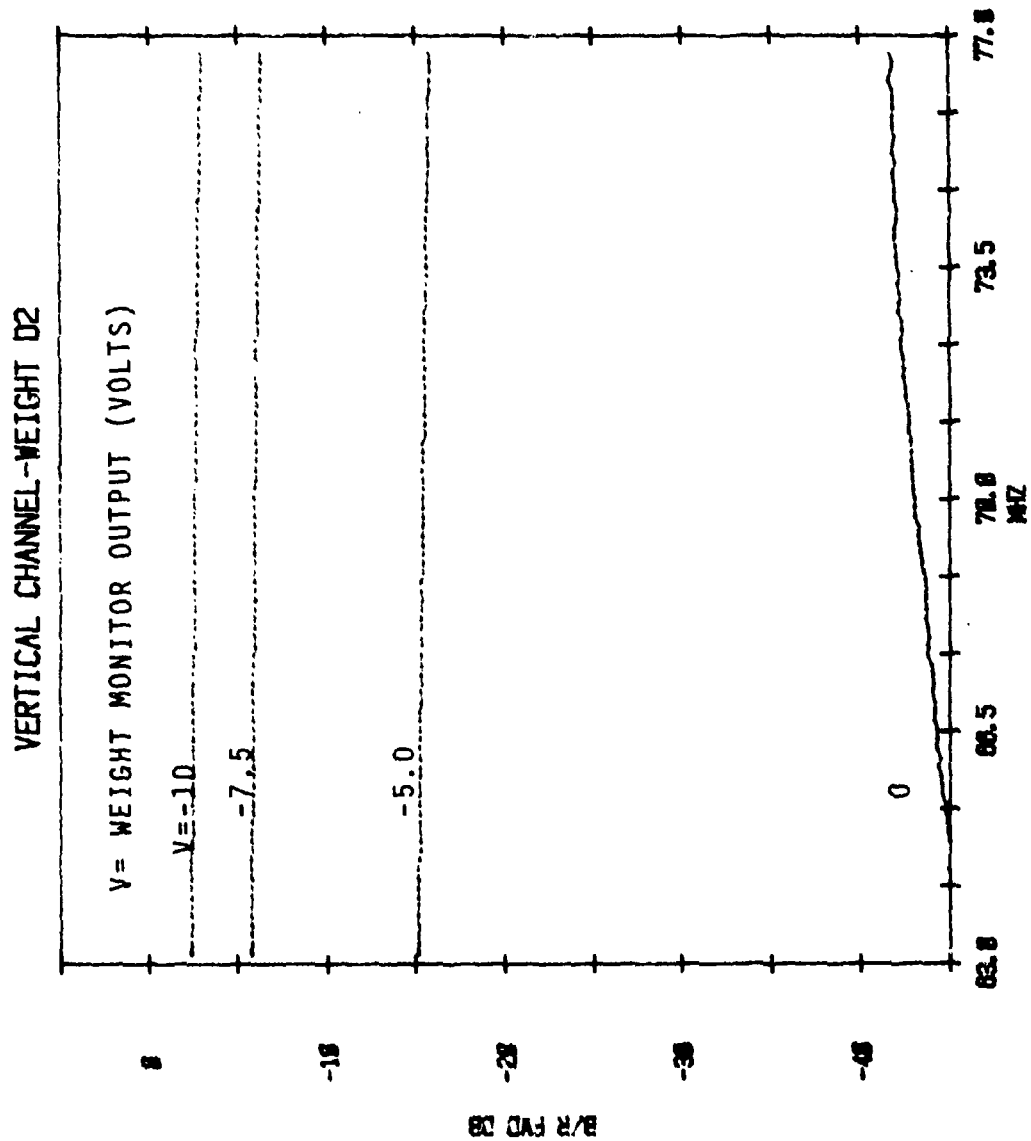


Figure 51. Attenuation of Weight D2 with Negative Control Voltages - Vertical Channel

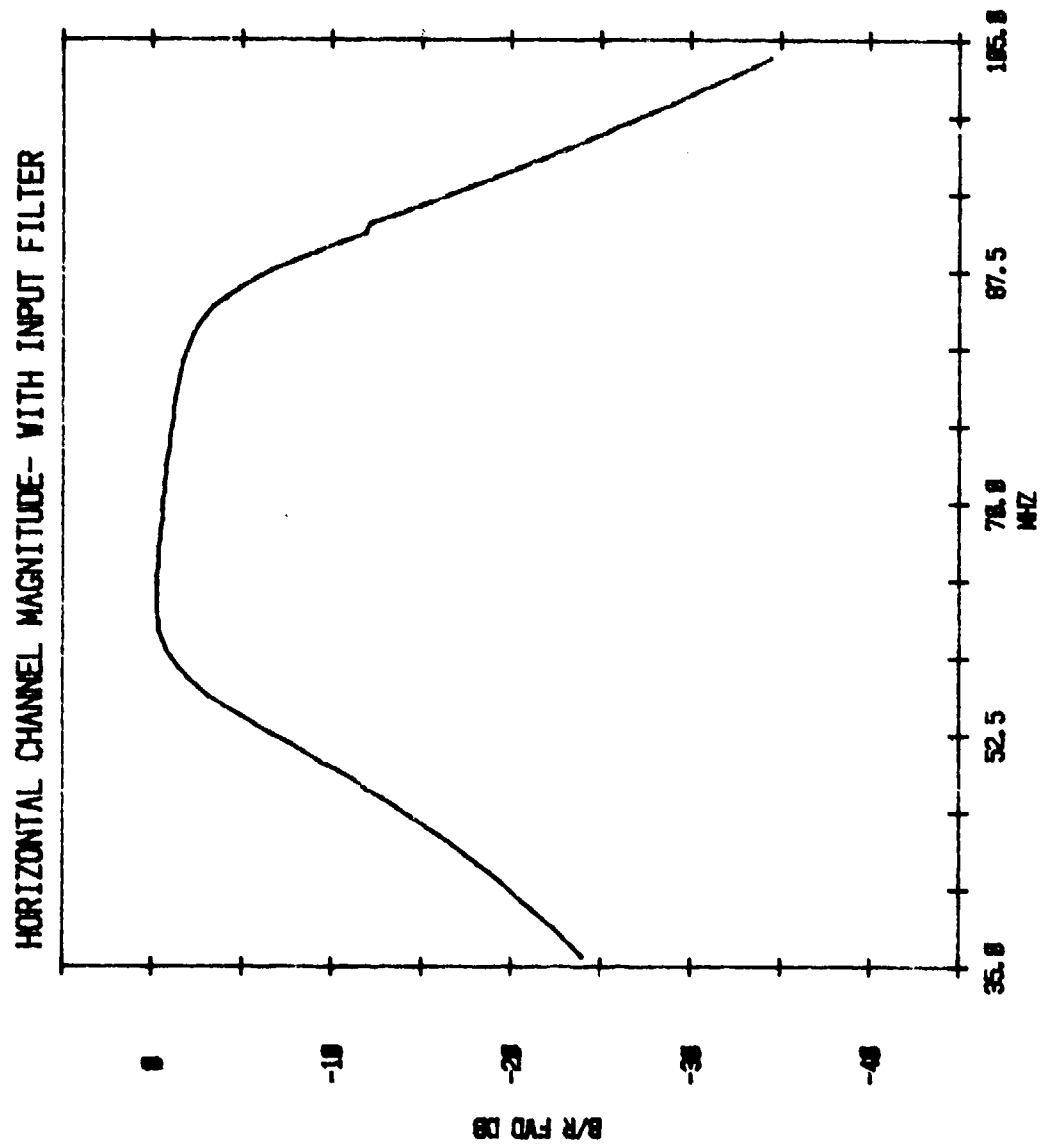


Figure 52. Horizontal Channel Amplitude Response  
With Input Filter (35 MHz-105 MHz)

produced by the notch filters in the equalizer. The input filter supplies more than 24 dB of attenuation at 34 MHz and more than 35 dB at 105 MHz. The in-band amplitude slope induced by the filter is shown in greater detail in Figure 53. The slope is approximately 0.5 dB from 63 to 77 MHz. Insertion loss at 70 MHz about 0.5 dB. The Horizontal Channel delay with input is given in Figure 54. The delay is approximately 105 ns. The delay relative to that at 70 MHz is shown in greater detail in Figure 55. Removing the input filter we obtain the amplitude response in Figure 56. The slope decreased and mid-band gain is +0.5 dB. The input to output delay as seen in Figure 57 is close to 75 ns without input filter. The group delay normalized to 70 MHz is somewhat flatter without the filter as shown in Figure 58.

The Vertical Channel amplitude response with filter is depicted in Figures 59 and 60. Delay characteristics with input filter are shown in Figures 61 and 62. Without input filter the Vertical Channel amplitude response is as in Figure 63. Delay characteristics without filter are shown in Figures 64 and 65. The Vertical Channel characteristics are closely matched to those of the Horizontal Channel.

#### 4.1.3 Performance Testing Results

The design objective for the CPIRE was operation with cross-polarization discrimination ratios (CPDR) from 5 dB to 40 dB. Optimization of the various CPIRE internal parameters for link usage requires a knowledge of actual cross-polarization interference dynamics. As information on this subject is limited, arbitrary decisions regarding CPIRE adjustments were made. For test purposes, the dither size,  $\Delta$ , was set such that the residual interference caused by the dither in each weight was -43 dB relative to the output signal power. Thus, with a complex weight pair operating in quadrature, the residual interference is approximately -40 dB, theoretically permitting operation to the design goal of a CPDR of 40 dB. Tests revealed the limiting performance factor to be control loop jitter. Integrator time constants were then chosen for maximum loop bandwidth allowing for a margin of stability. Filter bandwidths and the timing parameters of dwell and wait time were chosen for optimum bit-error rate (BER) performance with Broadband II Modem in the 2 B/Hz mode. Although no

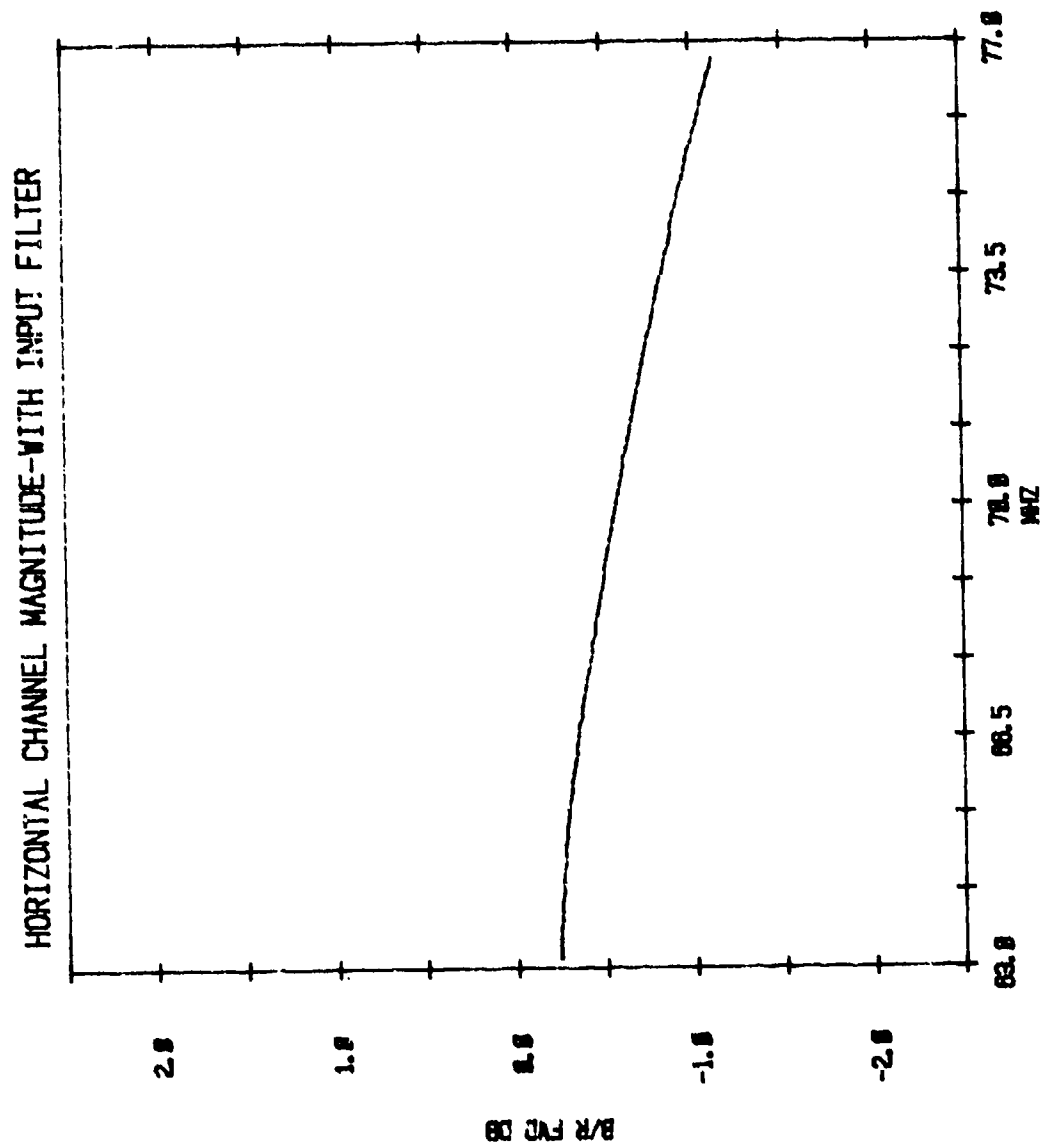


Figure 53. Horizontal Channel Amplitude Response  
With Input Filter (63 MHz-77 MHz)

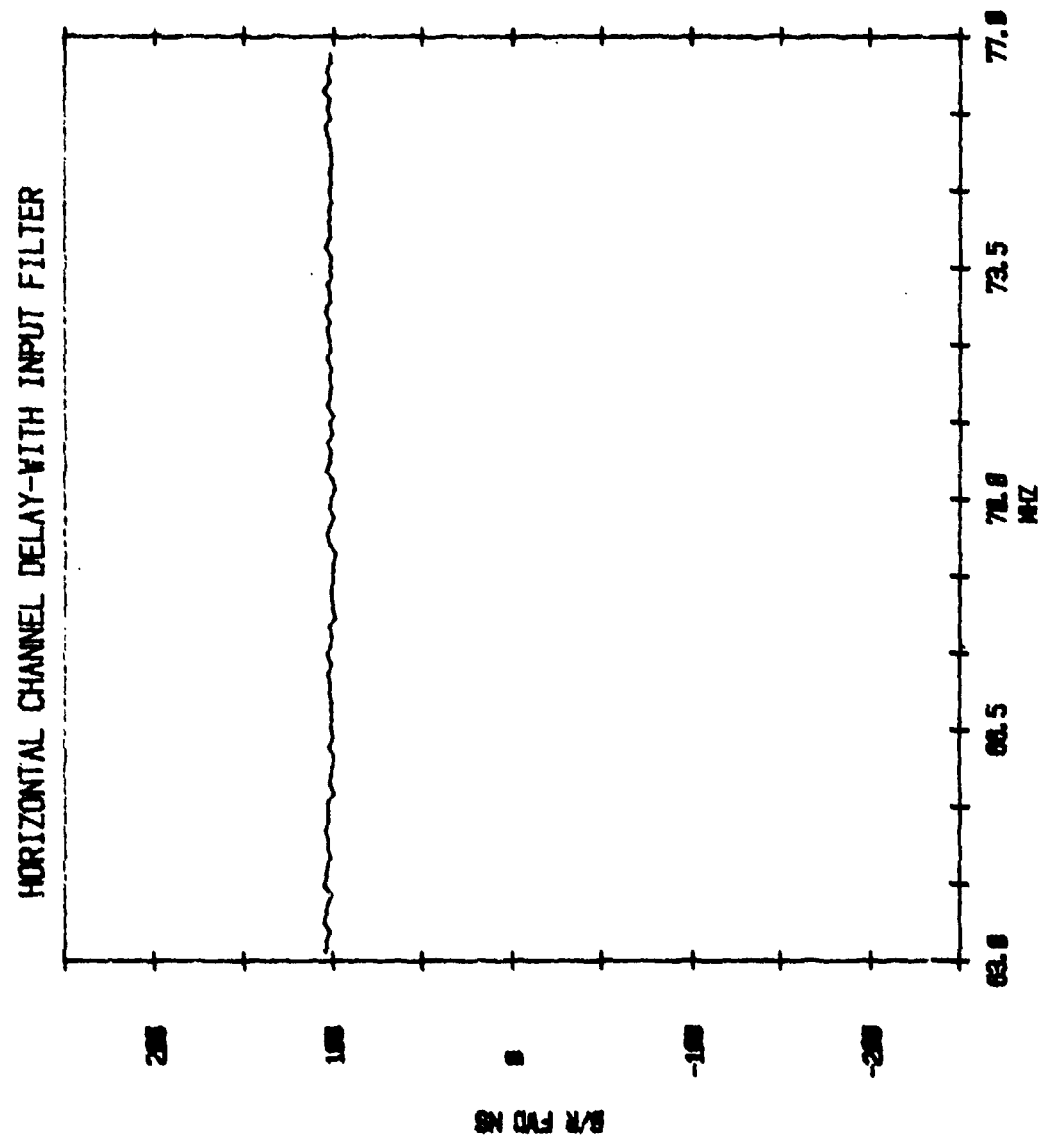


Figure 54. Horizontal Channel Delay With Input Filter

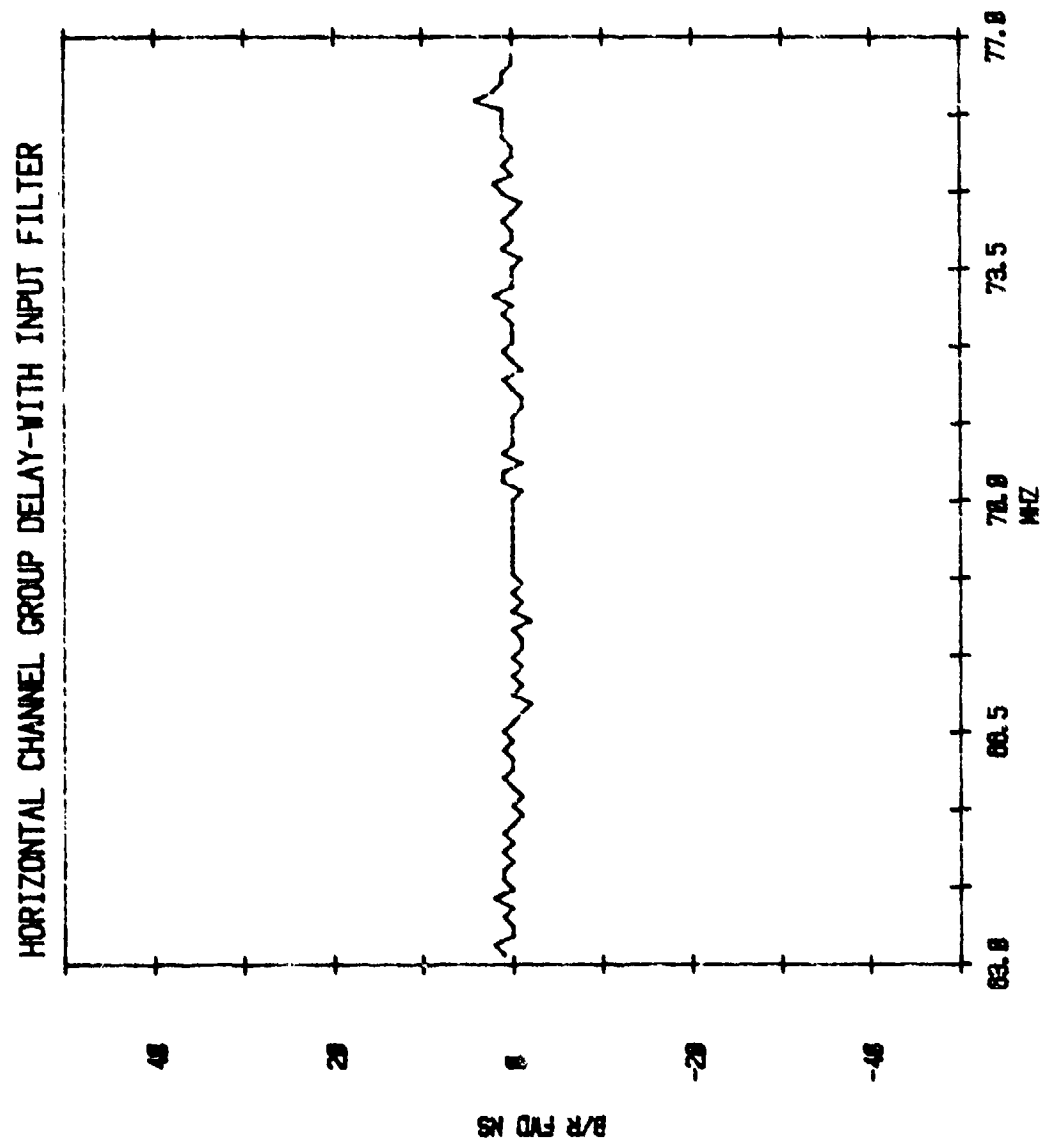


Figure 55. Horizontal Channel Group Delay  
With Input Filter

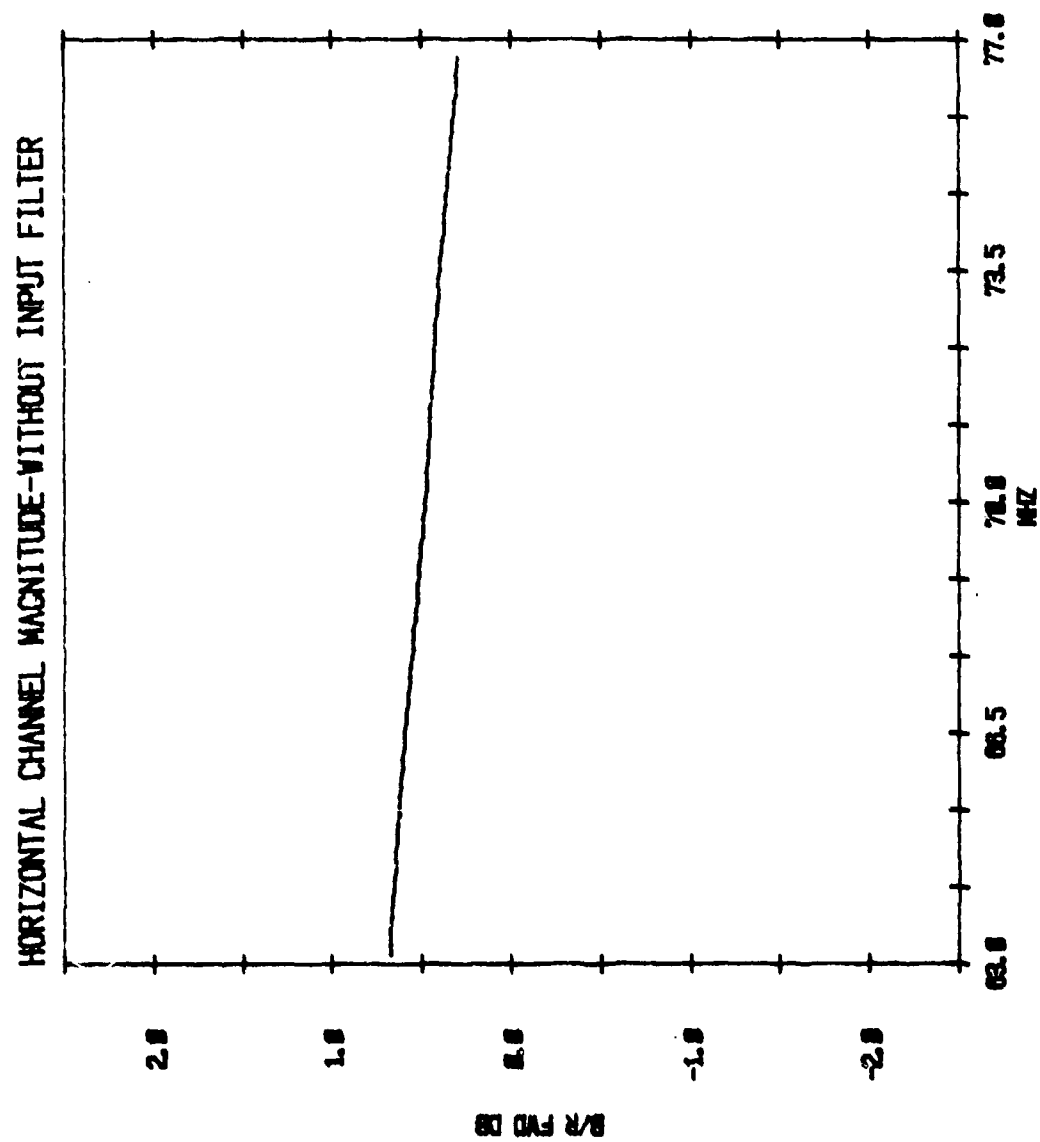


Figure 56. Horizontal Channel Amplitude Response Without Input Filter

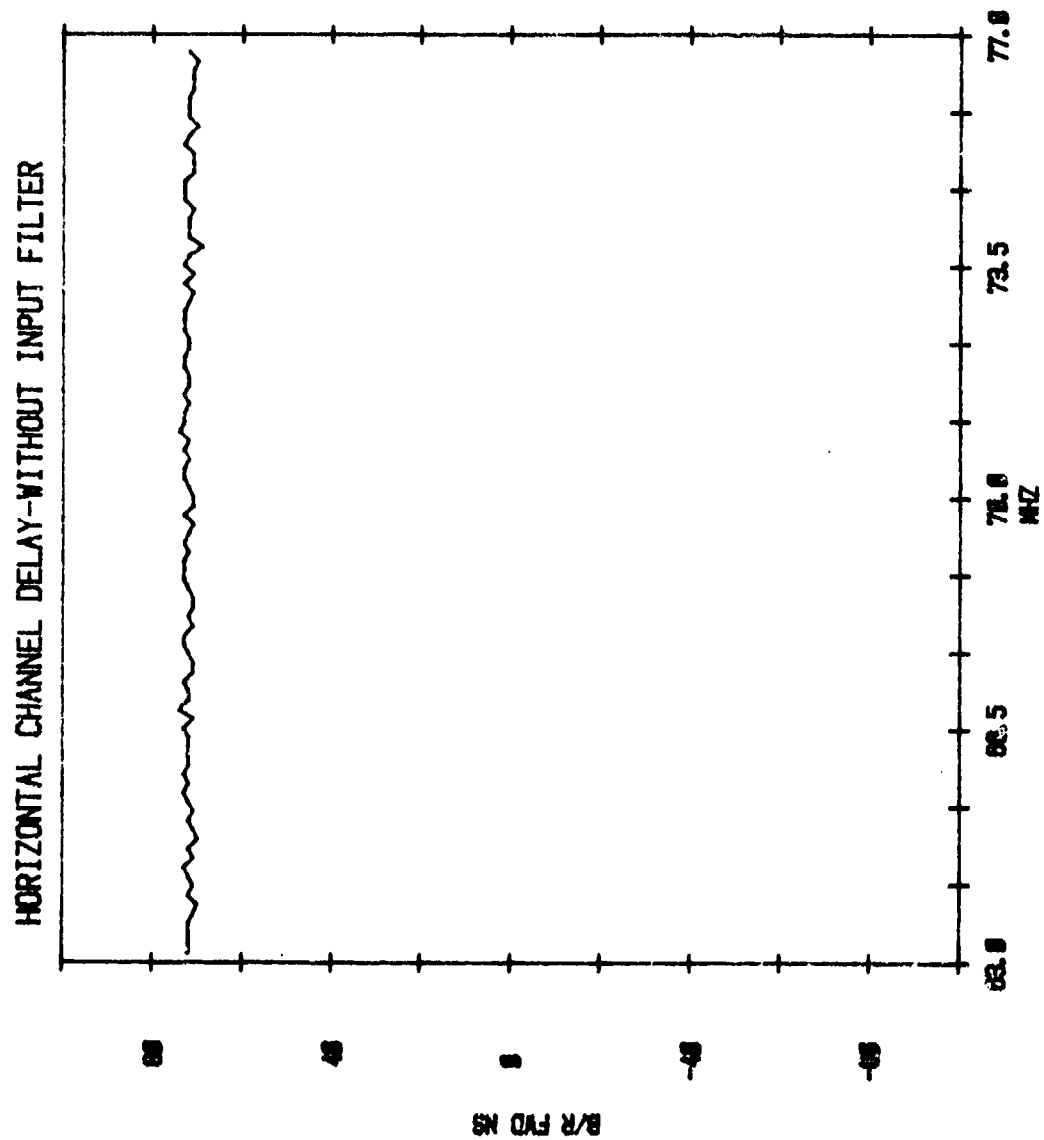


Figure 57. Horizontal Channel Delay Without Input Filter

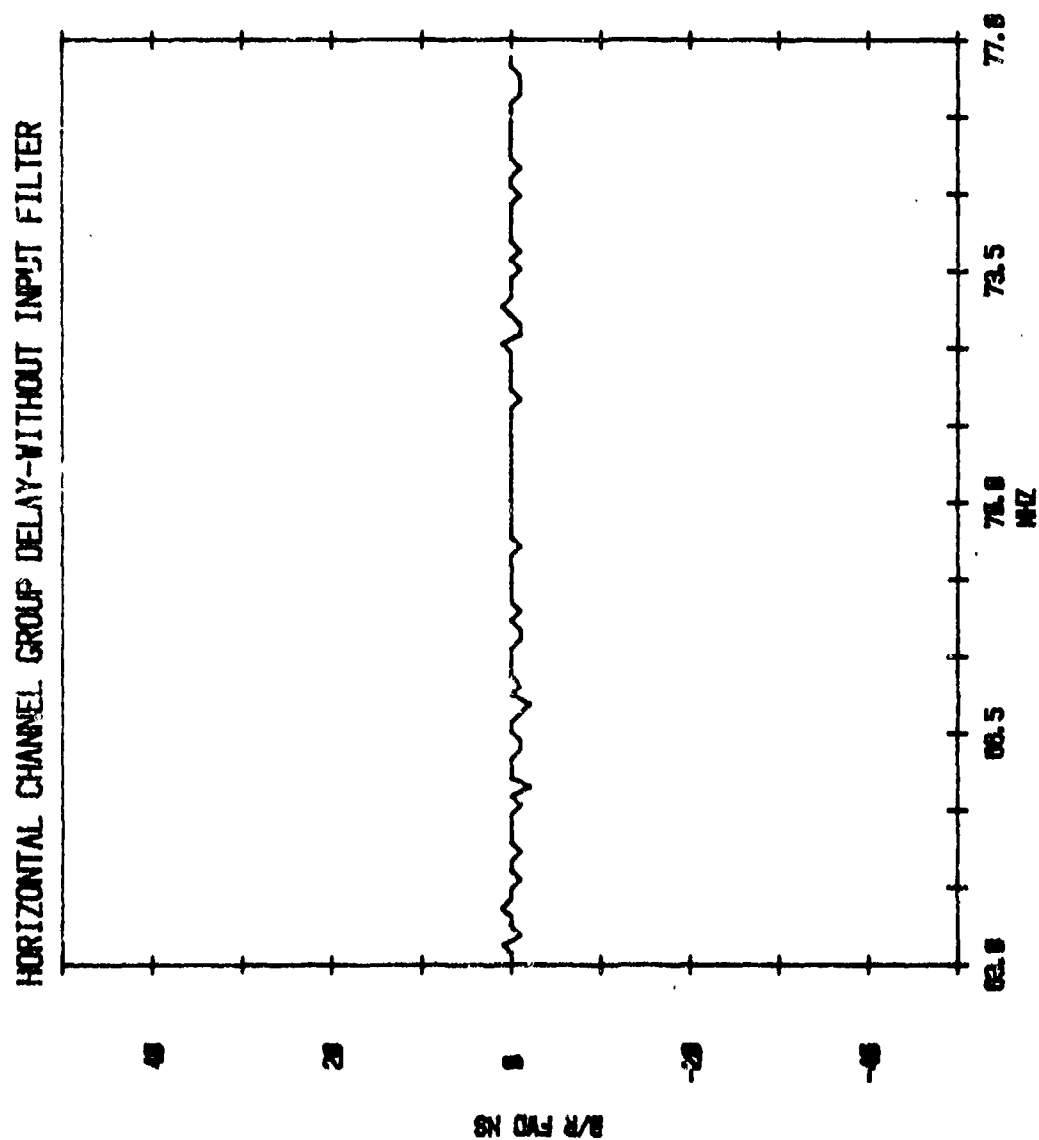


Figure 58. Horizontal Channel Group Delay Without Input Filter

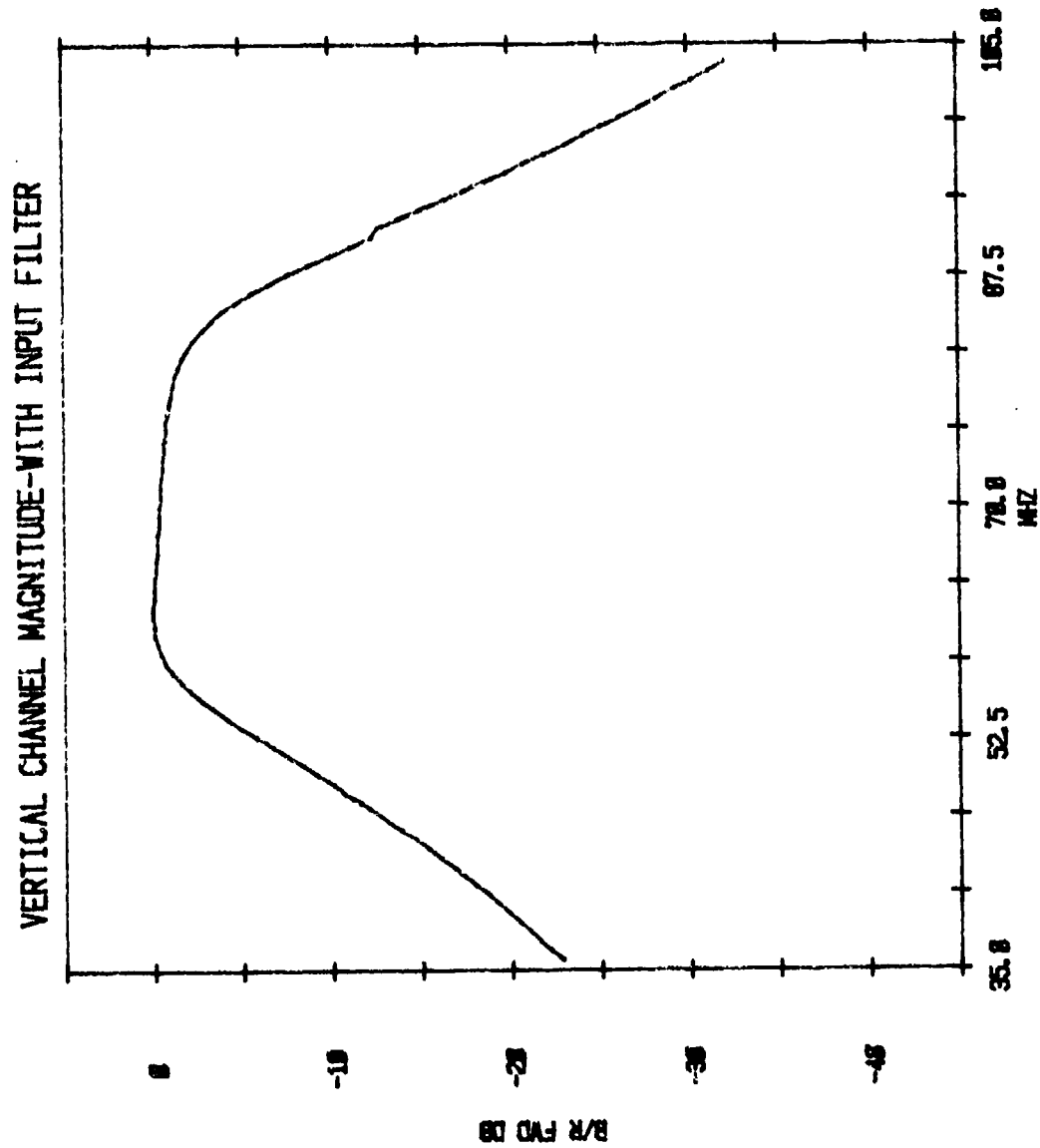


Figure 59. Vertical Channel Amplitude Response  
With Input Filter (35 MHz-105 MHz)

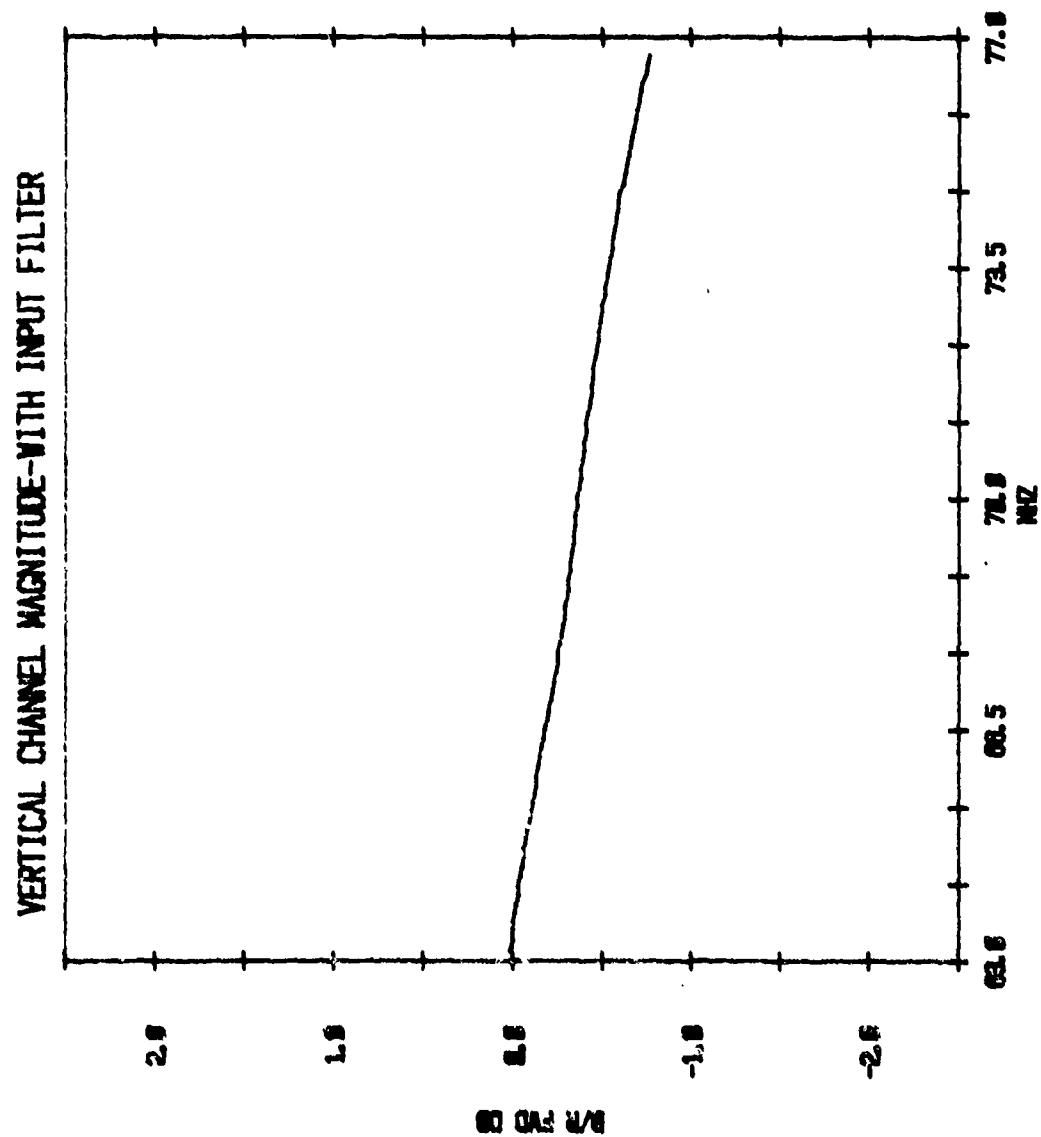


Figure 60. Vertical Channel Amplitude Response  
With Input Filter (63 MHz-77 MHz)

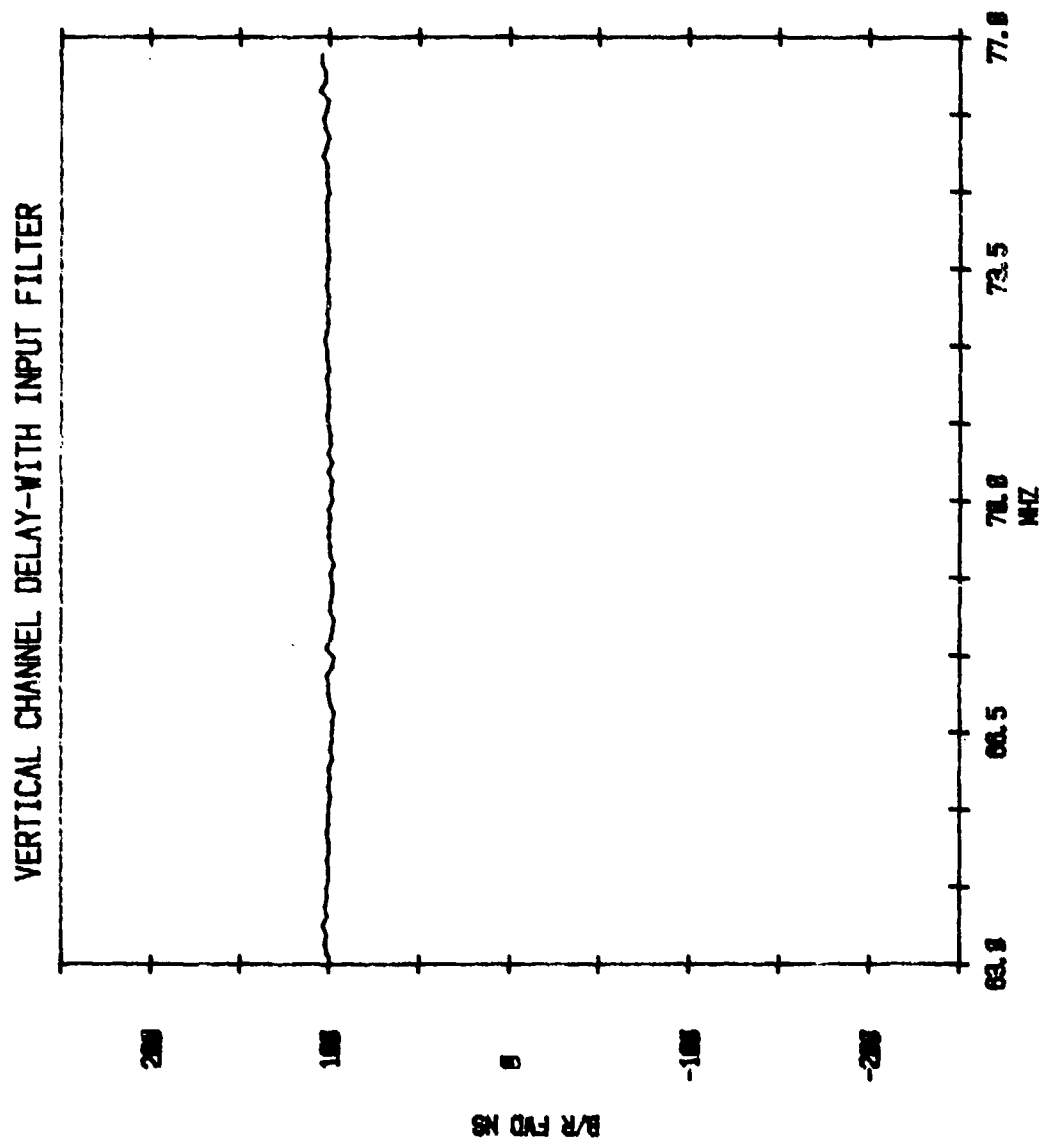


Figure 61. Vertical Channel Delay With Input Filter

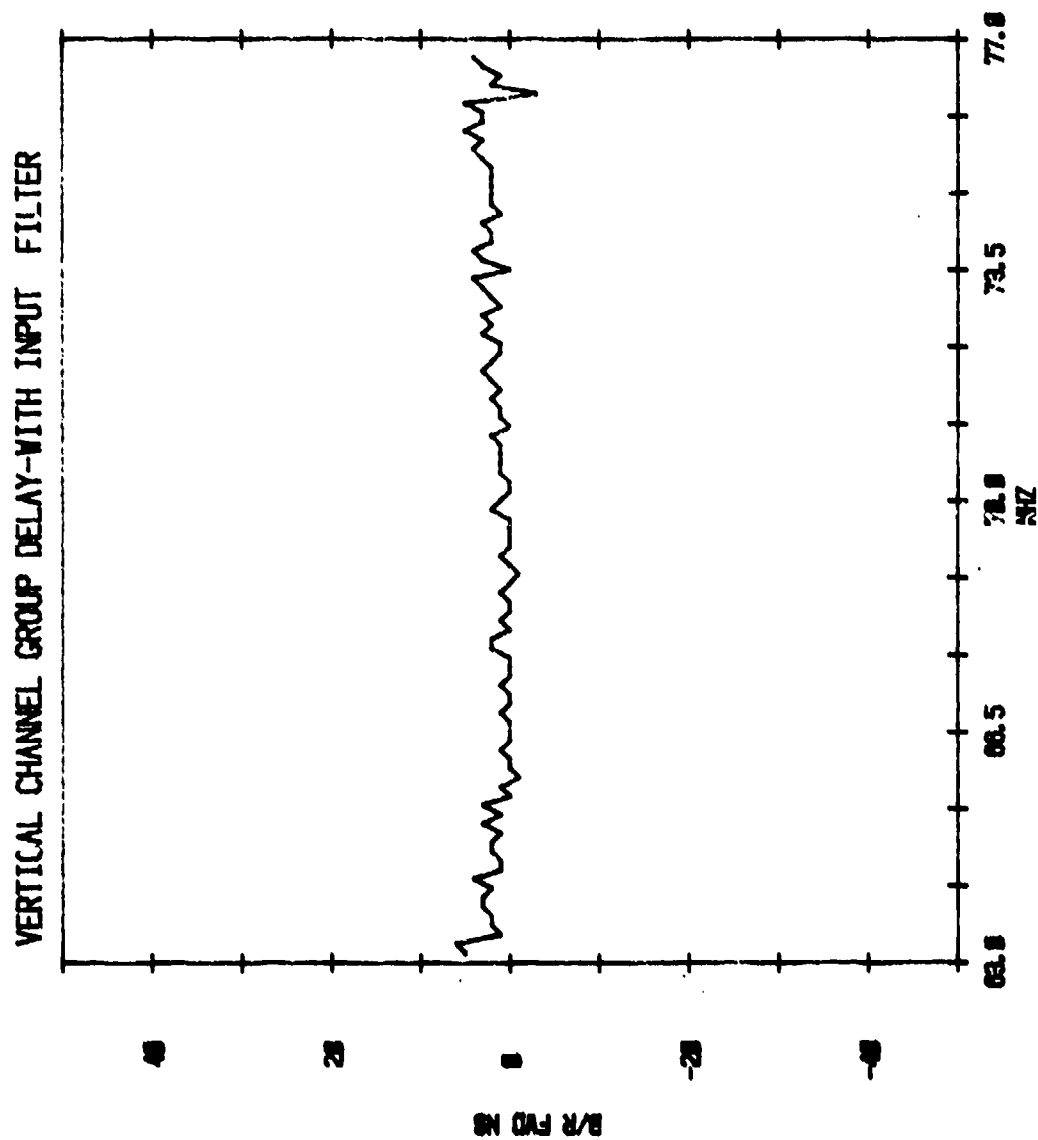


Figure 62. Vertical Channel Group Delay  
With Input Filter

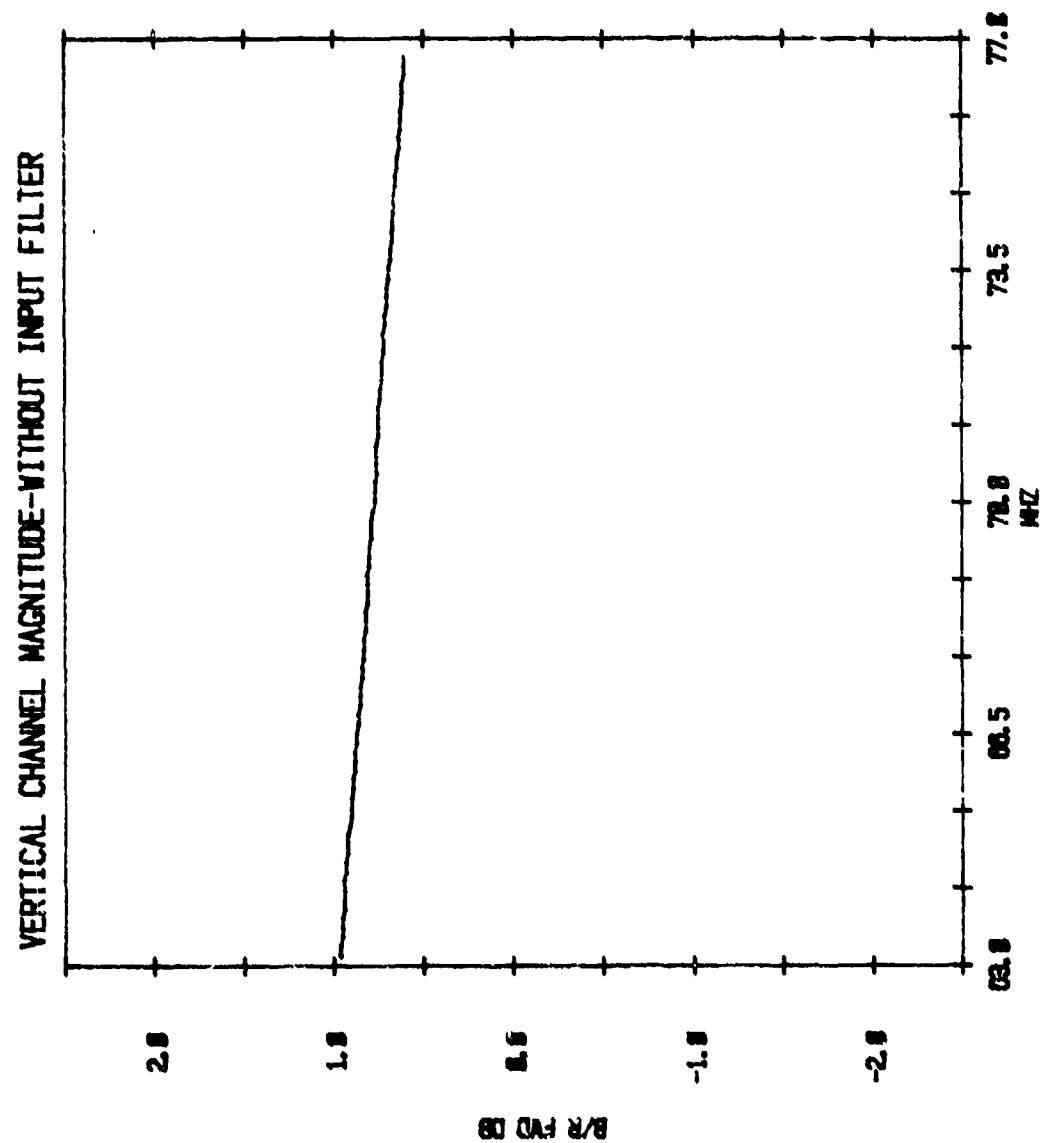


Figure 63. Vertical Channel Amplitude Response Without Input Filter

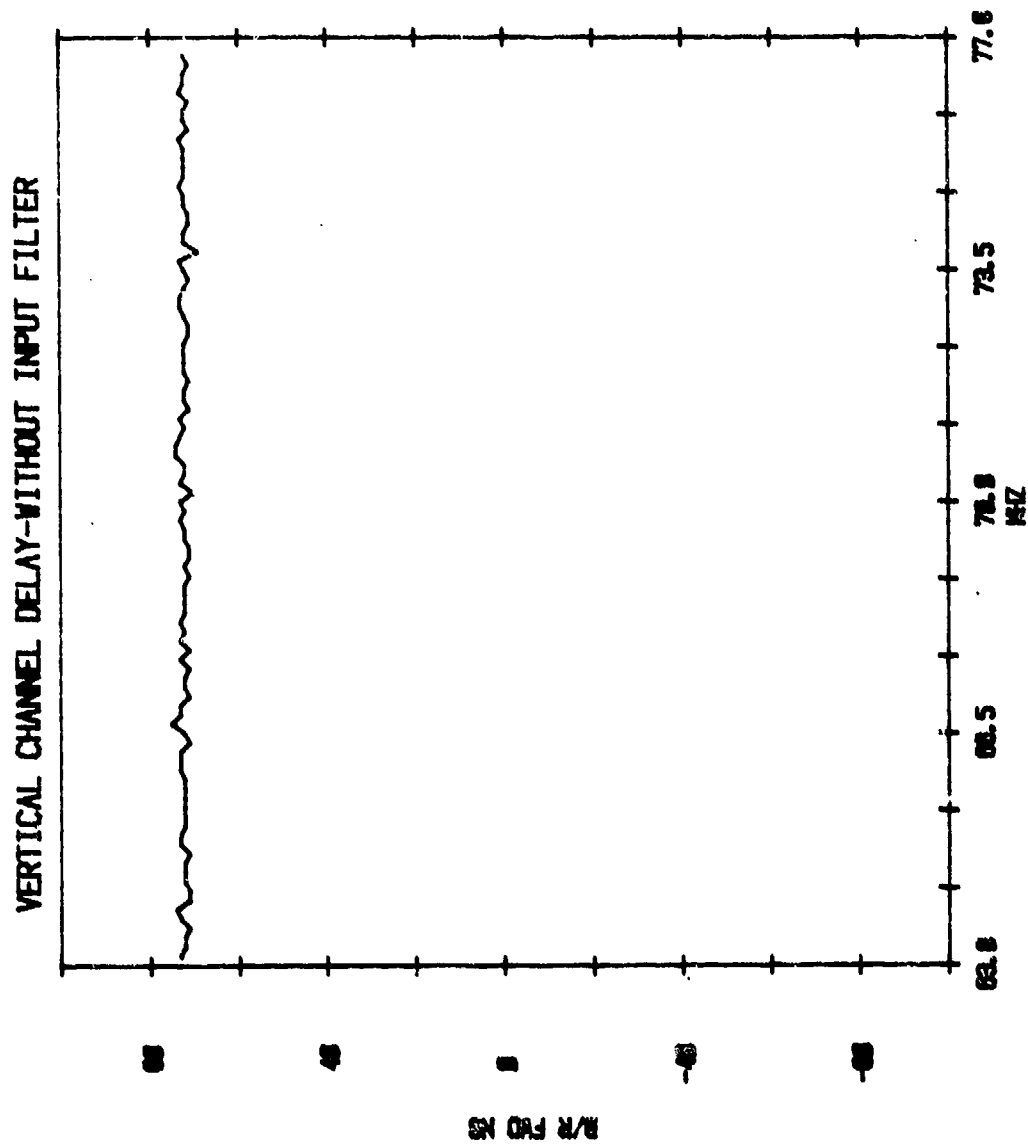


Figure 54. Vertical Channel Delay Without Input Filter

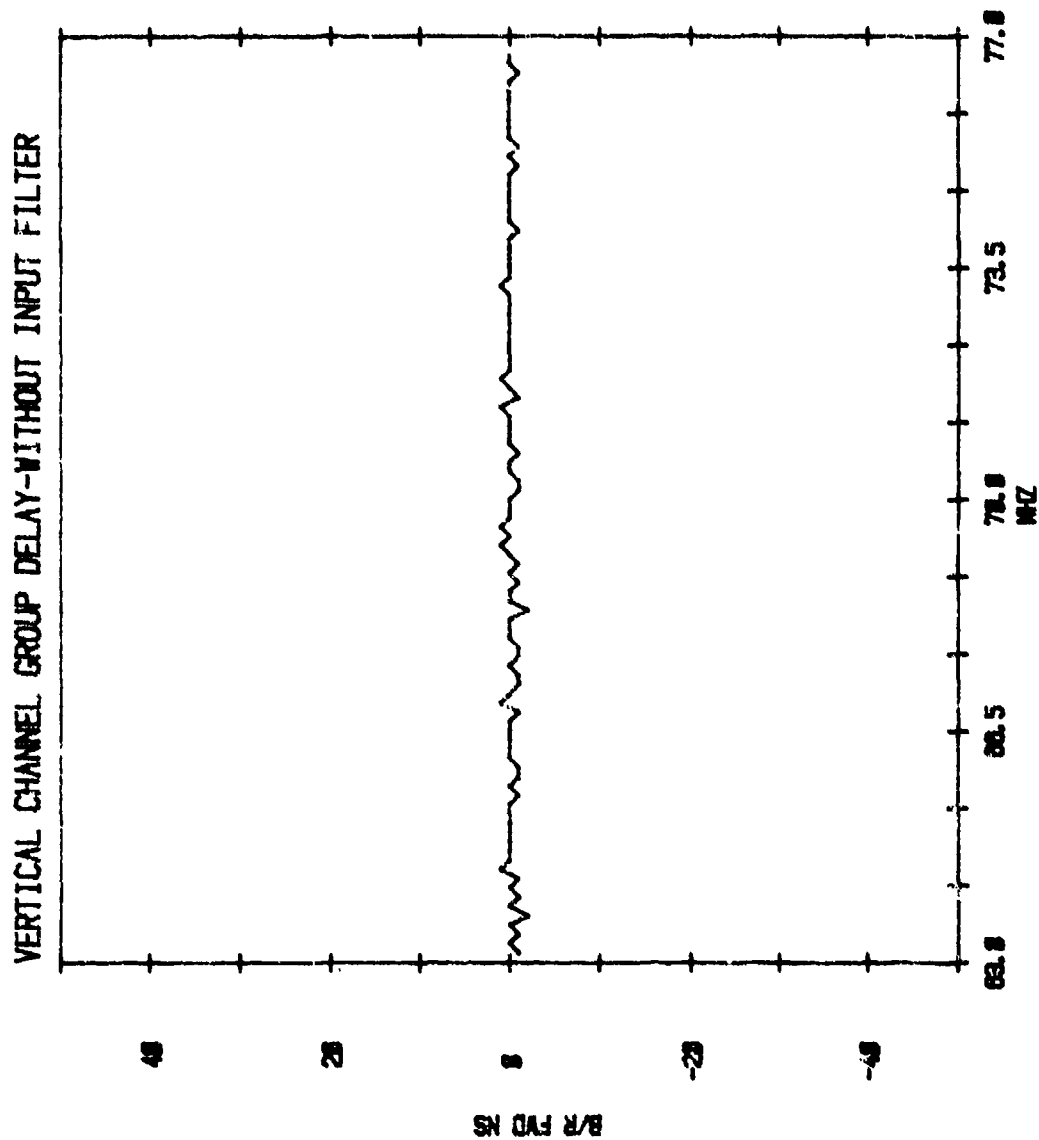


Figure 55. Vertical Channel Group Delay  
Without Input Filter

attempt was made to optimize 1 B/Hz performance, a complete series of tests were run in this mode as well. Tests revealed that optimum timing parameters for the two channels differed slightly. As independent timing control was not provided, the parameters were adjusted for best average performance between channels.

The test configuration utilizing the Decorrelator (described in Appendix B) to simulate Horizontal and Vertical channels from a single Broadband Modulator is treated in detail in Appendix C. A discussion of theoretically achievable signal to noise ratio (S/N) improvement is given in Appendix D. The improvement possible is a function of CPDR and phase angle of the crosstalk. Even with perfect cancellation of the cross-pole component, variations of several dB in performance are possible, depending on the phase angle of the interference. This effect is minimized for small amounts of cross pole. The test configuration chosen for in-plant tests differs from a real radio installation in that the noise is added to the modulator output before the second channel is synthesized and the cross pole introduced. In reality, the noise would be generated in the radio receiver inputs after the cross-pole mechanism. Although chosen for simplicity, the in-plant configuration has the advantage of minimizing cross-pole angle effects. Also, for consistency in measurement, the test setup, including interconnecting cables, remained unchanged throughout in-plant testing.

BER measurement tests were run under a variety of conditions, as described below. Measurements were duplicated for both channels and for 2 B/Hz and 1 B/Hz modem operation.

#### 4.1.3.1 Two B/Hz Test Results

To obtain baseline performance data, the modulator and demodulator were connected through the test fixtures at 70 MHz without the CPIRE. Without cross-polarization interference, the solid curve of Figure 66 was obtained. This represents the best obtainable performance. Then, various amounts of interference were introduced. The cross-pole mechanism simulated was nondispersive and symmetrical; i.e., the same crosstalk on both channels. BER curves for CPDR's of 5 to 30 dB are shown in the figure.

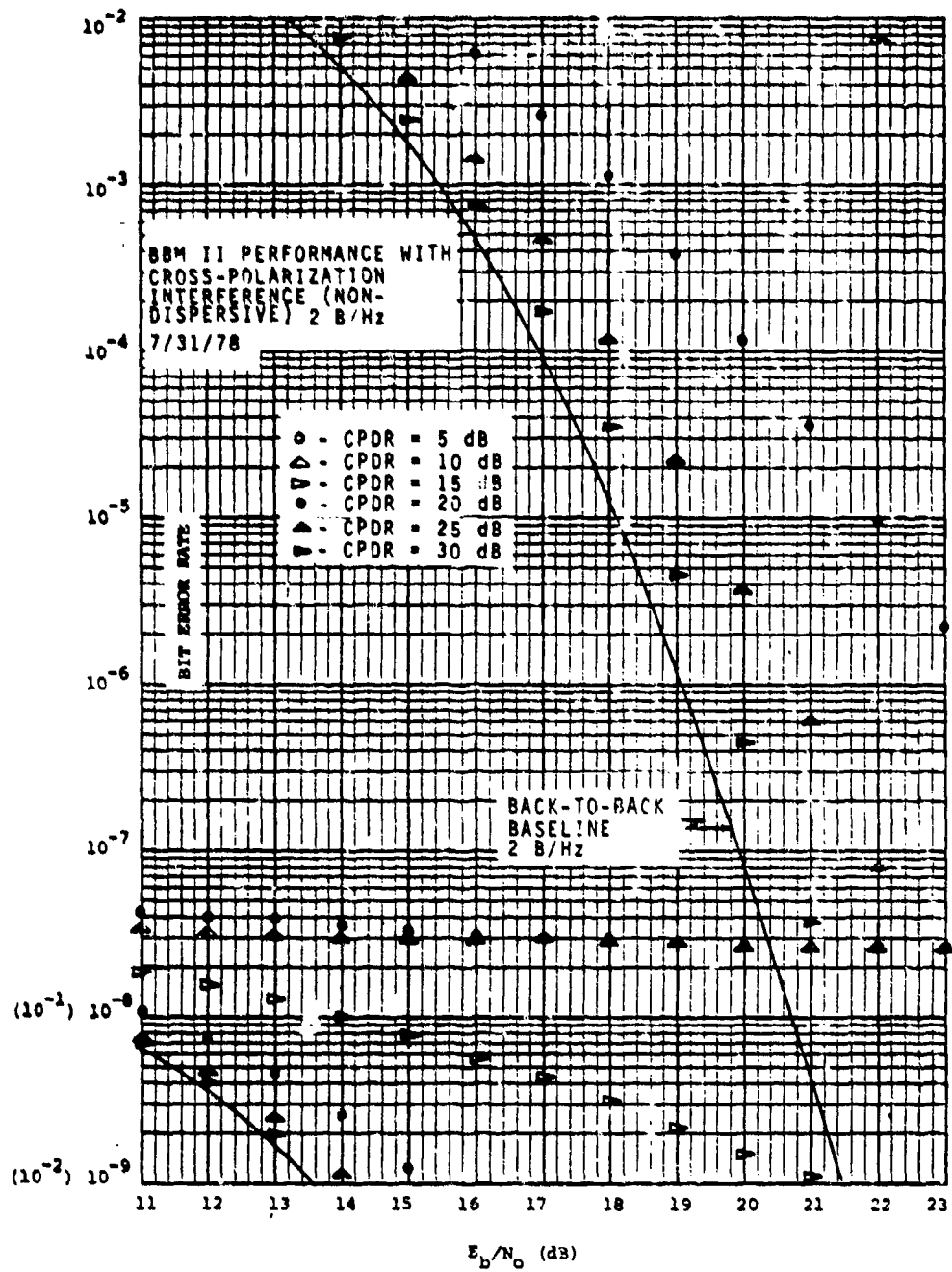


Figure 66. BBM II 2 B/Hz Performance With Cross-Polarization Interference

Next, the CPIRE without input filter was introduced into the signal path. Referring to Figure 67 for the Horizontal Channel, it may be seen that the CPIRE in the manual mode with all weights set to zero degrades the baseline performance less than 0.3 dB in the vicinity of a  $10^{-7}$  BER. Without interference and the CPIRE in the automatic mode, the degradation is perhaps 0.4 dB from the baseline curve. The slight increase is a result of the dither applied to the weights. With cross-polarization interference down 10 dB from the signal on both channels, the degradation is approximately 0.5 dB at a  $1 \times 10^{-7}$  BER. With a worst-case CPDR of 5 dB, the BER is within 0.8 dB of the baseline at  $1 \times 10^{-7}$  for the test setup used. As explained in Appendix D, performance becomes increasingly angle dependent with decreasing CPDR. Thus, the curve taken at a CPDR of 5 dB is representative of the test configuration used. With CPDR's of 10 dB or more, the performance shown in Figure 67 should be fairly representative of expected performance over an actual radio link. Figure 68 shows the measured performance of the Vertical Channel. Bit error rates are slightly lower than on the Horizontal Channel for CPDR's of 10 dB or higher, and slightly higher at a CPDR of 5 dB.

To simulate dispersive cross-polarization interference, a test filter was introduced into the signal path of the opposite channel from that being measured. A delay line in the channel being measured compensated for the filter's delay. Under these conditions, the CPIRE must equalize out the test filter to permit cancellation of the interference. The test filter, a single pole Butterworth filter 20 MHz wide and centered at 70 MHz, has the amplitude response of Figure 69. A more detailed curve over the bandwidth of interest is given in Figure 70. The group delay characteristics of the filter are shown in Figure 71. With the test filter in Vertical Channel path, the Horizontal Channel produced the BER data of Figure 72 with a CPDR of 5 dB. Performance is within 0.75 dB of the baseline at a BER of  $1 \times 10^{-7}$ . This is somewhat better than the nondispersive test. Data for the Vertical Channel with the test filter in the Horizontal path is given in Figure 73. Here, the data is within 1.2 dB of the baseline at a BER of  $1 \times 10^{-7}$ . This is very close to the results of the nondispersive test.

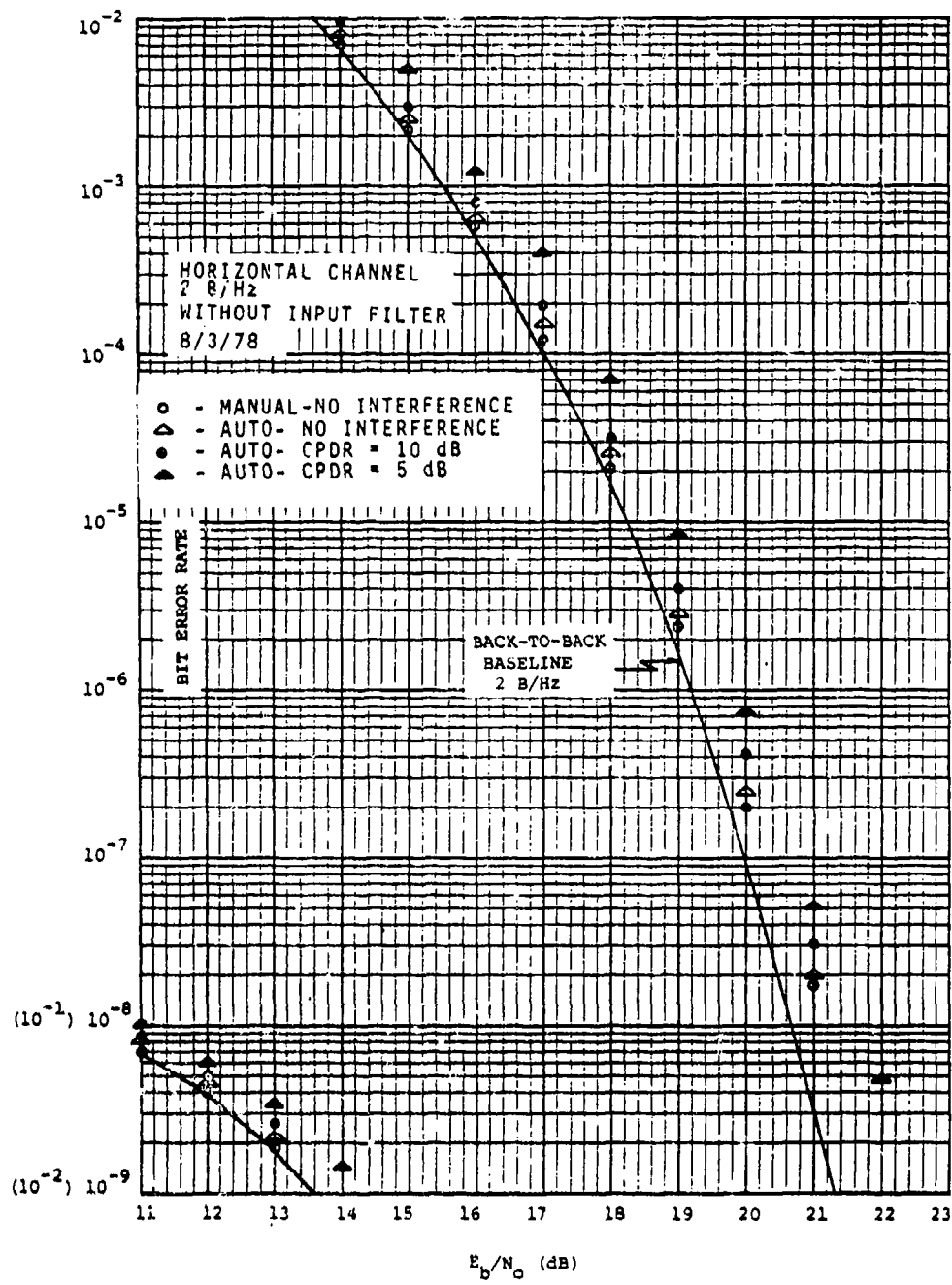


Figure 67. CPIRE Horizontal Channel 2 B/Hz  
Performance Without Input Filter

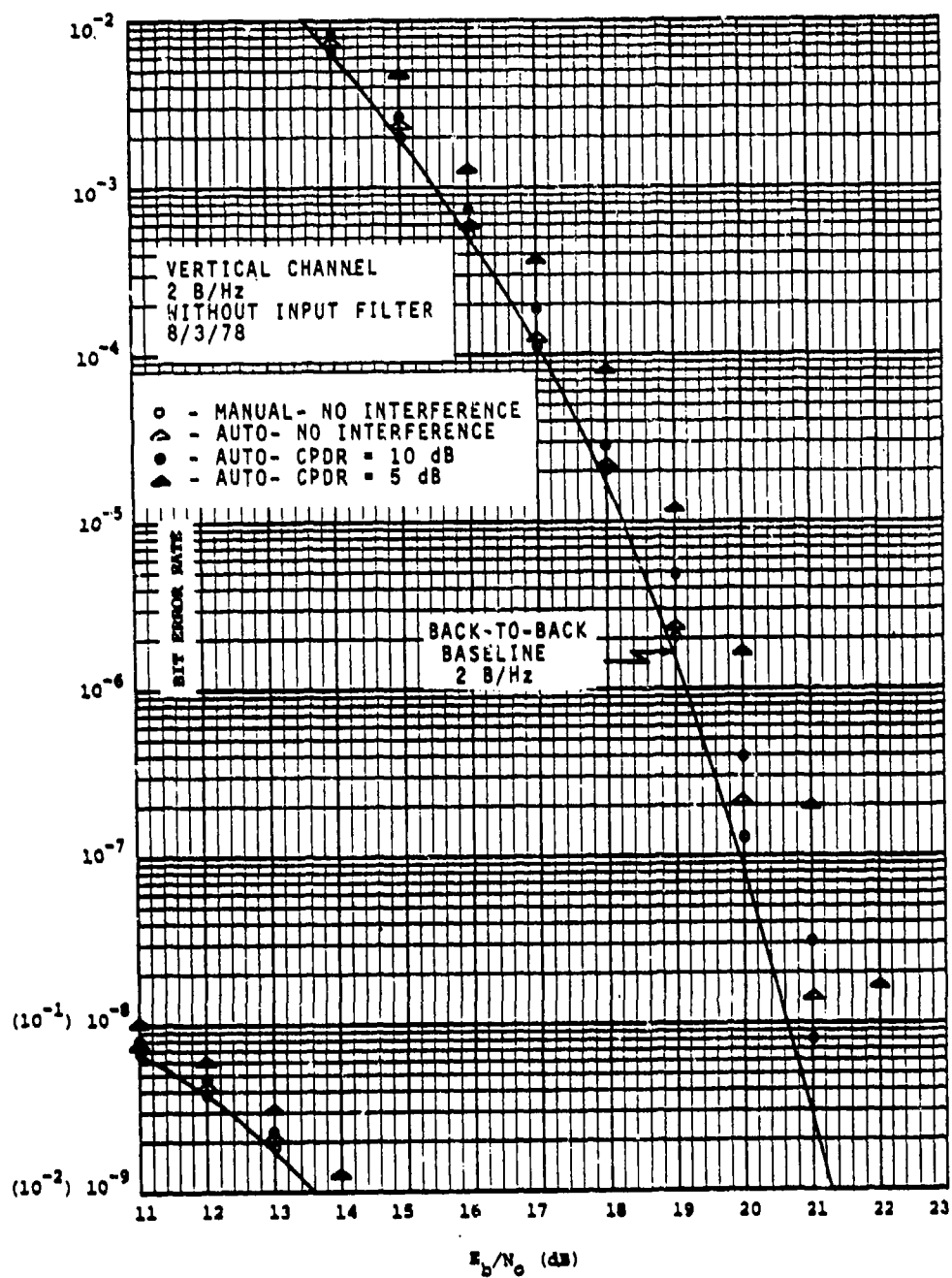


Figure 68. CPIRE Vertical Channel 2 B/Hz  
Performance Without Input Filter

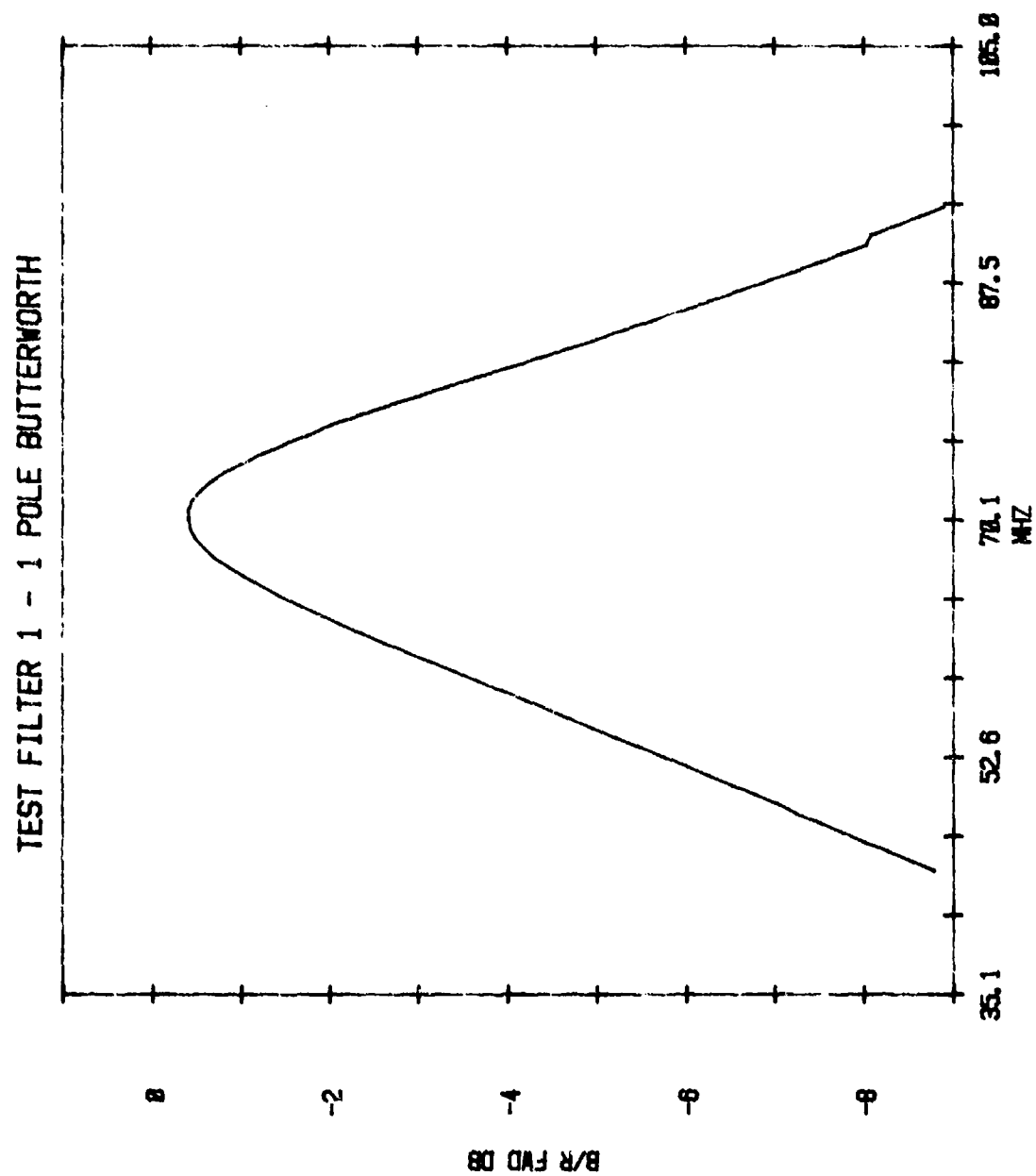


Figure 69. Dispersive Cross-Polarization Test  
Filter Amplitude Response (35 MHz - 105 MHz)

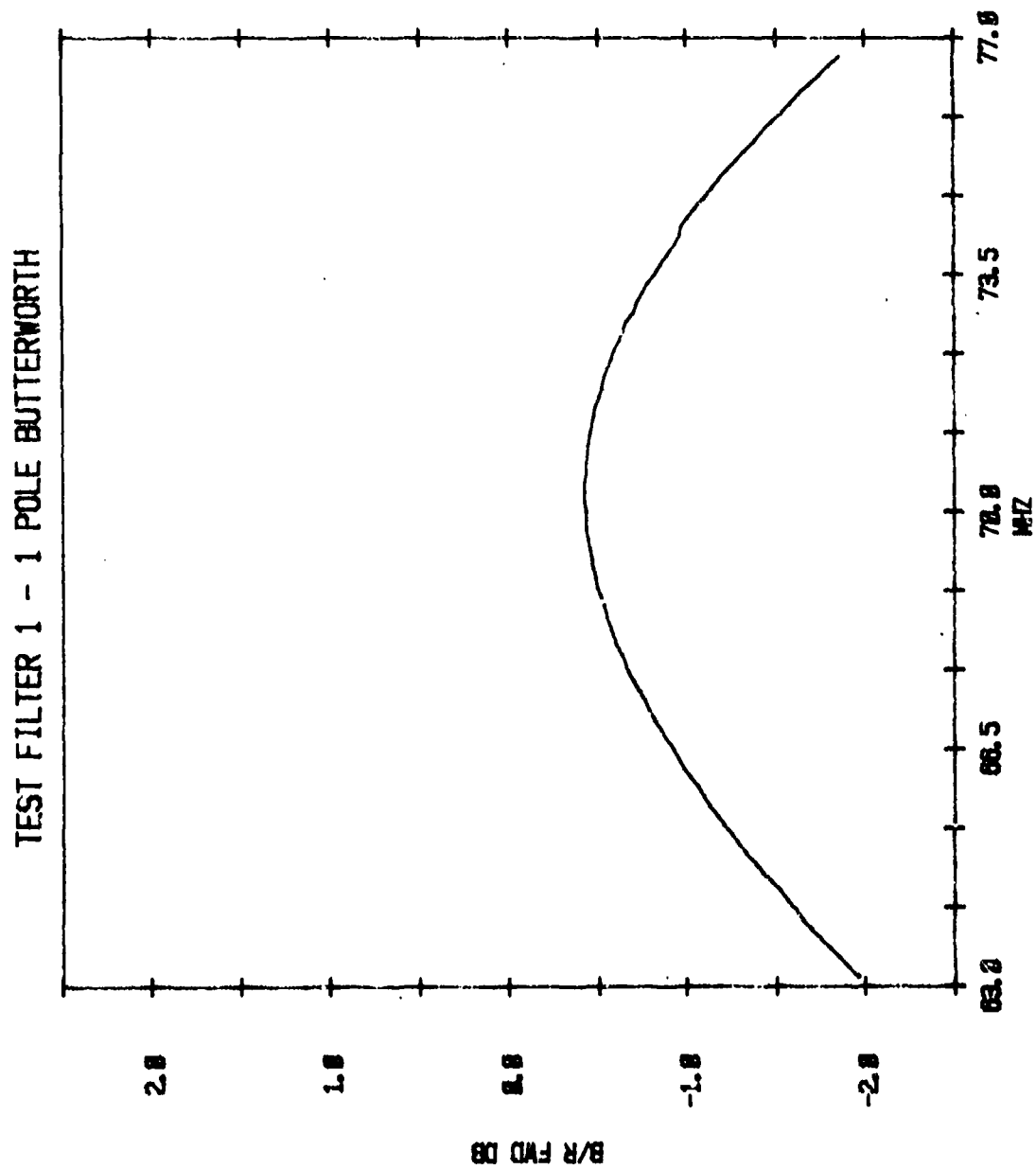


Figure 70. Dispersive Cross-Polarization Test  
Filter Amplitude Response (63 MHz - 77 MHz)

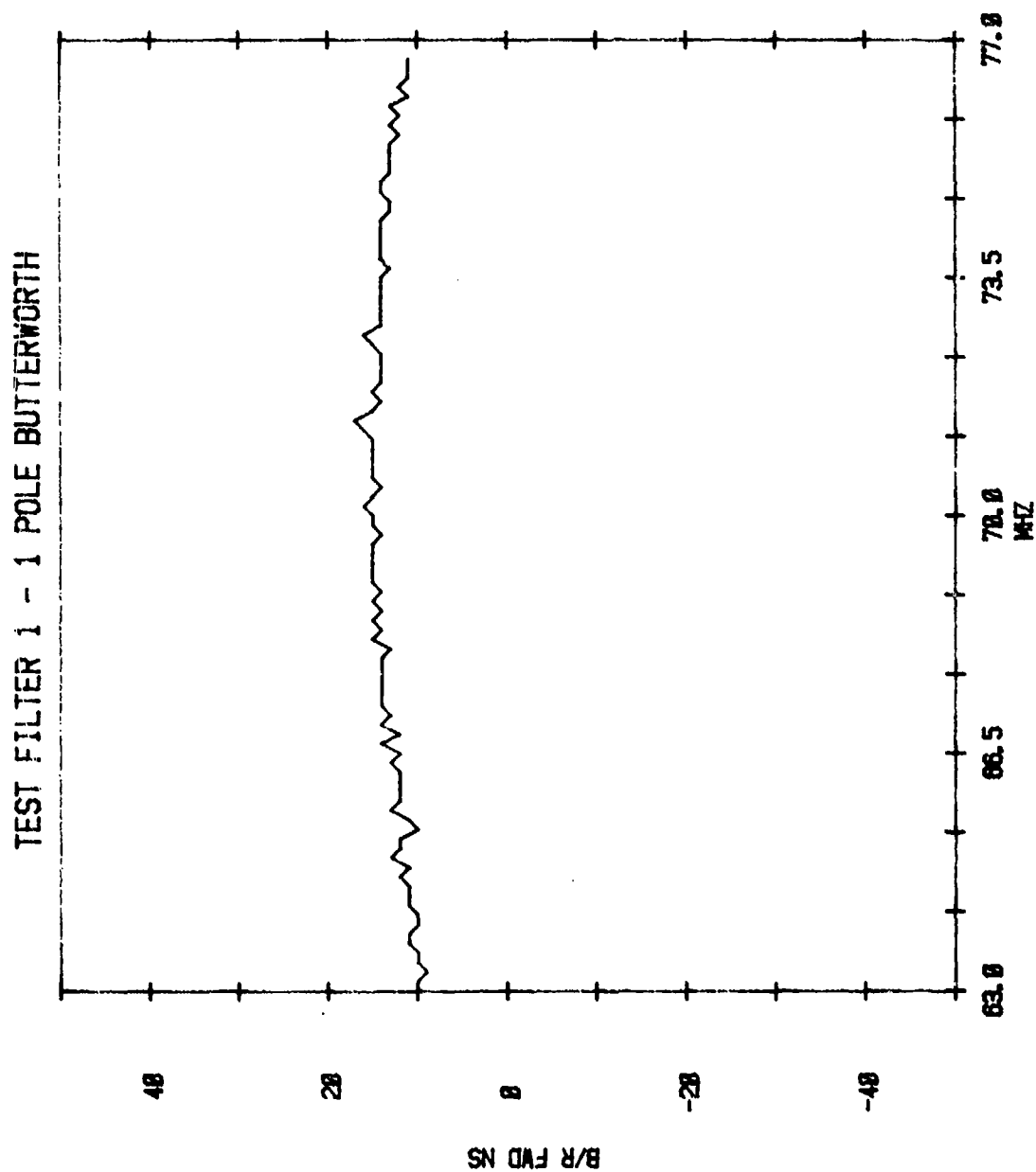


Figure 71. Dispersive Cross-Polarization Test  
Filter Group Delay Characteristics

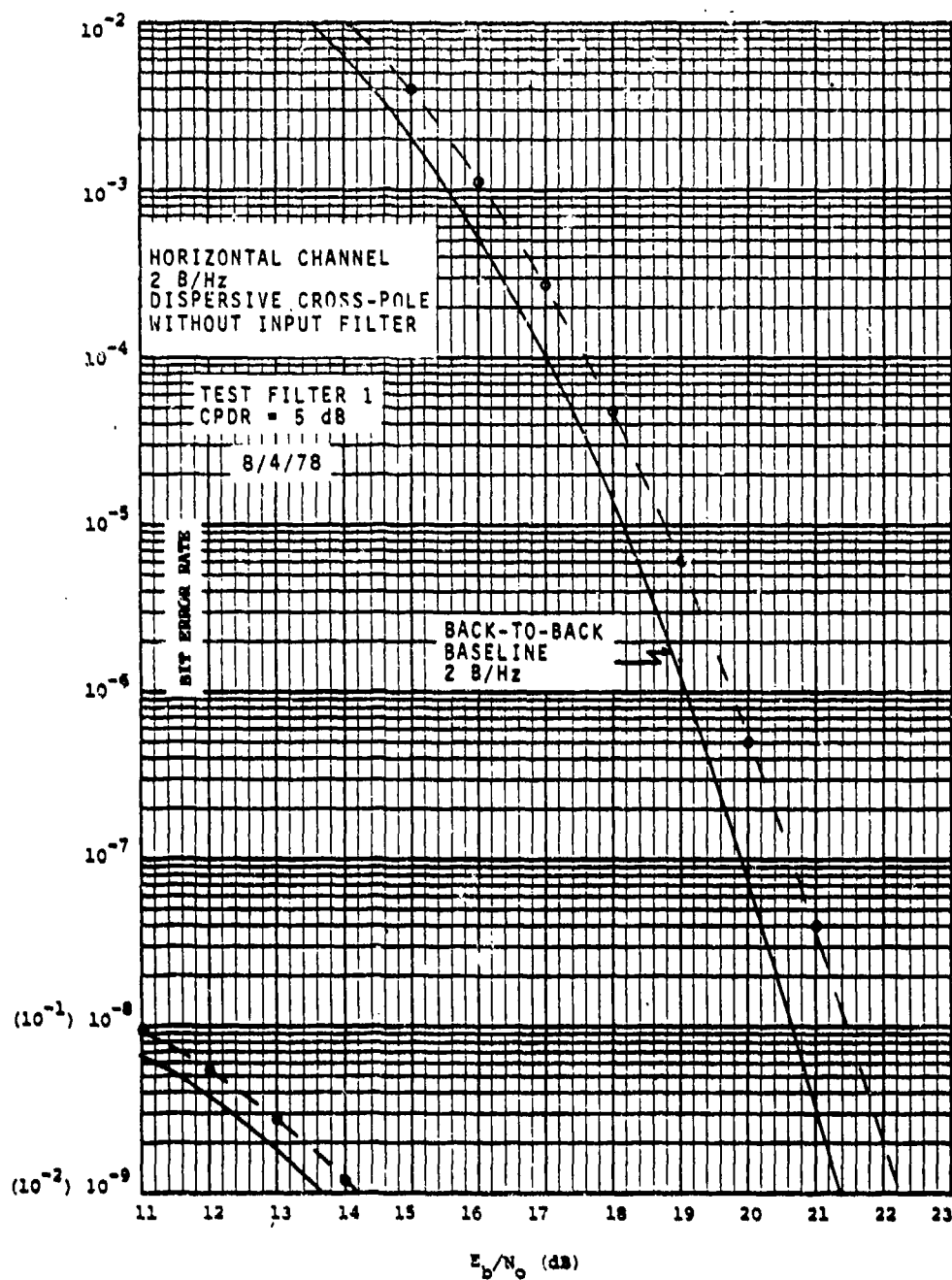


Figure 72. CPIRE Horizontal Channel 2 B/Hz  
 Dispersive Cross-Pole Performance  
 Without Input Filter

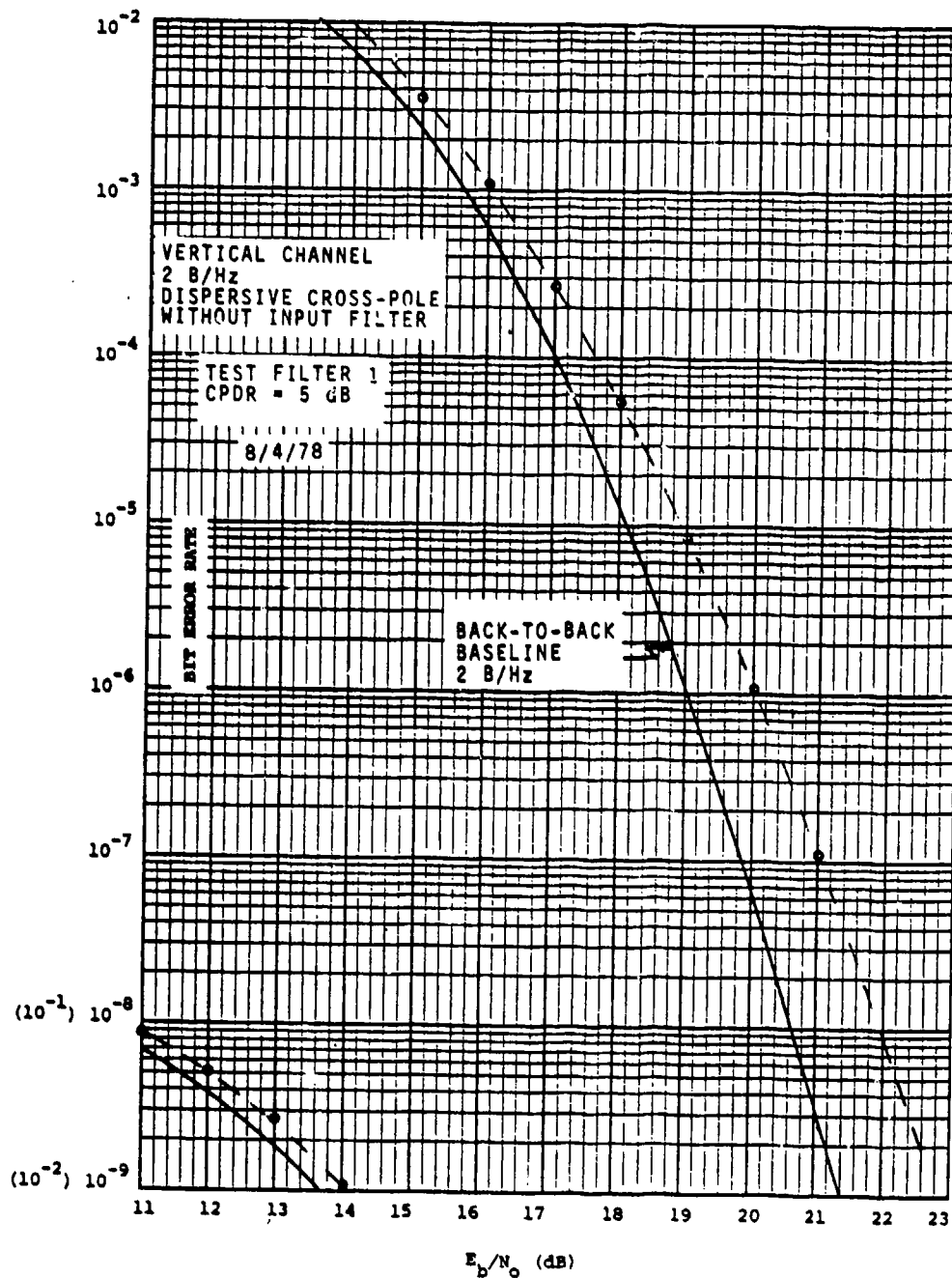


Figure 73. CPIRE Vertical Channel 2 B/Hz  
Dispersive Cross-Pole Performance  
Without Input Filter

To test CPIRE performance with time-varying cross-polarization interference, the amount of cross pole was modulated with a sine wave. The peaks of the sine wave corresponded to CPDR's of 10 and 40 dB. BER versus  $E_b/N_0$  performance for varying modulation rates is shown for the Horizontal Channel in Figure 74. The baseline curve is the static performance with a CPDR of 10 dB. With 1 Hz modulation rate, the data points are essentially unchanged. A 10 Hz rate produces about 0.4 dB degradation at a BER of  $1 \times 10^{-7}$ . The curve is displaced almost 2 dB at the same point for a 20 Hz modulation signal. This indicates a loop bandwidth around 10 Hz which was the chosen design goal. The Vertical Channel exhibits a slightly narrower loop bandwidth in Figure 75. Again, with a 1 Hz modulation rate, the data matches the static performance. With 10 Hz modulation, performance is degraded approximately 1.5 dB in the vicinity of a  $1 \times 10^{-7}$  BER.

BER curves were also run with the input filters installed in both channels. The tests were performed with static, nondispersive cross-polarization interference. The results are shown for the Horizontal Channel and Vertical Channel in Figures 76 and 77, respectively. The Horizontal Channel exhibits 0.1 dB better performance without filter (see Figure 67) for a CPDR = 10 dB in the vicinity of a  $1 \times 10^{-7}$  BER and almost 0.6 dB better performance with a CPDR = 5 dB. The Vertical Channel behaves similarly as can be seen by comparing Figures 68 and 77. Although the degradation is not great, performance is superior without input filter if out-of-band noise is limited.

#### 4.1.3.2 One B/Hz Results

Broadband Modem II performance in the 1 B/Hz mode in the presence of cross-polarization interference without the CPIRE is shown in Figure 78. The baseline BER versus  $E_b/N_0$  curve was measured through the test fixtures. As in the 2 B/Hz mode, performance degrades rapidly with decreasing CPDR, though not quite as quickly.

Basic CPIRE performance without input filter is shown in Figure 79 for the Horizontal Channel. Worst-case BER curves are within 0.9 db of the baseline curve in the vicinity of a  $1 \times 10^{-7}$  BER. Though slightly worse, this is comparable to the 2 B/Hz performance. CPIRE parameters were,

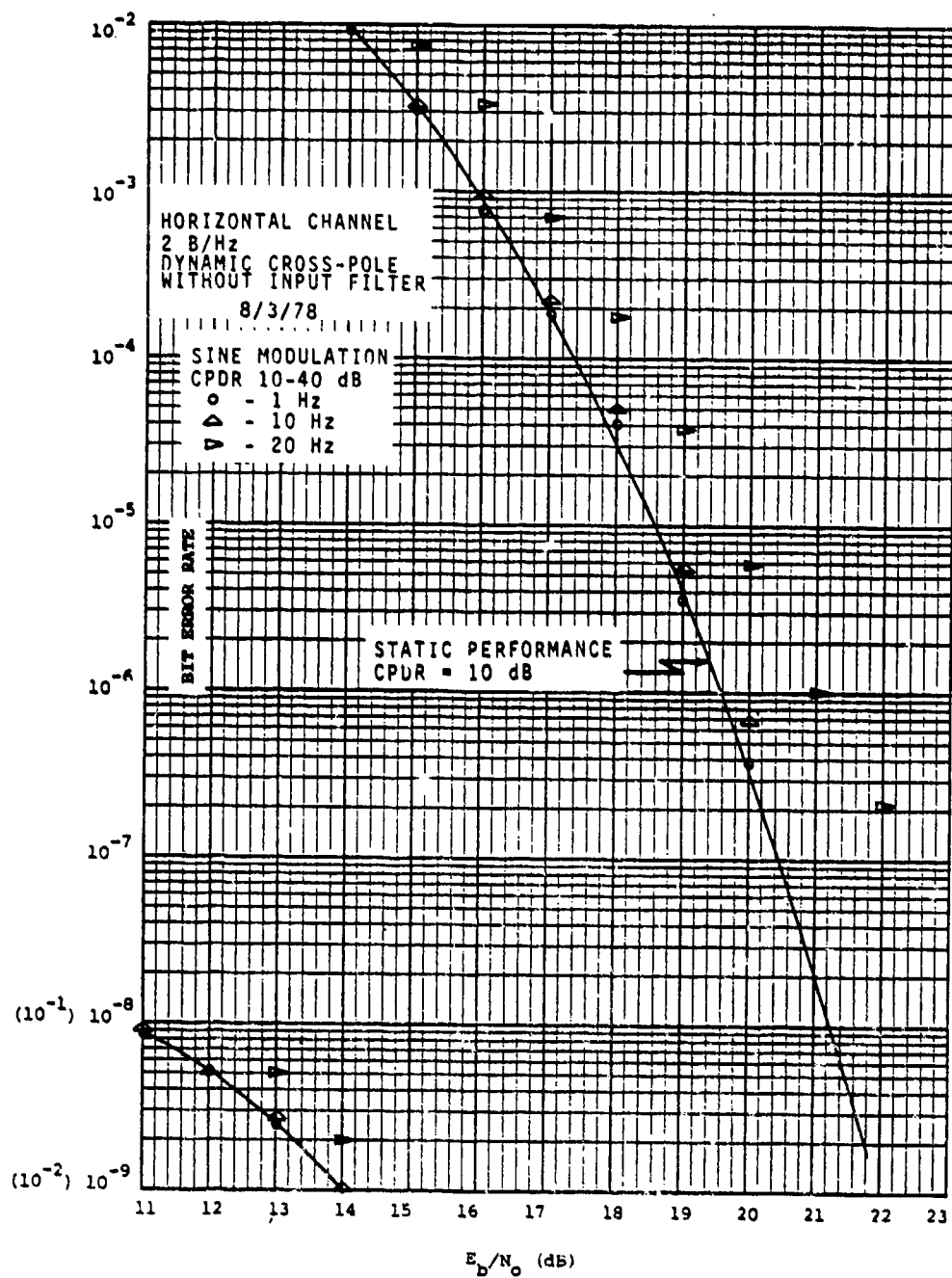


Figure 74. CPIRE Horizontal Channel 2 B/Hz  
Dynamic Cross-Pole Performance  
Without Input Filter

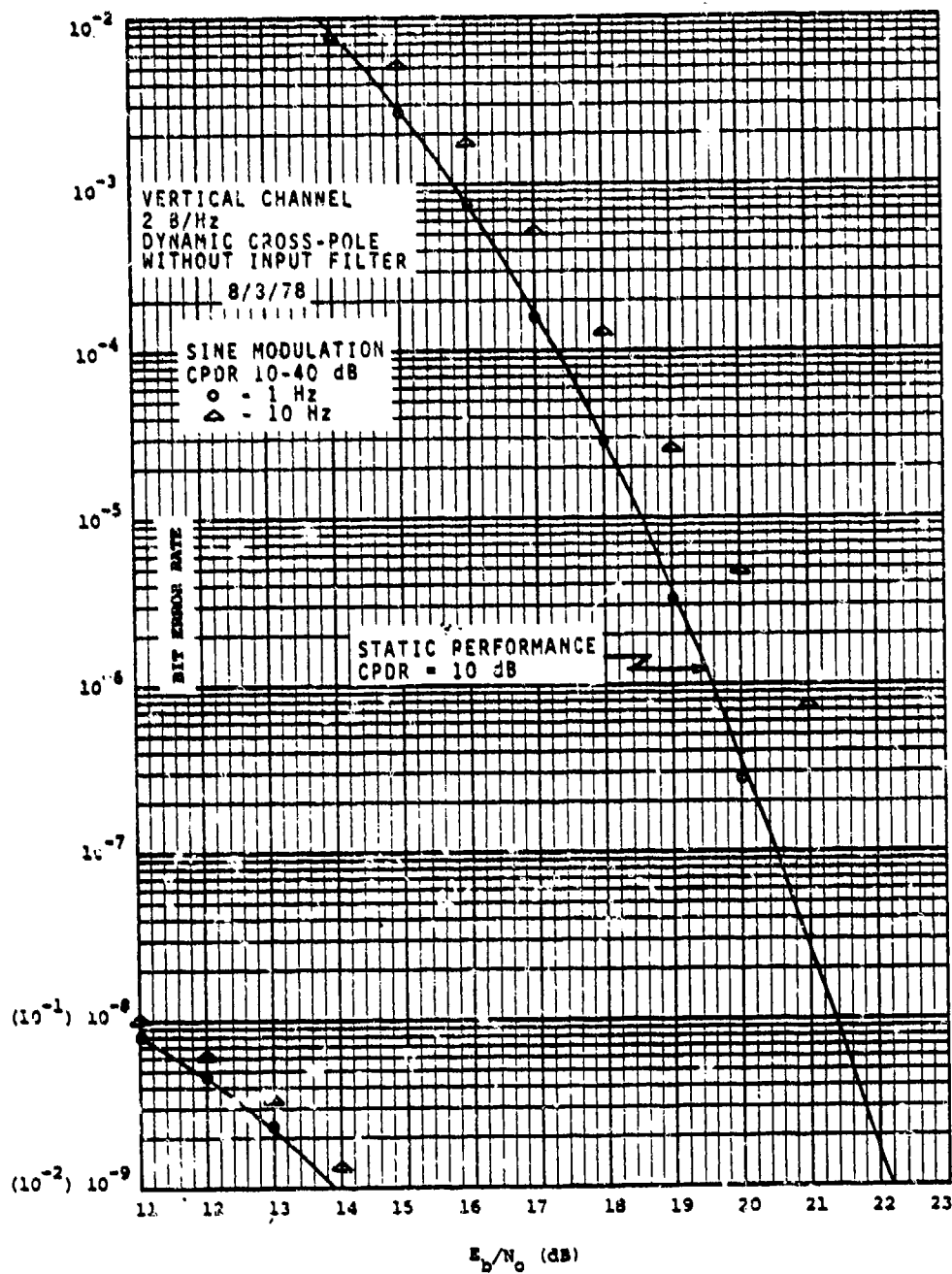


Figure 75. CPIRE Vertical Channel 2 B/Hz  
Dynamic Cross-Pole Performance  
Without Input Filter

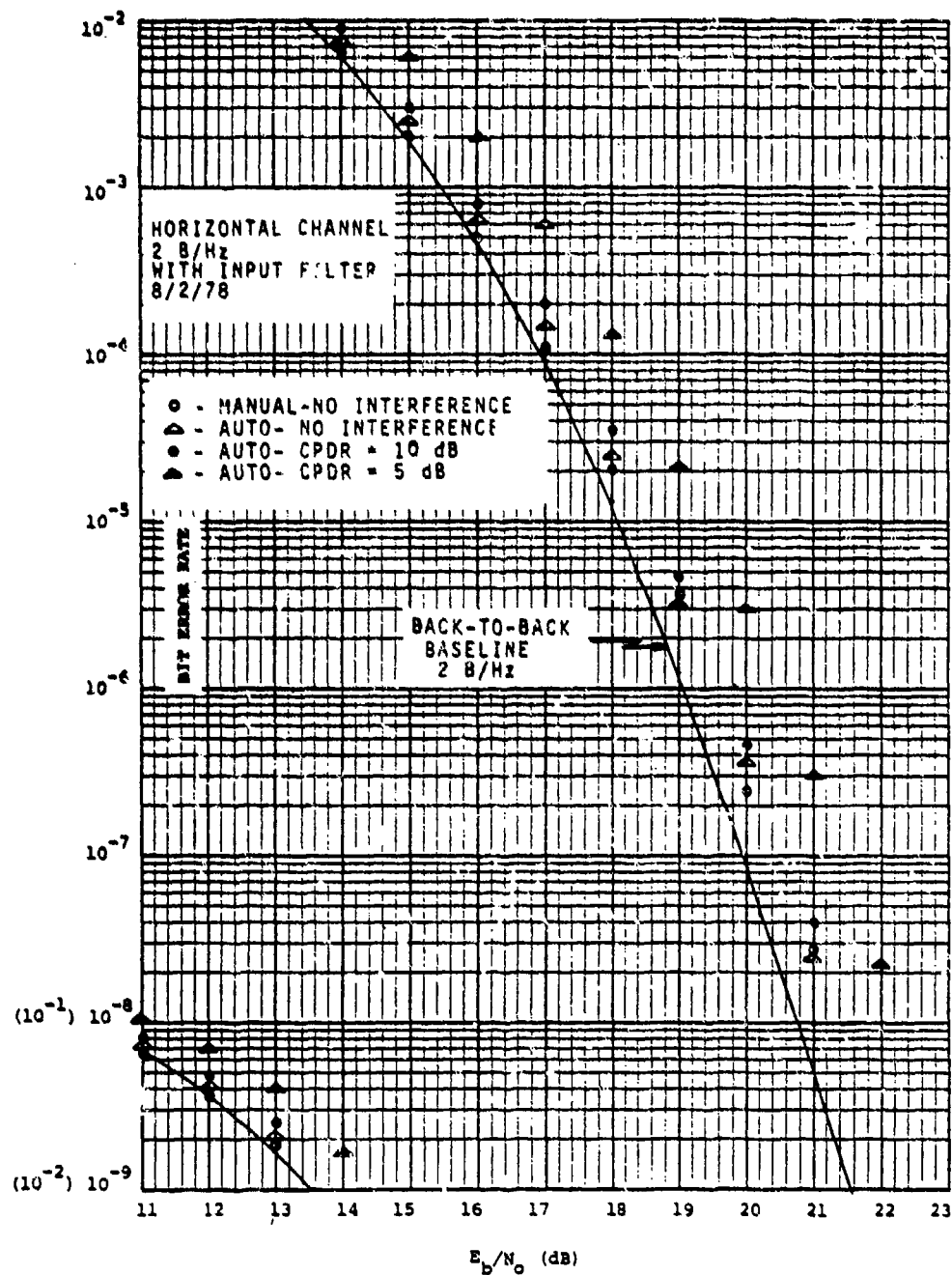


Figure 76. CPIRE Horizontal Channel 2 B/Hz  
Performance With Input Filter

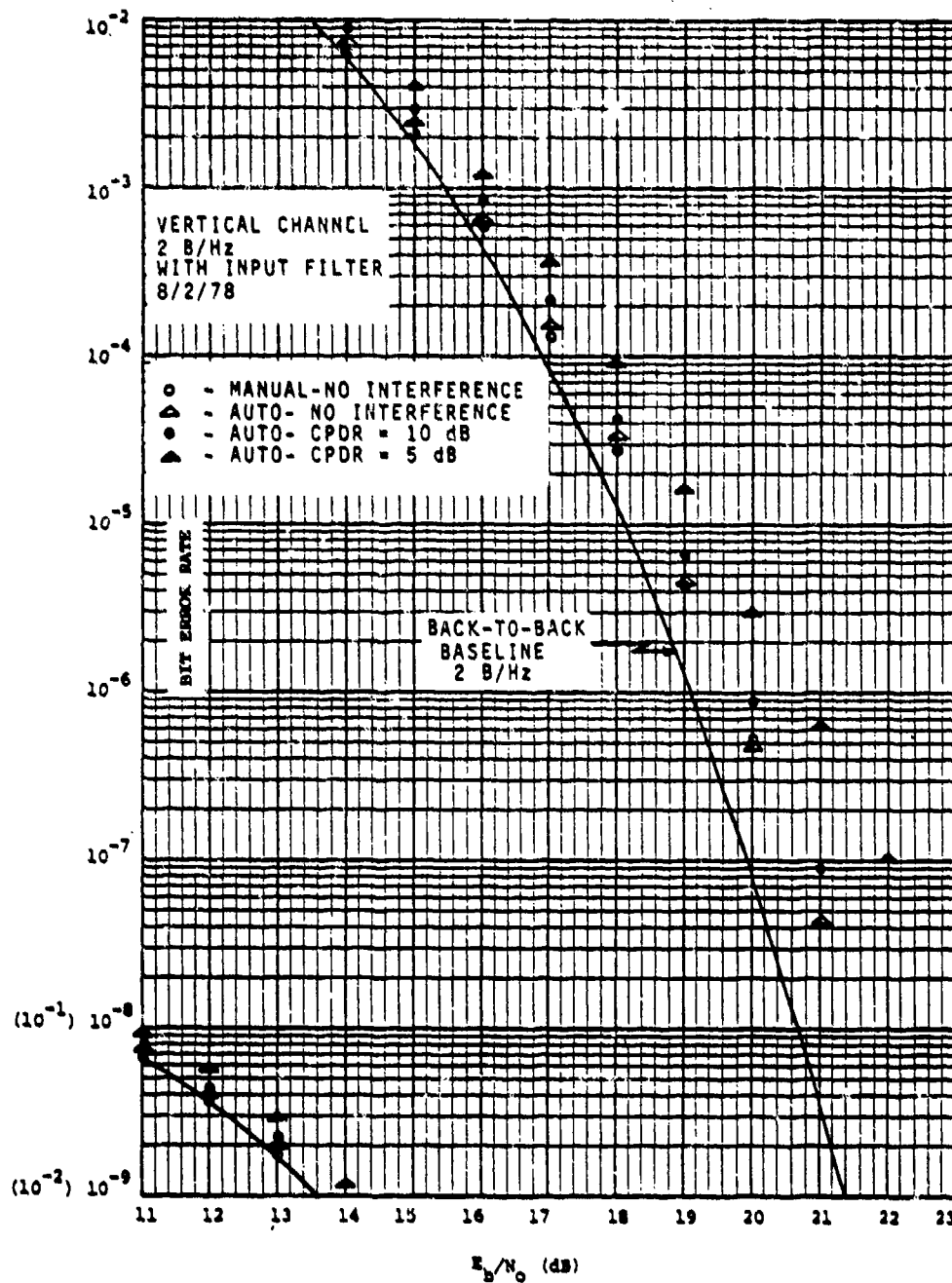


Figure 77. CPIRE Vertical Channel 2 B/Hz  
Performance With Input Filter

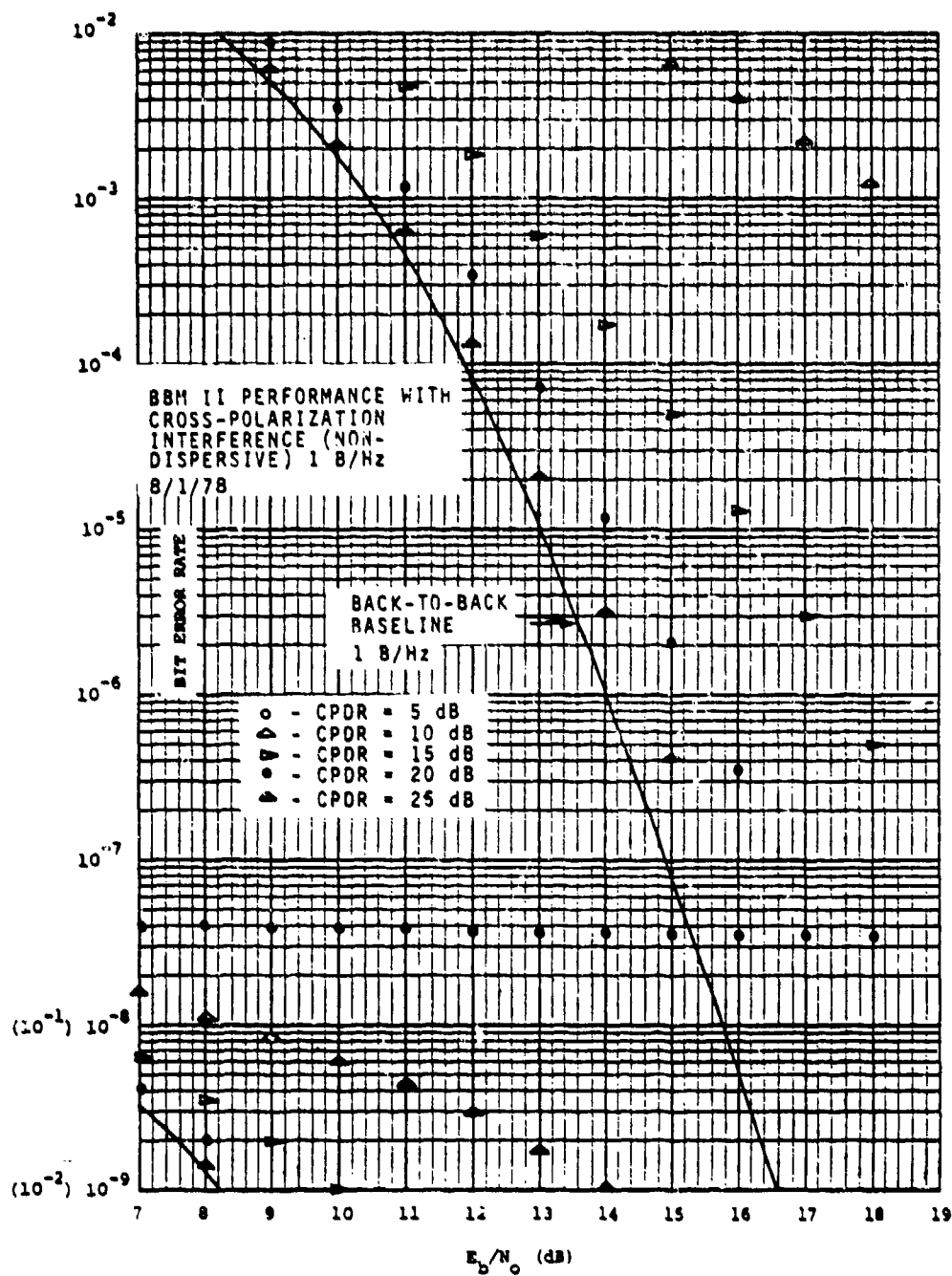


Figure 78. BBM II 1 B/Hz Performance With  
Cross-Polarization Interference

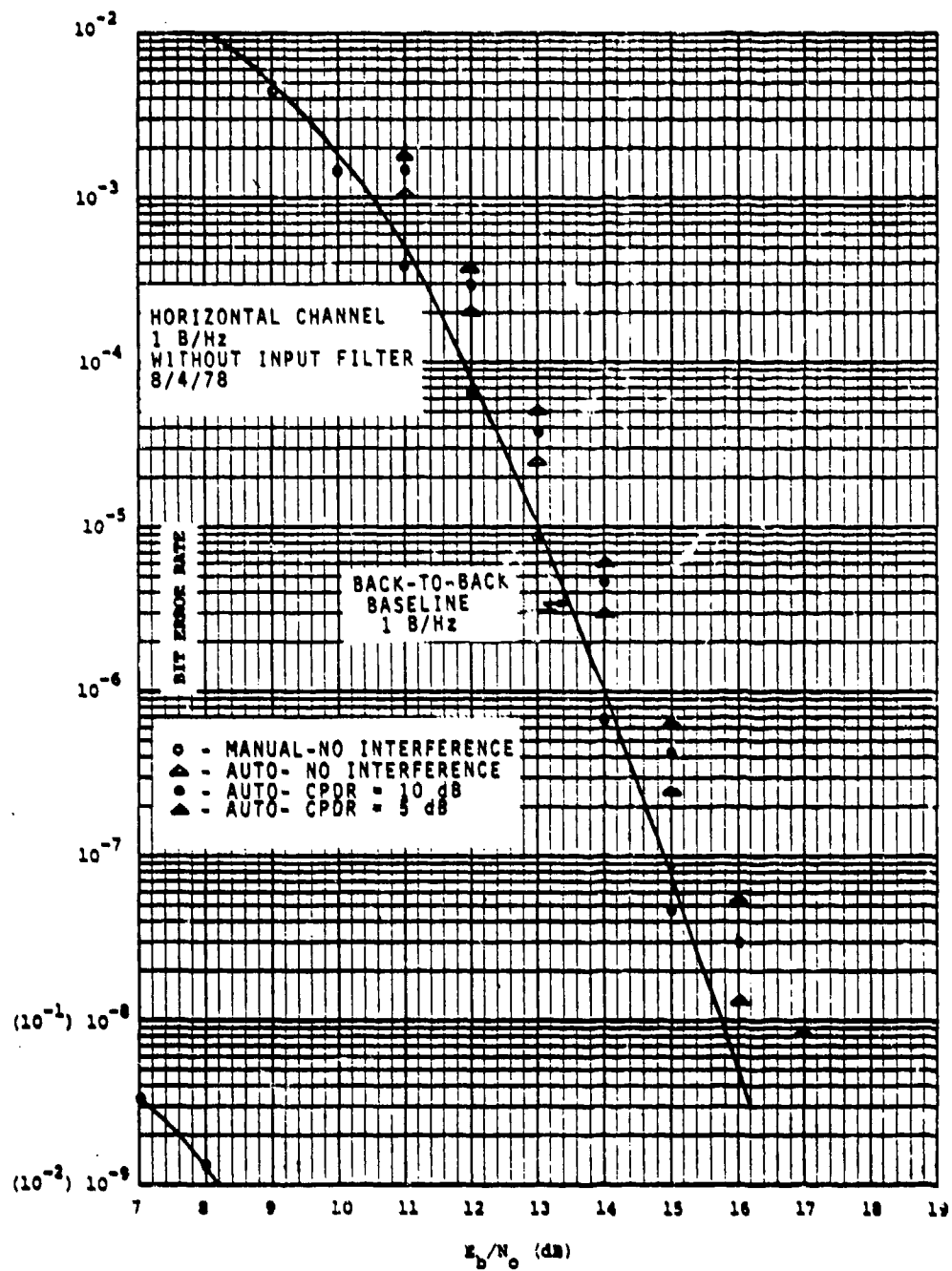


Figure 79. CPIRE Horizontal Channel 1 B/Hz  
Performance Without Input Filter

however, optimized for the 2 B/Hz mode not the 1 B/Hz performance. Vertical channel, 1 B/Hz performance is given in Figure 80. Worse-case Vertical Channel performance is within 1.5 dB of the Baseline at a BER of  $1 \times 10^{-7}$ .

Dispersive cross-pole tests were performed as in the 2 B/Hz case. The results are given in Figures 81 and 82 for the Horizontal and Vertical Channels, respectively. Results are essentially the same as the nondispersive tests.

Dynamic cross-pole interference effects for 1 B/Hz modem operation are shown in Figures 83 and 84. Again, the Horizontal Channel exhibits slightly wider loop bandwidth. Both channels perform well even with a 10 Hz modulation rate.

Use of the input filters degrades Horizontal Channel BER performance by approximately 0.6 dB at a BER of  $1 \times 10^{-7}$ . This can be seen by comparing Figures 79 and 85. Vertical Channel performance with filter, shown in Figure 86, is actually slightly better than without filter (Figure 80).

#### 4.1.4 RADC Witnessed In-Plant Testing Results

A random curve set was duplicated with RADC representatives to verify previously obtained in-plant data. Nondispersive, static cross-polarization interference tests were performed on the Horizontal Channel with the modem in the 2 B/Hz mode. The results are shown in Figure 87. These tests were performed after a 2-week burn-in period without realignment of the CPIRE. With a CPDR of 10 dB, the results are within measurement accuracy of 0.1 dB of those obtained earlier (Figure 67). At a ratio of 5 dB, results are within 0.4 dB.

#### 4.2 RADC Tests

This paragraph presents data acquired at RADC in Rome, New York, October 30, 1978 through November 3, 1978.

##### 4.2.1 FCC 19311 Waveguide Filter Results

A waveguide filter designed to shape the Broadband Modem II modulator output to meet FCC Docket 19311 requirements was supplied for tests involving two cross-polarized microwave channels. This filter was constructed to the same specifications as the original filter supplied on Contract F30602-76-C-0434. The two filters ("new" and "old") were installed

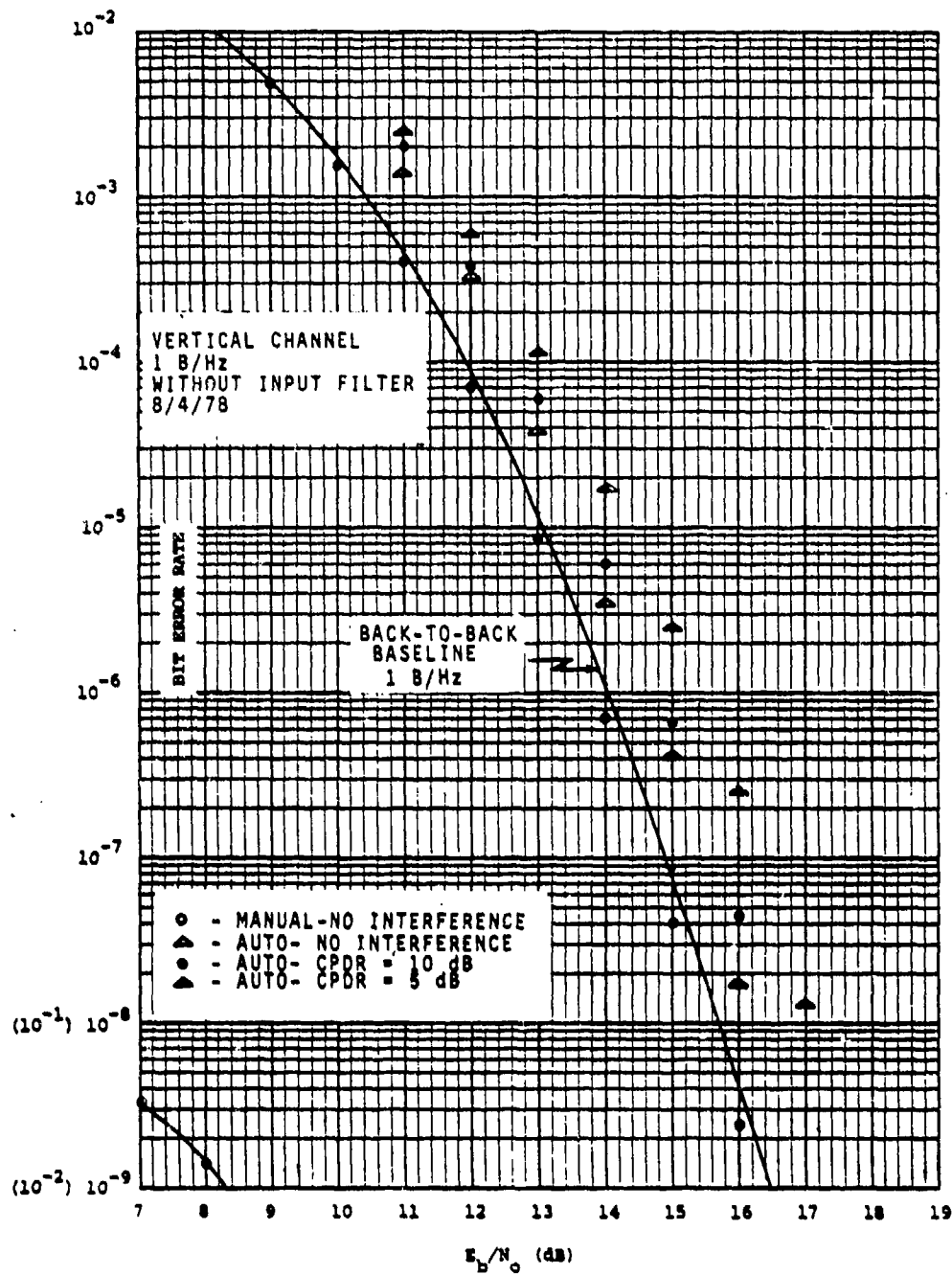


Figure 80. CPIRE Vertical Channel 1 B/Hz  
Performance Without Input Filter

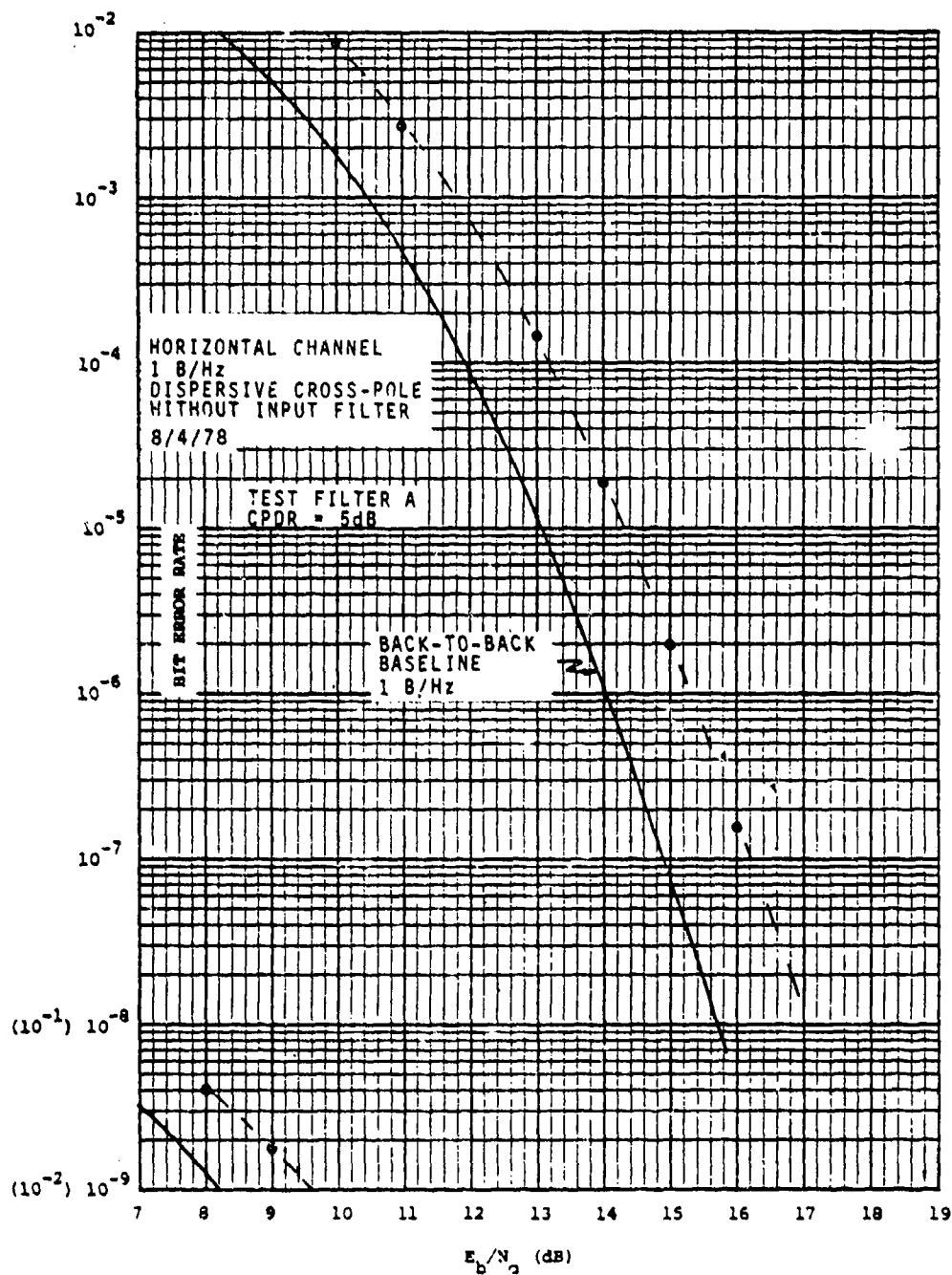


Figure 81. CPIRE Horizontal Channel 1 B/Hz  
Dispersive Cross-Pole Performance  
Without Input Filter

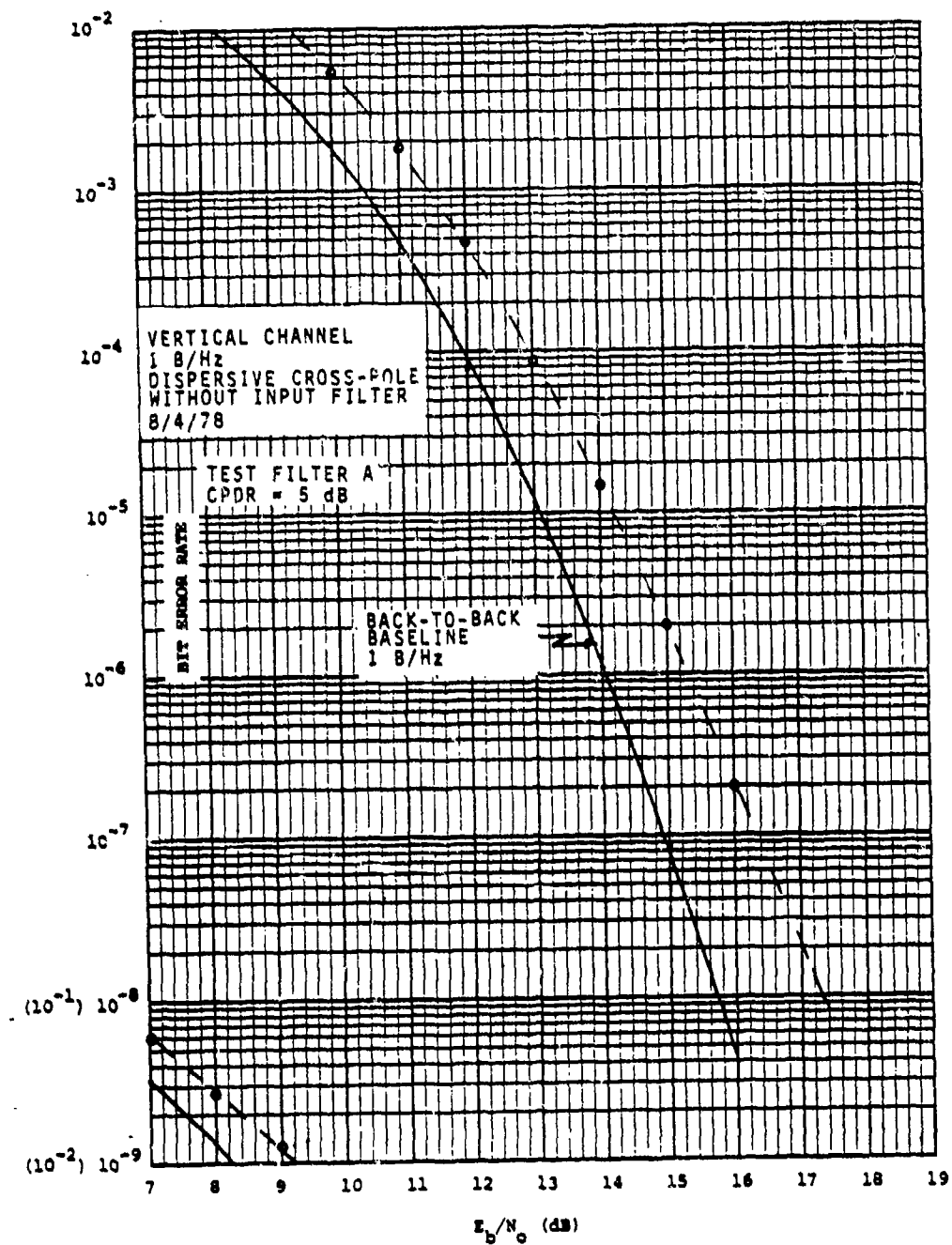


Figure 82. CPIRE Vertical Channel 1 B/Hz  
Dispersive Cross-Pole Performance  
Without Input Filter

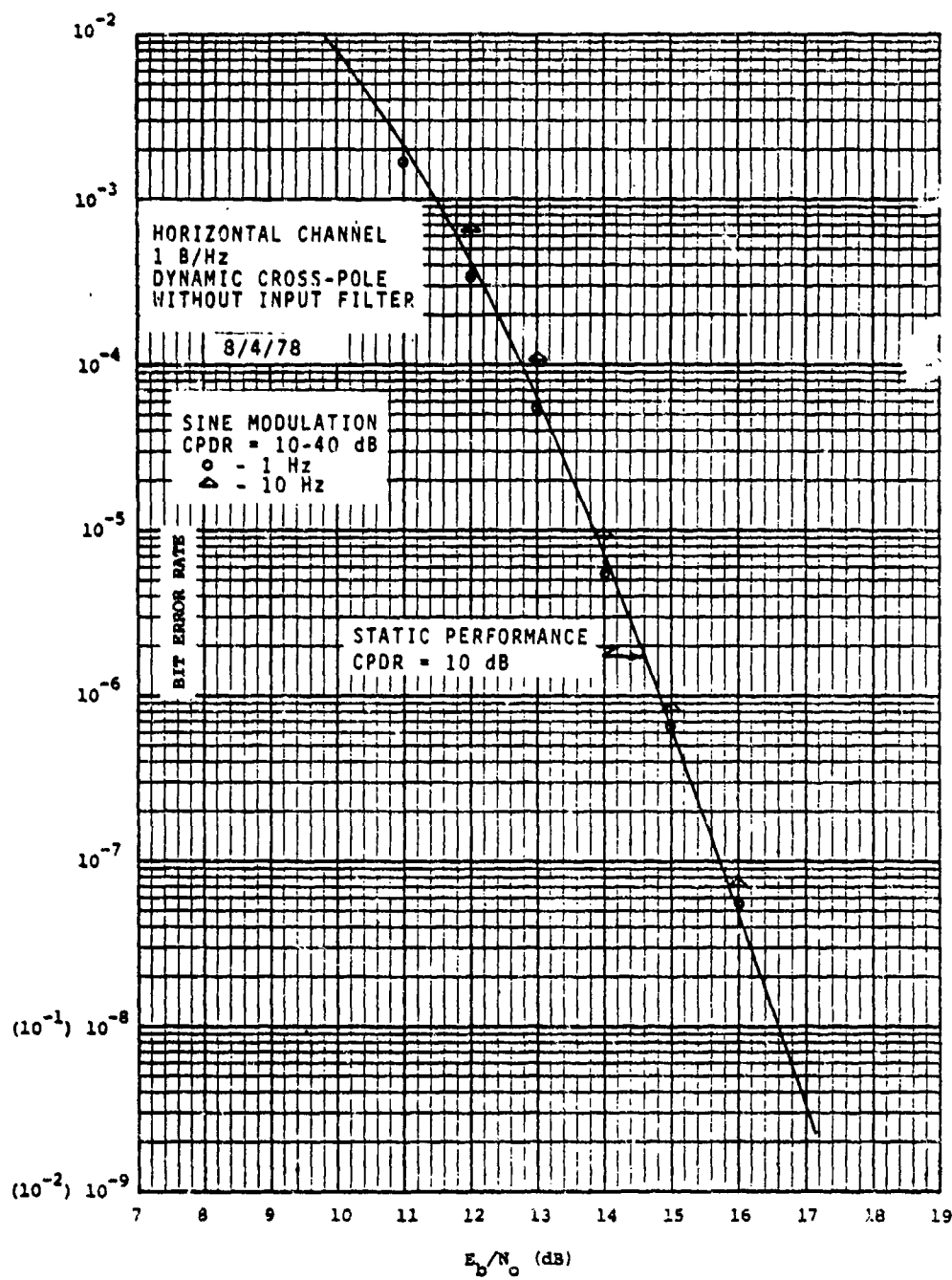


Figure 83. CPIRE Horizontal Channel 1 B/Hz  
Dynamic Cross-Pole Performance  
Without Input Filter

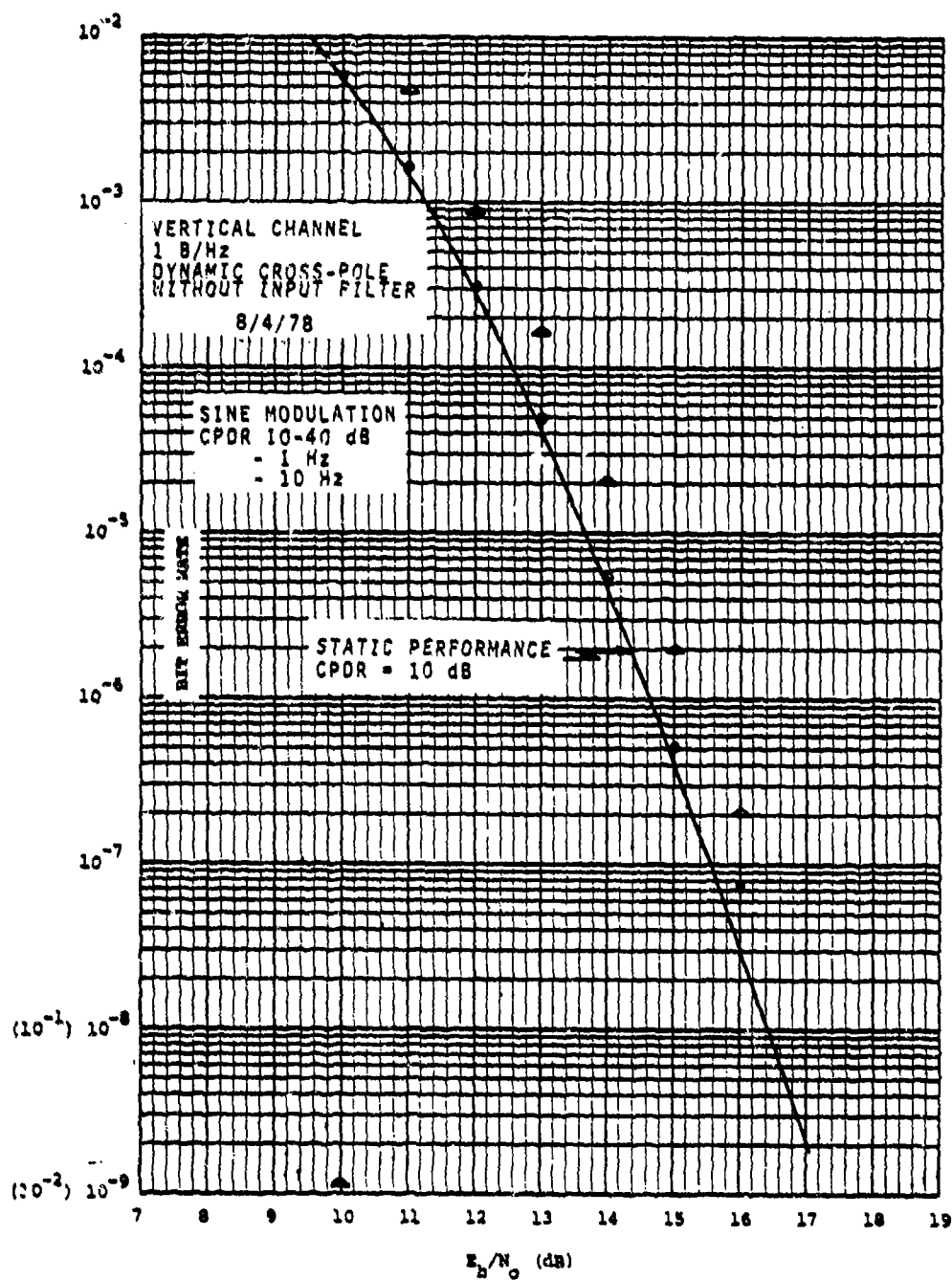


Figure 84. CPIRE Vertical Channel 1 B/Hz  
Dynamic Cross-Pole Performance  
Without Input Filter

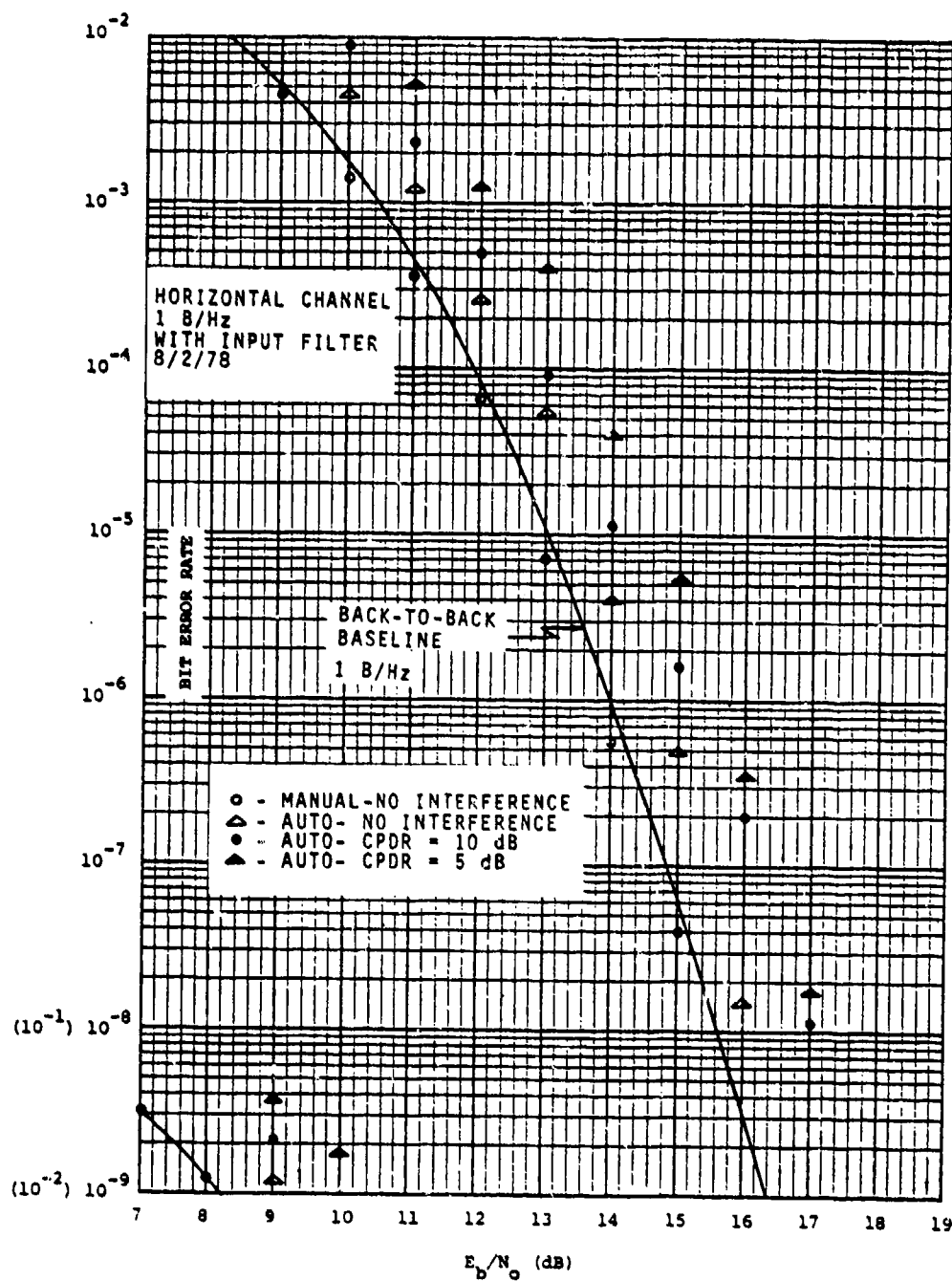


Figure 85. CPIRE Horizontal Channel 1 B/Hz  
Performance With Input Filter

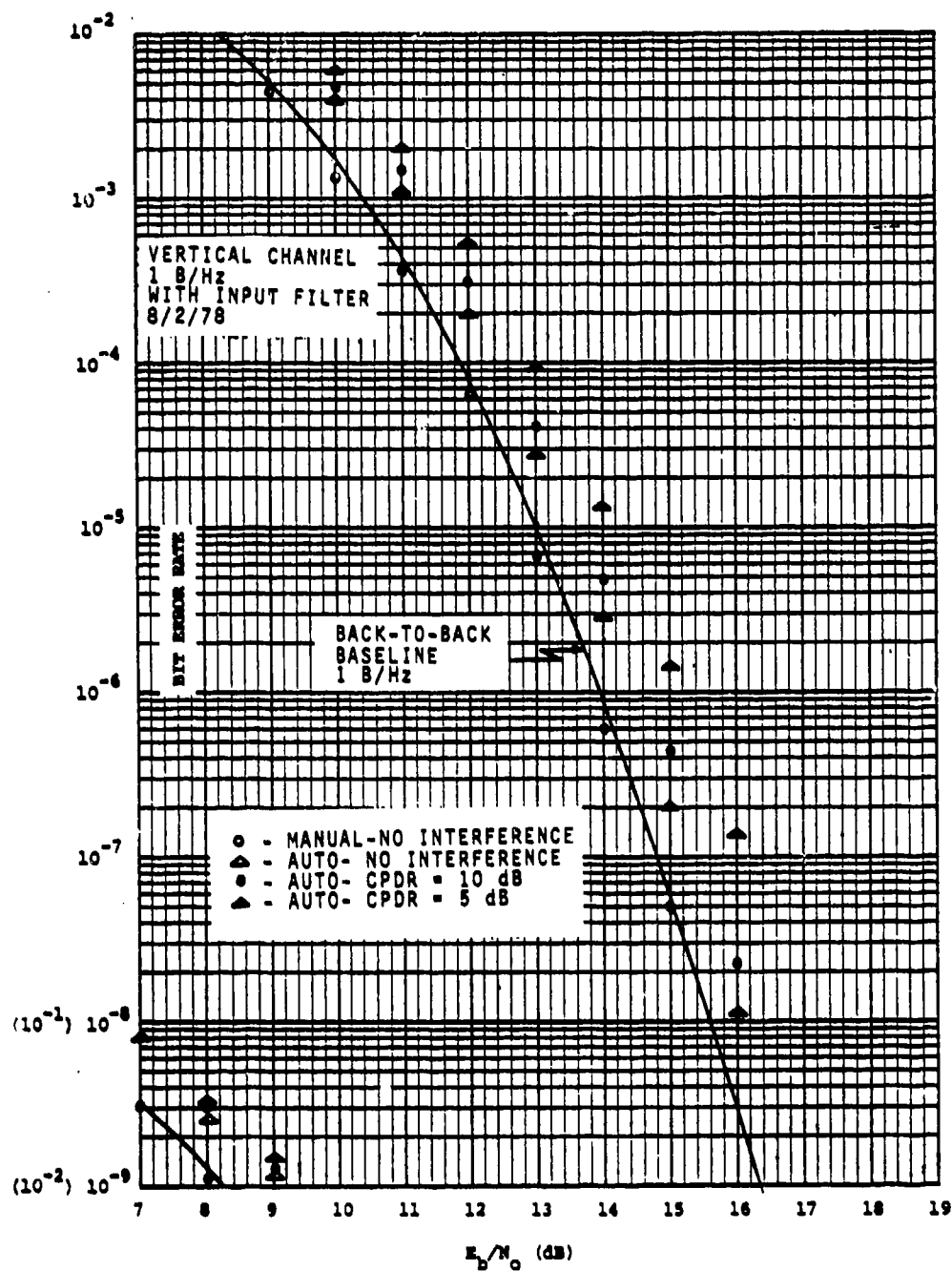


Figure 86. CPIRE Vertical Channel 1 B/Hz  
Performance With Input Filter

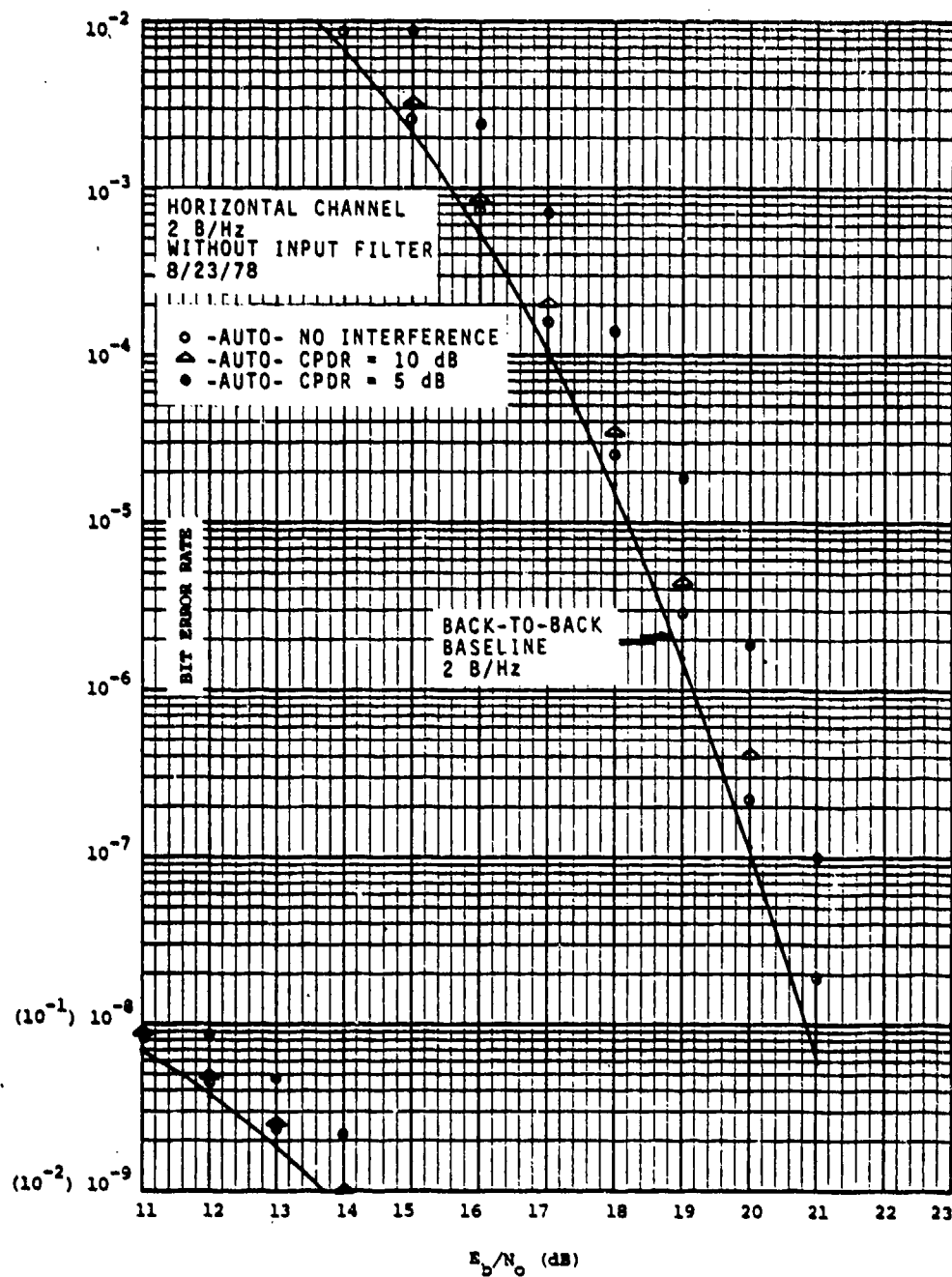


Figure 87. CPIRE Horizontal Channel 2 B/Hz  
Performance Without Input Filter

in the LC8D radio used with the microwave simulator. A visual examination of the spectra of the two radio channels revealed a match to within  $\pm 1$  dB. As the original filter met FCC 19311 requirements with a margin of several dB (refer to Report F30602-76-C-0434), the new filter also meets these requirements. Thermal noise was added to the radio receiver outputs and bit error rate (BER) measurements were made using both filters, providing a sensitive test of amplitude and group delay matching between filters. This data is presented in Figure 88. BBM II performance with the new filter is within 0.2 dB of that with the old filter down to an error rate of  $1 \times 10^{-6}$ . This is very close matching, especially considering that separate radio transmitters were used with the two filters.

#### 4.2.2 Performance Verification Testing Results

Initial RADC tests of the CPIRE were conducted with the test configuration used for the in-plant tests at Harris (Appendix C, Figure C-2). This was done to ensure proper operation of the unit. As realignment was required, some variations from the in-plant results were expected. The Horizontal Channel performance is shown in Figure 89. The tests were performed without input filter and with the modem in the 2 B/Hz mode. The corresponding in-plant data is given in Figure 67. Modem baseline performance was slightly improved at the RADC tests as was CPIRE performance with CPDR's greater than 10 dB. Performance with a CPDR of 5 dB was degraded slightly from that measured in-plant. The difference of 0.7 dB at a BER of  $1 \times 10^{-7}$  could be explained by a slightly different interference phase angle or increased loop jitter in the equalizer portion of the CPIRE. Vertical channel performance as shown in Figure 90 was slightly better under all conditions than that measured in-plant as seen by comparison with Figure 68.

#### 4.2.3 Radio/Simulator Performance Testing Results

Following initial performance verification of BBM II and the CPIRE, the LC8D radio and simulator were placed in the signal path. The modulator output was upconverted to 8.075 GHz with one of the two radio channels, filtered with a FCC 19311 waveguide filter, and fed through the simulator to one of the radio receivers where it was downconverted to 70 MHz. This IF output was then fed to the same test configuration used for

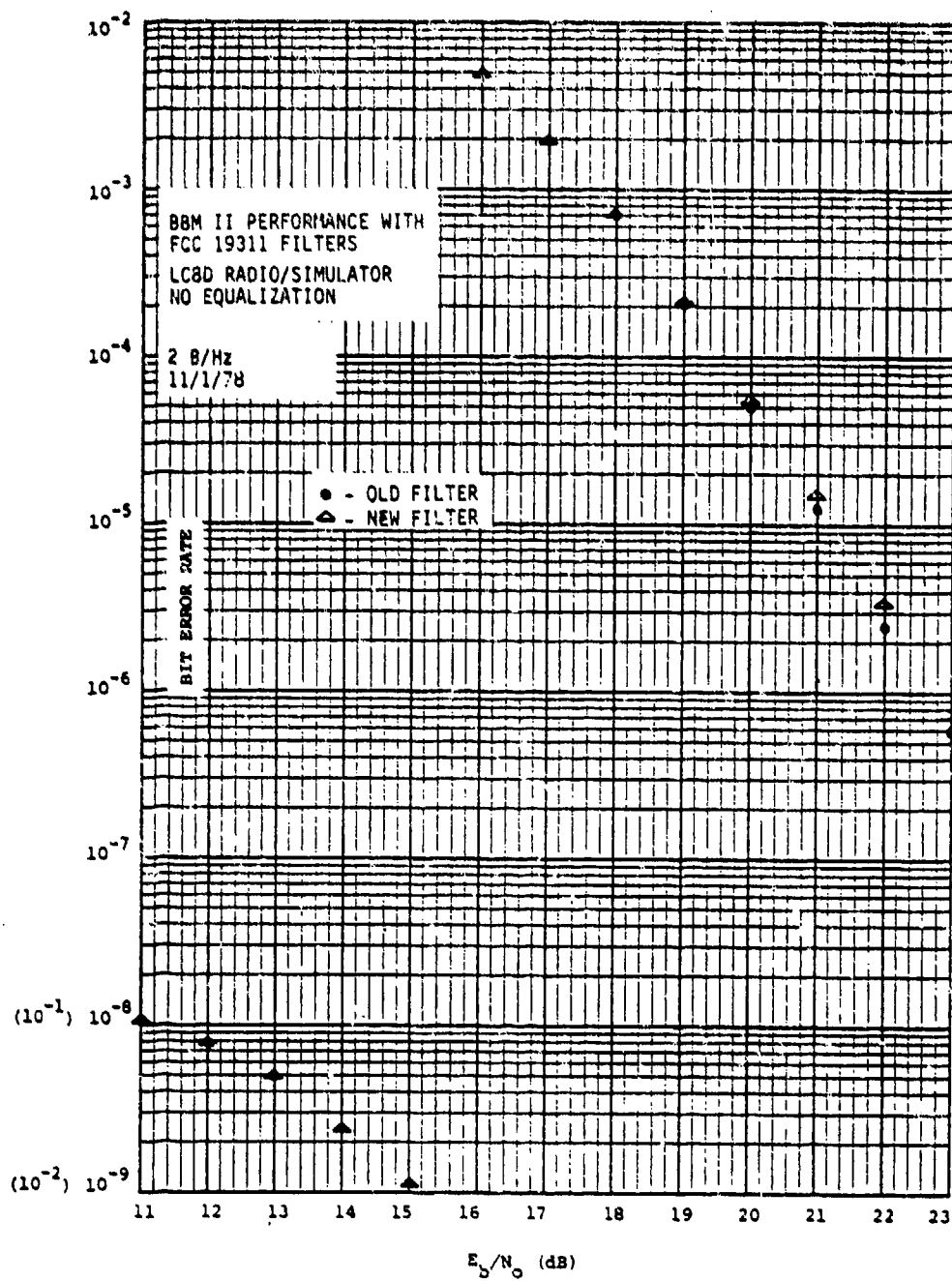


Figure 88. BBM II Performance With FCC 19311 Filters

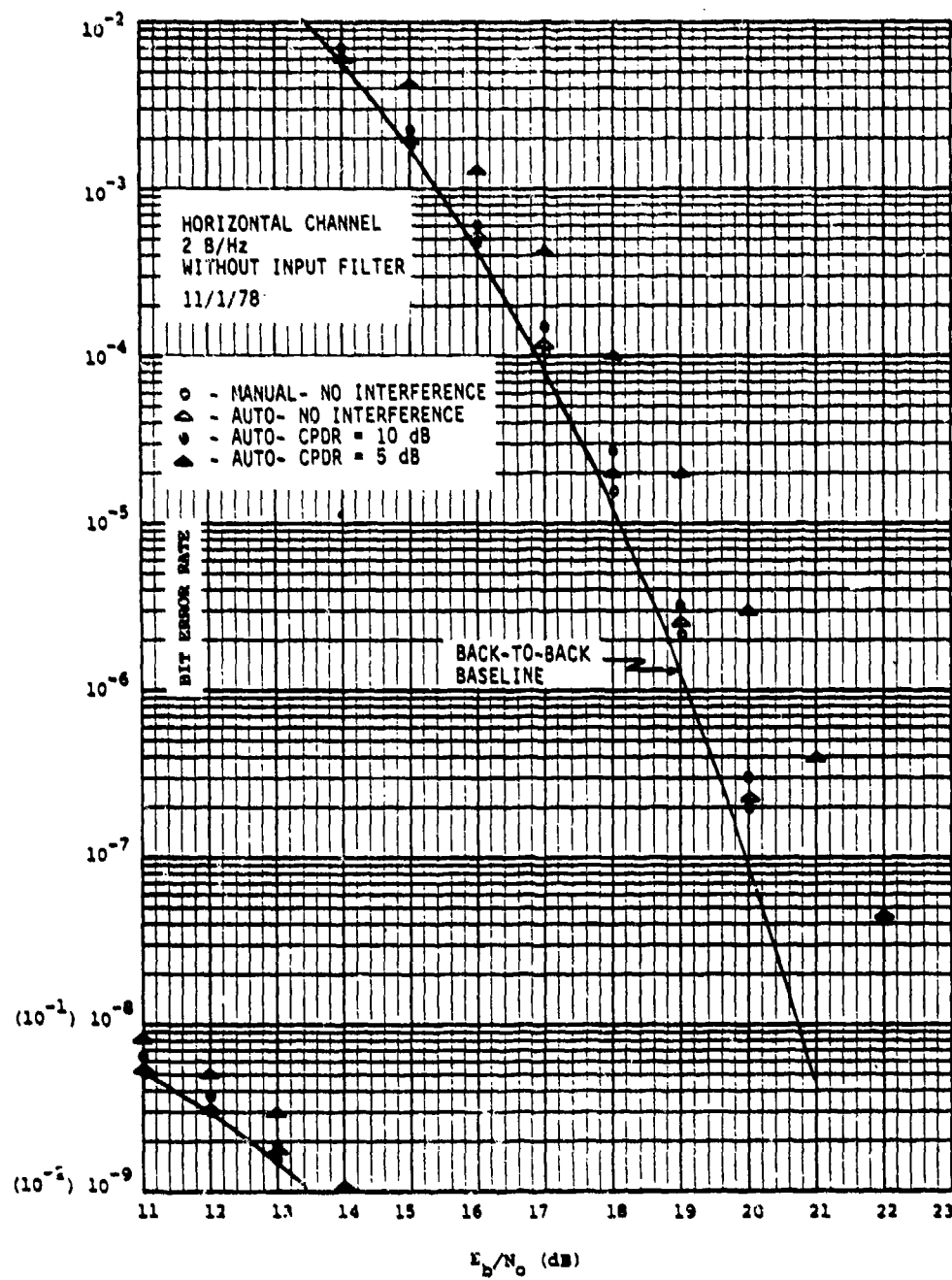


Figure 89. CPIRE Horizontal Channel 2 B/Hz  
Performance Without Input Filter

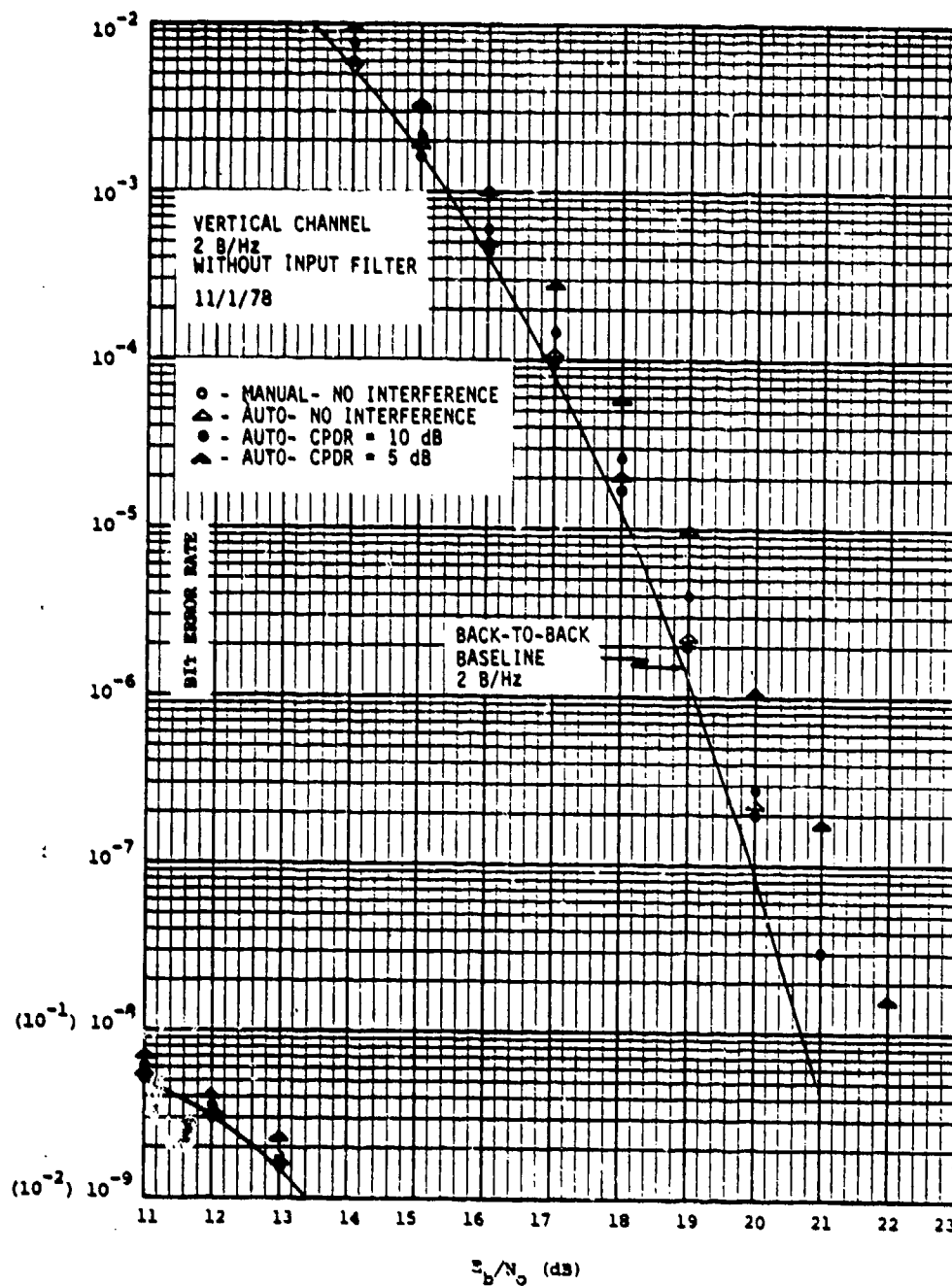


Figure 90. CPIRE Vertical Channel 2 B/Hz  
Performance Without Input Filter

the initial verification tests. Although insertion of a single radio link between the modulator and decorrelator does not fully simulate true operational link conditions, it does force the CPIRE to operate with a signal whose envelope is corrupted by the 19311 filtering and frequency translations of the radios. The peak-to-peak value of the AM introduced by the filtering was approximately 10 percent of the peak-to-peak envelope value. This is somewhat greater than anticipated and will degrade CPIRE performance as the unit operates by measuring AM content of the signal envelope. A possible modification to the CPIRE to improve performance with the heavy filtering would be the inclusion of a sample and hold circuit ahead of the AM measuring circuitry synchronized with symbol timing. This might allow samples to be taken at a point where the filtering-induced AM is minimized.

Most of the Radio/Simulator tests were run with the modem in the 2 B/Hz mode as this is of primary interest. A few tests were, however, performed to characterize 1 B/Hz operation.

The LC8D's IF noise spectrum was narrow enough ( 25 MHz) to allow CPIRE operation without the internal input filters. For all RADC tests, the filters were bypassed.

#### 4.2.3.1 2 B/Hz Radio/Simulator Results

The Broadband Modem's performance in the presence of cross-polarization interference introduced at IF after the signal passes through the radio and simulator is shown in Figure 91. The FCC 19311 filter was installed in the radio and  $4/25 \text{ ns/MHz}^2$  parabolic group delay correction was used at IF to equalize the radio/filter combination. This value of correction was determined during testing performed on Contract F30602-76-C-0434. The solid line depicts back-to-back IF performance. The dotted line depicts performance through the simulator without interference. Figure 91 shows BER versus  $E_b/N_0$  for CPDR's between 10 and 30 dB.

CPIRE performance over the radio without parabolic correction for the Horizontal Channel is shown in Figure 92. Similar data for the Vertical Channel is given in Figure 93. The baseline curve reflects the absence of the group delay correction. The two channels perform almost identically under these conditions. Without interference, the curve is within 0.8 dB of

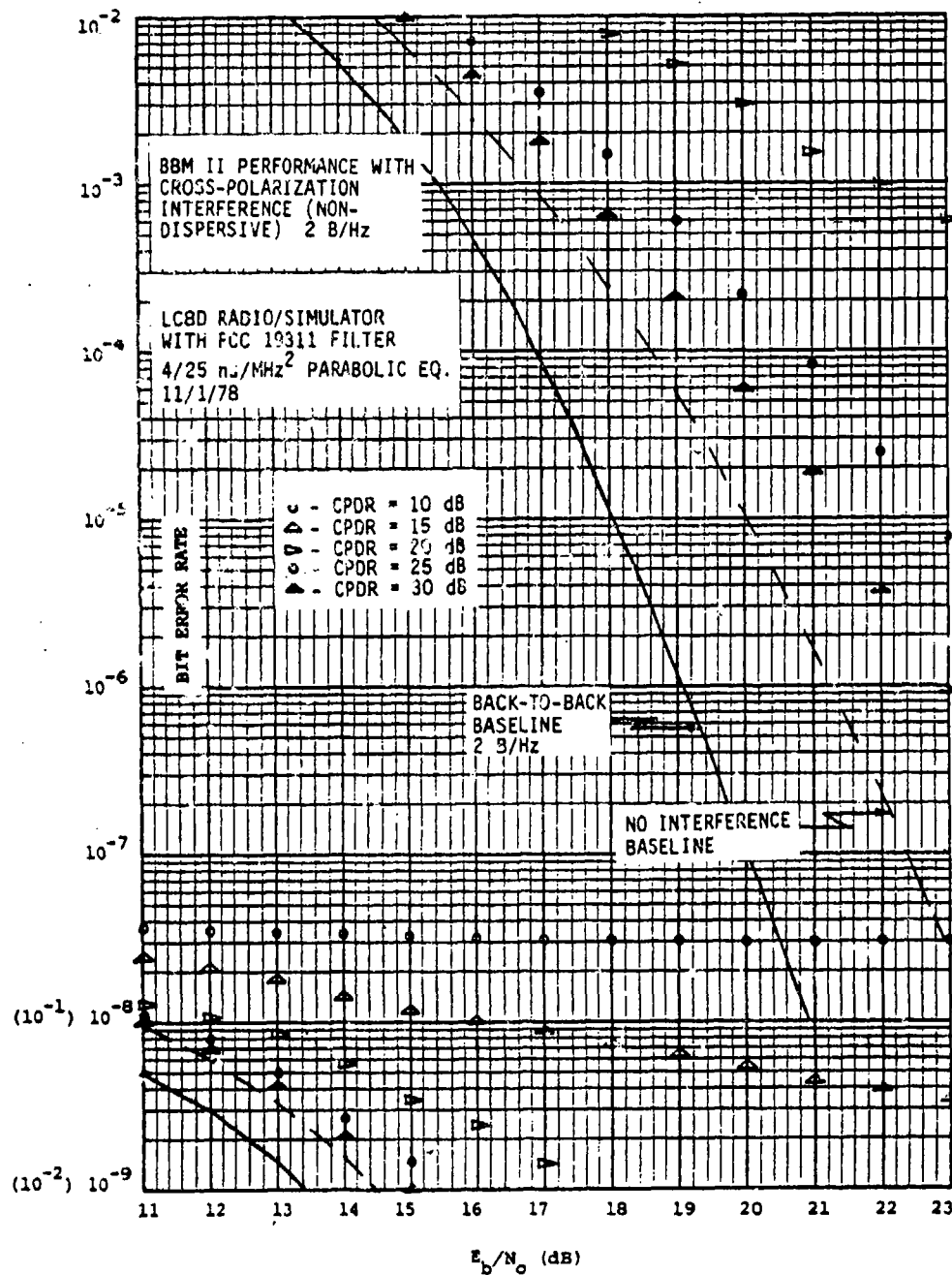


Figure 91. BBM II 2 B/Hz Performance Over LC8D Radio  
With Cross-Polarization Interference

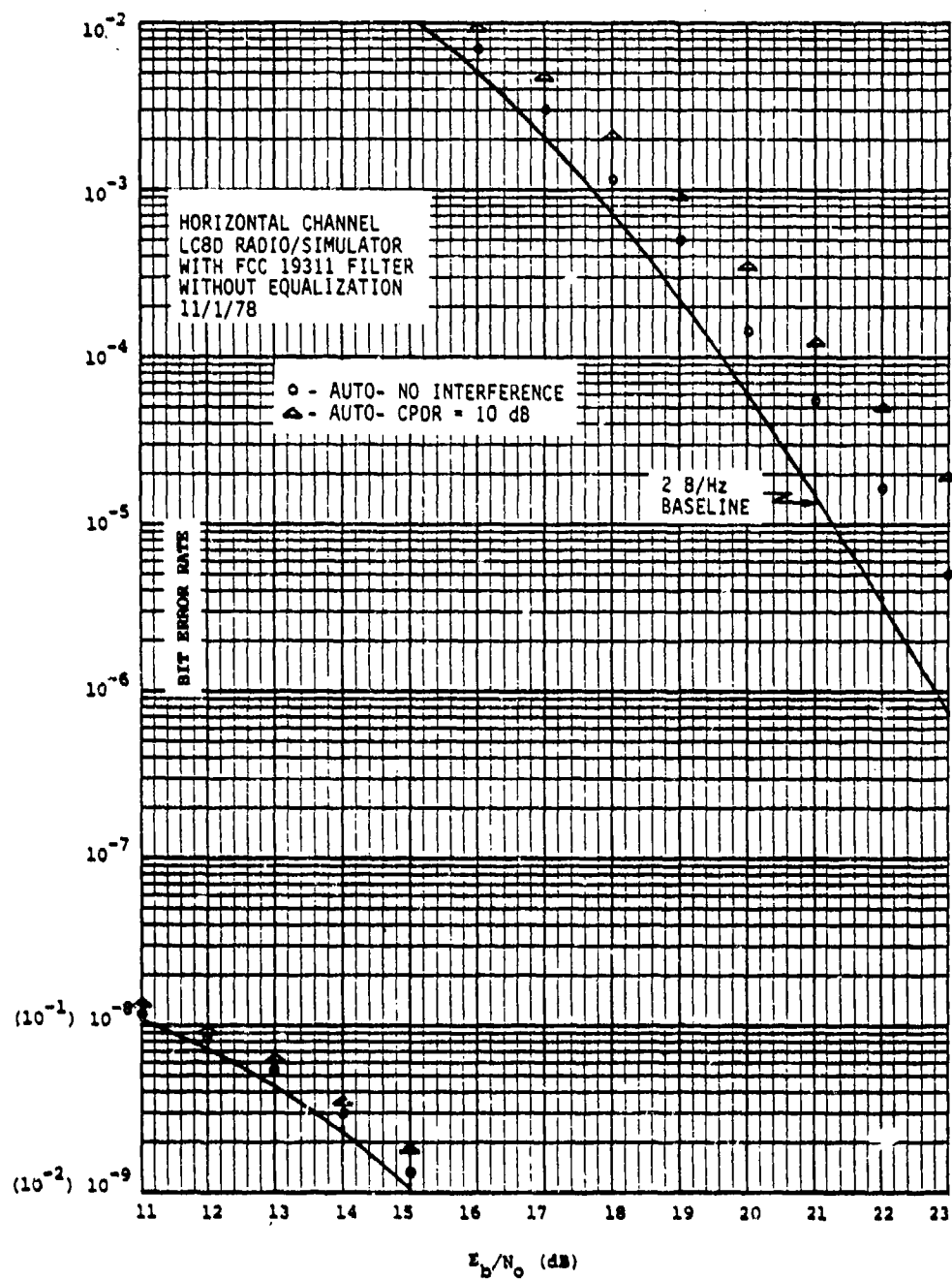


Figure 92. CPIRE Horizontal Channel 2 B/Hz Performance  
With LC8D Radio/Simulator Without Equalization

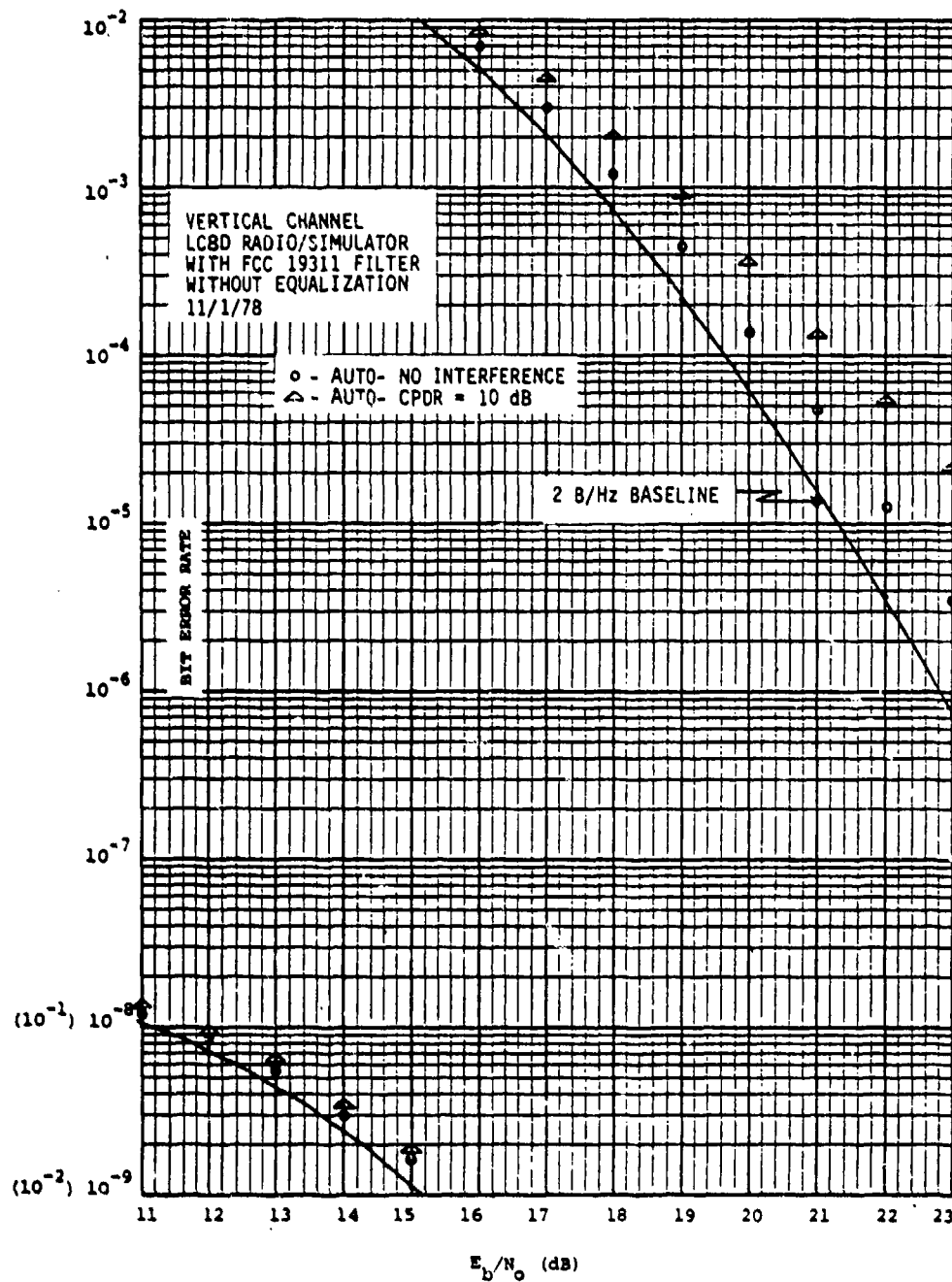


Figure 93. CPIRE Vertical Channel 2 B/Hz Performance With LC8D Radio/Simulator Without Equalization

the baseline at a BER of  $1 \times 10^{-4}$ . With a CPDR of 10 dB, the curve is within 1.6 dB of the baseline at the same BER. Without the CPIRE, the BER would be a nearly constant 40 percent.

Since the two channels perform so closely over the radio/simulator, the Vertical Channel was used for all additional tests. Figure 94 shows CPIRE operation with the parabolic group delay correction installed after the receiver downconversion to IF. Here, performance without interference is within 1 dB of the baseline in the vicinity of a  $1 \times 10^{-6}$  BER. With a CPDR of 10 dB, the BER curve is within 2 dB of the baseline in the vicinity of a  $1 \times 10^{-5}$  BER. With a CPDR of 5 dB, the flair is more pronounced, indicating residual loop jitter in the equalizer portion of the CPIRE. Comparing this figure with Figure 91, it may be observed that the CPIRE reduces an input CPDR of 5 dB to a CPDR of approximately 25 dB under these conditions. Starting with a CPDR of 10 dB, the CPIRE can reduce the interference to a CPDR near 28 dB. The residual interference level is better than 30 dB down.

An additional 2 B/Hz mode test was run with the CPIRE's equalizer section bypassed. Only the cross-pole weight was allowed to operate. As seen in Figure 95, operation in this mode (with nondispersive cross-polarization interference) is virtually independent of CPDR and equivalent to the noninterference case. It is thus obvious that the equalizer section should be bypassed if naturally occurring cross-pole mechanisms are found to be essentially nondispersive. It is also apparent that the equalizer control loops are more susceptible to noninterference-induced AM than are the cross-pole loops.

#### 4.2.3.2 1 B/Hz Radio/Simulator Results

CPIRE performance with the modulator output going over the radio with FCC 19311 filter and with  $4/25 \text{ ns/MHz}^2$  parabolic group delay equalization is shown in Figure 96. The no-interference curve is within 0.6 dB of the baseline curve in the vicinity of a  $1 \times 10^{-6}$  BER. With a CPDR of 10 dB, this is degraded by 0.5 dB. With a CPDR of 5 dB, the curve is within 1.9 dB of the baseline at a BER of  $1 \times 10^{-5}$ . As noted earlier, with small CPDR's, performance is highly phase angle dependent.

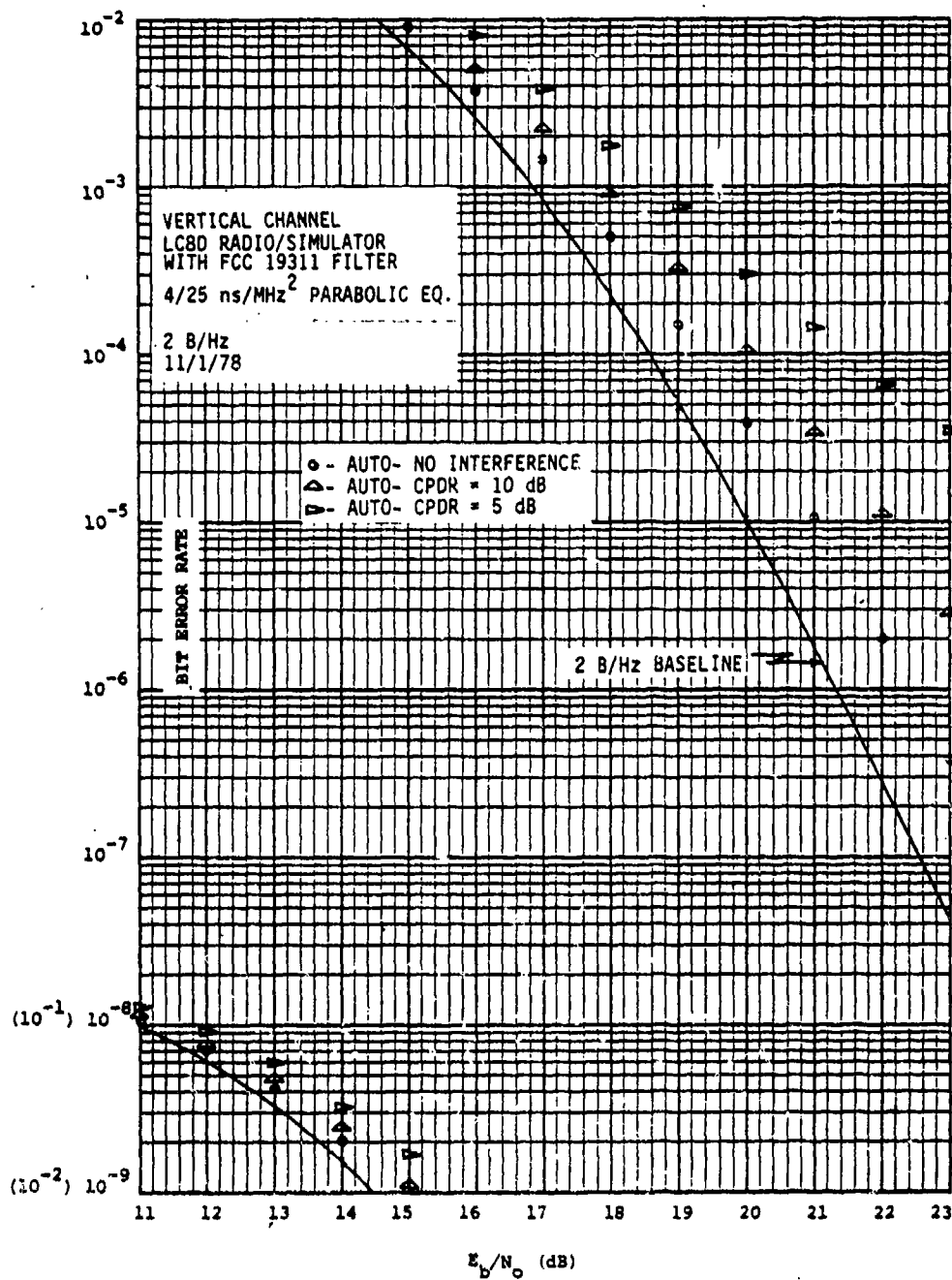


Figure 94. CPIRE Vertical Channel 2 B/Hz Performance With LC8C Radio/Simulator With Equalization

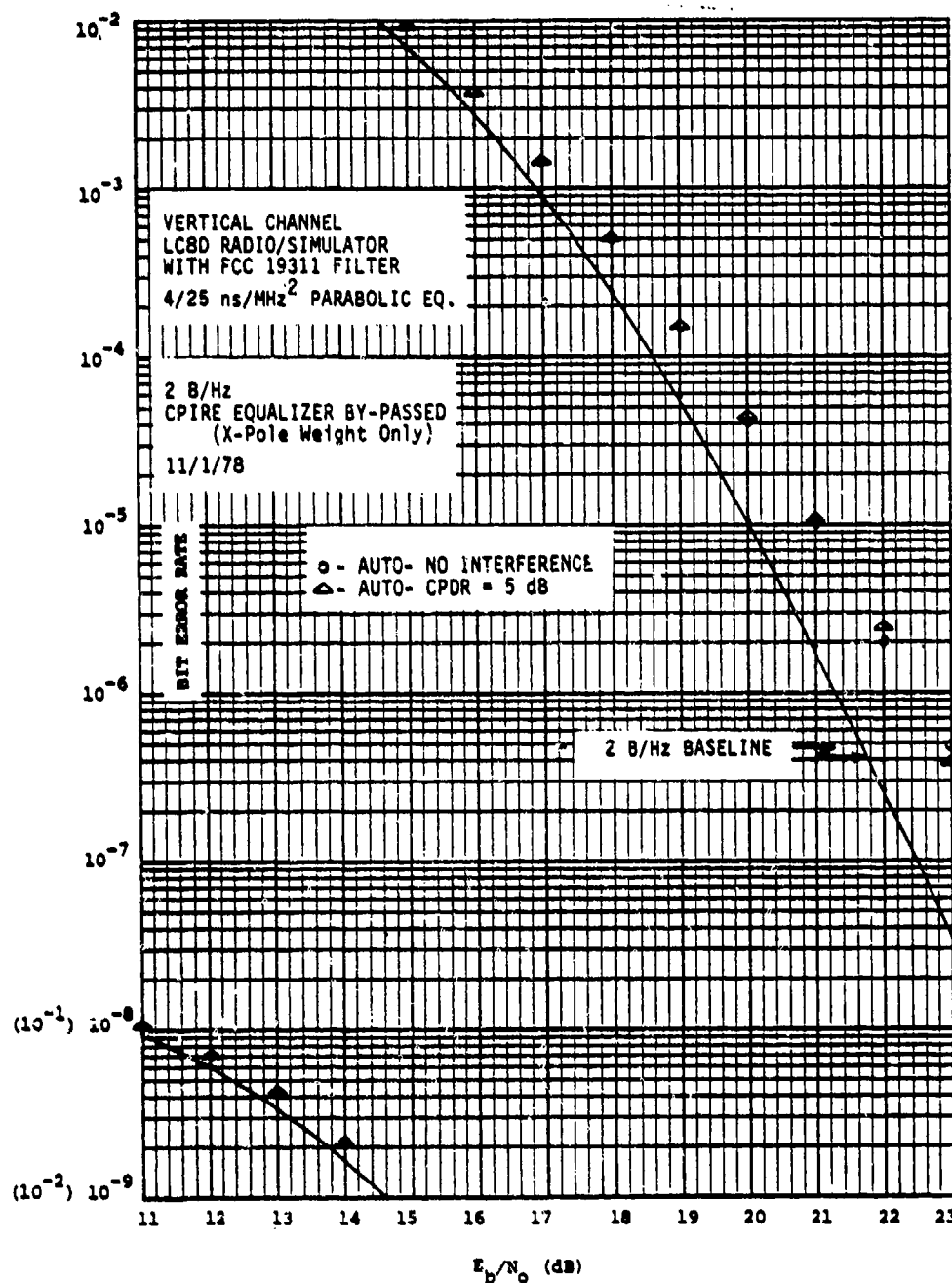


Figure 95. CPIRE Vertical Channel 2 B/Hz Performance With LC8D Radio/Simulator - Equalizer Bypassed

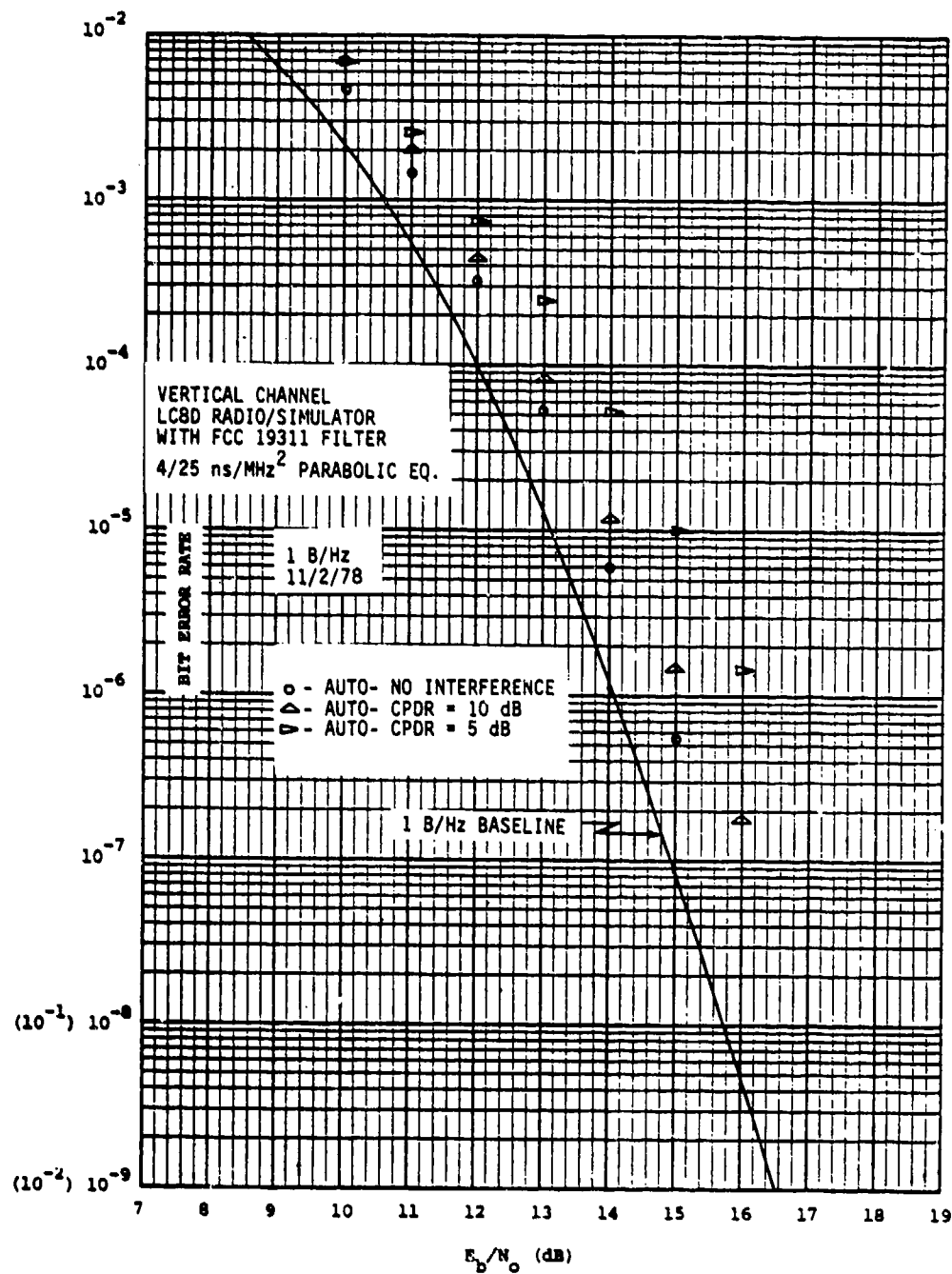


Figure 96. CPIRE Vertical Channel 1 B/Hz Performance With LC8D Radio/Simulator

With the CPIRE's equalizer section bypassed, the curve in Figure 97 was obtained with a CPDR of 5 dB. Comparison with Figure 96 reveals that performance under these conditions is virtually the same as the no-interference case with the equalizer enabled. As in 2 B/Hz operation, improved performance can be obtained with nondispersive cross-polarization interference by disabling the equalizers.

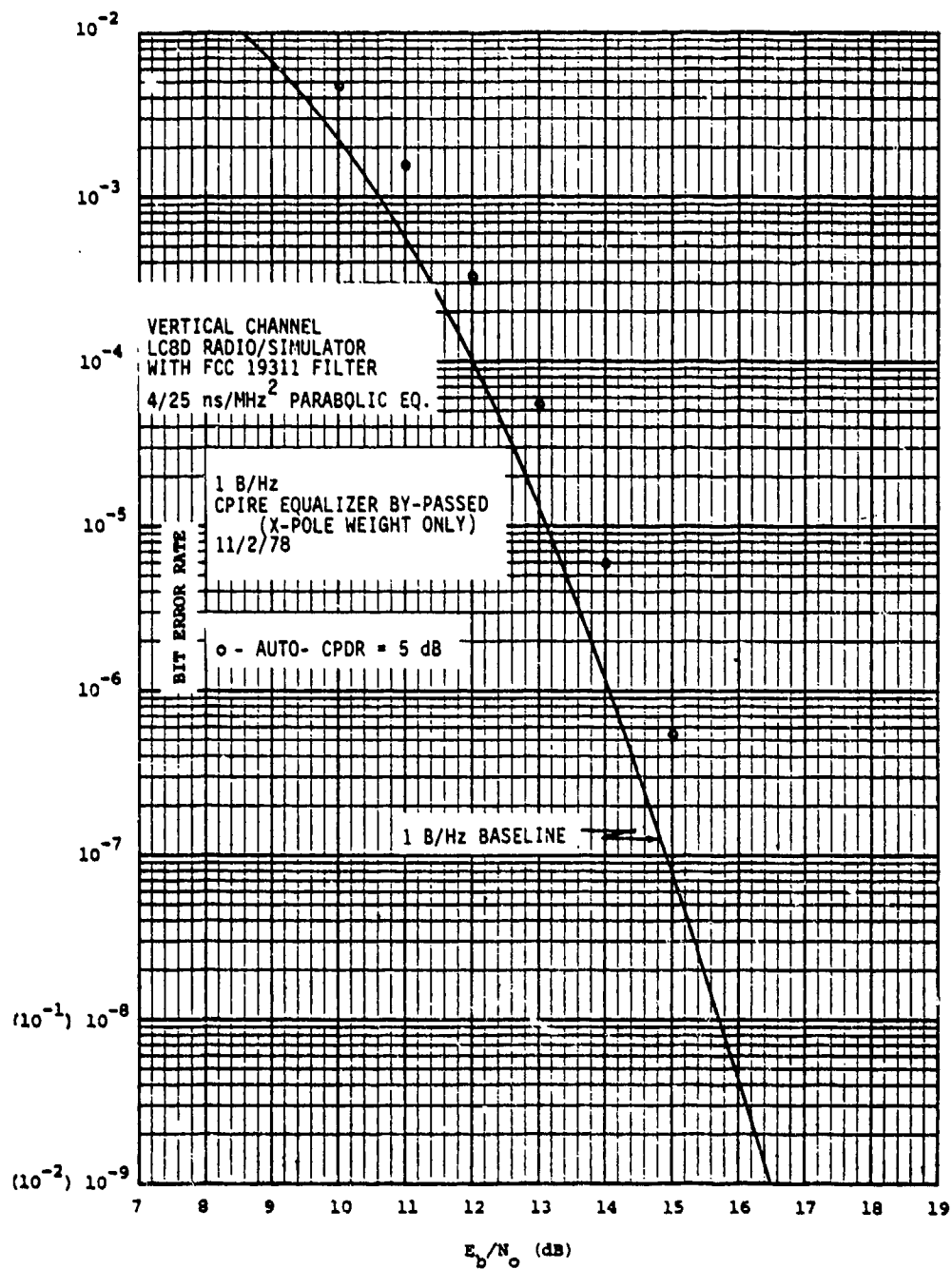


Figure 97. CPIRE Vertical Channel 1 B/Hz Performance With LC8D Radio/Simulator - Equalizer Bypassed

**SECTION 5.0**  
**CONCLUSIONS AND RECOMMENDATIONS**

## 5.0 CONCLUSIONS AND RECOMMENDATIONS

### 5.1 Conclusions

A breadboard adaptive equalizer providing improved performance on cross-polarized line-of-sight microwave channels was constructed and successfully tested.

The equalizer provides the required 20 ns of linear and parabolic group delay compensation at the band edges (70 MHz  $\pm$  7 MHz). In addition, the equalizer can provide 8 ns of straight delay compensation and more than 3 dB of linear, parabolic, and cubic amplitude correction at the band edges. With the Broadband Modem II signal going through the LC8D radio with FCC 19311 microwave filter, a 20 dB improvement may be obtained starting with a cross-polarization discrimination ratio (CPDR) of 5 dB. Residual interference levels in the automatic mode are more than 30 dB below the signal level. For nondispersive cross-pole interference, removal of the amplitude and group delay equalizer portions can result in 25 dB of cross-pole suppression starting with an initial CPDR of 5 dB. Performance is also improved if the modem signal is free of filter-induced amplitude modulation. This was demonstrated in the tests without the radio. Here, residual interference levels were close to the design objective of a CPDR of 40 dB, and a CPDR of 5 dB was reduced to a CPDR near 28 dB. A CPDR of 10 dB was reduced by more than 20 dB. Tests also demonstrated that the equalizer can track time varying interference at 1 Hz rate without degradation and up to a 10 Hz rate with less than 1.5 dB degradation in the vicinity of a  $1 \times 10^{-7}$  BER.

### 5.2 Recommendations

It is apparent from the tests that increased knowledge of naturally occurring cross-polarization interference mechanisms could result in a more effective interference reduction equalizer. The control loop parameters could be optimized for existing conditions. An extended study utilizing the Cross Polarization Interference Reduction Equalizer (CPIRE) as a test instrument on existing microwave links could obtain valuable information concerning the nature of cross-pole interference. Such a test program is recommended.

It is further recommended that a program be undertaken to refine the CPIRE to provide improved performance with signals having filter-induced AM and to provide automatic copolar operation. Simultaneous automatic cross-polar and copolar operation could provide previously unattained performance with the Broadband Modem over the microwave radio while meeting FCC 19311 requirements. Both goals could possibly be accomplished by investigation of performance criteria other than envelope AM content. Measurement of eye pattern closure at the output of the Broadband Demodulator may provide the optimum control system for an equalizer providing simultaneous copolar and cross-polar operation.

APPENDIX A  
ACHIEVABLE TIME DELAY

# APPENDIX A

## ACHIEVABLE TIME DELAY

Definite bounds exist for the group delay compensation range of the chosen equalizer implementation. After an  $n$ th order notch filter we have voltage given by

$$jA \sin^n \pi f T$$

where  $A$  is the maximum value of the weighted voltage with respect to the normalized reference voltage, and  $T$  is the time delay of the delay lines used to construct the notch filter. In this design,  $T = 14.29 \times 10^{-9}$  seconds. The maximum value,  $A$  occurs at  $f_c \pm \frac{1}{2T}$  where  $f_c$  is the notch frequency. The amplitude at the band edge (7 MHz from the carrier) is 10.04 dB below the peak value. The phase shift is

$$\phi(f) = \tan^{-1} (A \sin^n \pi f T)$$

and the time delay is

$$\tau(f) = \frac{1}{2} \frac{d\phi}{df}$$

$$\tau(f) = \frac{T}{2} \frac{A n \sin^{n-1}(\pi f T) \cos(\pi f T)}{1 + A^2 \sin^{2n}(\pi f T)}$$

At the band edge ( $\pm 7$  MHz) the time delay is

$$\begin{aligned} \tau(7) &= \frac{7.15 A n \sin^{n-1}(18^\circ) \cos(18^\circ)}{1 + A^2 \sin^{2n}(18^\circ)} \\ &= \frac{7.15 A n (0.309)^{n-1} (0.951)}{1 + A^2 (0.309)^{2n}} \end{aligned}$$

For a first order notch,

$$\tau(7) = \frac{6.8A}{1 + 0.0955A^2} \text{ ns}$$

Delay increases with  $A$  for small values of  $A$  and decreases with  $A$  for large values of  $A$ . The maximum value of delay is achieved with  $0.0955A^2 = 1$  or  $A = 3.24$  and is 11.0 ns.

For a second order notch the time delay at band edge is given by

$$\tau(7) = \frac{7.15 A^2 (0.309)(0.951)}{1 + A^2 (0.309)^4}$$

$$= \frac{4.20 A}{1 + 0.00912 A^2}$$

Maximum band edge delay is realized with  $0.00912A^2 = 1$  or  $A = 10.47$  and is 21.99 ns.

For a third order notch, the band edge delay is given by

$$\tau(7) = \frac{7.15 A(3)(0.309)^2(0.951)}{1 + A^2 (0.309)^6}$$

$$= \frac{1.95 A}{1 + 0.00087A^2}$$

Maximum delay is realized with  $A = 33.90$  and is 33.06 ns.

**APPENDIX B**  
**DECORRELATOR**

## APPENDIX B

### DECORRELATOR

The Decorrelator was constructed as a test fixture to simulate two independent Broadband Modem channels, ("horizontal" and "vertical") with a single Broadband modulator. This is accomplished by splitting the output of the modulator into two channels and introducing sufficient delay into one of the channels to remove correlation between them. Amplifiers restore the original modulator output level. A block diagram is shown in Figure B-1.

The Decorrelator is contained in a 3.5-inch high chassis designed to be mounted in a standard 19-inch rack. A photograph of the unit's front panel is shown in Figure B-2. The unit contains an integral power supply and requires no special cooling provisions. Input and output connectors are BNC type and are located on the front panel. The maximum input level is +1 dBm into 75 ohms. The Horizontal Output is the minimum delay path, the Vertical Output the maximum delay path. Output levels are within  $\pm 0.25$  dB of the input at 70 MHz. This can be seen in Figures B-3 and B-4 where output magnitude is plotted versus frequency across the bandwidth of interest for the Horizontal Channel and Vertical Channel, respectively. The slight (approximately 0.75 dB) slope across the band on the Vertical Output is a result of dispersion in the delay line. Delay versus frequency is plotted in Figure B-5 and B-6. The delay through the Horizontal Channel is less than 5 ns, while the delay through the Vertical Channel is approximately 310 ns. The differential delay is approximately 4.1 symbol times when the Broadband Modem is operating in the 2 B/Hz mode. The minimum time required for the ending phase nodes to advance a full 360 degrees is 2.67 symbol times. Complete decorrelation would require many symbol times. The delay selected represents a good compromise between correlation and dispersion. The effects of the small amount of remaining correlation were minimized during in-plant testing by maintaining the exact test configuration for all measurements, thus preserving phase relationships between channels and interference.

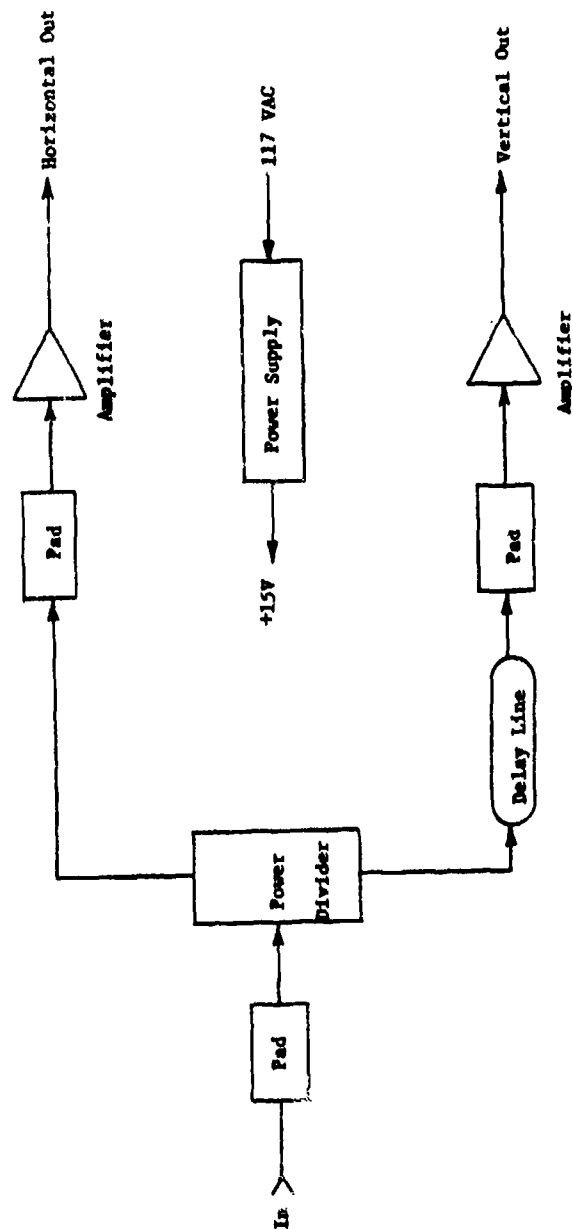


Figure B-1. Decorrelator Block Diagram

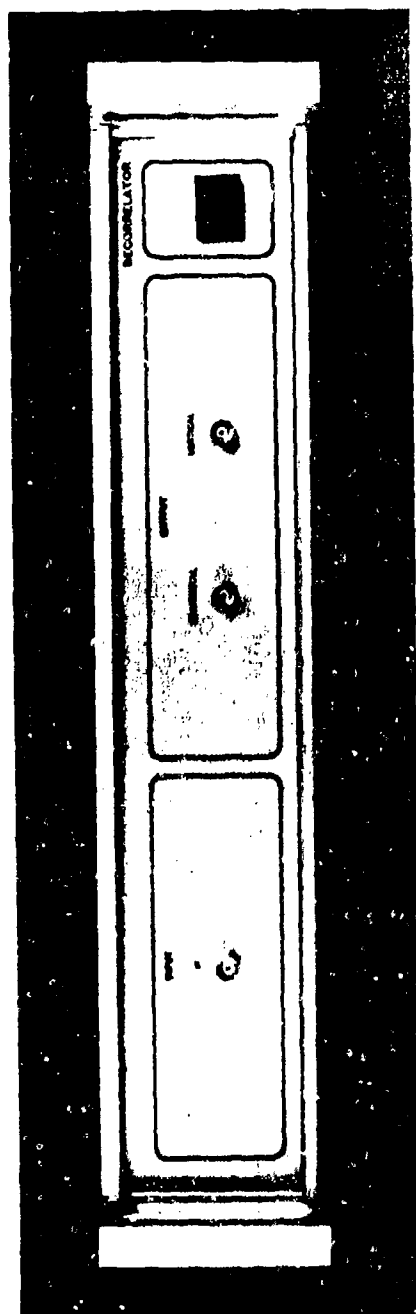


Figure B-2. Decorrelator Front Panel

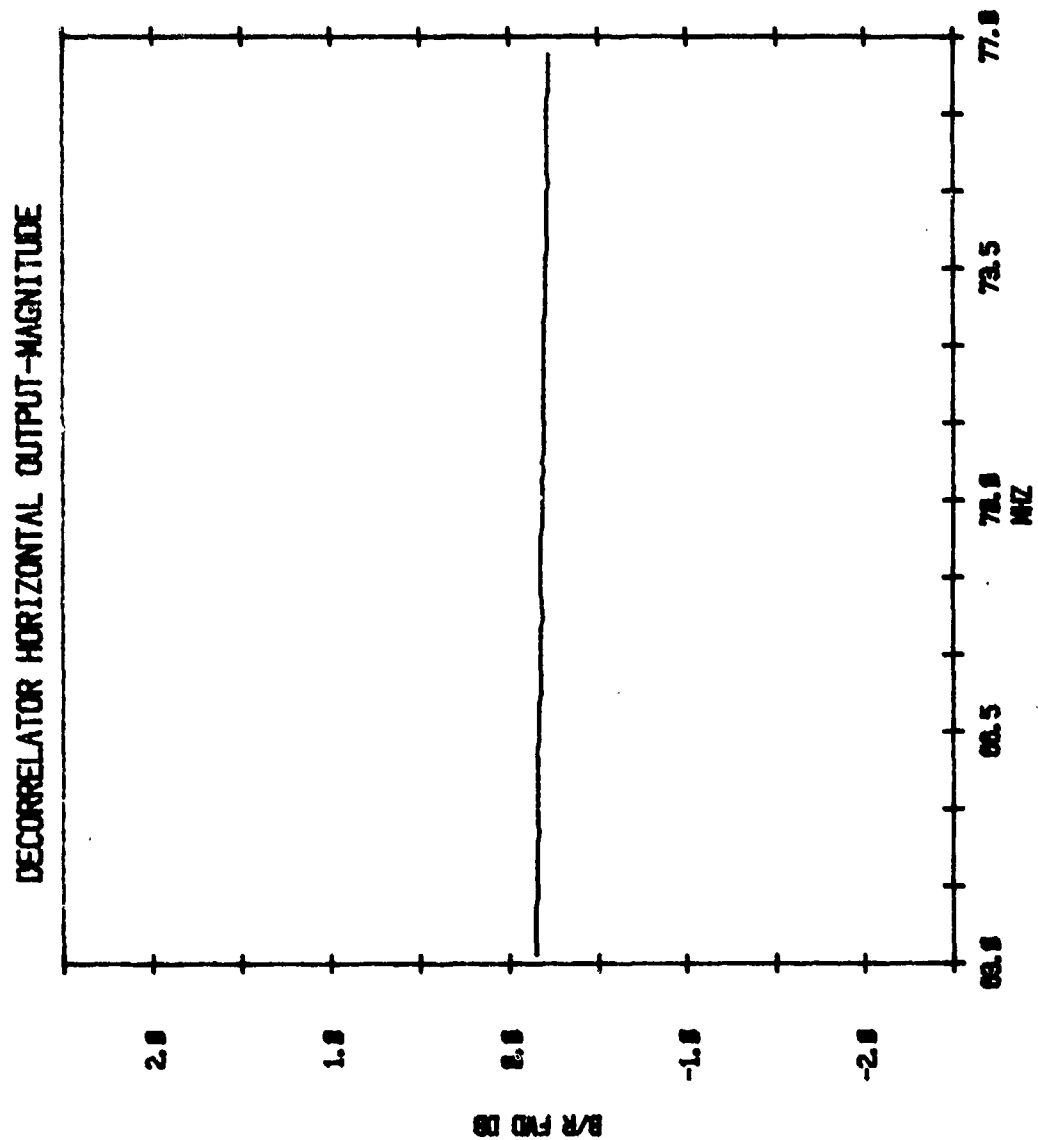


Figure B-3. Decorrelator Horizontal Output Amplitude Response

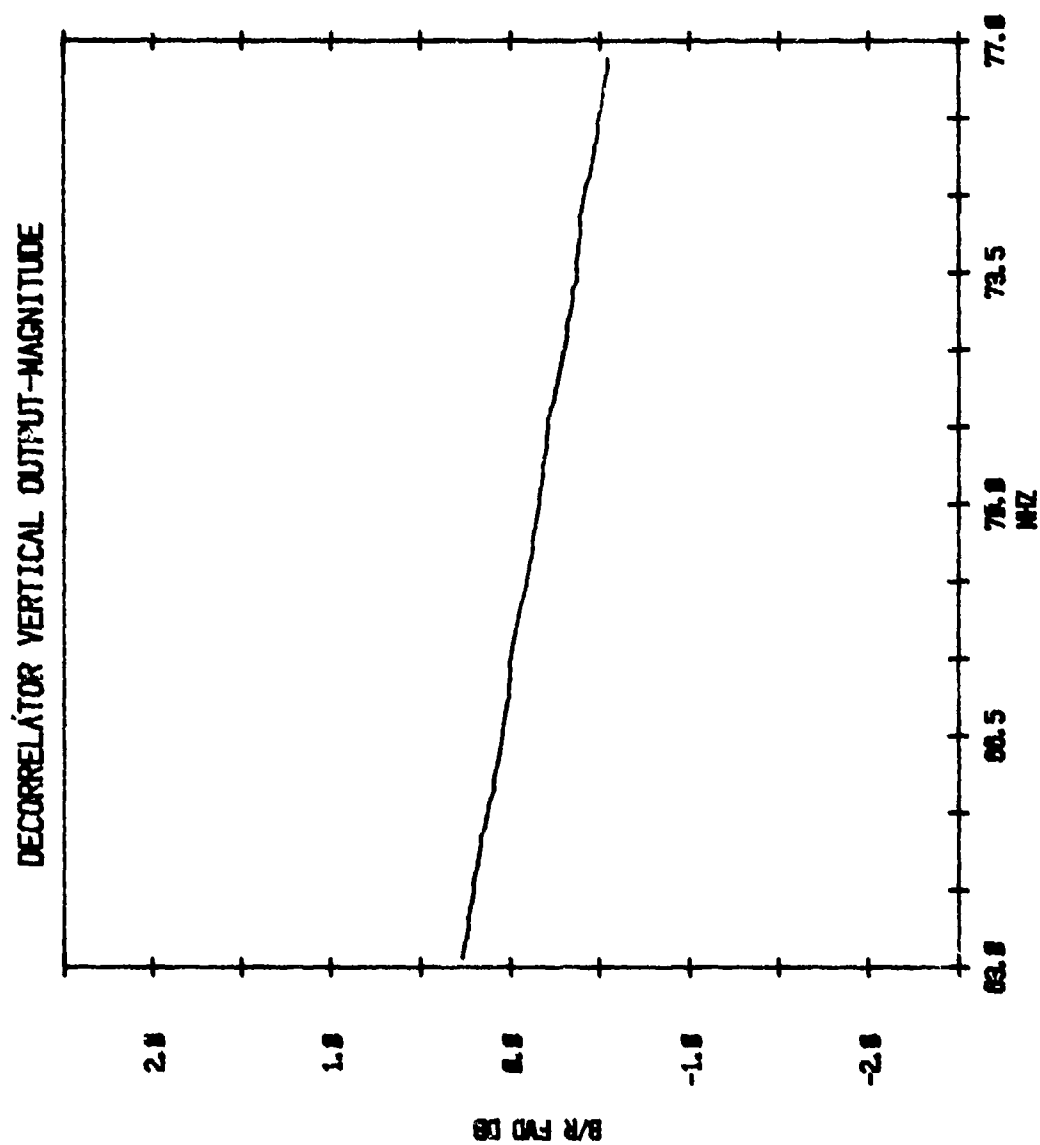


Figure B-4. Decorrelator Vertical Output-Amplitude Response

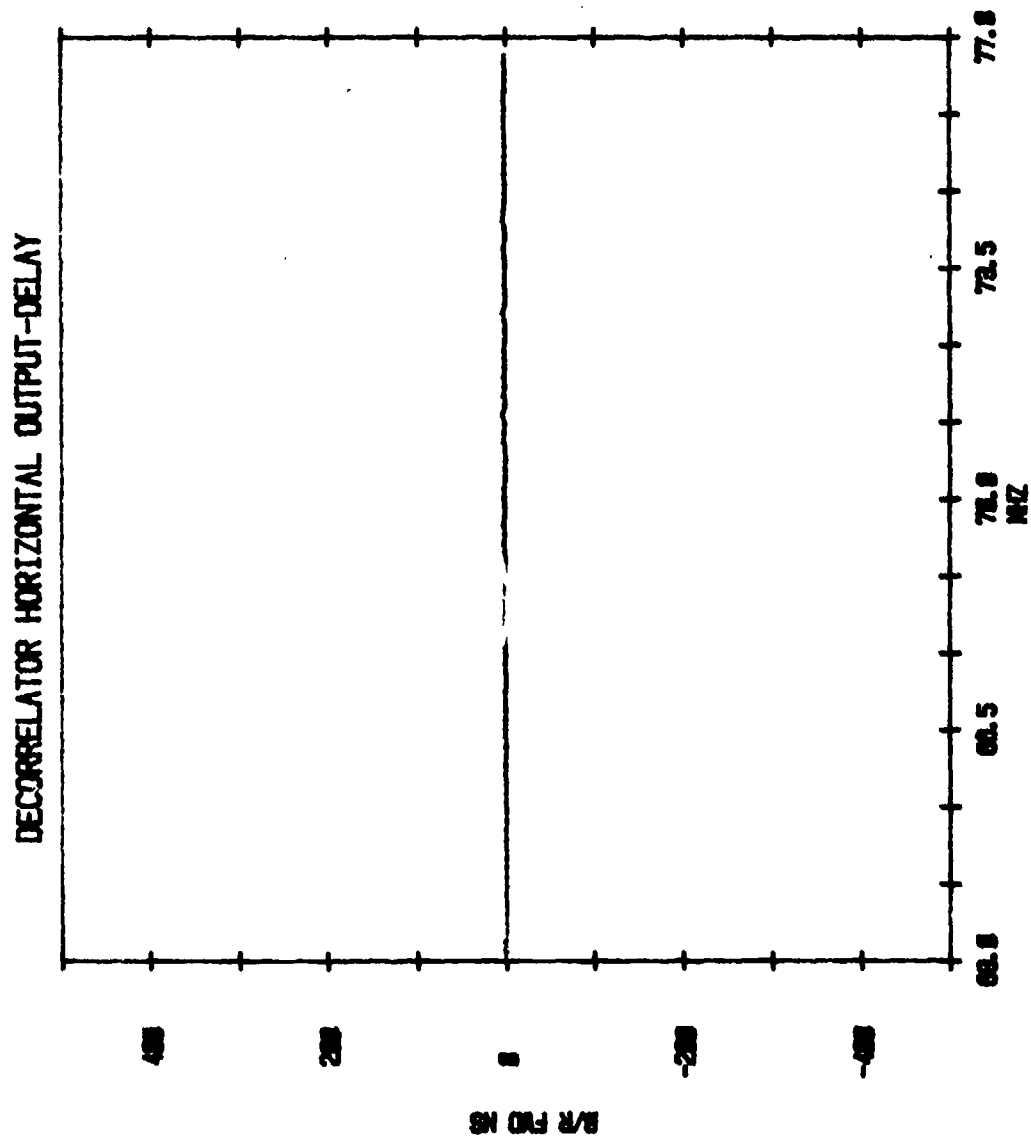


Figure B-5. Decorrelator Horizontal Output Delay

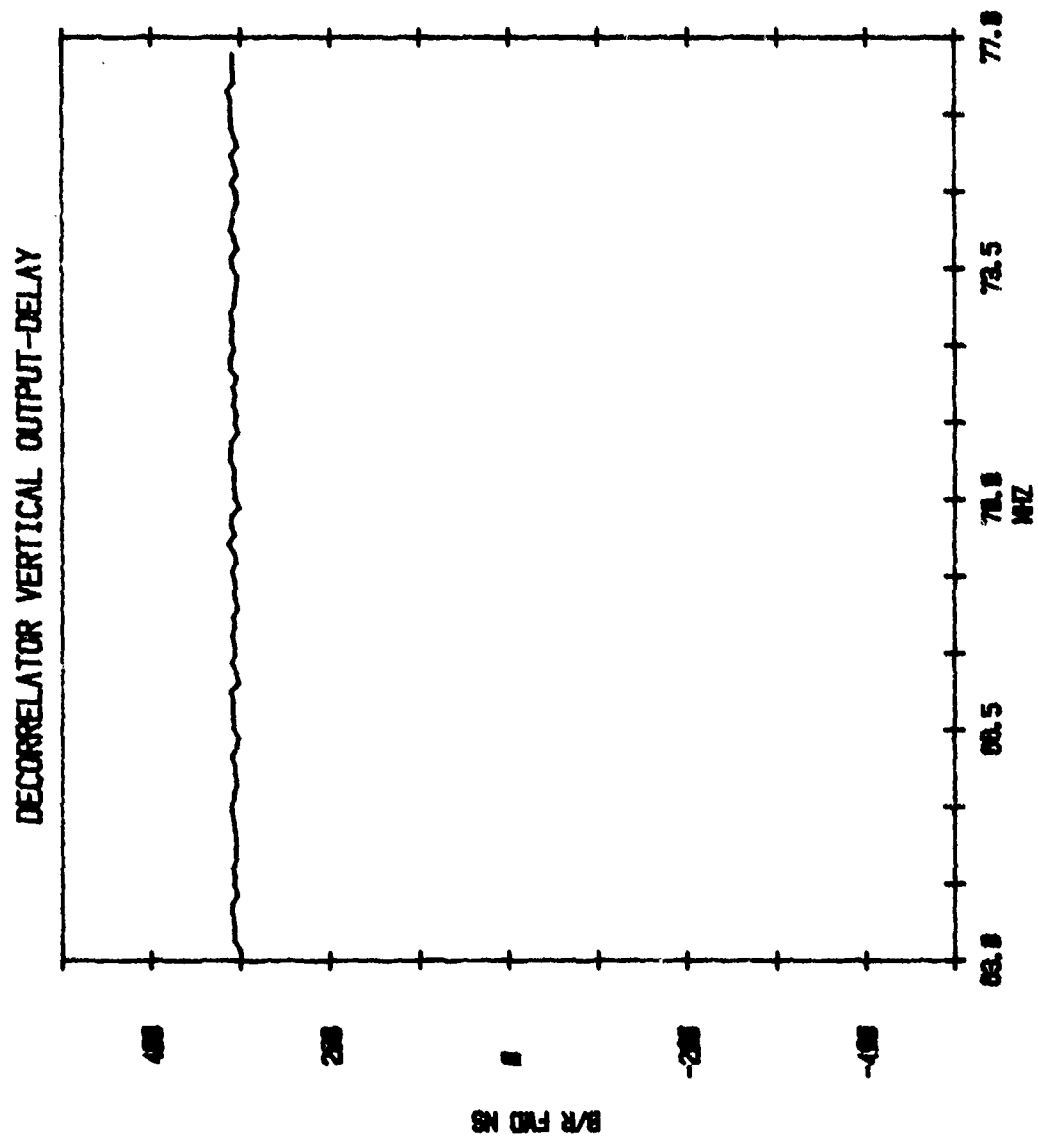


Figure B-6. Decorrelator Vertical Output Delay

APPENDIX C  
TEST PLAN

## APPENDIX C

### TEST PLAN

#### 1.0 SCOPE

This plan describes a test program for Cross-Polarization Interference Reduction Techniques (Cross Pole). The test will be conducted at RADC and at Harris GCSD in Melbourne, Florida.

#### 2.0 OBJECTIVE

The overall objective is to characterize the critical performance parameters of the Cross Pole breadboard. Specific tests include:

- a. Equalization Range
- b. Nondispersive Cross-Polarization Interference Reduction
- c. Dispersive Cross-Polarization Interference Reduction
- d. Dynamic Cross Polarization Interference Reduction

#### 3.0 HARDWARE DESCRIPTION

The Cross Polarization Interference Reduction Equalizer (CPIRE) is packaged in a single 19-inch chassis with integral power supplies and provides dual channel operation. Each channel consists of an adaptive equalizer designed to compensate for cross-polarization interference between two microwave modem channels. The unit operates by adjusting the phase and amplitude of a preequalized component of one channel and summing it with the other to cancel the interference. The two equalizers are capable of linear, parabolic, and cubic amplitude correction, as well as straight delay and linear and parabolic group delay correction. A basic block diagram is shown in Figure C-1. Each received channel is split three ways. One component, the main signal path, is fed to a summer where the correction signal is added. The other two components are fed to the equalizer for the opposite channel. Each equalizer consists of three cascaded notch filters (N.F.). The filter outputs are adjusted by complex weights ( $W_n$ ) and summed with a delayed component of the input. This provides equalization to match the interference that must be removed. The equalized signal is adjusted in amplitude and phase with the cross-pole weight,  $W_4$ , and summed with the other channel, cancelling the interference on it. The "cleaned up" channel is fed to the demodulator and to the control circuitry for the equalizer weights. The output signal is examined for amplitude modulation on its

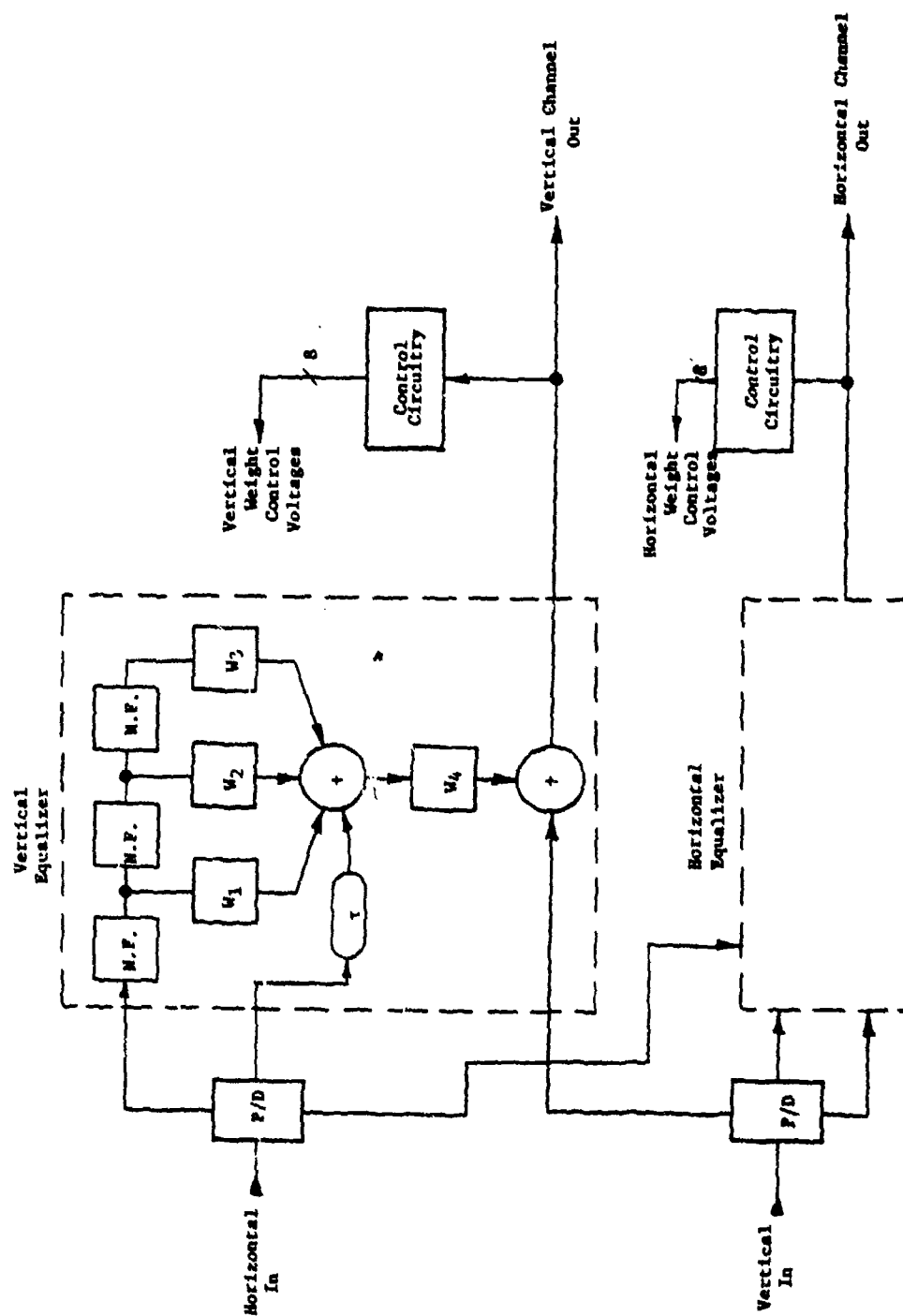


Figure C-1. CPIRE Basic Block Diagram

envelope. Adjustments are made to the weights to minimize the AM, thus minimizing the cross-polarization interference.

#### 4.0 TEST PROGRAM

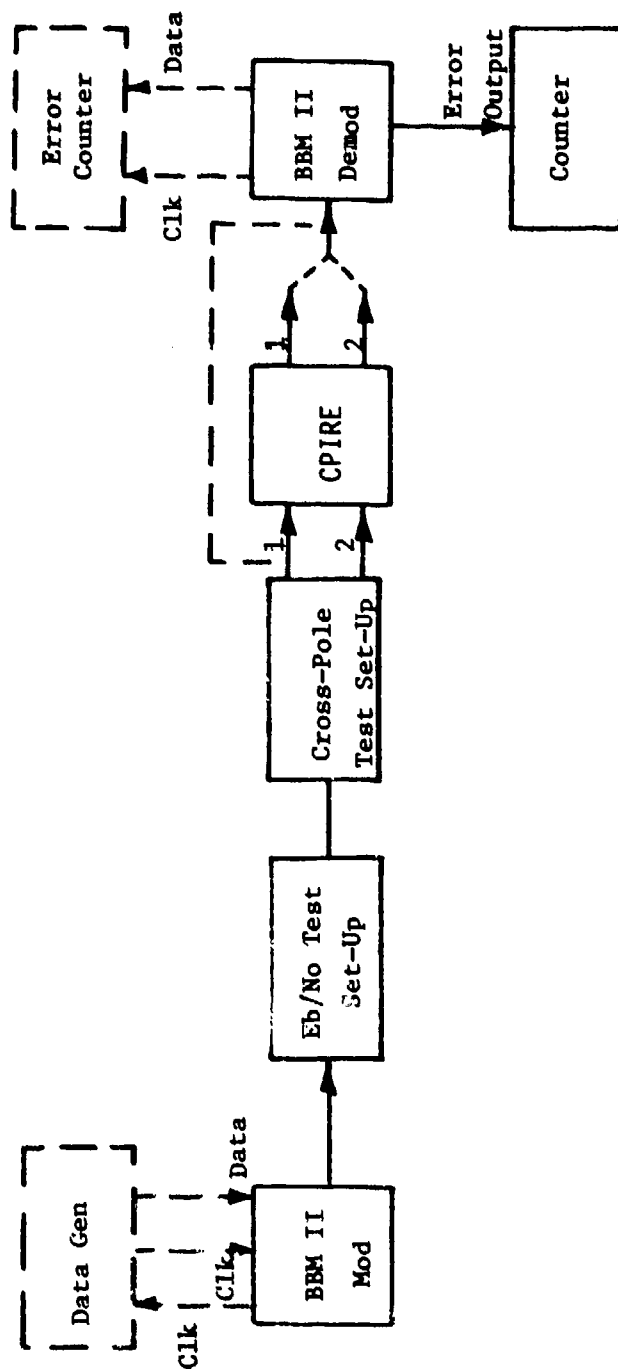
The test program includes tests at Harris GCSD in Melbourne, Florida, and at RADC. The in-plant tests are designed to provide a performance baseline from which to interpret results from the later radio and link tests and to verify the characteristics of various internal parameters. Most of these tests will be performed in conjunction with the GFE Broadband Modem. The modulator output will be split into two signals with one signal delayed to prevent correlation with the other channel. The delayed signal will simulate the second channel. Mixing between channels will introduce interference. Noise can be summed with the modulator output to measure bit error rate (BER) at the demodulator output. All tests at Harris will be run at 70 MHz. The RADC tests will include link tests utilizing the LC8D radio.

#### 4.1 In-Plant Tests

Initial tests of the CPIRE will be performed on the Hewlett Packard 8505A Network Analyzer, with the equalizer in the manual mode. Phase and amplitude equalization capabilities will be characterized. The remainder of the test will be performed with the basic test configuration of Figure C-2. Here, the interference reduction capabilities of the CPIRE are tested in conjunction with the Broadband Modem implemented under Contract F-30602-76-C-0434. Details of the  $E_b/N_0$  Test Setup, Decorrelator, and Cross Pole Test Setup are shown in Figures C-3, C-4, and C-5.

##### 4.1.1 $E_b/N_0$ Calibration

The test setup of Figure C-3 is used to provide a reference error rate for the Broadband Modem. Thermal noise power at the output of the test setup is measured with the signal attenuator set to maximum attenuation. This measurement is recorded. The noise attenuator is then set to maximum attenuation and the signal attenuator is adjusted to give the same meter reading as the noise power did previously. The noise attenuator is then restored to its original position, establishing a 0 dB SNR in the filter bandwidth.  $E_b/N_0$  is then determined by adding a correction factor that



For Self Test Mode  
of Modem

Figure C-2. In-Plant Test Configuration

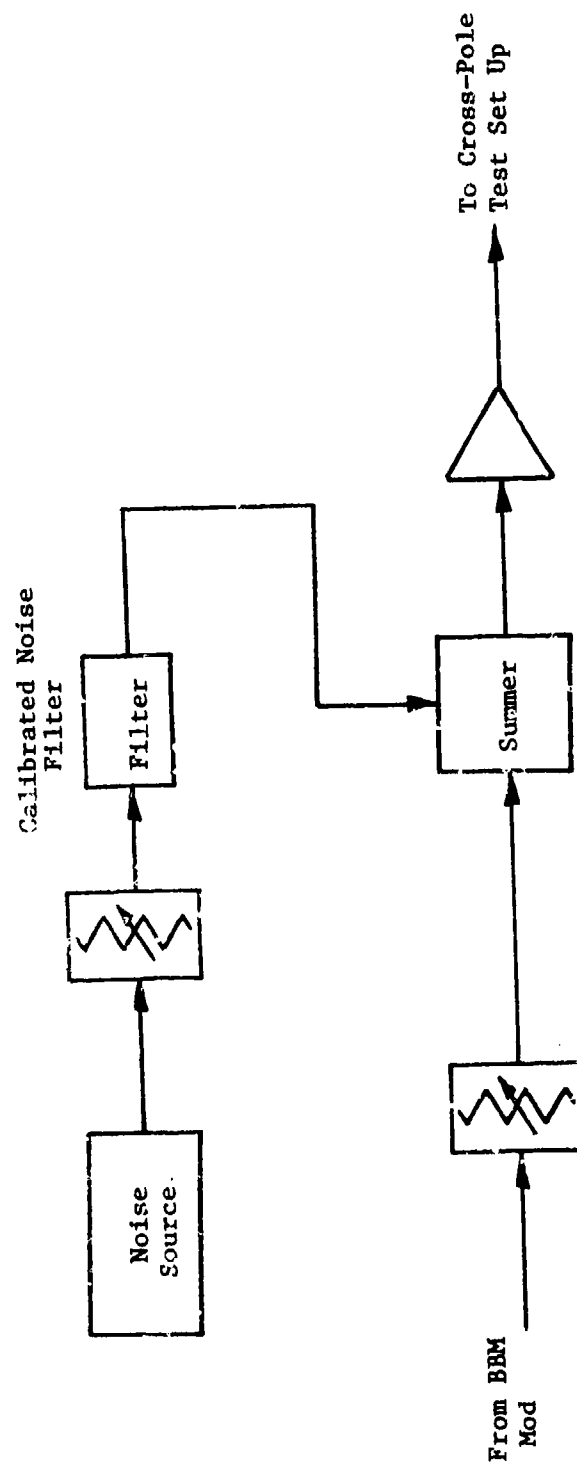


Figure C-3.  $E_b/N_0$  Test Setup

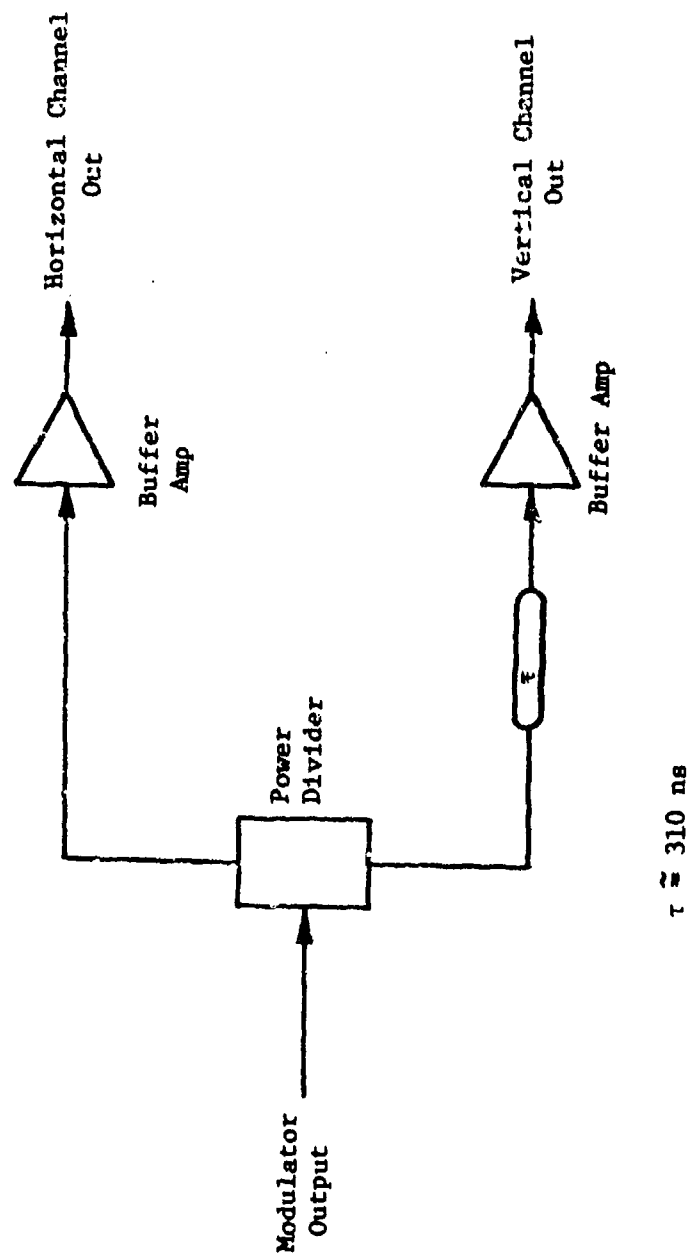


Figure C-4. Decorrelator Block Diagram

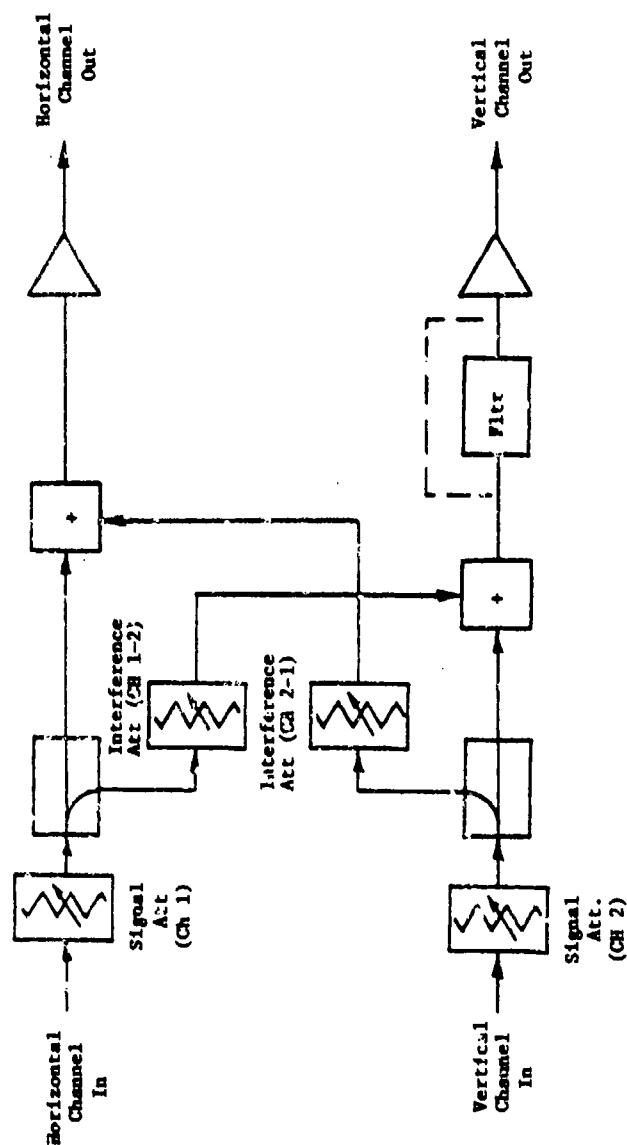


Figure C-5. Cross-Polarization Test Setup

is equal to  $10 \log \frac{NBW}{BR}$  where NBR is the measured noise bandwidth of the calibrated filter and BR is the bit rate. The desired  $E_b/N_0$  is obtained by adjusting the attenuator settings.

#### 4.1.2 Cross Polarization Discrimination Ratio Calibration

The Test Setup of Figure C-5 is used to provide adjustable interference between the two modem channels. Two uncorrelated channels are simulated by delaying part of the modulator output by approximately four symbol times in the Decorrelator. Electronically controlled attenuators sum a portion of one channel with the other. Electronically controlled attenuators are used rather than manual ones to allow dynamic tests with the cross-polarization discrimination ratio as a function of time. With the cross-pole attenuators set to maximum attenuation, the main signal power can be measured. Then the signal attenuator of one channel can be set to maximum and the interference attenuator adjusted to provide the desired level of interference. This is repeated for the other channel and then the signal attenuators are restored to their original positions.

#### 4.1.3 Nondispersive Cross-Polarization Interference Reduction

To test the basic cross-polarization interference reduction capability of the breadboard, the filter shown in Figure C-5 is removed. The test set then simply mixes the channels together without any frequency selectivity. Performance should be identical on both channels. For a baseline reference, the CPIRE is bypassed and a BER curve is plotted versus  $E_b/N_0$  with minimum cross-talk. The measurements are then repeated with various amounts of cross-polarization interference to determine modem performance with interference. The CPIRE is then inserted in the signal path and the measurements are repeated. The improvement in error rate is noted. The design goal is an operation range of cross-polarization discrimination ratios from 5 to 40 dB.

#### 4.1.4 Dispersive Cross-Polarization Interference Reduction

To test for interference reduction with frequency selective fading, a filter is introduced into the signal path on one channel (see Figure C-5). The BER measurements are performed on the other channel. The equalizer portion of the CPIRE must eliminate the effects of the filter in order that the cross-pole weight might cancel the interference. The filter

is chosen to introduce group delay and amplitude distortion within the design requirement range of 20 nanoseconds across a 14 MHz frequency band. A delay line is inserted into the signal path of the channel being measured to reduce the differential delay between channels to a level that the CPIRE can handle ( $\pm 10$  ns). The tests are then conducted as in Paragraph 4.1.3.

#### 4.1.5 Dynamic Cross-Polarization Interference Reduction

By modulating the amount of cross-talk with electronically controlled attenuators, the ability of the CPIRE to track changes in interference can be measured. Modem BER versus  $E_b/N_0$  is plotted with modulation frequency as a parameter for a sine wave control voltage whose peak amplitude produces a known amount interference.

#### 4.2 RADC Tests

The primary objective of the RADC tests is to test the CPIRE in conjunction with the LC8D radio, utilizing one of the microwave links available. The test configuration is shown in Figure C-6.

##### 4.2.1 Initial Tests

Initial test at RADC will consists of simple back-to-back tests of the Broadband Modem and CPIRE to verify proper operation after shipment. Modem performance will be measured back-to-back with additive thermal noise as described in Paragraph 4.1.1. CPIRE performance will be verified at a given  $E_b/N_0$  with a fixed amount of cross-polarization interference calibrated as in Paragraph 4.1.2.

##### 4.2.2 Link Tests

After proper operation of the hardware has been verified, it will be tested over an actual microwave link at 8 GHz. The Modem Modulator will be installed at one site, driving two transmitters by use of the Decorrelator. The Broadband Demodulator and CPIRE will be installed at another microwave site. Modem performance over the link with the without the CPIRE will be measured using the self-test feature of the Broadband Modem. BER performance in the presence of cross-polarization interference should be improved considerably with the CPIRE. Additional cross-polarization interference can be introduced by use of the LC8D Simulator which can allow part of one transmitter output to be summed with the other. Performance with and without the CPIRE can then be measured.

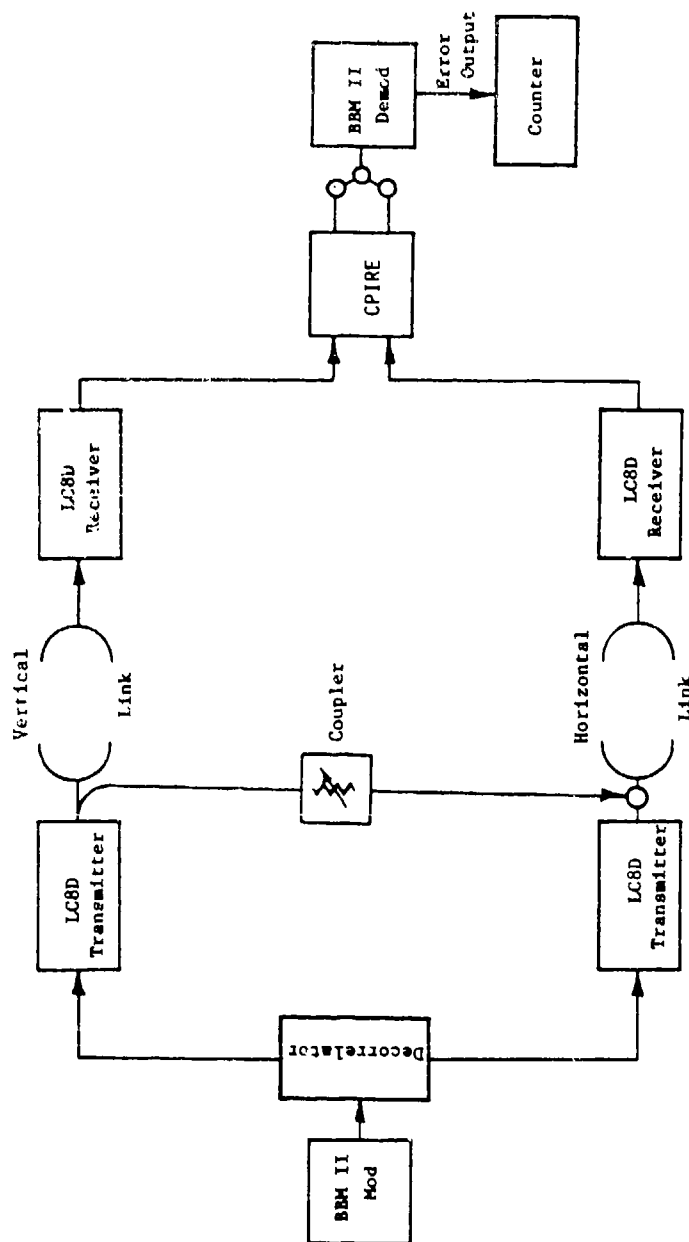


Figure C-6. RADC test Configuration

APPENDIX D  
ACHIEVABLE S/N IMPROVEMENT

## APPENDIX D

### ACHIEVABLE S/N IMPROVEMENT

The amount of signal to noise ratio (S/N) improvement possible with the interference reduction technique used for this contract is a function of initial interference level and interference phase angle. The cancellation scheme is shown in Figure D-1. The main channel signals  $s_1$  and  $s_2$  are assumed uncorrelated and have a component of the other channel added to them with amplitude  $r_n$  and angle  $\phi_n$ . Noise is added at the receiver inputs after the introduction of the cross-pole components. The noise in each channel is uncorrelated with the noise in the other. To cancel the cross talk, a component of one channel is weighted with the proper amplitude and phase angle and subtracted from the other channel resulting in the expressions given in Figure D-1. If  $r_1 = r_2 = r$ ,  $n_1^2 = n_2^2 = N$ ,  $n_1 n_2 = 0$ , and  $s_1^2 = s_2^2 = s$ , then

$$\frac{S}{N_o} = \frac{S}{N} \frac{(1 - r_1 r_2 e^{j(\phi_1 + \phi_2)})^2}{1 + r^2}$$

and,

$$\frac{S}{N_o, \max} = \frac{S}{N} (1 + r^2), \phi_1 + \phi_2 = \pi$$

$$\frac{S}{N_o, \min} = \frac{S}{N} \frac{(1 - r^2)^2}{1 + r^2}, \phi_1 + \phi_2 = 0$$

Figure D-2 plots the minimum and maximum output S/N expressions above versus  $r$ , the amount of coupling. The 0 dB S/N reference refers to the S/N at the input without cross-polarization interference. Thus, with perfect cancellation of the cross-pole components, the resulting S/N can be either better or worse than the S/N in the absence of cross pole, depending on the angles  $\phi_1$  and  $\phi_2$ . The effect of phase angle becomes negligible for small amounts of coupling as shown in Figure D-2.

The test configuration used for in-plant testing (see APPENDIX C) differed from the more realistic situation described above in that the noise was added to the signal before the cross-pole interference was introduced.

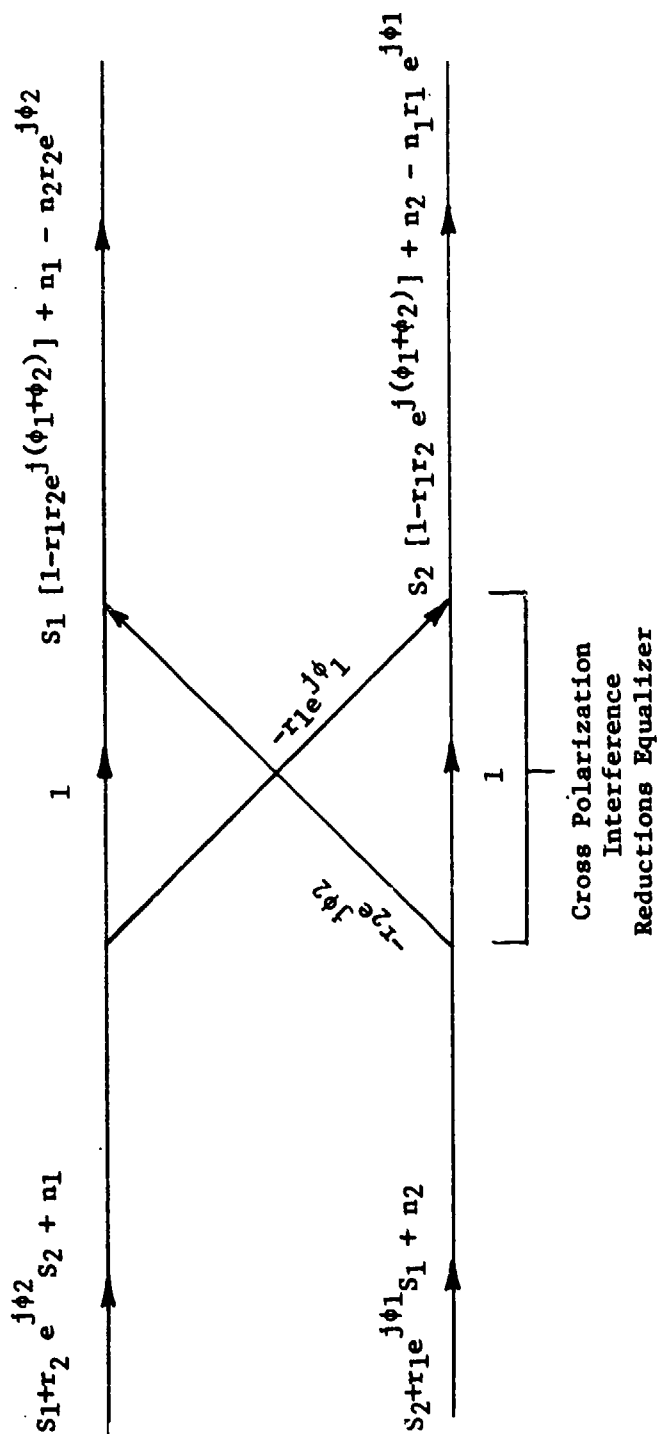


Figure D-1. Cross-Polarization Interference Cancellation Scheme

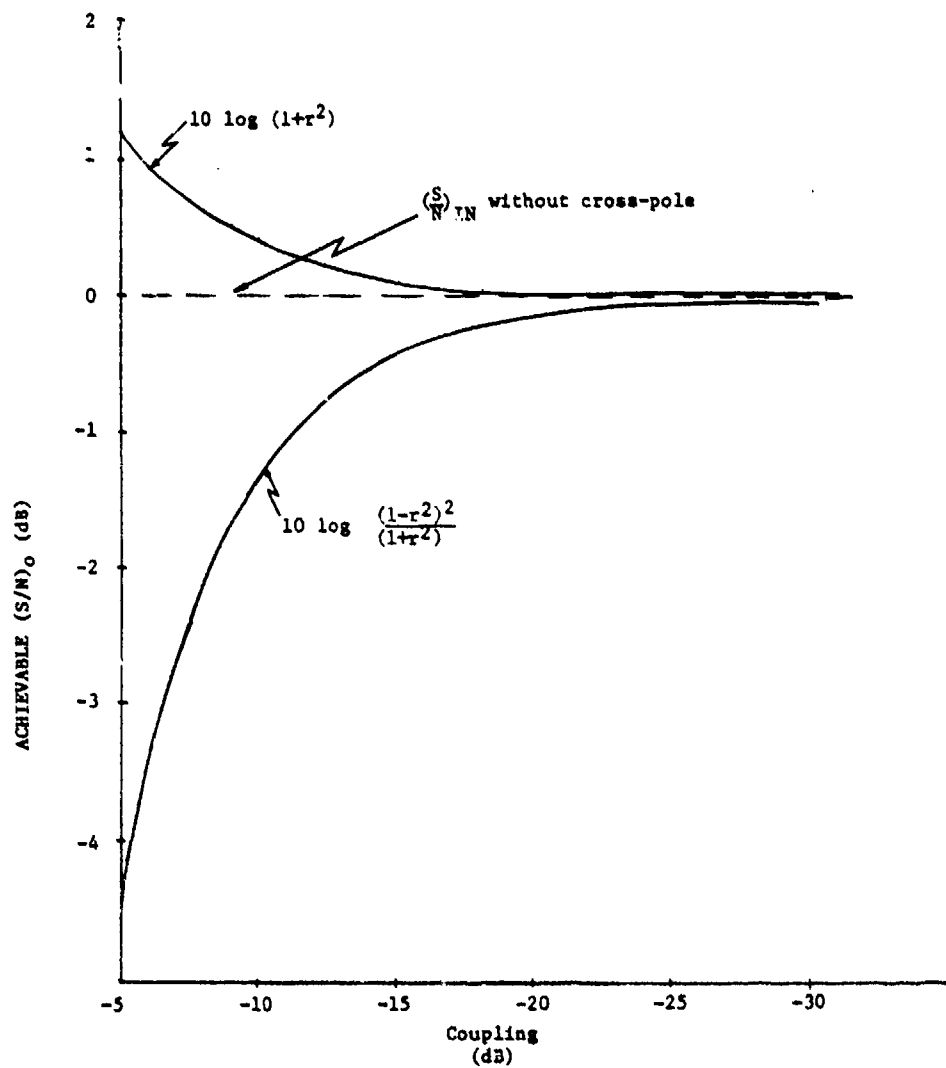


Figure D-2. Achievable  $(S/N)_0$  Bounds

Thus, if perfect cancellation of the cross talk is achieved, then the noise introduced from one channel to the other by the cross-pole mechanism will also cancel, restoring the original S/N. Ideally then, any discrepancy between measured S/N at the output and S/N at the input without cross-pole should be independent of cross-pole phase angle and reflect imperfect cancellation of the interference. This is complicated somewhat by the frequency dependant out-of-band gain produced by the notch filters in the equalizers. Cancellation of the noise will thus be imperfect and the output S/N will differ from the input S/N. This effect can be minimized by the use of narrow-band noise. In all in-plant tests, the noise bandwidth was approximately 28 MHz at the equalizer inputs which is twice the bandwidth of interest. Angle dependancy was noted during testing but the effect was only a few tenths of a dB with a cross-polarization discrimination ratio of 5 dB. For consistency in measurement, the test setup remained unchanged through testing.

APPENDIX E  
REFERENCES

## APPENDIX E

### REFERENCES

1. Baird, C. A. and Pelchat, G. "Cross Polarization Techniques Investigation", RADC-TR-77-244, July 1977. A043395.
2. Gillingham, Bruce E. and Davis, Robert C., "Broadband Modem II, RADC-TR-78-92, April 1978. A055269.